DISSERTATION PRESENTED FOR THE DEGREE OF DOCTOR OF NATURAL SCIENCE (DR. RER. NAT.)

A CO-TUTELLE OF THE UNIVERSITY OF MONTPELLIER AND THE UNIVERSITY OF REGENSBURG

Characterization of a metal-extracting water-poor microemulsion

Presented by Tobias LOPIAN

29/09/2017

Under the supervision of Prof. Thomas Zemb
An Prof. Werner KUNZ

Composition of the jury

Werner KUNZ, Prof., Universität Regensburg	Reporter / Ph. D. Director
Michael GRADZIELSKI, Prof., Technische Universität Berlin	Reporter
Yves CHEVALIER, Directeur de Recherche, Université Lyon 1	Reporter
Julian OBERDISSE, Directeur de Recherhe, Université Montpellier	Adjudicator
Richard BUCHNER, Prof., Universität Regensburg	Adjudicator
Thomas ZEMB, Prof., Université Montpellier	Adjudicator / Ph. D. Director
Sandrine DOURDAIN, Dr., CEA	Supervisor

UNIVERSITÉ DE MONTPELLIER

Preface

This PhD thesis was Co-Tutelle between the partner-universities of Montpellier, France and Regensburg, Germany, between December 2014 and November 2017. In France, this work has been carried out at the Laboratoire du Tri ionique par les Systèmes Moléculaires auto-assemblés (LTSM), which is part of the Institut de Chimie Séparative de Marcoule (ICSM) at the French commissary for atomic energy (CEA). It is implemented in the ERC-project REEcycle in the work-package IV (Exploring new formulations increasing pH window and selectivity). In Germany, this work has been carried out at the Institute of Physical and Theoretical Chemistry, Faculty of Natural Science IV, University of Regensburg. Prof. Dr. Thomas Zemb and Prof. Dr. W. Kunz have guided this work as PhD directors and supervised by Dr. Sandrine Dourdain. This work would not have been possible without the great support from many people. Therefore, I want to express my profound gratitude to the following, who contributed to the completion of my dissertation:

First of all, I would like to express my deepest gratitude for Prof. Dr. Thomas Zemb for giving me the opportunity to participate at this ERC-project, the chance to work at the ICSM and the financial support in order to complete this thesis. I am very grateful for inspiring discussions and his fruitful lessons in physical chemistry. Without his encouragement and drive, this work would have not been possible.

I want to express my sincere gratification towards Prof. Dr. Werner Kunz and his support through this PhD. His calm and patient attitude enabled establishing the Co-Tutelle contract in an Odyssey between the two partner universities. Further, I highly appreciate the possibility to carry out a considerate part of the experiments at his institute.

In addition, I want to thank Prof. Dr. Richard Buchner for the possibility to carry out conductivity and permittivity measurements in his laboratory, as well as the productive discussions.

Sincere thankfulness is owed to Sandrine Dourdain for her professional and moral support through this work. Together, we explored novel domains and learned "petit-à-petit" how to establish a red thread through this work.

I deeply want to show my tanks to Dr. Sylvain Prévost from the ILL in Grenoble. Not only did he find much interest in the subject and helped me advance in many fruitful discussions, but he also became a dear friend.

Dr. Didier Touraud is gratefully acknowledged for the great discussions about phase diagrams and helping me to find specific literature.
Thanks to Prof. Dominik Horinek and Sebastian Schöttel for the collaboration on the UFME-subject and the great publications we were able to diffuse.
I'd like to express a special thanks to Hélène Martin and Vainina Russello for their incredible effort and help in administrative tasks and paper-work.
I gratefully want to thank my team of the LTSM for the pleasant time in the laboratories, in particular our chef, Dr. Stéphane Pellet-Rostaing. Thank you Guilhem, Carlos, Arthur, Beatrice, Alex and Tamir for this great time. Additionally, I want to thank all the other colleagues at the ICSM, whom I didn't name individually.

Further, I would like to sincerely thank all my friends of the German fraction (Michael, Maximilian, Markus, Mario and Robert) and the French fraction (Julien, Alban, Laurant, Michael, Camille, Périne, Thibault, JB and many more). You made this stay in France an exceptional life-time and experience in my life. I will always cherish

Of course to my loving parents, Fritz and Evi Lopian, and my sister Dinah, for their never-ending support throughout the last years.

Last but not least my beloved girlfriend Carolin – We endured three tough years and I am endlessly grateful for your support, love and friendship throughout this work. From the bottom of my heart, I thank you.

Contents

Introduction	**1**
Chapter I – Introduction in fundamental concepts	**5**
Chapter II – Exploring stability domains in extracting microemulsions	**43**
Chapter III – Exploring the conducting properties of a metal-extracting microemulsion	**101**
Chapter IV – Relation of the reference model with a solvent extraction system	**137**
General conclusion	**155**
References	**159**
Annex	**179**

Introduction

Rare-earth elements (REE) are a set of 17 metallic elements in the periodic table, counting all 15 lanthanides and completed by Scandium and Yttrium. They become increasingly important in the transition towards a green and sustainable economy and are the origin for the technological advances in the 21st century. These metals are essential for a wide range of modern inventions, which are indispensible for the development of efficient carbon-free and environmentally benign technologies. They are an important ingredient for modern hydride batteries, hybrid and electrical cars, smartphones, HD-displays, laser-technology, refinement of crude oil, catalysis as well as for permanent magnets used in wind turbines.[1]
A procedure to retrieve these elements from electronic wastes in order to close the so-called "life-cycle" of electronic devices has not been established on an industrial scale. This is reflected by the fact that less than 1% to the world wide annual production of rare earths stems from recycling projects. A major problem is caused by the chemical and physical similarity of these elements, which poses severe problems to the task of separating these metals from each other. The separation procedure of choice is solvent extraction, also called liquid-liquid extraction. In this procedure, two non-miscible solvents (usually water and an apolar organic solvent) are contacted with each other and at proper conditions a mass transfer of a desired species from one liquid to the other can be triggered. In order to retrieve rare earths from an aqueous solution, this is done using complexing agents, also called extractants, which form a reverse aggregate in the organic phase, encapsulating an extracted metal in an apolar environment. On a laboratory scale, very efficient extractant molecules have been synthesised and promising systems have been developed. However, up to date it is not possible to formulate a continuous, adaptive and predictive solvent extraction procedure on an industrial scale. One of the main reasons is the lack of a comprehensive fundamental understanding. On a laboratory scale, extraction is done in dilute conditions of the extractant in the organic phase, where interactions between complexes can be neglected. For an efficient extraction however, high concentrations of extractants are needed, leading to non-ideal behaviour in the organic phase. The origin of these interactions between complexes is yet poorly understood.

In an attempt to challenge major questions on the extraction of rare earth elements from electronic waste, the European Research Council (ERC) has granted a funding for the project REE-Cycle.[2] Using a combined empiric and theoretical approach, this project aims to

formulate general laws, which will allow increasing the predictability for extraction processes. A very successful route to describe the non-ideal behaviour is the so-called colloidal approach.[3] Interpretation of metal-extractant complexes as reverse micelles enables to revert to concepts known from surfactant science. Linking thermodynamic concepts of complex formation with self-assembly allows explaining why a critical concentration of extractant is often necessary to be considered in the organic phase. Further, co-extraction of water in the micellar cores has assigned such systems the term of *extracting microemulsion*.
Besides fundamentally understanding the physico-chemical mechanisms of a metal-extracting microemulsion, the project REEcycle aims to explore new routes in order to enhance the efficacy of an extraction. One route is the application of an external electrical field. This requires exact knowledge on the mechanisms of charge formation in apolar environment.

Therefore, in the frame of this ERC-project and in compliance with the colloidal approach, this work addresses two fundamental questions, which have yet been poorly reviewed in solvent extraction science: the macroscopic phase behaviour and the conductivity properties.

The macroscopic phase behaviour of a solvent extraction procedure is poorly understood. However, knowledge of the phase behaviour is indispensible for chemical engineers in order to find an “optimum formulation”, i.e. when the microemulsion selectively extracts a desired metal species and possesses appropriate mechanical properties for application in continuous procedures. Additionally, mapping of the phase behaviour in diagrams shows a chemical engineer how to avoid undesired phases (such as stable emulsions and third phase formation, also called “three-phase catastrophe”).
Phase diagrams are a powerful way to describe and visualize the phase behaviour of a multi-component system and summarize a large amount of experimental data.[4] In surfactant science, phase diagrams do not only map the phase behaviour of microemulsions, but they provide a link between the macroscopic behaviour and internal interactions, e.g. evolution of phase boundaries are a direct link to the solubilization capacity on a microscopic scale.

The second aspect of this work concerns the conducting behaviour of metal-extracting microemulsions. Up to date, micelles in an apolar environment are often considered as electrically neutral. Therefore, the origin of attractive interactions between reverse aggregates is always assigned to dispersion forces. Nevertheless, formation of charged micelles by either dissociation or dismutation mechanisms earned an increasing attention in recent years.[5] In the frame of the colloidal approach in solvent extraction, formation of

charged aggregates may explain a yet neglected origin of interaction between reverse aggregates: Coulomb interactions. On the long run, if these mechanism are well understood exploiting this feature may help enhance the extraction efficacy.

To achieve these objectives, the thesis has been divided in four chapters. The first chapter of this work gives a fundamental introduction of the three pillars of this work: solvent extraction, colloidal science and electrodynamic properties in apolar media. The second chapter is devoted to explore the stability domains of an extracting microemulsion. Solvent extraction systems used in an industrial formulation are complex multi-component formulations, containing at least six different components (aqueous phase composed of water, the desired metal species in form of an electrolyte and acid – the organic phase of the complexing agent, a diluent and a modifier to adjust mechanical properties of the liquid). Thus, a simplified model system was defined. The evolution of the phase behaviour is investigated by establishing a Gibbs phase prism for four different solvents (toluene as a reference solvent, as well as isooctane, dodecane, nitrobenzene). Using the Gibbs prism as a comprehensive map, the conductivity profile of extracting microemulsions is evaluated in chapter III. The results are correlated using small angle scattering experiments as a supporting experimental method. Since the results of chapter 2 and 3 are based on a model system, the fourth chapter is a comprehensive conclusion and outlook on the importance of the macroscopic phase behaviour and conductivity in solvent extraction.

(1) Binnemans, K.; Jones, P. T.; Blanpain, B.; Van Gerven, T.; Yang, Y.; Walton, A.; Buchert, M. Recycling of Rare Earths: A Critical Review. *J. Clean. Prod.* **2013**, *51*, 1–22.

(2) REE-CYCLE ERC http://reecycle-erc.blogspot.com/ (accessed Sep 28, 2017).

(3) Zemb, T.; Bauer, C.; Bauduin, P.; Belloni, L.; Déjugnat, C.; Diat, O.; Dubois, V.; Dufrêche, J.-F.; Dourdain, S.; Duvail, M.; et al. Recycling Metals by Controlled Transfer of Ionic Species between Complex Fluids: En Route to “Ienaics.” *Colloid Polym. Sci.* **2014**, *293* (1), 1–22.

(4) Chevalier, Y.; Zemb, T. The Structure of Micelles and Microemulsions. *Rep. Prog. Phys.* **1990**, *53* (3), 279.

(5) Hsu, M. F.; Dufresne, E. R.; Weitz, D. A. Charge Stabilization in Nonpolar Solvents. *Langmuir* **2005**, *21* (11), 4881–4887.

(6) Kahlweit, M.; Strey, R.; Haase, D.; Kunieda, H.; Schmeling, T.; Faulhaber, B.; Borkovec, M.; Eicke, H.-F.; Busse, G.; Eggers, F.; et al. How to Study Microemulsions. *J. Colloid Interface Sci.* **1987**, *118* (2), 436–453.

Chapter I

On solvent extraction and microemulsions

–

Introduction in fundamental concepts

1. LIQUID-LIQUID EXTRACTION – A VERSATILE SEPARATION METHOD 9

1.1) THE BASIC CONCEPT OF SOLVENT-EXTRACTION 9

1.2) SOLVENT EXTRACTION AS THE CORE SEPARATION PROCEDURE IN HYDROMETALLURGY . 12

1.3) HOW TO EXPLAIN THE SOLUBILIZATION OF POLAR ELECTROLYTES INTO AN APOLAR ENVIRONMENT 13

1.4) THE COLLOIDAL APPROACH: COUPLING SOLVENT EXTRACTION WITH THE FORMATION OF SELF-ASSEMBLING HIGHER ORDERED STRUCTURES 15

2. SELF-ASSEMBLY AND MICELLES 17

2.1) SURFACTANTS AND THE INTERFACE OF LIQUIDS 17

2.1.1) General introduction of surface active compounds 17

2.1.2) Classification of surfactants 18

2.2) SELF-ASSEMBLY INTO MICELLES AND THE CRITICAL MICELLAR CONCENTRATION 19

2.2.1) A theoretic experiment 19

2.2.2) The thermodynamic driving forces for self-assembly in aqueous solutions 20

2.2.3) Self-assembly in an apolar environment of low permittivity 21

2.2.4) Consistent definition of a critical micellar concentration in apolar media and solvent extraction 22

3. MICROEMULSIONS – THERMODYNAMICALLY STABLE MIXTURES OF WATER AND OIL 23

3.1) ORIGIN OF THE THERMODYNAMIC STABILITY OF MICROEMULSIONS 23

3.2) CONDITIONS FOR FORMULATION OF A MICROEMULSION AND REQUIRED ADDITIVES 24

3.2.1) Defining the amphiphilic character of a surfactant 24

3.2.2) Additives to further decrease the interfacial tension between water and oil 25

3.2.3) Geometrical interpretation of the interface – the packing parameter and curvature 26

3.2.4) Macroscopic phase behaviour and the Winsor-Phases 28

3.3. LOCATION OF THE DIFFERENT PHASES ON A MAP: INTRODUCTION IN PHASE DIAGRAM ANALYSIS 30

3.3.1) How to read phase diagrams 30

3.3.2) Phase diagrams in surfactant science – Ternary representation 32

3.3.3) Variation of the temperature – the Gibbs prism and prism analysis 34

4. CONDUCTIVITY IN APOLAR MEDIA AND MICROEMULSION SYSTEMS 37

4.1) ON THE FORMATION OF CHARGED SPECIES IN LIQUID MEDIA 37

4.2) REVERSE MICELLES AS CHARGE CARRIERS 38

4.3) MODELS TO EXPLAIN THE CONDUCTIVITY IN REVERSE (SWOLLEN) MICELLAR SOLUTIONS 39

4.4) TRANSITION FROM DISCRETE REVERSE MICELLES TO BICONTINUOUS MICROEMULSIONS: PERCOLATION.....39

5. CONCLUSION 41

1. Liquid-liquid extraction – A versatile separation method

One of the biggest challenges in chemistry and related disciplines is the availability of pure compounds: isolation of a desired protein from a cell, extraction of a natural product from a biological matrix, production of gasoline from crude oil, or purification of products after a chemical reaction, just to name a few. Therefore, separation procedures are ubiquitous, on a laboratory as well as on an industrial scale. Scientists developed an arsenal of different tools, exploiting the differences of chemical and physical properties in order to isolate and enrich a desired target from undesired by-products. Apparently simple methods such as centrifugation, pioneered by Svedberg in the twenties,[1] allows the segregation of dense molecules from less dense ones. Chromatography, with all its facets plays with the polarity of molecules, electrophoresis exploits the mobility of charged entities in an electric field. Thermally driven processes, such as distillation separates volatile products depending on the boiling temperatures – the amount of possibilities is shear endless.

One of the oldest, yet very successful separation procedure is *solvent extraction*, also called *liquid-liquid extraction*. It finds a daily application in laboratories of organic chemist to purify their products after a chemical reaction. Perfume industry uses large columns to extract a few droplets of good-smelling essential oils.[2] In the field of nuclear fuel cycle management, solvent extraction allows separation and isolation of radio-active fission products (namely the PUREX and DIAMEX processes at the French CEA agency or TALSPEAK processes in the USA).[3,4] These processes allow to separate valuable Uranium and Plutonium from fission products (e.g. Americium and Caesium). Though previously considered as waste, these fission products are new used in a closed fuel cycles for generators of the IVth generation. Further, solvent extraction allows to selectively separate rare earth elements from raw ores and electronic waste.[5] A comprehensive treaty, as recent as 2004, was assembled by an international team of four editors.[6]

1.1) The basic concept of solvent-extraction

The basic idea behind a liquid-liquid extraction experiment is simple: One needs two liquids, which are (at least partially) immiscible, and a third compound, which will unevenly distribute between these two phases. The two immiscible liquids are called *solvents*, whereas the solubilized compounds to separate are called *solutes.*[7]

Since this work will only deal with water and organic liquids, the terminology “aqueous phase” is introduced for a *polar* phase and respectively the “organic phase” for an *apolar* or *oil phase*.

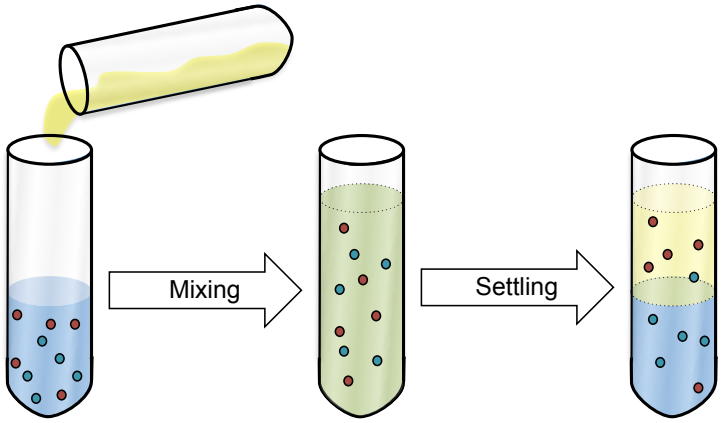

Figure I-1 – Schematic representation of a solvent extraction experiment. Two liquids, e.g. water and oil are not miscible. Two compounds are solubilized in the aqueous phase. After contacting the aqueous phase with an organic phase, the solutes distribute between the two phases according to their solubility in each of the respective phases.

In figure 1, a schematic representation of such an extraction experiment is demonstrated: Two different types of solutes (red and blue) have been solubilized in an aqueous matrix. An organic solvent is added and the solution is thoroughly mixed. After phase separation of the two liquids due to their immiscibility, the two solutes will distribute unevenly between the aqueous and the organic phase.

Solvent extraction is an *equilibrium process*, which means that the system is in a thermodynamic equilibrium and the transfer of an ion between the two phases is a dynamic equilibrium process. Distribution of the solutes between the two phases is determined by their intrinsic “affinities” towards the aqueous or respectively the oil phase. This is reflected by their reference chemical potential $\mu_i^{0,phase}$ in each of the phases. Since the system is at a thermodynamic equilibrium, the free energy of the system is at a minimum. Therefore, the chemical potential μ_i^{phase} of a solute i is equal in both phases:

$$\mu_i^{aq} = \mu_i^{org} \qquad (i)$$

Where “aq” denotes the aqueous phase and “org” the organic phase. The chemical potential can be split into the reference chemical potential $\mu_i^{0,phase}$ in the designated phase and a second term related to the activity a_i^{phase}

$$\mu_i^{0,\ aq} + RT \cdot \ln\ a_i^{aq} = \mu_i^{0,org} + RT \cdot \ln\ a_i^{org} \qquad (ii)$$

The difference of the reference chemical potentials defines the free energy to transfer a solute from one phase to the other. Since the particular interest is to transfer a solute i from the aqueous to the organic phase, rearrangement of equation (ii) leads to:

$$\Delta_{Trans}G^{aq\rightarrow org} = \mu_i^{0,aq} - \mu_i^{0,org} = RT \cdot \ln a_i^{org} - RT \cdot \ln a_i^{aq} = RT \cdot \ln \frac{a_i^{org}}{a_i^{aq}} \quad (iii)$$

Therefore, the free energy of transfer $\Delta_{Trans}G^{aq\rightarrow org}$ is determined by the activity of the component in both phases. Assuming ideal behaviour, i.e. no interactions of the solute molecules between each other, the activity can be reduced to the concentration c_i^{phase} of the solute (the mathematical formalism can be found here [8]). Thus, the free energy of transfer can be defined as the ratio of the concentrations of solute i in each individual phase:

$$\Delta_{Trans}G_i{}^{aq\rightarrow org} = RT \cdot \ln \frac{c_i^{org}}{c_i^{aq}} = RT \cdot \ln D_i \quad (iv)$$

D_i defines the *distribution ratio* and was first introduced by Nernst in 1891 and is a measure for the efficacy of an extraction.[9] In case of the red solute in figure 1, $D_{red} > 1$, since the majority of this component accumulates in the organic phase. In contrast, $D_{blue} < 1$, as it preferably stays in the aqueous phase.

To come back to the usage of solvent extraction as a separation procedure, the "separation-efficiency" can by determined by comparing the free energy of transfer between two solutes i and j as:

$$\Delta_{Trans}G_i{}^{aq\rightarrow org} - \Delta_{Trans}G_j{}^{aq\rightarrow org} = \Delta\Delta_{Trans}G_i{}^{aq\rightarrow org} = RT \cdot \ln \frac{D_i}{D_j} = RT \cdot \ln S_i \quad (v)$$

This is a double-difference: on one hand, the distribution of the solute between the two phases and secondly the direct comparison with a second solute. The *separation factor* S_i is therefore a measure for the selectivity of an extraction system.

The scheme in figure 2 gives an overview on how an extraction process can be coupled with the thermodynamic driving forces. In 2(a), the reference chemical potential of a solute in the initial aqueous phase (blue bar) is higher than the reference chemical potential in the final organic phase after contact (red bar). Thus it is transferred into the organic phase, as it is thermodynamically favourable.

In 2(b), a second solute (ion 2) is considered, for which the reference chemical potential in the organic phase is lower, than for the "ion 1". As a consequence, the difference of the reference chemical potentials (green bars) of the second solutes is higher and thus the free

energy of transfer favours a transfer of “ion 2” into the organic phase. The difference of the free energies determines the selectivity of the system.

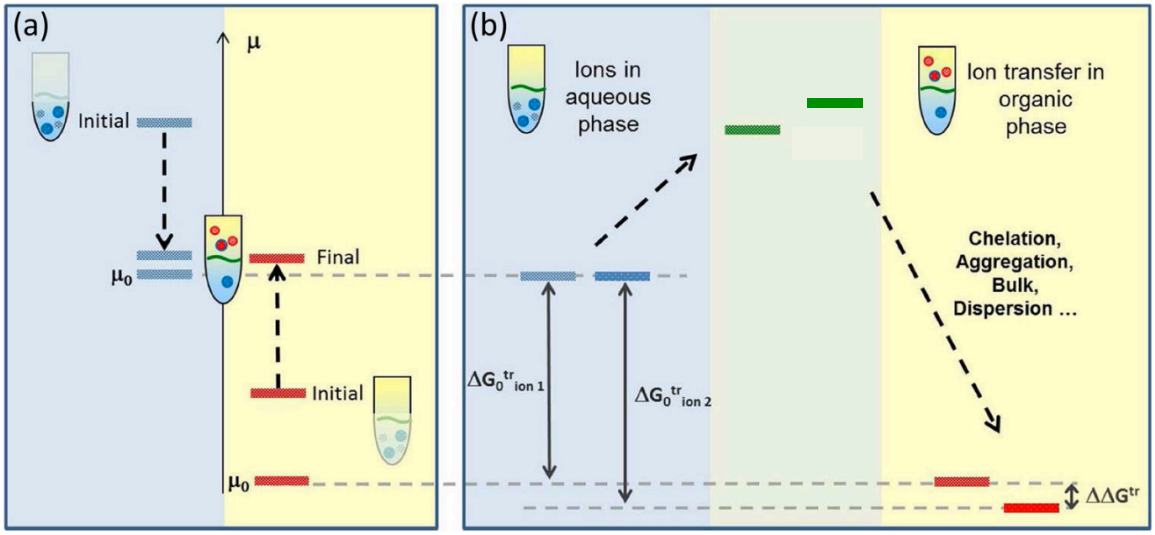

Figure I-2 – Schematic representation of an extraction process based on the distribution of ions between an aqueous and an organic phase. Reproduced and adapted from [10].

1.2) Solvent extraction as the core separation procedure in hydrometallurgy

One of the major field of applications of solvent extraction is hydrometallurgy, that is the art to retrieve precious metals from ores and minerals,[11] but also from electronic and metallic wastes.[12]

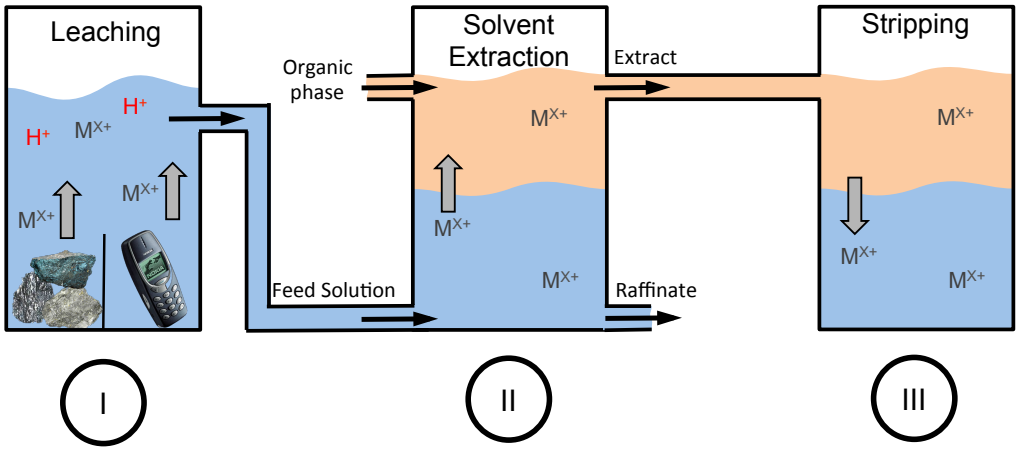

Figure I-3 – Simplistic scheme of a hydrometallurgical process with solvent extraction as the core separation step. The first step is the leaching of metals from ores or waste material with an acidic solution. The second step is the enrichment of desired metal species from the feed solution with a formulated organic solution. In the third step, the precious metals are recuperated from the organic phase by a stripping step.

Hydrometallurgy has a huge industrial importance and the complexity lies in particular within the multi-stage systems of a whole process. Since this is the field of chemical engineers, only the most essential basics are highlighted, in order to illustrate the importance of solvent extraction as the key separation process.[13]

The first step to recover metals from a solid matrix is the so-called "*leaching*". The metals are transferred into a liquid matter of state using an acidic aqueous phase, as shown in step I. The loaded aqueous phase, called *feed solution* is then pumped into a second basin and contacted with a formulated organic phase. It is designed to selectively and efficiently extract the desired metal species into the organic phase, where we enter the realm of solvent extraction. After loading of the organic phase, the next step is the back-extraction or *stripping*, back into a fresh aqueous phase, after which the targets can be recuperated.[14]

1.3) How to explain the solubilization of polar electrolytes into an apolar environment

Electrolytes are composed of ions, which exhibit strong electrostatic forces on each other upon dissociation. Extraction into an apolar phase of low dielectric permittivity ε_r is thus counter-intuitive. However, it is very possible to solubilize electrolytes in an organic phase: One of the earliest reports of solvent extraction has been the extraction of uranium nitrate using ether[15] and even today, retrieving tantalum and niobium with octan-1-ol,[16] or octan-2-ol as organic phase has proven to be efficient.[17]

Nowadays, more appropriate alternatives are used, on one hand, to comply the safety regulations and on the other hand for more versatile and adaptive modes of application. Complexing agents, also called *extractants*, enable the transfer of electrolytes into an apolar solvent. Extractants posses a polar head-group and an apolar tail. Since pure extractants are either in a solid matter of state or liquid, but very viscous (e.g. HDEHP, TODGA), they need to be solubilized in an organic solvent (in general linear or branched alkanes, e.g. iso-octane or dodecane). Since this organic matrix does not actively participate in the complexation process, they are commonly classified as *diluents*.

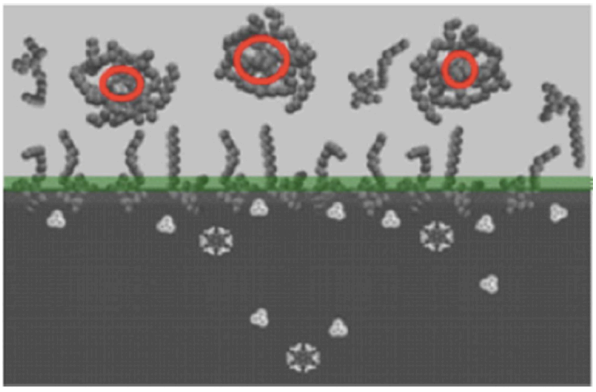

Figure I-4 – Artist view of a water-solvent interface (meniscus underlined in green) in a liquid-liquid extraction system on a nanometer scale. Amphiphilic extractant molecules pick up an electrolyte at this interface and encapsulated them into an organo-soluble complex. The red circle illustrates the polar cavity where the electrolyte is embedded after extraction. Figure reproduced from [18].

The extractants create a polar cavity in an apolar environment. The electrolyte is encapsulated by the head-groups and the apolar tails allow the solubilization of the whole complex in an organic solvent (as depicted in figure 4). The term "extractant" is not reserved for a single type of molecule, but there are different types of extractants, which have different mechanisms of complexation:[19]

1) **By cation exchange:** Organo-phosphorus acids, such as HDEHP[20] or Cyanex 272[21] and carboxylic acids, such as Versatic 10[22], donate their proton into the aqueous phase and in return complex a metal-cations. As a result of the proton-release, the distribution and selectivity is highly sensitive to the concentration of acid in the aqueous phase. Therefore, fine tuning of the formulation allows not only the extraction of a broad range of metals, but also high selectivity (e.g. isotope separation of Europium using HDEHP).[23]

2) **By formation of ion pairs:** Amines, such as Alamine 336,[24] form an adduct with an acid molecule (so-extracted from the aqueous phase). In return, the adduct forms an ion-pair with a cation, dragging it into the organic phase. In contrast to the first type, no proton is released. On one hand, this mechanism is less tuneable, but on the other hand, the system is more prone to high quantities of acid in the aqueous phase.

3) **By "Solvation":** Representatives of this class are phosphine oxides (TOPO), acid esters (TBP),[25] and malonamides (DMDOHEMA, TODGA).[26] These non-ionic extractants extract a metal cation by forming a solvation shell, competing with the hydration shell of ions in the aqueous phase. Typically, high amounts of acid in the aqueous phase are necessary to trigger a transfer in the organic phase. They are

frequently used in recycling of nuclear fission products due to the low amount of water solubilized in the organic phase.

Combination of extractants from different types can modify the overall reaction mechanism. The general international textbook for solvent extraction identifies 17 different categories, based on variation of acid, temperature, pH and type of extractant(s). The 17th category is somewhat special, since it concentrates all documented cases which could not be attributed to the first 16 classes.[6]

Though the mechanisms for complexation may differ, from a thermodynamic point of view, extraction of a neutral species is always described in the manner. Therefore, in order to "predict" the outcome of an extraction, early theories in the 1960s based on regular solution theory.[10] Using a "molecular approach", extensive experimental screening of the distribution ratio versus the experimental variables (temperature, pH, acidity) was conducted, in order to derive independently the solubilization of metal species in the organic phase.[27]

1.4) The colloidal approach: Coupling solvent extraction with the formation of self-assembling higher ordered structures

Early works of McDowell and Coleman analysed the unusual extraction behaviour of Uranium between an aqueous and organic phase, using di-n-decylamine sulphate as an extractant and benzene as diluent.[28] The distribution ratio of the cation could not be explained with usual equilibrium studies. Therefore, the authors tried to shed some light into the extraction mechanism by analysing the surface properties of the system. The interfacial tension between water and benzene is $\gamma_{water-benzene} = 32.7 \frac{mN}{m}$.[29] Upon increase of either the extractant concentration in the organic phase or the acidic concentration in the aqueous feed, the interfacial tension decreased by up to a factor 3.

As mentioned earlier, extractants have a polar head-group and an apolar tail, thus they can be classified as *amphiphilic molecules* (which will be introduced in details in the next sub-section). A typical stereotype for each of the presented classes is depicted in figure 5, highlighting the polar complexing sites in blue, and the apolar moieties in orange. Due to their amphiphilic nature, consideration of metal-extractant complexes as a form of reverse micellar aggregation has been recognized since the early 1980s.[30]

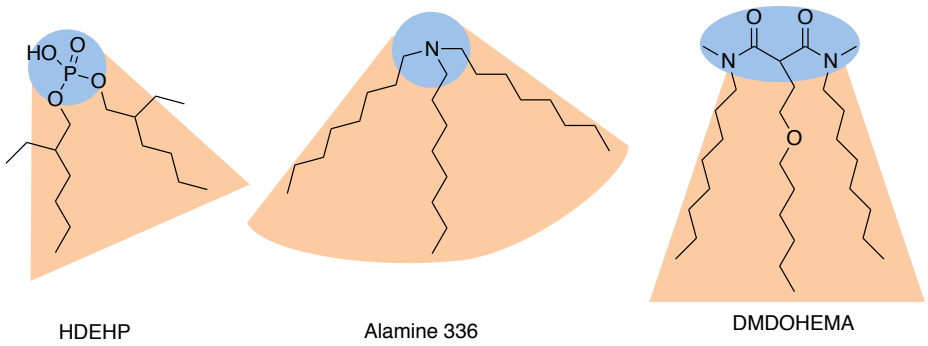

Figure I-5 – Molecular structure of commonly used amphiphilic extractants. The blue areas denote the hydrophilic head-groups, responsible for complexation of cations. The orange areas show the lipophilic tails, solubilizing the complex in an apolar environment.

The pioneering works of Osseo-Asare confirmed the interpretation that complexes can be compared to reverse micelles, by showing that extractant molecules "self-assemble" beyond a critical concentration in the organic phase.[31] Through NMR, osmometry and surface tension measurements, the presence of reverse micellar structures was postulated, as well as the formation of liquid crystalline phases strongly indicated the assembly of extractant-molecules into higher-ordered forms of molecular aggregation.[32,33] Direct proof has been given in 1998, when Erlinger *et al.* was able to detect a scattering signal in the small-angle regime using X-ray and neutron scattering experiments (DMDOHEMA as extractant for Uranium nitrate).[34] Fitting of the scattering signal with a globular geometry revealed a polar micellar core of $R \sim 1\,nm$ and typically 6-12 apolar chains in the shell. Further, formation liquid crystals phases have been observed, similar to surfactant systems.[35,36] Thus, as an analogous to water-soluble surfactants, extractants can be viewed as solvent-soluble surfactants.

Nowadays, the colloidal interpretations has been commonly accepted and established in solvent extraction of metal species and referring to extractive organic phases as metalloamphiphilic solutions.[10,37] In the molecular approach self-assembly was hidden under a phenomenological set of activity coefficients in order to predict the outcome of an extraction. Considering the water-oil interface as a highly curved film (as in figure 4) allows coupling of the free energy of transfer with the free energy of micellization i.e. formation of a reverse micellar complex. This enabled to identify entropic terms as the origin of origin of synergism in certain cases.[38] On the long run, the colloidal approach will allow the elucidation of predictive theoretic models and thus the fundamental origin of the previously introduced 17th "miscellaneous" category.[39]

2. Self-assembly and micelles

As the name implies, the colloidal approach in solvent extraction (also soft matter or supramolecular approach) is based on the scientific domain of colloids, i.e. entities which are too big to "feel" the effects of quantum mechanics, yet too small to succumb the gravitational force of the earth – thus the common length scale is in the range of 1 nm – 100 nm.[40] Colloidal chemistry is a large inter-disciplinary subject, combining physics, chemistry and biology. This introduction targets only the specific section of surface active molecules and their self-assembling properties, in order to elucidate the thermodynamic driving forces applied in the colloidal approach in solvent extraction: the science of surfactants, self-assembly and microemulsions.

2.1) Surfactants and the interface of liquids

2.1.1)General introduction of surface active compounds

The term "surfactant" is an abbreviation for **surf**ace-**act**ive **a**ge**nt**, which literally addresses molecules that "actively want to go to the surface". Surfactants are the prototype of amphiphiles, thus they possess both, a water-soluble and a water-insoluble component, as depicted in figure 6.[41] The term "amphiphile" (from the Greek words "*amphi*" = both and "*philis*" = love/friendship) arises from the double nature: the hydrophilic head-group likes to

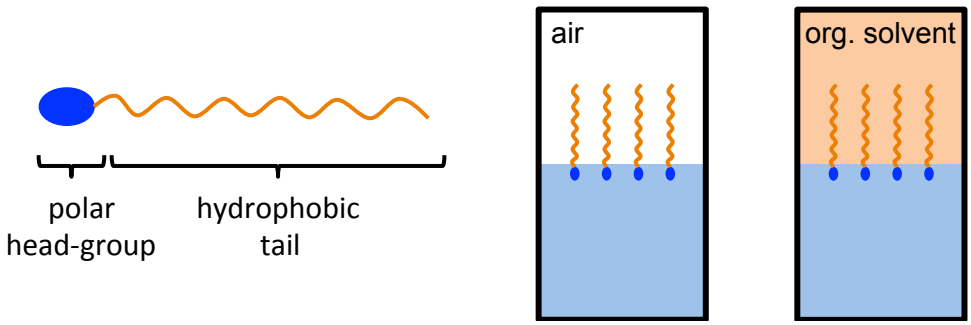

Figure I-6 – Schematic representation of the molecular structure of an amphiphile and the organisation at the interface of a two-phase system containing water and oil.

interact water and the hydrophobic tail prefers to interact with apolar, organic species. When dissolved in water, the insoluble hydrophobic group extends out of the bulk water phase towards air, or (if present) into the oil phase. The water-soluble head-group on the other hand, remains in the water phase.[42]

The driving force for the adsorption at the interface is mainly attributed to the bad solubility of the apolar chain in the bulk aqueous phase, thus the chemical potential favours a migration towards the interface and decreasing the free energy at the interface by decreasing the interfacial tension.[43]

2.1.2)Classification of surfactants

Similar to extractants, the word “surfactant” is not reserved for a special type of molecules, but many different molecules comply with this definition, provided the polar and apolar moieties have a sufficiently large affinity towards water and oil to form micelles (introduced in next sub-section).

Surfactants are primarily defined by the nature of the head-group. Further, the hydrophobic part is composed of one or more alkyl chains, which can be linear or branched. The chain-length is mostly in the range of 8-18 carbon atoms. The degree of chain branching, the length of the chain, and the position and nature of the polar head-group are all parameters, which affect the physicochemical properties of the surfactant.

In figure 7, a general overview on the most common classes of surfactants is given. The polar head-group is divided into two classes: non-ionic versus ionic. For ionic surfactants, the classification can be further divided in cationic, anionic or zwitter-ionic. The list is by far not complete, but should be sufficient for a general introduction.

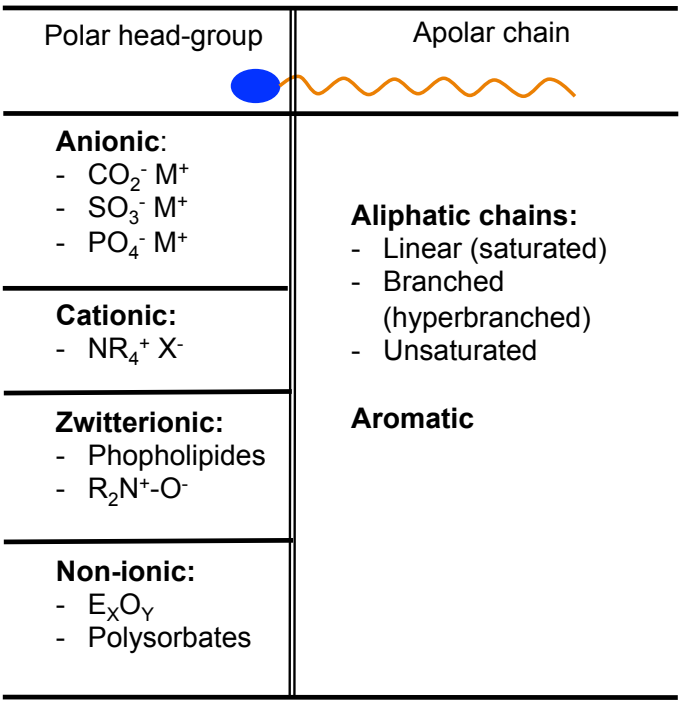

Figure I-7 – Classification of surfactants according to their head-groups and apolar chains. Adapted from [38].

2.2) Self-assembly into micelles and the critical micellar concentration

2.2.1)A theoretic experiment

Let us consider a theoretical experiment: the concentration of a surfactant molecule is successively increased in an aqueous environment. The majority of the surface-active molecules will adsorb at the interface, while a minor fraction is dissolved in the bulk. As a consequence the surface tension is decreasing constantly as the concentration is increased. If the interface is saturated, the residual surfactants are forced to solubilize in the bulk. In order to avoid the unfavourable interaction of the non-polar chains with water they will self-assemble into spherical clusters called *micelles*, as depicted in figure 8.[40]

The critical concentration above which this phenomenon is observed is called *critical micellar concentration* (cmc). Above this concentration, a surfactant-monomer can be located at three different positions: at the interface, as a monomer in the bulk (the monomer concentration is equal to the cmc) or inside a micelle.

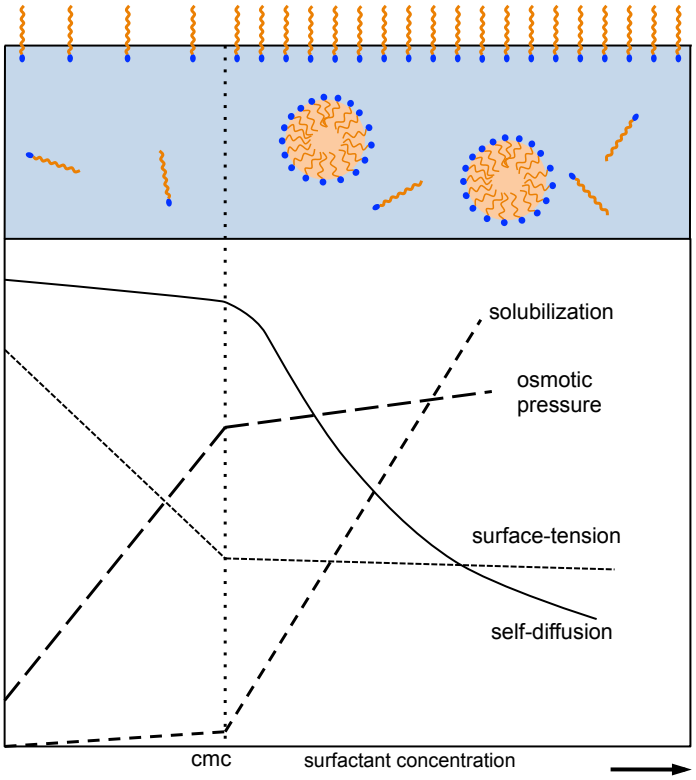

Figure I-8 – Change of some physico-chemical properties of a micellar solution before and after the cmc. Adapted from [44].

The *aggregation number* N_{Agg}, i.e. the number of surfactants per micelle, is constant. Therefore, the addition of more amphiphiles results in the increase of micelles per unit

volume.[40] The critical concentration varies highly, depending on the nature of the surfactant and the conditions of the system (pressure and temperature). Nevertheless, to give an example, one of the most studied surfactants in literature, sodium dodecyl sulfate (SDS), has a critical micellar concentration of $cmc = 8.2\,mM$ and an average aggregation number of $N_{Agg} = 62$ molecules per micelle.[45,46]

As illustrated in figure 8, the physico-chemical properties of the solution change drastically if micelles are formed. As already mentioned, the surface tension decreases drastically upon increase of the surfactant concentration, however above the cmc it is nearly constant, since the interface is completely saturated. Given the apolar nature inside the micellar core, organic solutes can be solubilized inside, thus increasing the solubility of such solutes in an aqueous phase. Further, mobility of a surfactant drastically decreases, given that it is captured into a higher ordered cluster. Due to the higher inertia moment, the average diffusion coefficient per surfactant decreases. Colligative properties, such as the osmotic pressure are also influenced, since the system recognizes a micelle as one unit, not as ensemble of many surfactants.[43]

Micellar solutions are ordered on a nanometer scale, however isotropic on larger scales. If the concentration is further increased and the micellar solution becomes denser, micellar solutions become ordered even over large distances. This results in the formation of so called *mesophases* or *lyotropic liquid crystals*, but is not further reviewed.[47]

2.2.2)The thermodynamic driving forces for self-assembly in aqueous solutions

The distribution of a solute in a solution is generally favoured by a gain in entropy of mixing.[48] The main mechanism for assembly of surfactants into mesoscale structures is the same as the reason why oil and water do not mix: water and oil do not repeal each other, but they are able to interact due to attractive Van der Waals interactions. The bad solubility arises from the favourable hydrogen bonding of water with molecules of its own kind.[49] In the vicinity of an apolar solute, water will interact attractively, resulting in a low gain in enthalpy. On the other hand, water molecules, which are next to a non-polar solute, cannot participate freely to the hydrogen network. Hence, they have fewer conformations available than “free” water molecules and are associated with negative entropy and is the origin of the so-called *hydrophobic effect*.[50]

Further, the hydrophobic effect arises from the volume work, which is necessary to form a cavity in the continuous hydrogen-bond network of water. This cavity needs to be large

enough to accommodate the non-polar solute. The required energy for this contribution is large due to the high cohesion in water arising from the hydrogen-bonding connectivity on the one hand and the small size of water molecules compared to, e.g. alkanes on the other hand. Thus, an important consequence is that the magnitude of the hydrophobic effect is proportional to the area of hydrophobic contact between the water and the solute.[51]

2.2.3)Self-assembly in an apolar environment of low permittivity

So far only binary water-surfactant systems have been discussed. Considering now the solubilization of a surfactant in an organic diluent (e.g. n-heptane or n-dodecane). The scientific question on the driving forces for reverse micellization (i.e. spherical aggregates where the polar head-groups are oriented towards the micellar core) are still controversial. This starts already with the definition of a clear critical micellar concentration.[47]

Solubilized in oil, the surfactant has no real obligation to adsorb at the solvent-air interface, since both types of orientation of the surfactant at the interface is unfavourable for the free energy of the interface, as depicted in figure 9. Therefore, a direct correlation towards water systems can be excluded.

As mentioned earlier, the solubilization of a solute in a pure liquid is always favoured by a gain in mixing entropy. The self-assembly in apolar media is thus driven by attractive interactions between polar head-groups. This aggregation is unfavourable from an entropic point of view, since the system is has an increase in order. The self-assembly is strongly influenced by strength in interaction between polar moieties and

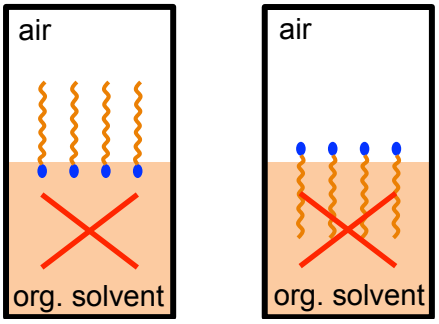

Figure I-9 – The two possible orientations of a surfactant in an organic solvent at the interface towards air. Since both are unfavourable for the free energy of the interface, the red crosses cross them out.

mostly attributed to attractive donor-acceptor interactions.[52] The presence of water favours these attractions, as it can adapt both, the role of both a donor and an acceptor. Further, it stabilizes electrical charges of head-groups by forming a hydration shell. Eicke and Christensen go even further and postulate that *true reverse micelles*, i.e. pure binary oil-

surfactant systems, do not exist and that the presence of a polar "impurity" as a structural nuclei is indispensible for the formation of a reverse micelle.[53,54] In order to challenge this view, Yu *et al.* showed that addition of water has the reverse effect: the scattering signal of a dry n-heptane/NaDEHP solution is lost upon addition of water, therefore declaring water as an "anti-micellization agent".[55] Therefore, the origin of reverse micellar formation and the presence is still under discussion in current literature: in some systems reverse micelles form in the absence of water,[56] while others require water to form reverse aggregates.[57]

2.2.4) Consistent definition of a critical micellar concentration in apolar media and solvent extraction

Since the aggregation is driven by attractive interactions, formation of dimers, trimers or oligomers at low surfactant-concentrations have been registered by different experimental methods (e.g. HDEHP tends to form dimers if dissolved in an apolar solvent).[58] The aggregation number on the other hand is often much lower than in aqueous solutions (e.g. $N_{Agg}(NaDEHP) = 12$).[59] Therefore, a sharp concentration, above which the surfactant self-assembles into reverse micelles of a preferred size is difficult to define and can also be presented as a multi-equilibrium reaction.[58] So it is important to point out that the expression a "critical micellar concentration" in non-polar solvents assembles two different concepts:

- The "cmc" as a critical concentration, above which "free monomers" are dissolved in the organic pseudo-phase and in equilibrium with reverse micelles. Considering the micellar solution as dilute allows taking the cmc as a measure for the free energy of aggregation as introduced by Tanford:[60]

$$\Delta_{mic}G = RT \cdot \ln cmc \qquad (vi)$$

  "Good" surfactants have intrinsically low values for the cmc ($cmc < 10\,mM$). For a critical aggregation in the range of $cmc \sim 100\,mM$, the micelles are called weak aggregates, since the free energy is in the range of $\Delta_{mic}G = 2 - 3\,k_BT$.[10]

- In chemical engineering, the cmc is defined as the concentration at which the solubilizing power of a binary system towards a third solute diverges (as depicted in figure 8). In an organic diluent, it specifies the concentration, above which an oil-soluble amphiphile "starts" to solubilize a polar species (e.g. water, acid or a metal-cation). This transition however is not sharp.[13] In ternary and quaternary systems,

some solutes may induce nucleation of micelles, as shown by Dejugant *et al.* in the case of common extractants.[61] Rigorous interpretation of the cmc requires to determine the *LAC*, i.e. the lowest aggregate concentration, as defined by Fontell *et al.*[62] If a neutral solute is extracted, this means that LAC is equal to the cmc. Nucleating charged solutes, such as nitric acid, induce a regime where $LAC < cmc$. It has been shown that some very hydrophilic solutes induce a situation for which $LAC > cmc$, for example HCl and the case of DOEHMDA in iso-octane.[61]

3. Microemulsions – Thermodynamically stable mixtures of water and oil

IUPAC defines a microemulsion as: "a dispersion made of water, oil and surfactant(s) that is isotropic and thermodynamically stable system with dispersed domain diameter varying approximately form $1\,nm - 100\,nm$, usually $10\,nm - 50\,nm$".[63] Thus, we enter the region where water, oil and surfactant are present in one single phase. In contrast to binary systems, the situation is now more complex, considering that not only the concentration of the surfactant can be increased, but also the ratio of water to oil. On one hand, microemulsions can be a dispersion of droplets, if only an insignificant amount of the dispersed solvent is present (either oil in water or water in oil). On the other, if both solvents are present in the same proportion, the system exhibits a bicontinuous sponge-like microstructure. In all three cases, an interfacial surfactant film separates water-rich and oil-rich domains.

3.1) Origin of the thermodynamic stability of microemulsions

The fact that microemulsions are optically transparent is attributed to the small size of the droplets. According to the Abbe-limit, objects with a diameter below $d \sim 200\,nm$ are not able to diffract visible light.[64] With typical sizes of the domains in the range of $10\,nm - 50\,nm$, transparency of microemulsions is therefore a consequence.

The critical parameter for thermodynamic stability is a drastic decrease of the interfacial tension between water and oil and thus the free energy of the interface. Only if the surface

tension can be sufficiently decreased, the gain in entropy by dispersing small fractions of water in oil (or vice versa) can compensate the loss in free energy by creating "more interface".[65] Therefore, the "interface" and the choice of the surfactant and its properties play a crucial role in the microemulsion stability.

3.2) Conditions for formulation of a microemulsion and required additives

The initial definition of microemulsions given by IUPAC is actually very elusive. Only few surfactants are able to solubilize large quantities of water and oil in a thermodynamically stable system without any additional additives (mostly non-ionic and hyper-branched ionic surfactants) and are thus true ternary microemulsions.[66] For most surfactants, the conditions of the systems have to be carefully adapted in order to achieve the ultralow surface tension (typically in the range of $\gamma_{microemulsion} = 10^{0} - 10^{-2}\ mN/m$) that is necessary to solubilize water and oil.

3.2.1)Defining the amphiphilic character of a surfactant

As elucidated, the crucial parameter to form a microemulsion is to lower the surface tension. An important property is the adsorption of surfactants at the interface. The first crucial parameter is the amphiphilicity of a surfactant and its driving force to adsorb at the oil-water interface.[48]

An empiric concept to quantify the preference of a surfactant towards either water or oil was introduced by Griffin.[67] The *Hydrophilic-Lipophilic Balance* (HLB) compares the molar masses of polar and apolar moieties:

$$HLB = 20 \times \left(\frac{M_{hydrophilic}}{M_{lipophilic}}\right) \qquad (vii)$$

where M_i is the molecular mass of the hydrophobic or hydrophilic parts of the surfactant. If the molecular mass of both moieties is equilibrated ($HLB = 10$), the surfactant has no preference and is a good emulsifier. For values below, the surfactant favours the solubilisation in the organic phase and respectively prefers the aqueous phase for values above. Though this concept has its origin for linear ethoxylated NIS, this classification has been adapted for many other surfactants to express their preferred solubility and will also be

done in this work. Other practical concepts, as the ratio *Winsor ratio R,*[68] or the *Phase Inversion Temperature* (PIT) have been developed later.[69]

Additional crucial parameters to point out are "thermodynamic parameters". The pressure and in particular the temperature have a great effect on the solubility of a surfactant. For non-ionic surfactants, increase of temperature decreases the solubility in water, due to dehydration of the head-group. The opposite is observed for ionic surfactants, where the increase in temperature favours solubility in the aqueous phase. This can be explained by the Bjerrum length, which decreases as the temperature is increased (see sub-section 4 for definition).[70]

3.2.2) Additives to further decrease the interfacial tension between water and oil

For the formulation of a microemulsion, high adsorption of a surfactant at the interface is not sufficient. From a historical point of view, Schulman first introduced the term *microemulsion*. He observed a decrease of turbidity for a ternary oil/water/soap system when adding a short-chain alcohol (pentan-1-ol).[71] If only soap is present (carboxylate, anionic surfactant), the interface is too stiff due to the electrostatic attraction and repulsion of the surfactant head-groups at the interface.[72] Addition of short-chain alcohol (as pentan-1-ol in case of Schulman), which has no real preference for neither water nor oil will eventually migrate at the interface. This creates disorder at the interface and thus a decreased interaction between neighboured surfactants. As a result, the fluidity of the interface is increased. The addition of a surface-active additive, which reduces the rigidity of the interfacial film is called *co-surfactant* or *co-solubilizer*.[73] This can be compared to cholesterol, solubilized in the lipid bilayer of eukaryote cells, which increases the fluidity of the film by decreasing the Van der Waals interactions between phospholipids.

Further, the electrostatic interactions between ionic head-groups can be additionally reduced by addition of *electrolytes* into the aqueous phase. The presence of ions screens the electrostatic potential between head-groups and thus the stiffness.

By carefully adjusting the formulation in terms of composition, additives and temperature, the interfacial tension can be decreases to values $\gamma_{oil-water} \leq 10^{-4}\ mN/m$.[74]

3.2.3) Geometrical interpretation of the interface – the packing parameter and curvature

On a nanometer scale, the interface between water and oil is not necessarily flat, but can be curved towards water or oil. A crucial factor for the orientation of the curvature is the geometrical shape of a surfactant.

In 1976, Ninham and co-workers have developed a theoretical approach to quantify the preferred geometry of a surfactant and the linked form of the interface: the *spontaneous packing parameter* p_0.[75] Depending on the length l_c and the volume v_{apolar} of the apolar chain, as well as the area of the head-group a_o, the ratio of the apolar surface $\frac{v_{apolar}}{l_c}$ and the polar surface a_o and defined as:

$$p_0 = \frac{v_{apolar}}{a_o \cdot l_c} \qquad (viii)$$

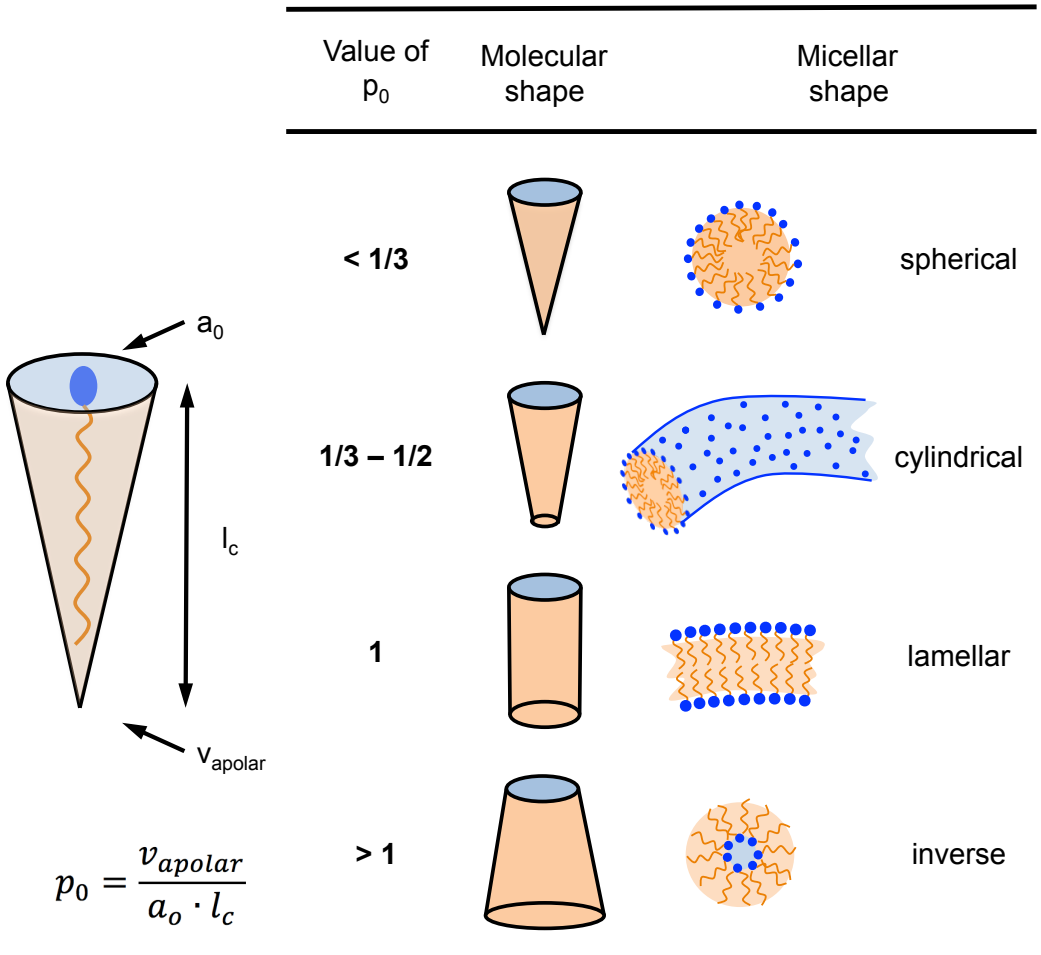

Figure I-10 – Definition of the packing parameter and illustration of the preferred spontaneous geometry. Reproduced from [76].

The spontaneous packing parameter specifies whether a surfactant prefers to curve towards oil (direct), water (reverse) or none (lamellar phases). Figure 10 shows an overview, how the molecular geometry has an impact on the resulting preferred shape. For surfactants with a high effective surface a_o, e.g. ionic surfactants with one aliphatic chain (SDS, cationic) the preferred aggregation is direct. For phospholipids where two aliphatic chains are present, there is no preference of the orientation. Therefore, the shape of the interface is planar. For surfactants with small head-groups and two or more aliphatic chains (e.g. Aerosol OT), the preferred aggregation is reverse.

The spontaneous packing can be linked to the macroscopic *average spontaneous curvature* H_0 of the interface, as illustrated in figure 11. The origin of this concept is actually much older than the packing parameter and has been developed by Gauss in the 19th century and used by Helfrich very thin shells of low curvature.[77]

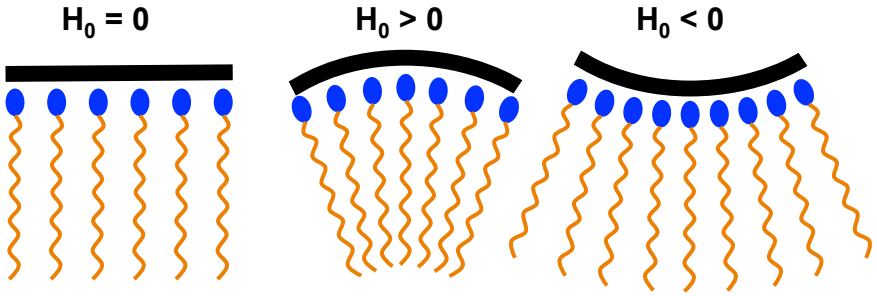

Figure I-11 – Orientation of the spontaneous curvature of an interfacial surfactant film. Redrawn from [78].

The stability of a microemulsion, in particular of the interface can be directly linked to the packing of the interface given by:[79]

$$\Delta G_{Bending} = \frac{1}{2}\kappa^*(p - p_0)^2 \qquad (ix)$$

Where $\Delta G_{Bending}$ is the *free bending energy* of the interface. The actual packing at a certain of water-to-oil ratio is represented by p. The stiffness of the interface is given by the generalized constant κ^*, which is a scalar. The free bending energy represents how much energy is necessary to "bend" the interface. It can be compared to the law of Hook to deform a spring from its natural state. The bigger the difference between the actual packing and the spontaneous packing, the more instable the interface until the system eventually phase separates. This is closely related to the "frustration" of a microemulsion (more detailed in section I-3.3.3).

The mathematical formalism behind the spontaneous curvature is not further introduced since this concept is only used qualitatively, but can be found in the book of S.H. Hyde (see [80]). In the main result chapters, the indication of a negative or positive curvature is associated with the tendency to curve either towards oil or water.

3.2.4)Macroscopic phase behaviour and the Winsor-Phases

So far only monophasic microemulsion systems have been considered. However at low concentration of surfactant (but above the cmc), mixtures of water and oil will separate, though the formulation would allow closing the miscibility gap, if enough surfactant were present. According to the preferred solubility of the surfactant (HLB), a microemulsion can co-exist with a second liquid phase in excess. The different types of phase behaviours have been named by Winsor and are represented in figure 12.[81]

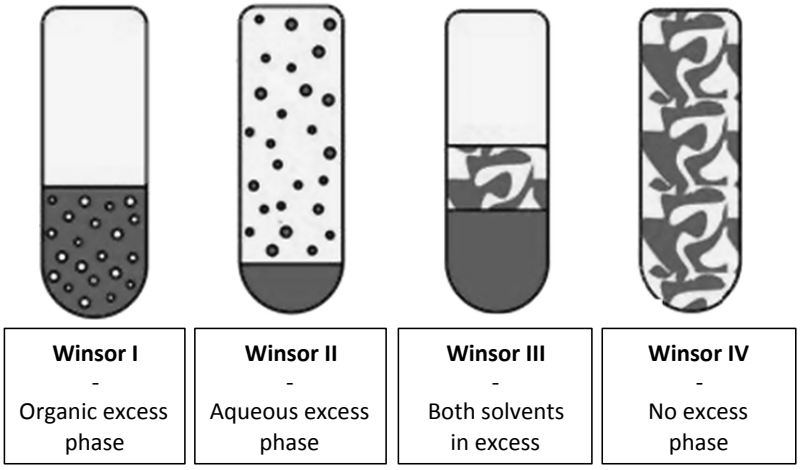

Figure I-12 – The four different types of phase behaviour in microemulsion systems named after Winsor. Ref taken from [82].

The simplest case, where enough surfactant is present to solubilize oil and water is called the *Winsor IV-phase*. The figure suggests that only bicontinuous microemulsions are *Winsor IV-phases*, however this is not a necessity. Monophasic systems with swollen direct micelles in a water-continuous medium or vice versa are also part of the Winsor IV class.

The *Winsor I-phase* is microemulsion in an aqueous-continuous environment and an organic phase in excess. The opposite, a microemulsion in an oil-continuous medium with an aqueous phase in excess is called *Winsor II-phase*. The *Winsor III* case arises, when the surfactant has no preferred solubility towards water or oil – i.e. the interactions of the head-groups with water and the tails with oil are nearly equal ($HLB \sim 10$). As a result, the surfactant as a strong affinity to assemble at the interface, for which water and oil are both necessary. If

the surfactant concentration is too low to cover this interface, excess water and oil are repelled from the microemulsion, thus resulting in two solvent phases in excess.

In the Winsor-nomenclature, the phase separation of a Winsor IV-phase into a Winsor I- or Winsor II-phase is due to a maximum swelling of aggregates. The free bending energy becomes too large to solubilize higher quantities of the dispersed phase. This can be imagined as a balloon, which is inflated by air. The elastic rubber of the balloon tolerates a certain amount of air. Above a critical volume however, the film rips and the balloon explodes. According to this reminder, in Winsor I- and II-phases, every excess molecule of the dispersed phase is expelled and forms a second phase in equilibrium. This phase separation is due to a maximum stress of the interface and is a *phase separation of type I*, as depicted in figure 13.[83] Since the microemulsion is unable to emulsify more volume of the dispersed solvent, in this work we refer to this type of phase separation as an *emulsification failure*. In a type I-phase separated system, the cmc will be in the same phase as the microemulsion.[84] Therefore, in figure 13, a monomer has been drawn in the same phase as the swollen micelles.

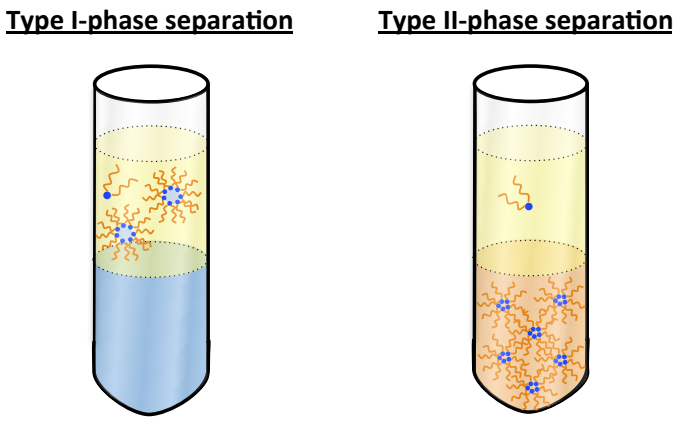

Figure I-13 – Schematic representation of the two types of phase separation. Type I is an *emulsification failure*, where mesoscopic aggregates are unable to solubilize higher quantities of the dispersed solvent. Type II is a *liquid-gas separation* and is a splitting of the organic phase into a "condensed" lower phase, and a gas-like organic phase, only containing negligible amounts of the amphiphile.

In contrast, and in particular reported for inverse systems, there is a second type of phase separation. The expulsion of a solvent is not driven by a maximum swelling, but due to an attraction between reverse micelles. This leads to a splitting of the organic phase. Reverse aggregates form a "condensed phase" in an oil-continuous medium, expelling residual oil into a second phase. A small fraction of the surfactant is solubilized in the excess organic phase, which is roughly around the cmc. The system is thus expelling the exterior medium. This is

the *type II-phase separation* and in this work, we refer to this type of phase separation as a *liquid-gas separation*.[85] Since the microemulsion is in equilibrium with an excess organic phase, we still refer to this solution as a Winsor I-type microemulsion phase, stretching the initial definition.

3.3. Location of the different phases on a map: Introduction in phase diagram analysis

Many different concepts about microemulsions have been discussed concerning their formulation, the interfacial film and different phase behaviours. Yet, what is missing is a big picture. Phase behaviour is typically mapped in phase diagrams, however since microemulsions are multicomponent systems, the visualization is restricted. This is an introduction on how to read ternary phase diagrams and how macroscopic observation can lead to conclusions on a microscopic scale.

3.3.1)How to read phase diagrams

The fundament for a multi-component system and the allowed phase transitions is phase rule of Gibbs[8]:

$$F = C - P + 2 \qquad (x)$$

Where P denotes the number of phases, C the amount of components and F the degrees of freedom.

In a system containing three components, a visual representation of the phase behaviour is presented in a *triangular or ternary phase diagram*. Such a phase diagram denotes the variation of the phase behaviour of a system upon changing the composition. The triangular phase representation is for a fixed temperature and pressure (otherwise an additional axis is required as will be shown later).

The three corners of the isosceles triangle represent the pure components. The sides represent the respective binary mixtures between the three components. The area inside the triangle records the phase behaviour if all three components are present. The relation of a component towards the other two is always given as a fraction. The fraction of each component at a certain composition of the sample can be read according to figure 14(i).

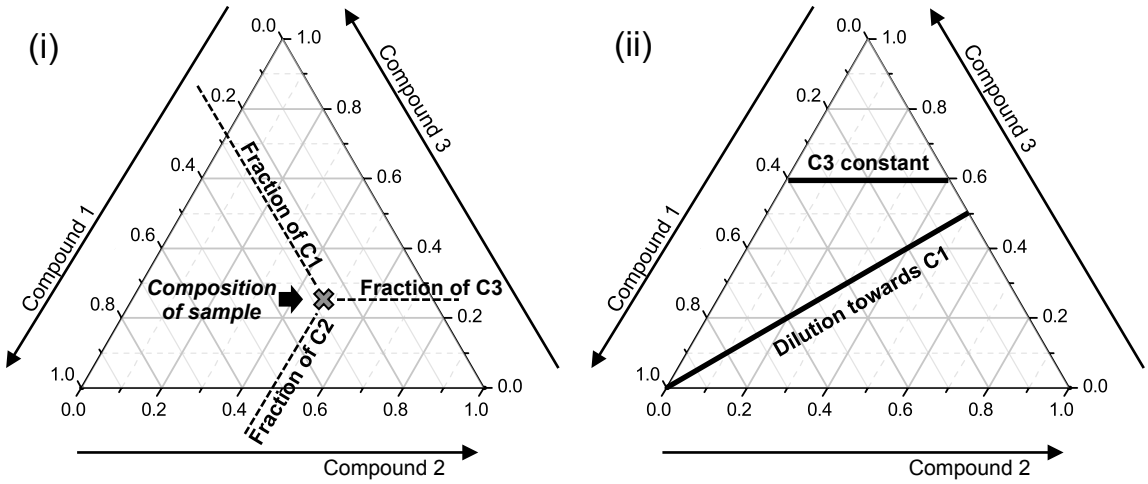

Figure I-14 – How to read a phase diagram. (i) Extracting the composition of a sample with respect to the fraction of each component. (ii) Line towards component 2: the ratio between C1 and C3 is constant; Line parallel to the base: along this line, C3 is constant and the ratio between C1 and C2 varies.

The composition of a sample is normalized. Thus, the fraction of a component is always between 0 and 1. There are three possibilities of normalization: the mole fraction x_i, the mass fraction w_i and the volume fraction ϕ_i.[40]

In figure 14(ii), two paths, which are often used for experimental evaluation, are shown. If for example the concentration of the surfactant is constant and the water-to-oil ratio is modified, the resulting path in the triangle is the one parallel to a base. If a solution is diluted (line towards corner of compound 1), the ratio of the two other components stays constant.

In many cases, the system is multiphasic, with two or more co-existing phases. The boundary between two phases is called *binodal*. If in a biphasic region, the system will separate into two phases, for which the composition is determined by *tie lines*. Along a tie line, the compositions of each phase are unchanged, however the ratio between the phases varies.

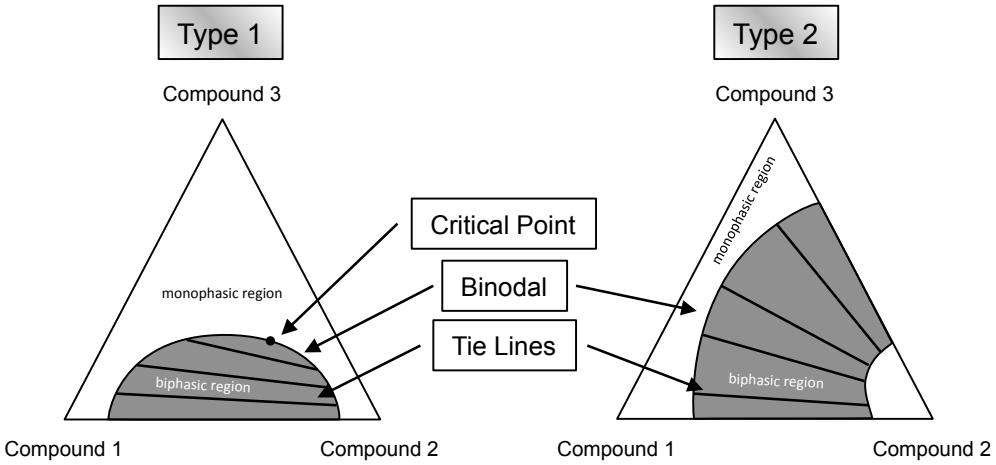

Figure I-15 – Differentiation between phase diagrams with miscibility gaps of type 1 and type 2.

One can distinguish between two types of miscibility gaps: for type 1, component 1 and 2 are immiscible, but both are miscible with the third component. In such systems, a critical point is present (figure 15(i)). For the second type, shown in figure 15(ii), two components are completely miscible, yet partially immiscible with the third.[86]

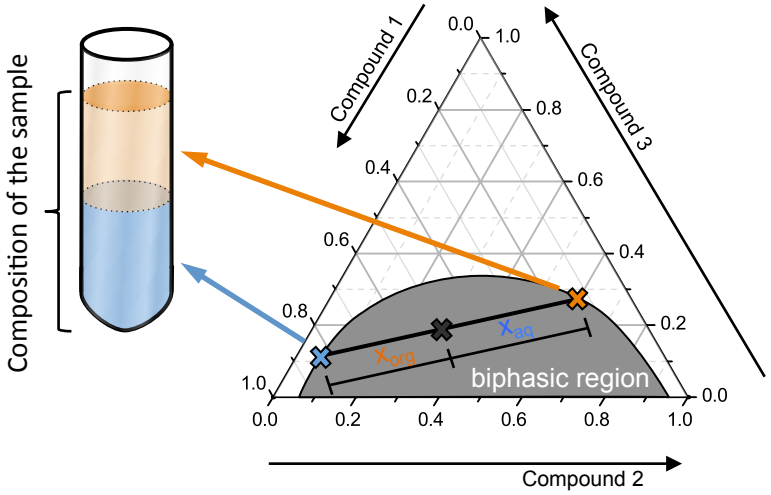

Figure I-16 – Tie line analysis in binary systems. A sample in the biphasic region will separate according to the orientation of the tie line. The compositions of the respective organic and aqueous phase can be deduced from the intersection of the tie line with the binodal. The ratio of the volumes is deduced from the lever rule.

The composition of the two phases can directly be read from the orientation of the tie lines as depicted in figure 16. Considering e.g. the phase diagram in volume fractions, the respective volumes of the two phases can be deduced using the lever rule:

$$\frac{V_{org}}{V_{aq}} = \frac{x_{org}}{x_{aq}} \qquad (xi)$$

Where $x_{org/aq}$ denotes the length of the partial tie line.

3.3.2)Phase diagrams in surfactant science – Ternary representation

In surfactant science, ternary phase diagrams are extremely helpful to trace the macroscopic phase behaviour as function of the composition. A typical example for a non-ionic surfactant, showing the wealth of different microemulsions is shown in figure 17.

The numbers inside the triangle delineate the number of co-existing phases for a giving composition. If two phases are present, the tie lines indicate the composition of the each phase.

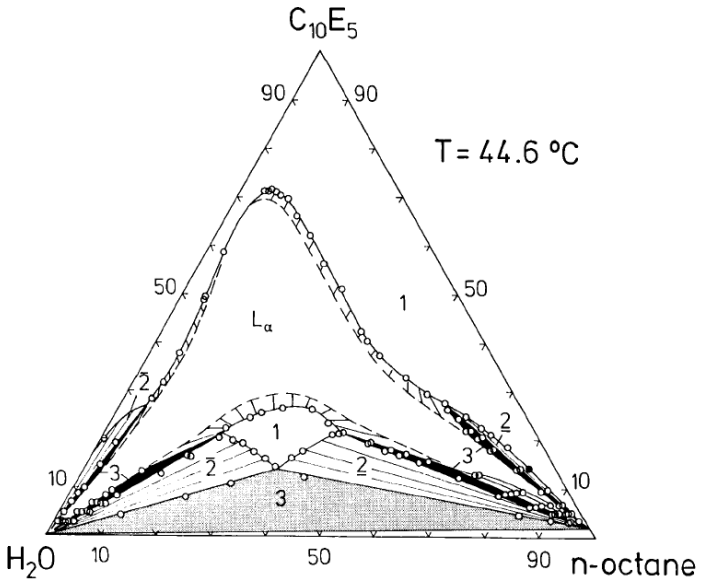

Figure I-17 – Ternary phase diagram of water, octane and a non-ionic surfactant at a fixed temperature of $T = 44.6\,°C$.[87]

For systems where more than three components are necessary to form a microemulsion, the appropriate way to represent the phase behaviour, in compliance with the Gibbs phase rule would be a multidimensional phase diagram. Each corner represents one component (e.g. for a system composed of water, organic solvent, surfactant, co-surfactant and salt, a 5-dimensional phase diagram would be necessary). However, the visualization is extremely complex and therefore a more straightforward approach is the pseudo-ternary representation, where two components are unified in one corner (e.g. water and salt or surfactant and co-surfactant). The ratio of the two components in a "pseudo-component" is fixed (e.g. fixed salt concentration in water, or ratio of surfactant to co-surfactant).

An example of such a pseudo-representation with five components is shown in figure 18.[88]

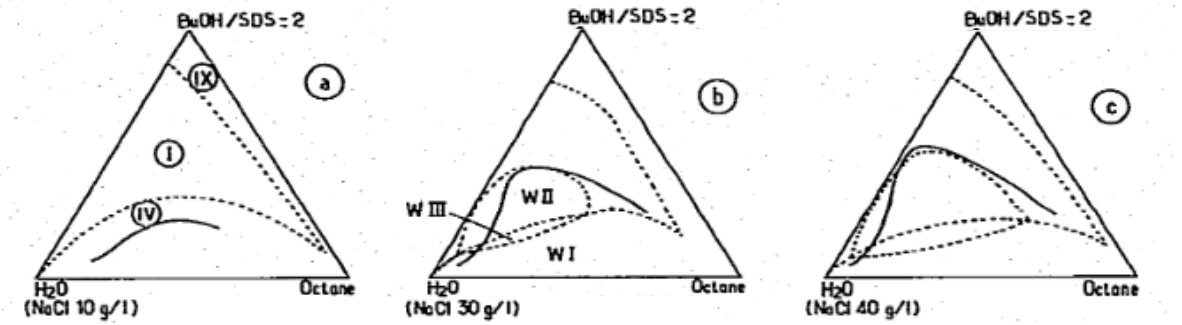

Figure I-18 – Pseudo-ternary phase representations of a 5-component system. The surfactant SDS and butan1-ol as co-surfactant are unified on the top corner; water and NaCl as electrolyte are unified as a common aqueous medium. The influence of the salt concentration on the macroscopic phase behaviour is shown in three different ternary diagrams.

3.3.3)Variation of the temperature – the Gibbs prism and prism analysis

The phase representation in a ternary phase diagram is for one fix temperature. However, as pointed out earlier, the solubility of surfactants is strongly dependent of the temperature of the solution. This affects also geometric constraints of the surfactant, i.e. the packing parameter and hence the curvature of the interface.

This change in solubility strongly affects phase behaviour and thus the topology of a phase diagram. Hence, to illustrate the temperature-dependent changes of the phase diagram an additional axis is required, transforming the two-dimensional representation in a 3-dimensional prism, with the temperature as an “edge” coordinate, as illustrated in figure 19.

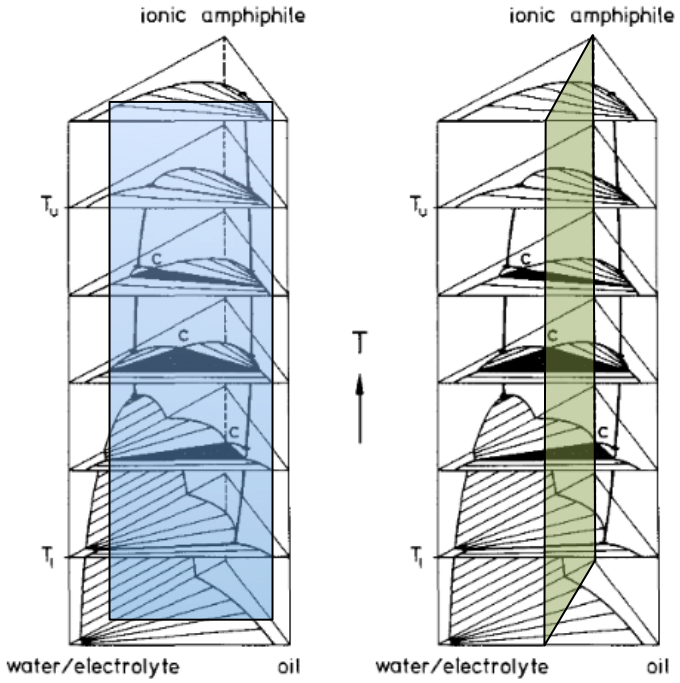

Figure I-19 – Gibbs prism of a quaternary system water + salt, oil and surfactant. Each triangle represents the phase behaviour at a specific temperature. Stacking of the triangles give a prism, for which the temperature-dependent phase behaviour can be analysed.[89] Two sections are shown, to represent the 3-dimensional in a more visual 2-dimensional phase diagram. The section in blue is a cut at a constant surfactant-concentration, in green at a fixed ratio of aqueous to organic solvent.

In his review, Kahlweit et al. summarized the most straight-forward way to analyse the phase behaviour, by first establishing a Gibbs prism, as shown in figure 19.[90] He defined three variables, for which any composition of the prism can be defined. Since all phase diagrams in this work are prepared in mass fractions, these variables are normalized with respect to the mass:

- The temperature T, to give the position on the Z-axis

- The surfactant mass fraction $\gamma_{surfactant}$:

$$\gamma_{surfactant} = \frac{m_{surfactant}}{m_{surfactant} + m_{aqueous\ solvent} + m_{organic\ solvent}} \quad (xii)$$

Where the m_i is the mass of each (pseudo-)component.

- The ratio of organic to aqueous solvent $\alpha_{solvent}$:

$$\alpha_{solvent} = \frac{m_{organic\ solvent}}{m_{aqueous\ solvent} + m_{organic\ solvent}} \quad (xiii)$$

The normalization of this ratio is with respect to the organic solvent. A value of $\alpha_{solvent} = 0$ indicates that no organic solvent is present. For $\alpha_{solvent} = 1$, no water is present.

According to these three variables, three different types of sections can be established in order to represent the phase behaviour in a more visual manner. The first one, which was already introduced, is at a fixed temperature: the ternary phase representation. Additionally, two representations have been established to visualize the effect of the temperature, by fixing one of the two remaining variables.

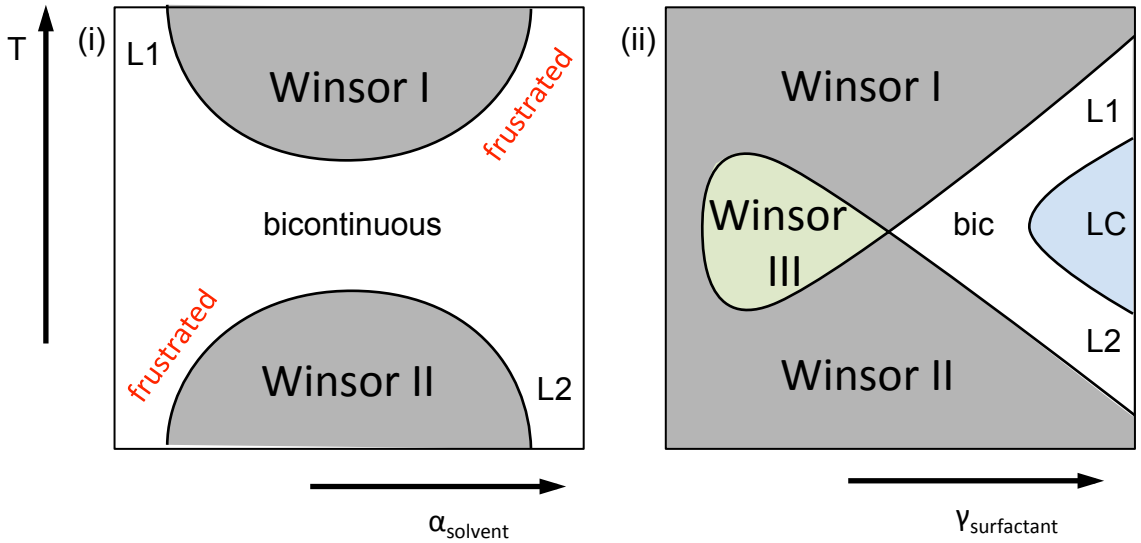

Figure I-20 – Cut-analysis of a Gibbs prism: schematic representation of a (i) χ-diagram and (ii) Fish-diagram for an ionic surfactant. The white areas are monophasic. The grey areas show two liquid phases in equilibrium. The green area indicates where three phases are in equilibrium and the blue phase shows the presence of liquid crystalline phases.

The first established representation was the *fish-diagram* or "Shinoda-Whale", due to the oddly shaped fish (see figure 20(ii)). It is a section of the prism at a constant solvent-to-water ratio, as depicted in figure 19 (green surface). The head is formed by a Winsor III-phase as and the tail is represented by a monophasic Winsor IV regime.[91]

The temperature for which the least amount of surfactant is necessary to form a monophasic microemulsion is called phase inversion temperature (PIT).[69] At this temperature, the

monophasic region is bicontinuous, as the surfactant has no preferred solubility towards water or oil, i.e. it has a value of $HLB = 10$. The microemulsion will therefore be bicontinuous. Below this temperature, ionic surfactants will prefer to solubilize in oil, therefore the structure on a microscopic scale will be reverse swollen droplets. If the solubility limit is reached, excess water is expelled from the system, forming a Winsor II-equilibrium (microemulsion with aqueous phase in excess). Above the PIT, the surfactant will prefer to solubilize in the aqueous phase, thus forming direct swollen micelles. If too much oil is present, it will phase separate, thus forming a Winsor I-phase. For non-ionic surfactants, this phase behaviour is inverted: By increasing the temperature, the surfactant is less water-soluble, therefore the Winsor II-phase is observed above the PIT and the Winsor I-phase below.

The second prism-section is the so-called χ-plot and has its name from the X-shaped monophasic region (from the Greek letter χ, as depicted in figure 20(i)). This representation is a section at a constant surfactant weight fraction, as indicated by the blue area in figure 19. The section is usually taken at a surfactant concentration just above the maximum solubility, which can be obtained from the fish-cut.

This representation allows the analysis of the so-called *frustrated-regimes*. As introduced earlier, the spontaneous packing parameter p_0 gives the preferred orientation of a surfactant at the interface. Therefore, if a surfactant e.g. prefers to curve towards oil, it is favourable that the volume-fraction of oil (i.e. a low $\alpha_{solvent}$) is favourable. This condition is called non-frustrated, since the packing parameter of the microemulsion will be close to the spontaneous packing. According to equation $(viii)$, the free bending energy will be therefore low.

If however the volume-fraction of oil is high, the system surfactant will be forced to curve against its nature. Nevertheless, the system can still form monophasic microemulsions and thus called *frustrated microemulsions*. The microstructure of such microemulsions is mostly very complex. The interface will try to locally compensate the curvature, giving rise to a very diverse morphology.[92]

4. Conductivity in apolar media and microemulsion systems

4.1) On the formation of charged species in liquid media

Chemical compounds with an ionic binding may dissociate into their anions (A) and cations (C) according to the reaction:

$$C_m A_n \leftrightarrow m\, C^{n+} + n\, A^{m-} \qquad (vix)$$

Where m and n is the respective valency of the anion and the cation. The dissociation is generally favoured by entropy and can be expressed by thermal energy:[48]

$$E_{Therm} = k_B T \qquad (vx)$$

With the temperature T and the constant of Boltzmann k_B. In contrast, attractive coulomb interactions antagonize the dissociation process (neglecting here alternative attractive interactions, e.g. Van der Waals).

$$E_{Coul} = \frac{|m \cdot n| \cdot q^2}{4\pi\varepsilon_r\varepsilon_0} \cdot \frac{1}{d} \qquad (vxi)$$

Where d is the distance between two charges, q the elementary charge, ε_0 the permittivity of free space and ε_r the permittivity of the surrounding medium.

By comparing the thermal energy, which is the main driving force for dissociation, with the coulomb-potential between two oppositely charged species, one can define a critical distance, above which two charged species stay separated and is defined as the Bjerrum-length λ_B:

$$\lambda_B = \frac{|m \cdot n| \cdot q^2}{4\pi\varepsilon_r\varepsilon_0 \cdot k_B T} \qquad (vxii)$$

For an electrolyte at a fixed temperature, the main criterion determining the critical distance is the permittivity of a solvent.[93] Table 1 gives a general overview on the Bjerrum-length of a symmetric 1:1 electrolyte in diverse solvents of different permittivity. In water the Bjerrum-length is 0.7 nm, therefore two ions can stay separated, considering that their hydration shell is sufficient to keep the anion and the cation above this critical distance.

In an aliphatic solvent, the two ions must be kept at a distance of $d = 31\ nm$ apart in order to stay as charged species in the medium. As a result, charge formation in apolar in apolar

Table I-1 – Permittivity and corresponding Bjerrum-length in different solvents, considering the valency of the ions: $m = n = 1$.

Solvent	ε_r	λ_B / nm
Water	80	0.7
Aliphatic solvent	1.8	31.1
Aromatic solvent	2.2	25.5
Nitrobenzene	34	1.6
Phenol	4.3	13.0

media is considered as not possible. Nevertheless, as the dissociation is expressed as a reaction (see equation (vix)), Fuoss came to the conclusion that the formation of charged species is a dynamic equilibrium.[94] Thus, if the size of an ion is below the Bjerrum-length, not all ions are associated, but a small fraction of ions can be charged.

4.2) Reverse micelles as charge carriers

Similar to the hydration shell in aqueous media, reverse micelles can be considered as containers, artificially increasing the distance between two charged species in a solvent of low permittivity.[95] With a typical diameter of $d = 2 - 5\ nm$,[96] the Bjerrum-length cannot be bridged completely to obtain fully charged micelles, yet the larger the radius of a reverse micelle, the higher charged fraction. In contrast to the dissociation mechanism as proposed above, the charging mechanism of reverse micelles M, is described by a disproportion:[97]

$$M + M \leftrightarrow M^+ + M^- \qquad (xviii)$$

Upon collision of two neutrally charged micelles, they will separate as one positively and one negatively charged aggregate. Measuring the conductivity, Weitz *et al.* was able to detect a linear increase of the conductivity signal as he increased the concentration of AOT in dodecane. The conductivity was significantly higher than in pure organic solutions (5 orders of magnitudes), therefore attributing the conduction to the formation of charged aggregates. From the linear development, he was able to deduce that 1.2 of 10000 micelles are charged. This was later confirmed by Schmidt *et al.,* who determined that the same phenomenon is observed for lecithin and aluminum(III)-3,5 diisopropyl salicylate.[98]

The group of F. Beunis developed a relatively new method called *Transient Current Measurements (TCM)* (earliest reports in 2008).[99,100] It enables to determine the fraction of charged micelles, as well as the generation rate, the mobility and hydrodynamic radii of charged micelles and confirms the previous findings of Weitz.[101]

4.3) Models to explain the conductivity in reverse (swollen) micellar solutions

As defined in section 2.2.3, consistent definition of a transition between a *true* binary reverse micellar solution and a transition towards a ternary microemulsion is difficult. Depending on the volume fraction of water dispersed inside the reverse micelles, different models have been developed. One variable of particular importance is therefore the ratio of surfactant to water which is expressed by the value W_0 (also w_0 and ω, depending on the literature):[102]

$$W_0 = \frac{n_{Water}}{n_{Surfactant}} \qquad (xix)$$

Where n_i is the number of molecules of component i.
Depending on the water-content W_0, several models have been proposed by Eicke:

- **Model for low W_0 and low concentrations of surfactant:**[103] This model gives the theoretic equivalent conductivity of dilute reverse micelles and predicts how the equivalent conductivity evolves with increasing water content.

- **The Charge-Fluctuation model for intermediate amounts of dispersed water:**[104] This model assumes reverse swollen micelles with free water in their core as electrically neutral, however it attributes a dynamic charge due to fluctuations, i.e. temporary coalescence and exchange of material. It allows to correctly predicting the conductivity in regimes where the size of reverse microemulsions is above 3 nm.

4.4) Transition from discrete reverse micelles to bicontinuous microemulsions: percolation

As introduced in section 3, microemulsion are thermodynamically stable dispersions of water and oil. One of the crucial parameter is the ratio of water to oil and therefore the preferred structure on a molecular scale. The transition from discrete reverse spheres to coalescing droplets and therefore a bicontinuous structure can be described by the mathematical model of percolation.[105]

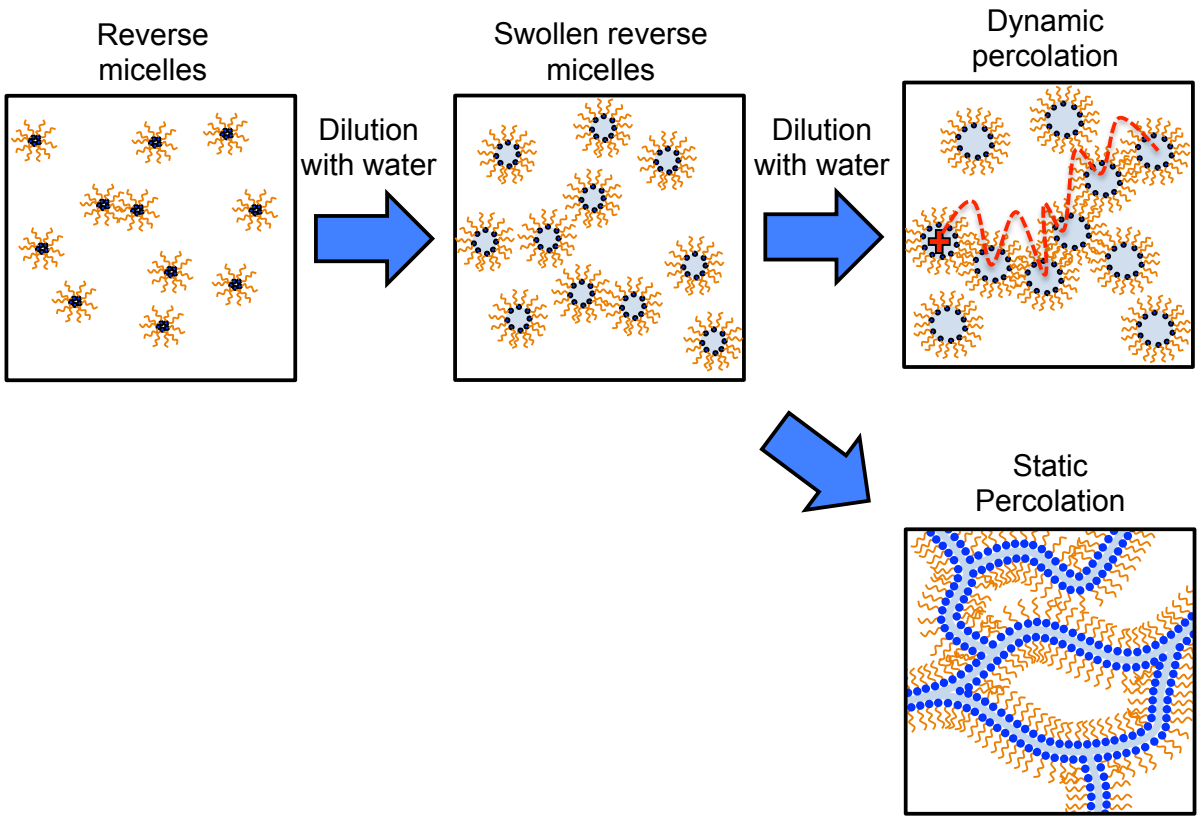

Figure I-21 – Schematic representation of a percolation phenomenon upon dilution. Increase of the volume fraction of the dispersed phase, in this case water for an inverse system, leads to a swelling of aggregates. Beyond a critical volume fraction of the dispersed phase, the system is percolating. Here, it can be differed between two distinct cases: (i) dynamic percolation, where the aggregates are still discrete, however due to reversible coalescence, charge carriers can hop from micelle to micelle. (ii) Static percolation, where the aggregates coalesce irreversibly to form continuous water-channels in which charge carriers can freely move.

Experimentally, the threshold upon which a reverse microemulsion transforms into a bicontinuous microstructure can be determined by conductivity measurements. As depicted in figure 21, addition of water to a reverse micellar solution, provided the interface is flexible, leads to a successive swelling of the aggregates. Above a critical volume fraction of water, the measured conductivity starts to increase significantly, since an ion can freely migrate in the water-continuous regime as the systems coalesce into a bicontinuous microemulsion.[106] However, if the speed of migration of an ion is smaller than the fluctuation rate of two reverse micelles. This results in a “hopping” of a charged species in a seemingly continuous environment, though the water-pools are not yet continuous. That is the so-called dynamic percolation.[107]

5. Conclusion

This chapter gives an introduction in solvent extraction as a separation method and the interpretation of such systems as extracting microemulsions. The fundamental driving forces in surfactant science, that drive amphiphilic molecules into self-assembly and higher-ordered structures are explained. The thermodynamically stable emulsification of water and oil is presented, that is the subject of microemulsions. Further, it gives an introduction in how to read and interpret ternary phase diagrams in surfactant science and the evolution of the phase behaviour vs. an external coordinate. At last, the formation of charged entities in apolar media is reviewed, with a focus on reverse micellar systems. In conclusion, this chapter gives the necessary tools and fundamental concepts to guide through this work.

Chapter II

Exploring stability domains in metal-extracting microemulsions

1. THE MACROSCOPIC PHASE BEHAVIOUR IN METAL-EXTRACTING MICROEMULSIONS 47

1.1) FORMULATION OF A SOLVENT EXTRACTION SYSTEM, ADAPTIVE FOR METALS 47

1.2) DEFINITION OF A "REFERENCE MODEL" 51

2. THE "REFERENCE" SOLVENT TOLUENE 56

2.1) THE TWO FACES OF THE PRISM 56

2.1.1) The bottom face of the prism – The ternary phase diagram of toluene/HDEHP/water 56

2.1.2) The top face of the prism – The ternary phase diagram of toluene/NaDEHP/water 57

2.1.3) Comparison of the two faces 60

3.1) IMPACT OF THE COUNTER-ION VARIATION Z ON THE MACROSCOPIC PHASE BEHAVIOUR – CONSTRUCTION OF A QUATERNARY PHASE PRISM 61

3.2.1) Observations along the prism 61

3.2.2) Evaluation of the macroscopic phase behaviour along the prism 66

3.2) EVIDENCE OF CO-SOLUBILITY 67

3.3) EVIDENCE OF FRUSTRATION 69

3.4.1) Horizontal cut of the prism: The "X-cut" 69

3.4.2) Vertical cut through the prism: the "Fish-cut" 71

3.4.3) Interpretation of the cut-representations 73

3.4) OFF-PLANE TIE LINES IN A QUATERNARY SYSTEM 77

3.4.1) Distribution of the extractant between the aqueous and the organic phase 77

3.4.2) Correlation of the distribution ratio with structuring and dissociation 79

4. VARIATION OF SOLVENTS 83

4.1) THE "THETA SOLVENT" – ISO-OCTANE 84

4.1.1) The two faces of the prism – Z = 0 and Z = 1 84

4.1.2) Impact of the counter-ion ratio on the development of the phase diagrams 85

4.2) PHASE BEHAVIOUR WITH A POORLY PENETRATING SOLVENT – N-DODECANE 88

4.2.1) The two faces of the prism – Z = 0 and Z = 1 88

4.2.2) Impact of the counter-ion ratio on the development of the phase diagrams 89

4.3) EFFECT OF HIGH POLARITY – NITROBENZENE 92

4.3.1) The two faces of the prism – Z = 0 and Z = 1 92

4.3.2) Impact of the counter-ion ratio on the development of the phase diagrams 93

4.4) COMPARING THE MACROSCOPIC PHASE BEHAVIOUR AS A FUNCTION OF THE SOLVENT ... 95

5. CONCLUSION 97

The macroscopic phase behaviour in metal-extracting microemulsions

1.1) Formulation of a solvent extraction system, adaptive for metals

Rare earth elements (REEs) find an ubiquitous implementation in a large variety of modern electronic devices. In permanent magnets (most common: NdFeB-magnets), which are used in wind power plants, minor additions of Dysprosium significantly increases the thermo-stability of the magnet against demagnetization.[108] Such magnets are further found in hard drive disks (HDDs), electrical bikes, hybrid cars, relays and switches and many other applications.[109] In Nickel-metal hydride batteries, an alloy containing Lanthanum allows to store considerable amounts of hydrogen, thus making the technology of cars running on hydrogen-fuel a graspable alternative.[110] Europium is found in old cathode ray tubes (CRTs), which in return is now needed in LCD, LED and plasma televisions.[111]

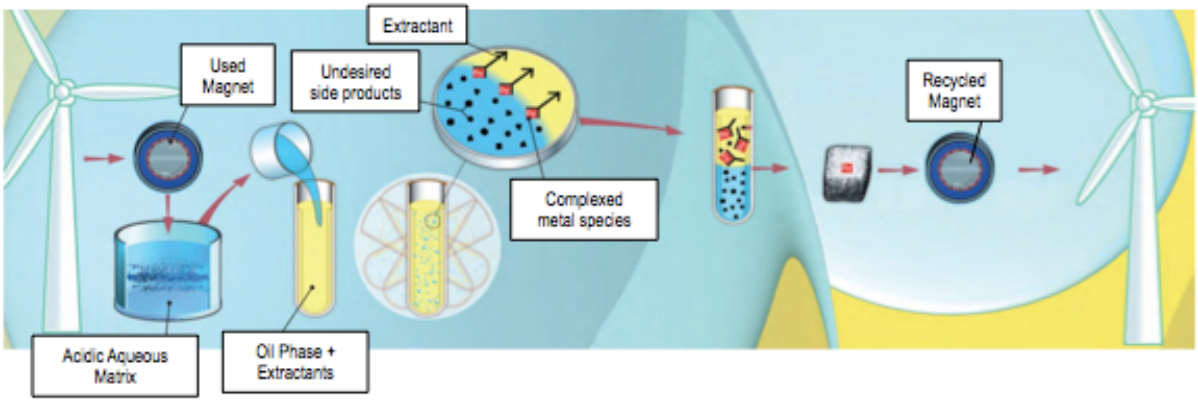

Figure II-1 – Life cycle of a permanent magnet used in a wind turbine, highlighting the role of solvent extraction as separation procedure.

Every of the abovementioned applications have a so-called *life cycle*, after which its use is fulfilled and it has to be replaced. This results in an enormous amount of waste containing precious rare earths.[112] The most versatile and straightforward recycling-process is hydrometallurgy, with solvent extraction as the key separation process). It is also the main route to retrieve rare earths from mineral ores. A major problem to recycle REEs from end-of-life-devices is the complex composition of the aqueous matrix after leeching. Due to the ubiquitous application, composition of the aqueous feed is never consistent and carries a divers number of by-products. A crucial factor is thus the origin of electronic wastes (the aqueous matrix is significantly different when dissolving either a permanent magnet or old HDDs). As a consequence, formulation of an adaptive and efficient solvent extraction process has proven to be highly complex. On a laboratory scale, selective transfer of specific rare earths could be successfully performed for a wide variety of rare earths, but adaption on

a large scale has yet not imposed as an economically favourable process.[113] The core target of the ERC-project *REEcycle* is therefore to make seemingly renewable energy from wind power plants actually renewable.[i]

A chemical engineer on the other hand has several crucial requirements on the formulation of a solvent extraction system, in order to apply it on a large industrial scale.[6] Apart from economic and ecologic aspects, a system needs to be efficient and selective, i.e. a distribution ratio $D_{REE} > 1$ as well as a separation factor $S_{REE} > 1$. Further, kinetic factors play an important role: on one hand, the transfer shall be fast, therefore a high contact area between water and oil is favourable. Thus, addition of surfactants to decrease the surface tension is a common approach. On the other hand, the separation of the aqueous phase from the organic phase must be fast.[114] Therefore, modifiers are added, which adjust the viscosity and density of the phases and thus the phase separation.

As a consequence, solvent extraction systems, as used in an industrial process, are composed of at least six essential components (water, electrolyte, acid, extractant, organic diluent and a modifier). Identification of an "optimum formulation", for which all abovementioned parameters apply is rarely predicted, but "identified by trial": Successive screening of the extraction behaviour by changing one variable while, fixing the ratio of the other components.[10] If an extractant has been identified to exhibit a favourable extraction towards a desired ion (i.e. a high distribution ratio), a quantitative extraction is obtained by drastically increasing the extractant concentration in the organic phase.

However, formulators encounter different problems when increasing the number of complexes in the organic phase. It is often observed, that the viscosity of the organic phase drastically increases, which is unfavourable for the continuous flow sheet.[115] Also, the formation of liquid crystalline phases or emulsification, and thus long separation times need to be avoided.[35] A drastic problem, in particular encountered in solvent extraction processes of actinides in the frame nuclear fuel reprocessing, is the formation of a third phase.[116] Using a colloidal approach by interpreting the metal-extractant-complexes as reverse micelles, the origin of this third phase has been identified as a splitting of the organic phase into two phases: Attractive Van der Waals interactions between polar cores of reverse micelles leads to the formation of a heavy "condensed" phase, expelling a light organic phase.[117]

[i] http://www.icsm.fr/erc.html
http://reecycle-erc.blogspot.fr/

In view of these constraints, plotting the phase behaviour in a phase diagram is a convenient approach to have a general overview of the system. In figure 2, a schematic representation of the ternary phase diagrams and the respective macroscopic observation in a test tube is illustrated. Due to the immiscibility of the aqueous and the organic phase, the regime where two phases are observed is very large. Further, since water should be ejected from the organic phase, the tie lines point towards pure water. In order to obtain an equal volume of the two phases and according to the lever rule, the tie lines must be cut at half the length, which is represented by the red line. Upon increase of the extractant concentration, the concentration of a desired ion decreases in the aqueous phase. This is represented by an increasing amount of reverse micelles in the organic phase, which selectively extract the red ion.

In figure 2(ii), the presence of a third phase due to splitting of the organic phase is illustrated. The green star represents the “optimum formulation”, for which the system is able to extract the highest amount of the desired ion. If the extractant concentration is increased, the organic phase will succumb to a third-phase formation.

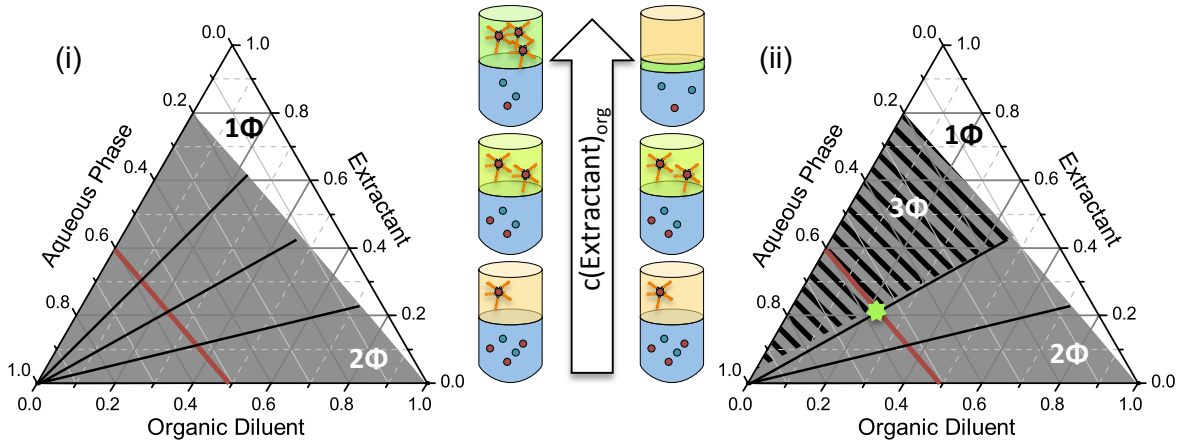

Figure II-2 – Schematic phase behaviour of a solvent extraction system expressed in a ternary diagram (in vol%). The grey and white areas denote the biphasic and monophasic areas. The striped area in (ii) shows a region where a splitting of the organic phase is observed. The red line indicates the compositions for which the volumes of the aqueous and organic phases are equal. The black lines show the tie lines. The test tubes with two phases represent the compositions in the diagrams, where the tie lines cross the red line.

Though a very clear direct method to demonstrate the phase behaviour, ternary phase diagrams are very complicated to obtain due to the high amount of components. Empiric studies on the phase behaviour are therefore scarce in literature. Predictive variation of the phase behaviour upon changing the concentration of one component is not available and thus also part of the “identification by trial” approach.

In the frame to predict the occurrence of the third phase, Bauer *et al.* evaluated the phase behaviour of the extraction system TBP-water-oil-acid-uranium nitrate.[18] Using a quaternary tetrahedron (components occupying the corners: water, extractant, solvent and electrolytes) she mapped the occurrence of the third phase reverting to a cut-analysis as introduced in the fundamental section. This allowed pointing out a qualitative trend, where the splitting of the organic phase can be encircled in a fish-cut. She deduced, that the main two factors for the occurrence of the third phase are the concentration of extractant in the organic phase and the amount of extracted ion.

To the best of our knowledge, Paatero *et al.* presented one of the few complete ternary phase diagrams known in literature for an extractant, as depicted in figure 3.[118,119] Using Cyanex 272 (bis(2,4,4-trimethylpentyl) phosphinic acid) as an extractant, he demonstrated the evolution of the phase behaviour as a function of the pH. The maximum of the three-phase regime shifts from the water-rich side at low concentrations of NaOH towards the

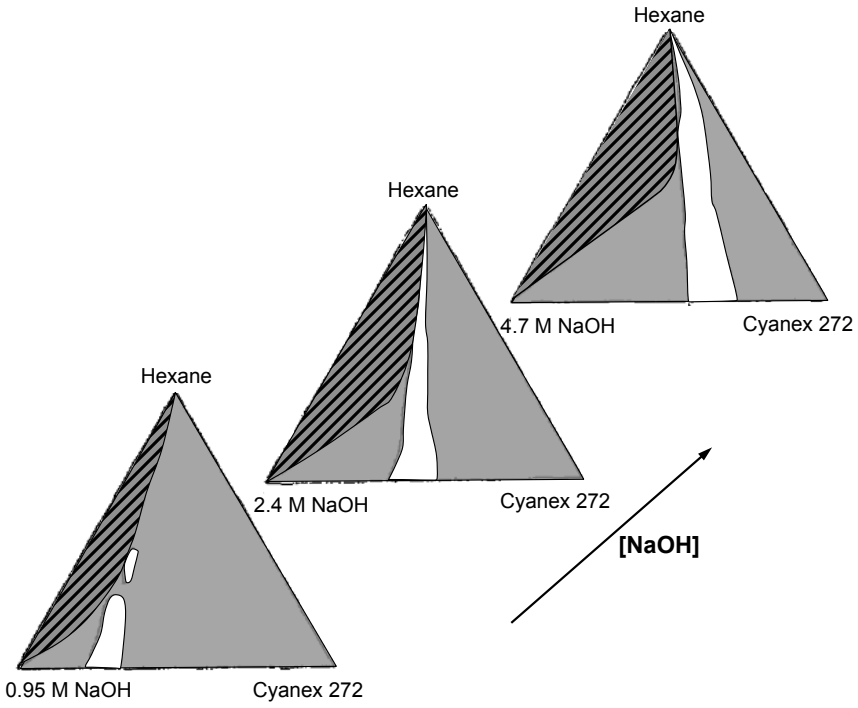

Figure II-3 – Pseudo-ternary phase diagrams of hexane/Cyanex/water + NaOH for different contents of NaOH in the aqueous solution. Monophasic regions are presented in white, biphasic domains in grey and regions where the system separates into three co-existing phases.[118]

hexane-rich side for high contents of the base in water. Additionally, The monophasic region observed on the water-rich side forms a continuous channel to the oil-rich side as the acidity is decreased.

As a result of the poorly available information on the phase behaviour in extracting microemulsions, the motivation for this work is a fundamental analysis in order to elucidate the phase behaviour as a function of well-chosen variables. The target is to give a predictive model for the phase development in solvent extraction.

1.2) Definition of a "reference model"

Due to the high amount of different components, the formulation of a solvent extraction system on an industrial scale very complex. Therefore, we define a "reference model", based components typically used in solvent extraction in order to elucidate the phase behaviour of a facilitated system. The two crucial variables, as defined by Bauer, is the concentration of extractant in the organic phase and the amount of extracted cations.[120]

In order to control the concentration of "extracted ion" in the organic phase, we revert to the model introduced by Paatero:[19,118,119] by neutralization of an acidic extractant with a strong base ensures a replacement of the proton by a cation. Therefore, a fixed ratio of the counter-ion Z^* can be defined as:

$$Z^* = \frac{n_{Extracted\ ion}}{n_{Proton} + n_{Extracted\ ion}} \qquad (i)$$

Where n_i defines the molecular amount of the extractant in either its protonated or complexed form. It can therefore be considered as a measure for the efficacy of an extraction.

As an extractant of choice, we elect bis(2-ethylhexyl) phosphorus acid (HDEHP, also DEHPA), which is represented in figure I-5 (fundamental). It is one of the most studied extractants in literature, namely due to its versatile extraction properties, as it extracts a very broad range of metals by exchanging its proton for a cation (extraction mechanism 1). It is of particular use in recycling of rare earths[20] and in nuclear fuel cycle management.[121]
As counter-ion we adopt the procedure of Paatero, using sodium hydroxide as neutralization agent, thus forming NaDEHP (or SDEHP). This may be a limiting factor in terms of imitating an authentic extraction complex, due to the valency (sodium being a mono-valent ion, whereas most heavy metals are multivalent). On the other hand, the sodium form of HDEHP has been extensively analysed in previous studies in terms of its phase behaviour,[122–124] aggregation,[55,59,125] dynamic properties,[126] conductivity[127] and interfacial properties.[128] Additionally, the molecular structure of NaDEHP is very close to the molecular structure of a

benchmark surfactant: Aerosol OT (AOT). Both molecules possess two 2-ethylhexyl chains as depicted in figure 4.

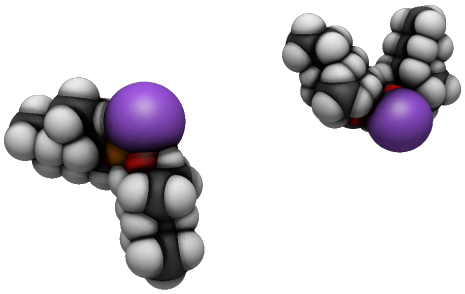

NaDEHP Aerosol OT

Figure II-4 – Molecular structures of NaDEHP and Aerosol OT in a Van der Waals representation.

Due to the branching of the apolar chains, they are classified in the amphiphile-class of hyper-branched surfactants, which are able to form microemulsions without addition of further additives.[129–131]

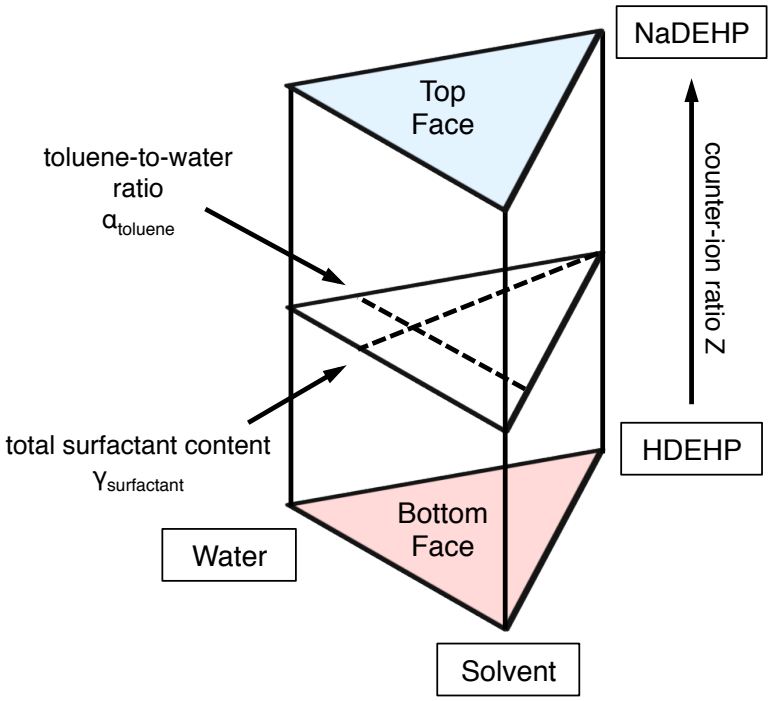

Figure II-5 – Scheme of a quaternary phase prism and introduction of the thermodynamic variable Z. The two faces represent the two limits for which the phase diagrams are true ternary systems. Every point of the prism can therefore be given as a function of the water-to-oil ratio, the extractant/surfactant concentration and the counter-ion ratio.

Completing the set with water and solvent we obtain a system with four essential components representing a solvent extraction system. The appropriate representation would be in form of a quaternary tetrahedron, in order to comply with the rule of Gibbs for phase

diagrams. However, we chose to omit this approach and consolidate the protonated form of the extractant (HDEHP) with the "extracted form" (NaDEHP) to one pseudo-component. This allows drawing a quaternary phase prism with the counter-ion ratio Z as an "edge" coordinate.

$$Z = \frac{w_{NaDEHP}}{w_{NaDEHP} + w_{HDEHP}} \qquad (ii)$$

Where w_i gives the mass fraction of the component i. This nomenclature has been chosen, since all phase diagrams presented are prepared in mass-fractions for the sake of experimental simplicity. Normalisation of Z by the total analytic weight fraction allows defining two limits of the axis:

- $Z = 0$ – The head-group is completely protonated
- $Z = 1$ – The head-group is completely deprotonated

The introduction of this axis and thus representation of the phase diagrams in form of a prism has several advantages. The edge coordinate is normally represented by temperature, as it modifies the spontaneous packing parameter p_0 of a surfactant and thus its solubility in water or oil. In case of the counter-ion ratio Z, modification of the head-group directly affects the effective surface a_0 of the head-group, while the apolar moieties remain unchanged.[75] Further, representation of the development of the phase behaviour in form of a prism allows applying tools known from surfactant systems, in order to better comprehend the macroscopic phase behaviour.[90]

In the treaty on the principles of solvent extraction, published in 2004, the solvents used for liquid-liquid extraction have been classified in five different categories, depending on their property to form hydrogen bonds (an overview is given in table 1).[6] All diluents are placed into the fifth category, as they possess neither donor, nor acceptor moieties. However, the significance of solvent penetration on the packing parameter and for phase stability is not only known in solvent extraction, but has been comprehensively studied for a solvent extraction system.[132] The attraction between metalloamphiphilic complexes can either be reduced by using a highly penetrating solvent (short and branched alkane) or by increasing the chain length of the extractant.

Therefore, we chose four different solvents for which the phase behaviour will be determined:

- **Toluene** – As it is often used in literature for analysis of physico-chemical properties of NaDEHP-systems, we will use toluene as a "reference" solvent. Further, the aromatic nature will allow a comparative study with aliphatic solvents.[59,126,128]
- **Iso-octane** – The molecular shape of this solvent is very close to the molecular structure of the apolar moiety of HDEHP. Therefore, we refer to iso-octane as a "theta solvent" as it highly penetrates the reverse micellar shell.
- **Dodecane** – Due to its long and relatively stiff nature, dodecane has poor penetration properties compared to toluene and iso-octane. It is however often the preferred choice on an industrial scale, since it has a significantly lower vapour pressure.
- **Nitrobenzene** – This molecule has a dipole moment of $\mu = 4.22$ and thus a permittivity of $\varepsilon = 35$. Though very polar, nitrobenzene (Nbz) is completely insoluble with water ($w_{Nbz\ in\ water} = 0.19wt\%$ and $w_{water\ in\ Nbz} = 0.24wt\%$). Given the low Bjerrum-length ($\lambda_B = 1.6\,nm$), this solvent is of particular interest for the second chapter on the formation of charged micelles in apolar media.

Table I-1 – Selected properties of water soluble and insoluble solvents. V is the molecular volume, μ the electric dipole moment, ε the dielectric permittivity and δ the Hildebrandt coefficient. Solvent of significance for this work are highlighted in orange.[6]

Solvent	M g/mol	V^b mL/mol	μ^c D	ε^b	δ $(J/mL)^{1/2}$
c-Hexane	84.2	108.7	0.	2.02	16.8
n-Hexane	86.2	131.6	0.09	1.88	15.0
n-Octane	114.3	163.5	~0	1.95	15.5
n-Decane	142.3	195.9	~0	1.99	15.8
n-Dodecane	170.4	228.6	~0	2.00	16.0
Decalin (mixed isomers)	138.3	157.4	0.	2.15	18.0
Benzene	78.1	89.9	0.	2.27	18.8
Toluene	92.1	106.9	0.31	2.38	18.8
Ethylbenzene	106.2	123.1	0.37	2.40	18.0
p-Xylene	106.2	123.9	0.	2.27	18.1
Dichloromethane	89.9	64.5	1.14	8.93	20.2
Chloroform	119.4	80.7	1.15	4.89	19.5
Carbon tetrachloride	153.8	97.1	0.	2.24	17.6
1,1-Dichloroethane	99.0	84.7	1.82	10.00	18.3
1,2-Dichloroethane	99.0	79.4	1.83	10.36	20.0
Trichloroethylene	131.4	90.7	0.80	3.42	19.0
Chlorobenzene	112.6	102.2	1.69	5.62	19.8
1,2-Dichlorobenzene	147.0	113.1	2.50	9.93	20.5
Carbon disulfide	76.1	60.6	0.	2.64	20.3
Water[a]	**18.0**	**18.1**	**1.85**	**78.36**	**47.9**[d]
Methanol[a]	32.0	40.7	2.87	32.66	29.3
Ethanol[a]	46.1	58.7	1.66	24.55	26.0
1-Propanol[a]	60.1	75.1	3.09	20.45	24.4
2-Propanol[a]	60.1	76.9	1.66	19.92	23.7
1-Butanol	74.1	92.0	1.75	17.51	23.3
Isoamyl alcohol	88.2	109.2	1.82	15.19	22.1
1-Hexanol	102.2	125.2	1.55	13.30	21.8
1-Octanol	130.2	158.4	1.76	10.34	20.9
2-Ethyl-1-hexanol	130.2	157.1	1.74	4.4	19.4
Diethyl ether	74.1	104.7	1.15	4.20	15.4
Diisopropyl ether	102.2	142.3	1.22	3.88	14.6
Bis(2-chloroethyl) ether	143.0	117.9	2.58	21.20	18.8
Acetone[a]	58.1	74.0	2.69	20.56	22.1
Methyl ethyl ketone	72.1	90.2	2.76	18.11	18.7
Methyl isobutyl ketone	100.2	125.8	2.70	13.11	17.2
Cyclohexanone	98.2	104.2	3.08	15.5	19.7
Acetylacetone	100.1	103.0	2.78	25.7	19.5
Ethyl acetate	88.1	98.5	1.78	6.02	18.2
Butyl acetate	116.2	132.5	1.84	5.01	17.6
Propylene carbonate	102.1	85.2	4.94	64.92	21.8
Nitromethane	61.0	54.0	3.56	35.87	25.7
Nitrobenzene	123.1	102.7	4.22	34.78	22.1

2. The "reference" solvent toluene

2.1) The two faces of the prism

To appropriately analyse the phase behaviour of a system containing four components by establishing pseudo-ternary phase diagram, one must first consider the phase behaviour of the respective binary and ternary systems.[89] As shown in figure 5, the prism is limited by two faces. Therefore, analysis of the phase behaviour is first analysed for these two limits, where the system is only composed of three components.

2.1.1)The bottom face of the prism – The ternary phase diagram of toluene/HDEHP/water

In general, phase properties of binary systems are discussed in a diagram where the temperature is plotted as a function of the two components.[133] However, as all measurements were carried out at ambient conditions, this analysis is done directly in the isothermal ternary phase diagram, depicted in figure 6.

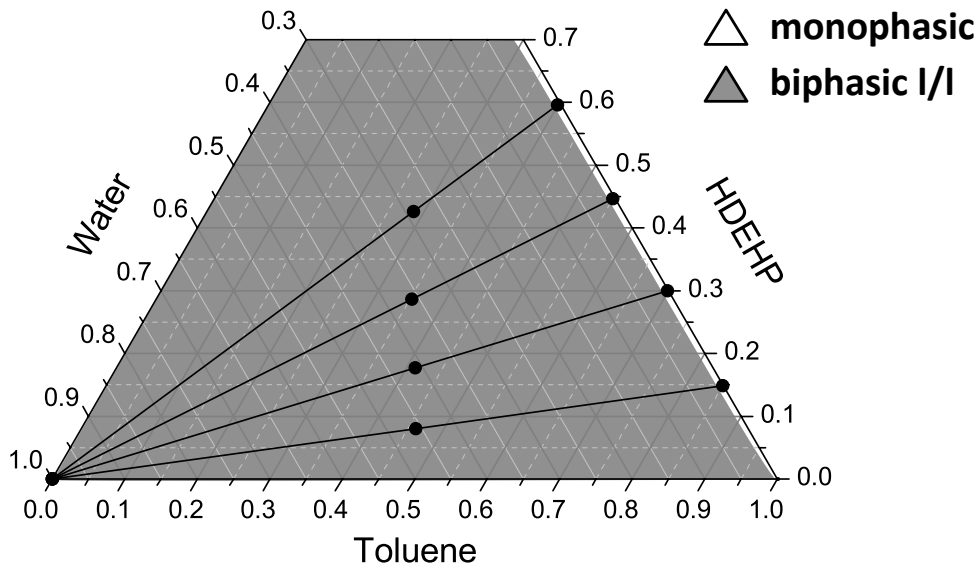

Figure II-6 – Ternary phase diagrams of toluene/HDEHP/water in wt%. The biphasic liquid-liquid domain is represented in grey, the monophasic region in white. The tie lines point towards pure water.

Due to their converse nature of interactions, water and toluene are completely immiscible (water in toluene: $w = 0.0635\ wt\%$; toluene in water: $w = 0.0515\ wt\%$).[134] The same feature can be attributed to the solubility of water and HDEHP. On the other hand, toluene and the extractant show a complete miscibility over the whole concentration range. The solubility

profile of the three binary mixtures can be extended to the ternary regime, where the system exerts a large miscibility gap. This results in a “triangle in a triangle”-morphology, where the whole triangle is a liquid-liquid regime, apart from the small monophasic stripe on the solvent-rich side. Miscibility gaps where two solvents are completely miscible with each other, but immiscible with a third are referred to as type 2.[86] The bad solubility of water in the organic phase is further confirmed by the direction of the tie lines, pointing towards water. The phase boundary runs along a constant W_0-value of $W_0 = 0.15$, therefore only insignificant amounts of water are soluble in the organic phase.

Considering that HDEHP forms small reverse aggregates in a toluene-continuous phase, it is unable to pick up more water. A phase separation where the internal bulk phase is ejected from the system is called *emulsification failure* or phase separation of type I.[135] Hence, the system can be declared as a *Winsor II* microemulsion.[68]

2.1.2)The top face of the prism – The ternary phase diagram of toluene/NaDEHP/water

In figure 7, the macroscopic phase property for $Z = 1$ is shown. NaDEHP is badly miscible in both solvents. In contrast to Aerosol OT, which is completely miscible in apolar solvents,[136] NaDEHP precipitates on the bottom of a tube. In water, gel-like liquid-crystalline phases are observed in the presence of an excess water phase.

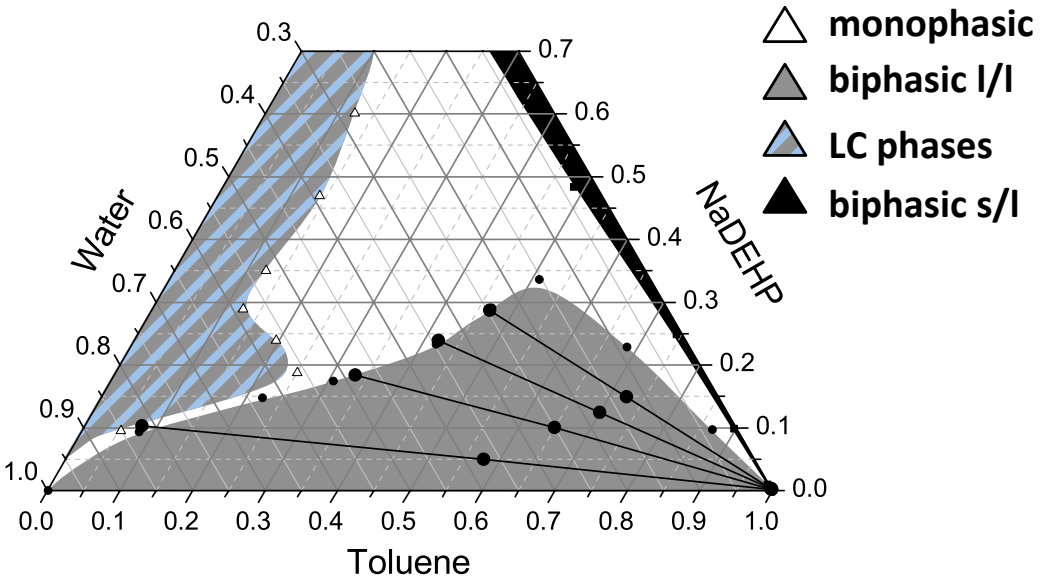

Figure II-7 – Ternary phase diagrams of toluene/NaDEHP/water in wt%. The biphasic liquid-liquid domain is represented in grey, the monophasic region in white, lyotropic mesophases in grey-blue and the biphasic solid-liquid regime in black. The tie lines point towards pure toluene.

All three binary miscibility gaps are closed upon addition of the third component and a large monophasic region is detected in the centre of the phase diagram. On the oil-rich side, the addition of small amounts of water transforms the biphasic solid-liquid phase (black area) into a monophasic transparent solution. The phase boundary runs along a constant value of $W_0 = 1.1$. The liquid-crystalline phase is present for toluene weight-fractions $w_{toluene} < 15wt\%$, with a peak at $w_{NaDEHP} = 21wt\%$.

The miscibility gap of water and toluene is closed upon increase of the surfactant concentration, showing a wedge-like form with a maximum at $w_{NaDEHP} = 30wt\%$. On the toluene-rich side, up to this maximum, the phase boundary runs along a constant water-to-surfactant ratio with a value of $W_0 = 6$. On the water-rich side, the biphasic l/l-regime is separated by the lyotropic phases by a narrow channel. As the direction of the tie lines point towards toluene, NaDEHP prefers to solubilize in water.

The phase behaviour of NaDEHP in the presence of oil and water has been previously reported only twice in literature to our best knowledge. Shioi *et al.* has mainly documented the development of the biphasic region upon introduction of an electrolyte. Hence, only the biphasic domain was analysed by decomposition of the tie lines (see figure 8(ii)).[123] In addition, Yu and Neuman have been pointing out the formation of lyotropic mesophases on the water-rich side.[122] Compared to our findings, no continuous path towards the water-rich corner has been detected. Another aspect, which has not been mentioned, is the "poor" solubility of the surfactant in an apolar solvent. A phase property that has been pointed out by Faure *et al.*, but not documented in a detailed phase diagram.[59]

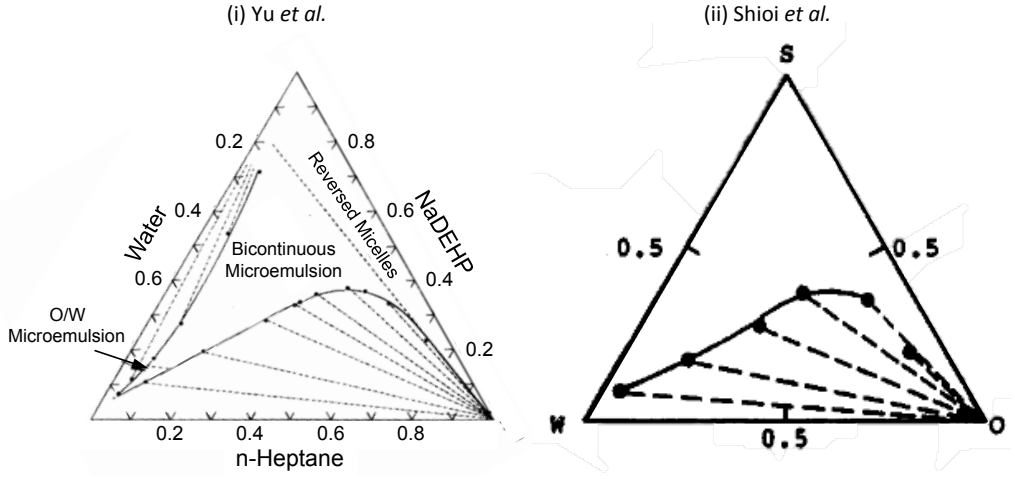

Figure II-8 – Ternary phase diagrams of n-heptane/NaDEHP/water in wt% presented by Yu and Neuman ($T = 20\,°C$)[122] (i) and by Shioi *et al.* ($T = 25\,°C$)[123] (ii).

Besides serving as a map, analysis of the macroscopic phase behaviour can give an insight on the microscopic structures, molecular forces and solubility properties related to the

topology of packing. With sodium as a cation, the DEHP-anion is able closing the miscibility gap water and toluene for any given ratio. Therefore, a continuous monophasic regime spans from the water-rich corner to the toluene-rich one. Due to this solubilization power and the amphiphilic properties of NaDEHP, this monophasic region is declared as a microemulsion, as previously mentioned in [122]. Converse to most commonly known ionic surfactants, no co-surfactant is necessary in order form a microemulsion.[137] The same feature is reported for AOT.[138] The formation of "co-surfactant-free" microemulsions using ionic surfactants is a particular property of so-called "hyper-branched" surfactants.[66,129] Branching of the chain allows significantly increasing the flexibility of the interfacial surfactant-film as well as decreasing the surface tension between water and oil. Therefore, no further additive is required to co-solubilize of water and oil.

As a result of the miscibility gap of type 1, the ternary phase diagram has a critical point that is located on the solvent-rich side (figure 9, red circle).[86] Following the blue dilution line towards water, the system will eject the organic solvent, though water is added. This means, that at low volume fractions of water (composition at red cross) phase separation is *liquid-gas phase separation*.[83] Further addition of water will eventually lead to an inversion of the phase separation type: on the water-rich side, the phase separation is due to an emulsification failure. This is a so-called phase separation of class I.[135] Here the system can correctly be compared to a Winsor I-phase.

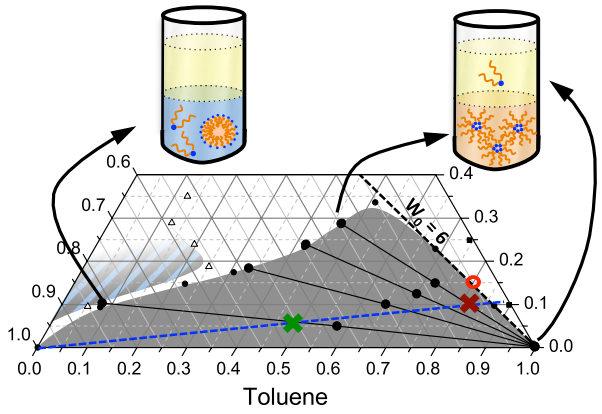

Figure II-9 – Miscibility gap of the ternary system toluene/NaDEHP/water in wt% at 25°C. The tie lines point towards pure oil, resulting in a critical point on the oil-rich side of the phase diagram (red circle). Two compositions (red and green cross) are represented on a dilution line towards water (blue line). The tubes illustrate the different types of phase separations, depending on whether the system is on the water-rich or solvent-rich side. The s/l-regime and most of the lyotropic phases have been omitted for clarity.

The existence of a narrow channel has been described by Fontell for the ternary system of caprylic acid, sodium caprylate, water, where the fatty acid adopts the function of an organic

solvent. This system has been extensively characterized in a set of 11 publications over two decades and is one of the most studied ternary systems known in literature.[62,139–147] The monophasic region in this channel is called an *anomalous liquid phase L3*, identical to what was expressed later as a DOC-lamellae structure for double chain cationic surfactants in the non-penetrating solvent n-tetradecane by Barnes *et al.*[148] X-ray scattering experiments revealed that the swelling by the oil is 1-dimensional,[144] i.e. this peculiar microstructure was the first locally lamellar phase of proven local structure at a mesoscale and was named later on as "sponge"-microemulsion and later as microemulsion with high internal phase (HIPME).[149]

2.1.3)Comparison of the two faces

It can be concluded, that the phase behaviour of HDEHP and NaDEHP with water and toluene are completely opposite. This is highlighted by directly comparing the phase properties that have been summarised in table 2. HDEHP essentially behaves like an organic solvent and exhibits a poor miscibility with water, but has a great co-solubility with toluene. On the other hand, NaDEHP is a surfactant and is able to successfully close the miscibility gap without addition of an additive.

Table II-2 – Consolidation and comparison of phase behaviour for the two ternary systems.

Properties		Z = 0	Z = 1
Miscibility Gap		Type 2	Type 1
Winsor-Phase		Winsor 2	Winsor 1
Phase Separation		Emulsification failure	Liquid-gas separation
Solubility of extractant with:	Water	no	no
	Solvent	yes	no

While the phase separation in the top face is an "emulsification failure", the main instability of the microemulsion in the bottom face is driven by an effective attraction and coalescence between the aggregates, leading to a "liquid-gas separation".

3.1) Impact of the counter-ion variation Z on the macroscopic phase behaviour – Construction of a quaternary phase prism

After thorough classification of the macroscopic phase behaviour of the binary and ternary compositions, many preliminary questions arise regarding the development of the phase behaviour in the pseudo-ternary-regime. As concluded in the previous section, the solubilization properties between HDEHP and NaDEHP are of complete converse nature. Therefore, a primary objective is to identify at which counter-ion ratio Z the phase properties invert and further to elucidate the driving forces that cause this inversion.

3.2.1)Observations along the prism

In total, five phase diagrams in the pseudo ternary regime have been prepared and are depicted in figure 10, alongside the two faces of the prism. An inconvenience of the pseudo-ternary representation is that the initially fixed ratio between the DEHP-derivatives may vary upon entering a multiphasic regime. As a consequence, no tie lines are represented in this section but are reviewed later. In figure 11, the seven phase diagrams have been put together to form the quaternary phase prism.

3.2.1.1) Lyotropic mesophases and impact of HDEHP evolution

For pure NaDEHP, an addition of $w_{toluene} = 15wt\%$ is sufficient to transform the LC-phase in a clear monophasic region, with a wedge-like extension at $\gamma_{\ NaDEHP} = 21wt\%$. For a counter-ion ratio of $Z = 0.9$, depicted in figure 10(vi), the phase triangle exhibits the same wedge-form at $\gamma_{\ NaDEHP} = 20wt\%$, however the area where LCs are found decreases for $\gamma_{\ NaDEHP} > 30wt\%$. The discontinuity from the liquid-liquid domain is still given. This discontinuity is lost for $Z = 0.7$. The pseudo-ternary diagram 10(v) shows that the lyotropic phases are completely embedded inside the grey multiphase domain, for intermediate surfactant concentrations $15wt\% \leq \gamma_{extractant} \leq 40wt\%$. At an equilibrium ratio of NaDEHP and HDEHP ($Z = 0.5$, figure 10(iv)), liquid crystalline phases are solely observed if the content of total extractant exceeds 50wt% and has a dent-like shape with a maximum at $\alpha_{toluene} = 50wt\%$.

To summarize, lyotropic phases have been observed for several ratios of HDEHP to NaDEHP along the prism, but have not been analysed further.

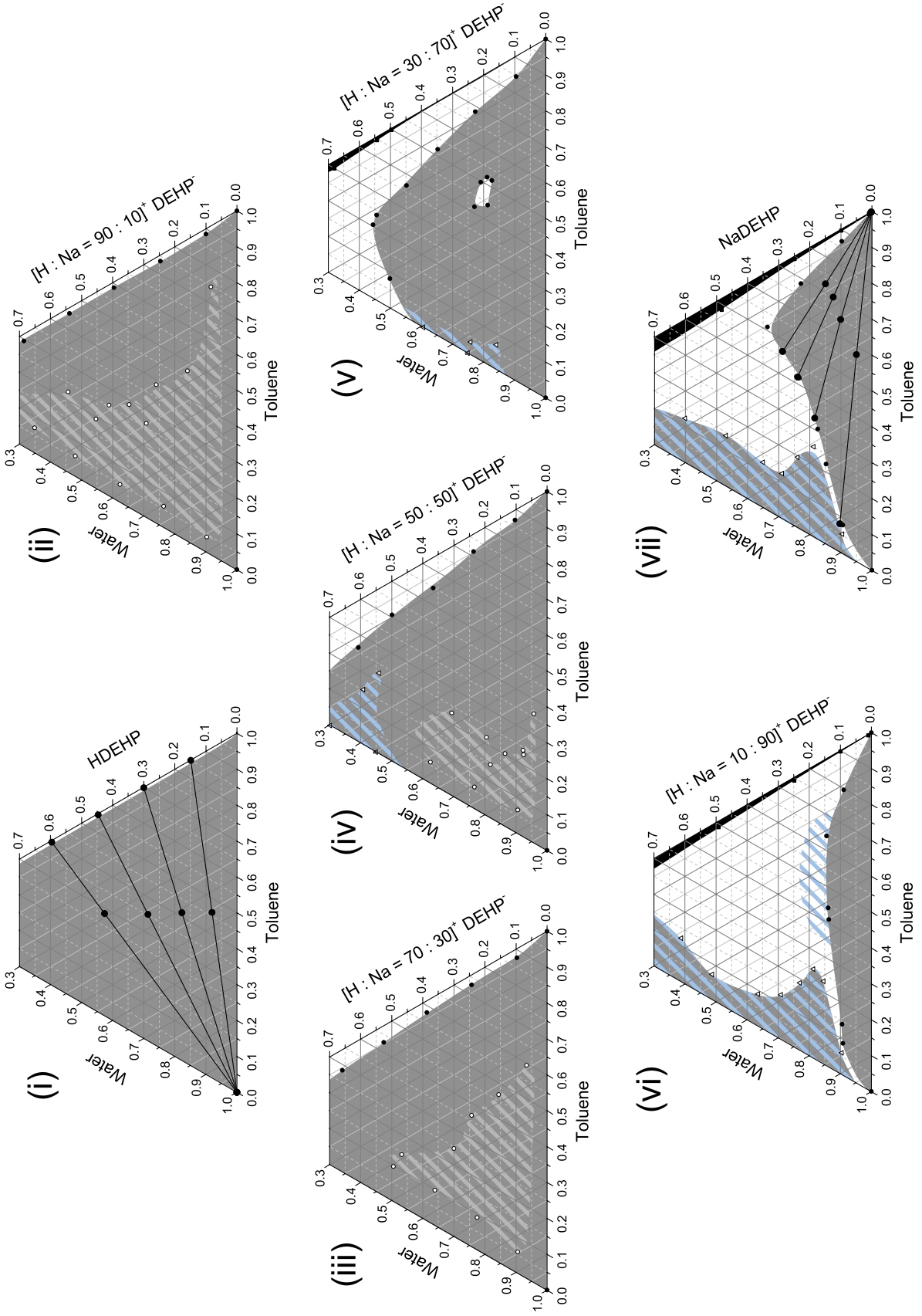

Figure II-10 – Pseudo-ternary phase diagrams of toluene/H-Na-DEHP/water in wt% for different ratios of H to Na. (i) $Z = 0$; (ii) $Z = 0.1$; (iii) $Z = 0.3$; (iv) $Z = 0.5$; (v) $Z = 0.7$; (vi) $Z = 0.9$; (vii) $Z = 1$.

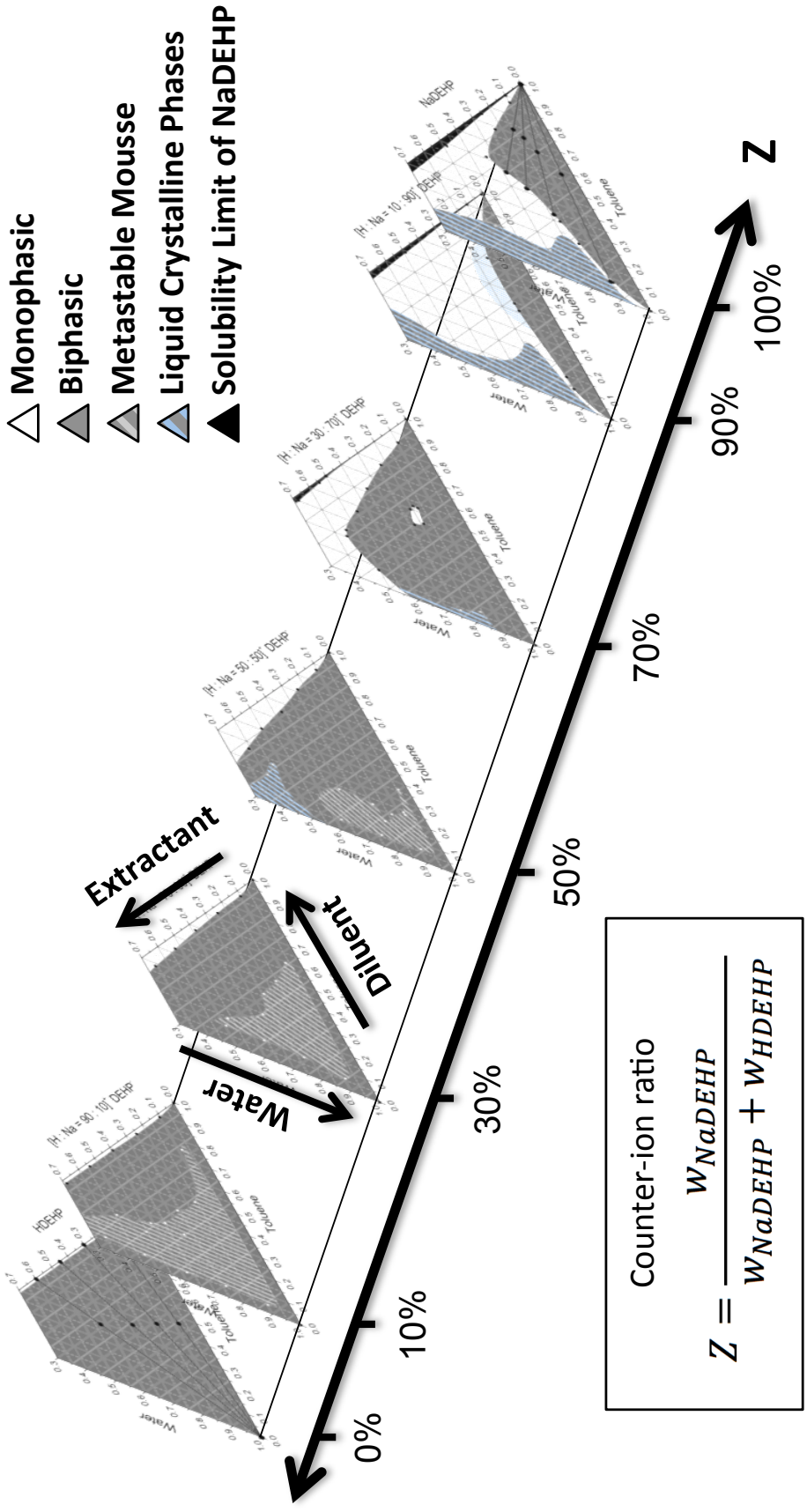

Figure II-11 – Quaternary phase prism of toluene/NaDEHP/HDEHP/water. The Z-axis gives the ratio of NaDEHP with respect to the total amount of extractant. 7 phase diagrams for different Z are plotted, including the two "faces" for $Z = 0$ and $Z = 1$.

3.2.1.2) The progression of the solid-liquid phase boundary

NaDEHP is essentially immiscible with toluene. As a result, a solid-liquid phase emerges near the NaDEHP-toluene base of the ternary phase diagram for $Z = 1$ (figure 10(vii)). Replacing the sodium cation successively by a proton leads to a disappearance of this phase for $Z \leq 0.5$.

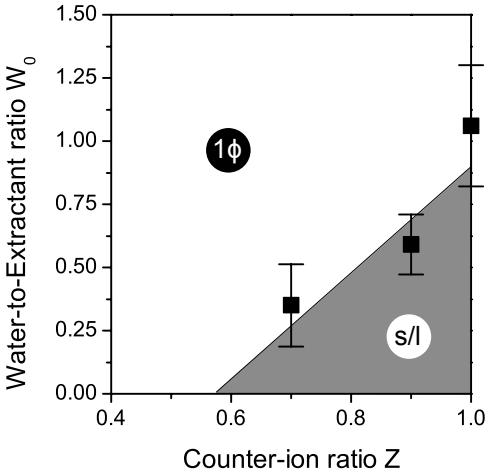

Figure II-12 – Amount of water molecules per molecule NaDEHP necessary in order to observe a phase transition, plotted as a function of Z.

The s/l-phase boundary observed for the diagrams in figure 10(v,vi,vii) run along constant W_0-lines. The phase behaviour is plotted as a function of the counter-ion ratio, defining $W_{0,Na}$ as:

$$W_{0,Na} = \frac{n_{Water}}{n_{NaDEHP}} \qquad (iii)$$

Where n_i is the molar number of component i. In figure 12, this ratio defines the necessary number of water molecules per molecule surfactant, in order to leave the biphasic s/l-regime.

For $Z = 1$, at least 1.1 water molecules per NaDEHP are necessary to form a monophasic, homogeneous solution. This water-to-NaDEHP ratio decreases linearly versus a decreasing counter-ion ratio. Therefore, it can be concluded, HDEHP actively increases the solubility of NaDEHP in toluene, and for $Z < 0.58$, no additional amount of water is necessary to form a homogenous ternary solution of toluene-HDEHP-NaDEHP. This can be confirmed, looking at the phase prism in figure 11 for $Z \leq 0.5$, where no solid-liquid phase was detected on the toluene-rich side.

3.2.1.3) Variation of the liquid-liquid miscibility gap with Z

For the bottom face of the prism ($Z = 0$), the amount of water that can be solubilized before the system separates into two phases is negligibly small. Increasing Z results in an increase of the monophasic region on the oil-rich side, as can be seen in the phase diagrams 13(i)-(v). The phase boundaries in these pseudo-ternary diagrams run along a constant water-to-extractant ratio and the value of W_0 is increasing with increasing Z.

A significant increase of the monophasic region is observed for $Z = 0.9$. Additionally, near the phase boundary, the monophasic clear solution exhibits a blue colouring. This bluish appearance, when observed in daylight, is sometimes referred to as Tyndall effect. This sample exhibiting this bluish colouring is shown in the photography in figure 13. The presence of a narrow channel is also observed, which is absent in the phase diagram for $Z = 0.7$ (figure 10(v)). Therefore, a transition of the miscibility gap from type 1 to type 2 is in this range for the counter-ion ratio. The evolution of this blue phase upon dilution is not abrupt but transient. Therefore, a sharp "boundary" cannot be given. The white-blue stripped area in figure 10(vi) encircles the area where this phase has been observed. It is also worthy to note that for samples in the liquid-liquid regime near this blue phase, the system separates into a transparent light phase and a bluish-transparent heavy phase.

Figure II-13 – Image of the apparently monophasic transparent low-viscous microemulsion for the system toluene/HDEHP/NaDEHP/water, exhibiting a bluish appearance designed as Tyndall effect corresponding to efficient diffusion of blue light (blue sky) without the strong diffusion due to local index variation that would produce a "milky" appearance.

In the pseudo-ternary phase diagram for $Z = 0.7$, a small monophasic region is located in the centre of the miscibility gap. Interestingly, the same bluish colouring was also observed for compositions inside this "lens".

The last feature to highlight, is the formation of a *liquid-foam-like (LFL)* third phase (depicted as grey-striped area) located within the biphasic region of the pseudo-ternary phase diagram for $Z = 0.1, 0.3, 0.5$. A photograph of the third phase appearing at the liquid-liquid interface is

shown in figure 14. This third phase has been observed for $0.1 \leq Z \leq 0.5$ and with decreasing area of the apparent regime as highlighted in the prism (figure 11).

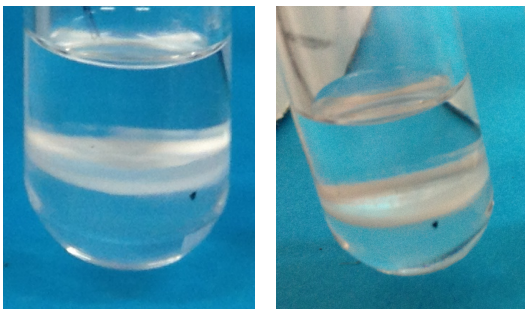

Figure II-14 – Images of a stable "*liquid-foam-like*" phase.

This "interfacial foam" is highly stable for several months for large extractant contents ($\gamma_{extractant} > 20wt\%$). However, for low extractant weight fractions ($\gamma_{extractant} \leq 5wt\%$), this LFL phase disappears over night. Therefore, the assumption is that this "liquid foam" formation is linked to microphase separation and is a kinetically trapped phenomenon.[150]

3.2.2)Evaluation of the macroscopic phase behaviour along the prism

As concluded in the previous section, NaDEHP is able to significantly solubilize any ratio of water and toluene at an appropriate content of the amphiphile. Thus, calling it a surfactant is justified, even in the absence of a co-solubilizing agent.[151] Addition of HDEHP enhances the solubilization significantly. In figure 10(vi), the necessary amount of total extractant is reduced to $\gamma = 14\,wt\%$ compared to $\gamma = 33\,wt\%$ for pure NaDEHP, in order to fully solubilized any ratio of water and toluene. Therefore, HDEHP shows properties of a co-surfactant.[73] Since the phase separation is a liquid-gas type separation, addition of HDEHP must decrease of the attractive potential, thus increasing the monophasic region.[135,152] The miscibility gap is still of type 1, therefore the system must exhibit a critical point. Due to the pseudo-ternary projection, the location this critical point cannot be determined by following the projection of the tie lines.[90] Nevertheless, the critical points should assemble on a line along the phase prism, shifting from the oil rich to the water rich side. This was comprehensively described for non-ionic surfactants of the C_XE_Y-type.[89,153]

Starting at the bottom face ($Z = 0$), addition of NaDEHP leads to an increase of the monophasic region on the solvent-rich side of the triangles. The phase boundary runs along a constant W_0-value in the respective phase diagrams. This means, that the phase separation is independent of the concentration of the water-solubilizing aggregate, but only

depends on the ratio of water to surfactant.[154] The nature of the phase separation is due to an emulsification failure.[135]

For $Z = 0.7$, a maximum of the miscibility gap is observed at $\gamma = 57\ wt\%$. This indicates that at a sufficiently large concentration, aggregates coalesce, hence increasing the amount of water that can be solubilized in the reverse micellar cores. Additionally, a second monophasic regime is observed, located in the centre of the biphasic liquid-liquid regime, which can be described as a *reentrant* effect: upon changing of a variable (volume fraction of water), the system undergoes a cyclic phase transition (monophasic – biphasic – monophasic).[155] The presence of a such a monophasic lens has been observed in the in the phase diagram highlighted in figure 3, however the origin of the reentrant effect is not further explained.[118] The structure on a nanoscopic scale has been investigated inside a lens that has been observed in a similar quaternary system: water, SDS, pentan-1-ol and dodecane.[156] Using small angle X-ray scattering, the aggregates have been identified to be locally lamellar structured.

3.2) Evidence of co-solubility

When working with ionic surfactant, the interfacial rigidity is very high due to the strong electrostatic interactions of the head-groups. As a result, the system is unable to co-solubilize high amounts of water and oil. Formulation of a microemulsion is only feasible, if a co-surfactant is added, i.e. a short-chained alcohol.[73] Though NaDEHP is able to close the miscibility between water and toluene, partial replacement of the sodium cation by a proton, further increases the monophasic regime. This is observed comparing the two triangles in figure 10(vi) and (vii).

In order to probe the maximum solubility, pseudo-binary toluene-extractant solutions have been prepared and diluted with water until phase separation. In figure 15, the resulting solubility profile is plotted as a function of the counter-ion ratio Z.

For $Z < 0.4$, both phase boundaries superpose and are at a constant value of $W_{0,Na} = 3.8$. In the regime of $0.4 \leq Z \leq 0.7$, the uptake of water increases linearly and exhibits a drastic increase for $Z > 0.7$. For the curve at $\gamma_{extractant} = 30wt\%$ of initial extractant content (circles), this increase in solubility is observed at $Z = 0.8$ and has its maximum at $Z = 0.9$. A similar tendency is observed for the curve with $\gamma_{extractant} = 10wt\%$ of initial extractant (squares), where a drastic increase is observed at $Z = 0.75$ and a maximum at $Z = 0.85$, before decreasing for $Z \geq 0.95$.

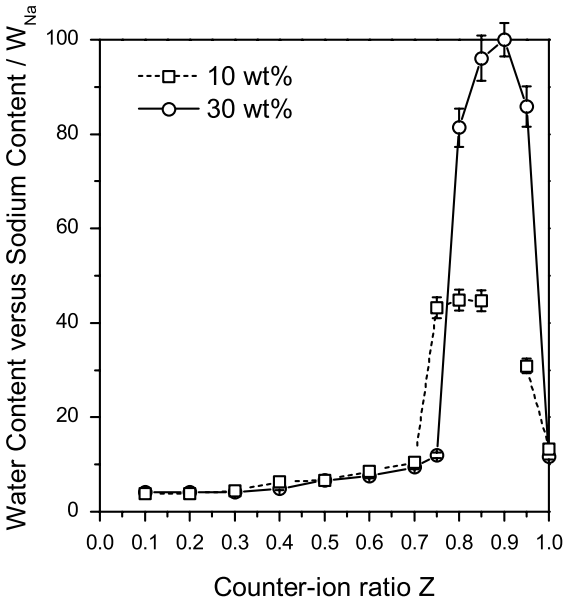

Figure II-15 – Solubility-limit of water in binary mixtures of extractant and toluene plotted versus different counter-ion ratios of Z.

Shah *et al.* proposed a model to explain the maximum solubility of a microemulsion based on two opposing effects.[83,157] On one hand, an increase in solubility can be achieved by decreasing the rigidity of the interface. The stiffness of the interface can be reduced by adding a co-solubilizing agent, e.g. short-chained alcohols,[158] aldehydes or ketones.[159] Phase separation in these systems is due to a maximum swelling of the aggregates and leads eventually to an emulsification failure, where the dispersed phase is expelled from the microemulsion to form a second phase in excess. On the other hand, at sufficiently high concentrations, phase separation can be explained by non-ideal behaviour: the discrete aggregates exert an attractive force on each other, leading to a phase separation. In reverse micellar systems, the nature of these interactions can be assigned to attractive Van de Waals interactions between polar cores. For ternary water, Aerosol, alkane systems,[96,160,161] this has been confirmed by fitting scattering spectra using the Perkus-Yevick equation for sticky hard spheres, as proposed by Baxter.[162]

As a result, the balance between these two opposing effects leads to a maximum of the solubility of water and oil, as depicted in figure 16. In case of the solubility behaviour in figure 15, the results can be explained as follows: For counter-ion ratios below the solubility maximum at $Z = 0.9$, the phase separation is mainly driven by a maximum swelling of the reverse micellar aggregates and thus an emulsification failure. For counter-ion ratios $Z > 0.9$, above the maximum solubility, solubility decreases due to attractive interactions resulting in a liquid-gas phase transition as observed in the top face.

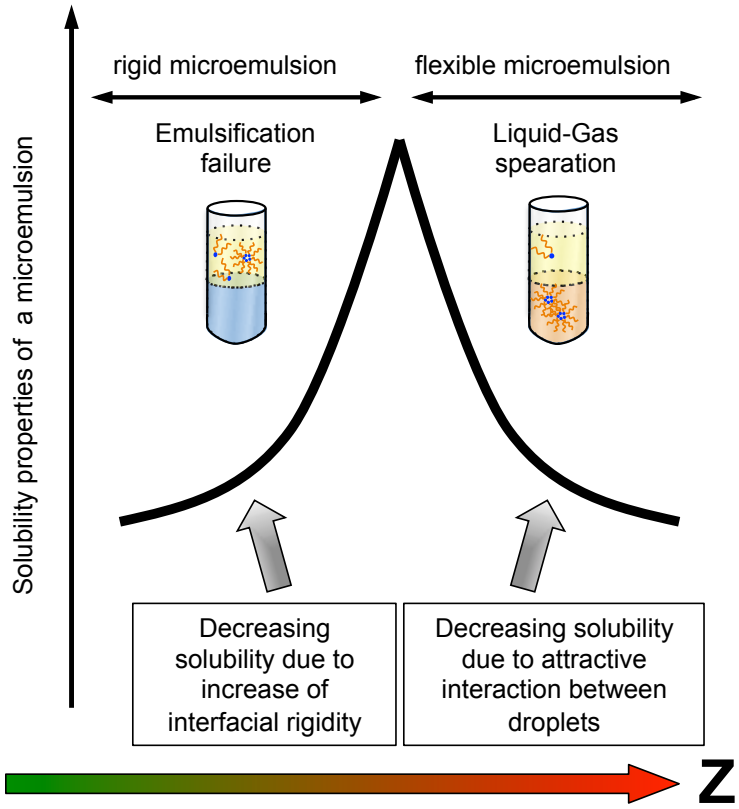

Figure II-16 – Schematic presentation of the transition for a phase separation of type II (attractive interactions) to type I (emulsification failure). Reproduced from [83].

This confirms that HDEHP can be considered as a co-surfactant. Considering NaDEHP as the "complexed" form of the extractant, it can be concluded that extractants, which do not actively participate in complexation, may still participate on the aggregation. This is in good accordance with the colloidal approach in solvent extraction, stating that the aggregation number (number of amphiphiles) of a complex is higher than the complexation number (number of extractants complexing a metal-cation.

3.3) Evidence of frustration

In this section, these two cases, respectively called fish-plot and χ-plot are presented, in order to comprehensively understand the macroscopic phase behaviour with the counter-ion ratio as a free variable.

3.4.1) Horizontal cut of the prism: The "X-cut"

A convenient representation to visualize the evolution of the phase behaviour as a function of Z is to cut a horizontal section through the prism, keeping the extractant concentration at a

constant level. Plotting the counter-ion ratio as a function of the toluene-to-water-ratio $\alpha_{toluene}$ reduces the 3 dimensional representation into a so-called "χ –cut".

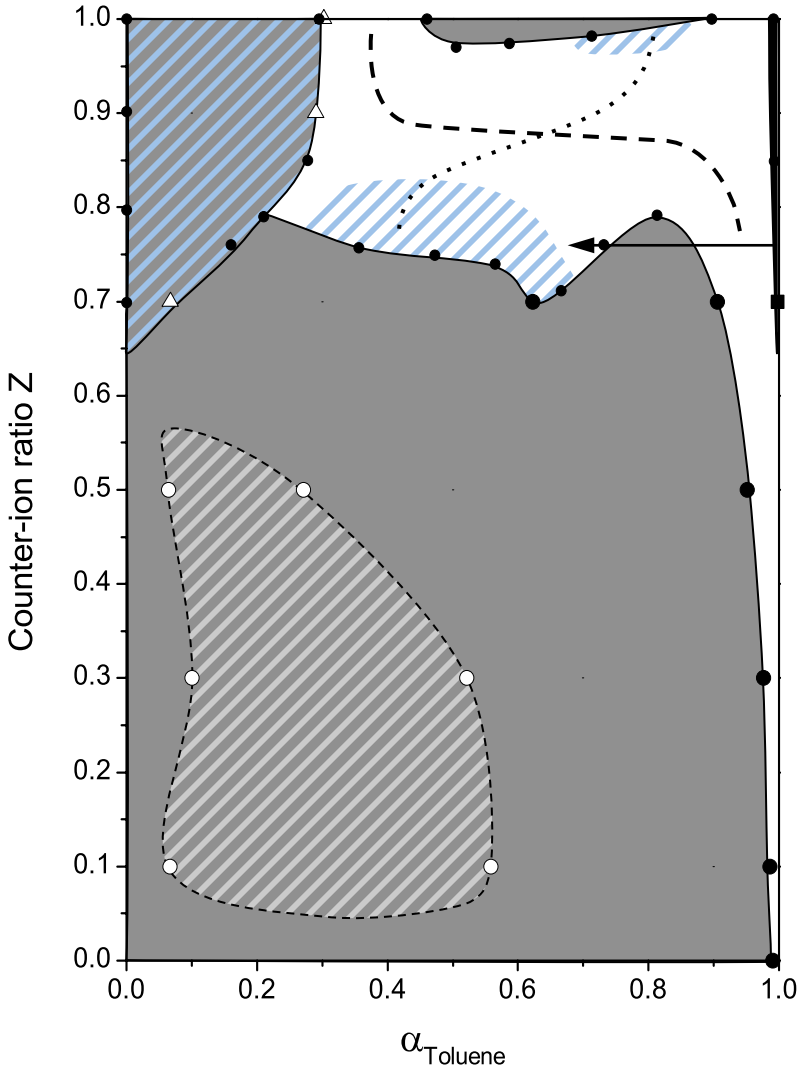

Figure II-17 – χ-cut the prism toluene/HDEHP/NaDEHP/water for $\gamma = 20wt\%$. The typical X-shaped form of the monophasic region has been highlighted by two lines. The dashed line represents the so-called "non-frustrated" regime. The dotted line traces the so-called "frustrated regimes".[40] The black arrow indicates a re-entrant pathway, where a monophasic-biphasic-monophasic transition is observed for decreasing α. Lyotropic phases; the s/l-phase and the LFL-phase are added for the sake of completeness.

Figure 17 depicts a χ-plot of the prism, established at a constant extractant weight fraction $\gamma_{extractant} = 20\ wt\%$. An objective of this plot is to verify if the monophasic lens observed for $Z = 0.7$ is connected with the "bulk" microemulsion observed for higher values of Z.

Starting from samples containing purely NaDEHP ($Z = 1$), a slight decrease of Z enhances significant the solubility of water and oil, which extends over the nearly whole range of α for $0.75 < Z < 0.95$ and flanked by LC-phases on the water-rich corner. A continuous path throughout the monophasic region can be traced from the water-rich corner at high Z, to the

toluene-rich corner, down to $Z = 0$, by trespassing a bicontinuous regime (dashed line in figure 14). Further, highlighted by the dotted line, a second continuous path can be drawn from the oil-rich region at high Z to the water-rich region with decreasing Z, up to a counter-ion ratio of $Z = 0.7$. Therefore, the typical χ-form, which gives this plot its name, is actually traceable in the phase prism. The centre of the cross denotes the region where the microemulsion exhibits a bicontinuous morphology on a mesoscopic scale. The microstructure in this region can be described as bi-liquid foam, alias HIPME in the name given by Hoffmann[149] or locally lamellar or symmetric sponge phase if spontaneous packing is close to $p_0 = 1$, and as disordered connected w/o or o/w cylinders, with a general theory given by Zemb.[79]

The monophasic lens is indeed connected with the bulk-microemulsion domain, showing a wedge-like form. Running along the arrow, indicated in figure 17 at a constant $Z = 0.75$, a re-entrant effect is observed. Starting with an oil-rich solution (for $\alpha > 0.9$), the sample enters a biphasic regime for $\alpha = 0.86$ and re-enters a monophasic region for $\alpha < 0.72$. Additionally, the emergence of a "bluish region" is not only found near the phase boundary on the oil-rich side for $Z > 0.9$, but also in the vicinity of the monophasic "lens" at low $\alpha_{toluene}$, thus in both *frustrated branches*.

3.4.2)Vertical cut through the prism: the "Fish-cut"

The usual notation of this plot is to make the "cut" at an equivalent ratio of water to oil. Nevertheless, two slightly displaced representations were chosen, thus one fish diagram on the water-rich side and respectively on the toluene-rich side. This was done in order to facilitate the discussion of the macroscopic phase behaviour. The presence of LC-phases and the liquid-foam-like phase have been added for the sake of completeness. Phase boundaries traced by a dashed line (such as the LFL regime and blue phases) indicate that the phase limit is afflicted with incertitude, but fulfil the purpose of demonstration.

The fish-plot on the water-rich side, at a toluene-to-water ratio of $\alpha_{toluene} = 0.25$, is depicted in figure 18(i). At $Z = 1$, the monophasic region is sectioned into two parts, separated by the wedge-like LC-region, observed in figures 13(vi and vii). Decreasing Z results in an increase of the solubility, with a maximum solubilization at $Z = 0.9$, where only $\gamma_{extractant} = 11.5\ wt\%$ are necessary in order to fully solubilize water with toluene. For $Z < 0.9$, the monophasic region is significantly reduced and passing by a frustrated brunch, the solution enters a domain where the monophasic region enhances a bluish shining, as detected in the χ-cut.

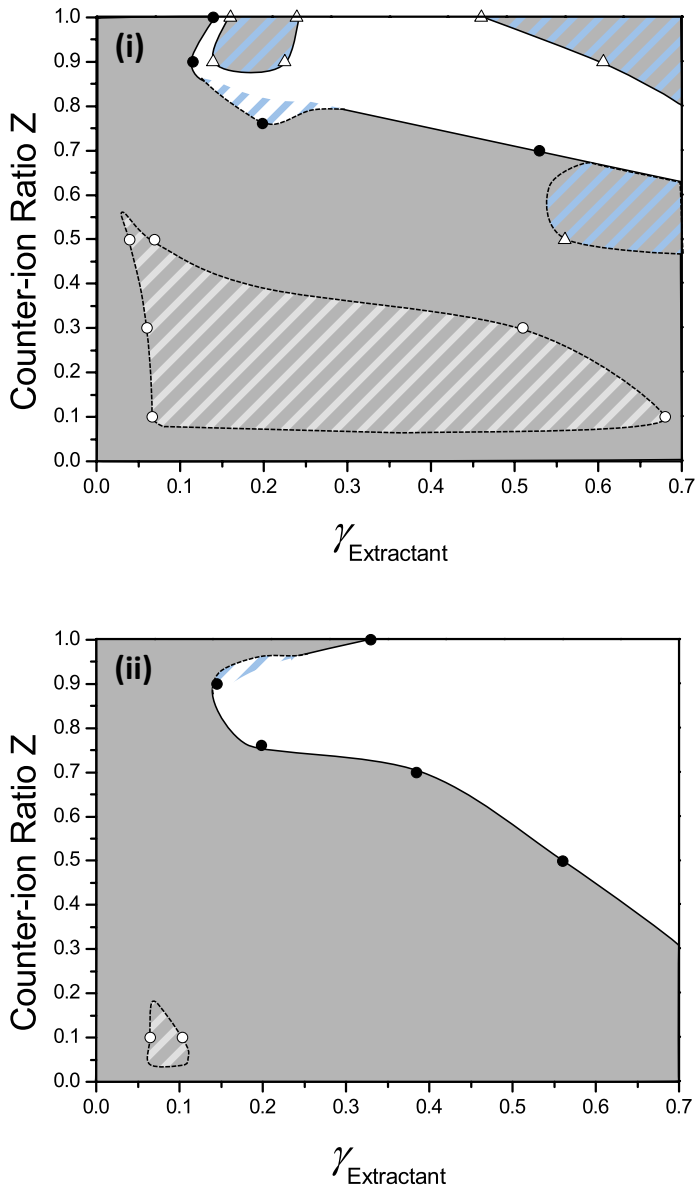

Figure II-18 – Vertical prism sections at constant water-to-toluene ratio. (i) $\alpha_{toluene} = 0.25$, (ii) $\alpha_{toluene} = 0.75$. A maximum solubility for in the water- as well as on the oil-rich side is detected for $Z = 0.9$. Lyotropic phases; the s/l-phase and the LFL-phase are added for the sake of completeness.

A similar phase behaviour is observed on the toluene-rich side, for $\alpha_{toluene} = 0.75$. No lyotropic phases have been observed, but a maximum solubility at $Z = 0.85$ confirms the results observed in the previous section (co-surfactant properties of HDEHP). In contrast to the fish-plot on the water-rich side, the bluish phase is detected on the "upper branch" of the tail.

No third phase was observed in the vicinity of the solubility maximum, giving this plot its typical name.

3.4.3)Interpretation of the cut-representations

3.4.3.1) Comparative analysis between NaDEHP and Aerosol OT

Aerosol OT and NaDEHP are special surfactants as they belong to the class of hyper-branched surfactants.[163] A single value for the spontaneous packing parameter p_0 cannot be attributed a priori: the area per head-group depends on degree of dissociation. If the sodium counter-ion is condensed, the surfactant has a spontaneous packing parameter in the order of $p_0 = 2.5$, thus giving rise to large inverse spherical domains.[138] Moreover, AOT is known to form large microemulsion domains even in the absence of salt or a co-surfactant and can carry water contents up to $W_0 = 40$, which in molar volume represents nearly ten times more water than surfactant.[164] For high volume fractions of oil, the aggregates are supposed to be reverse spheres and the size is aggregation number is mainly dependent on the ratio of water to AOT.[165] However, if Aerosol OT is in a dissociated form, it produces large lamellar phase domains. It has been solidly demonstrated, by evaluation of the scattering cross section versus volume fraction of water, using small angle X-ray scattering, that locally lamellar structures dominate in some parts of the large L2 region.[166] Moreover, branching of chains means easy "shape" modification, i.e. low κ^* and high flexibility.[66]

As known from the Krafft-temperature, increase of temperature raises the solubility of ionic surfactants in water, according to a decrease of the attractive London forces between aliphatic chains, but also due to an increase of the counter-ion dissociation, as the Bjerrum-length is reduced.[42] On the other hand, addition of an electrolyte decreases the solubility of ionic surfactants in water.[40] Chen and Strey made use of this converse solubility property to probe the macroscopic phase behaviour of AOT in the presence of small amounts of salt ($c_{NaCl} = 0.6\ mol/L$) versus the temperature.[167] In their χ-cut, depicted in figure 19, the *salting-out* effect of NaCl is competing with the *salting-in* effect of the temperature.

At ambient temperatures, AOT has a preferred solubility in the oily phase (a value $HLB < 10$). Therefore, the surfactant wants to curve towards water. On the solvent-rich side, the surfactant can disperse water in the organic medium by forming reverse globular aggregates and the resulting packing is close to the spontaneous packing. It is also called "non-frustrated", since the microscopic interface easily bends at room temperature towards the dispersed phase.

For low values of $\alpha_{n-dodecane}$, still at ambient temperature, water is the predominant solvent in the solution. Though AOT wants curve towards water, it is forced to curve towards oil. Therefore, packing of the surfactants differs greatly from the spontaneous packing parameter

and is thus called *frustrated* (depicted as red arrows).[92] Therefore, the local topology is likely to be made of disordered, only partly connected local structure, as described by the Disordered-open-connected DOC-model of microemulsions.[79]

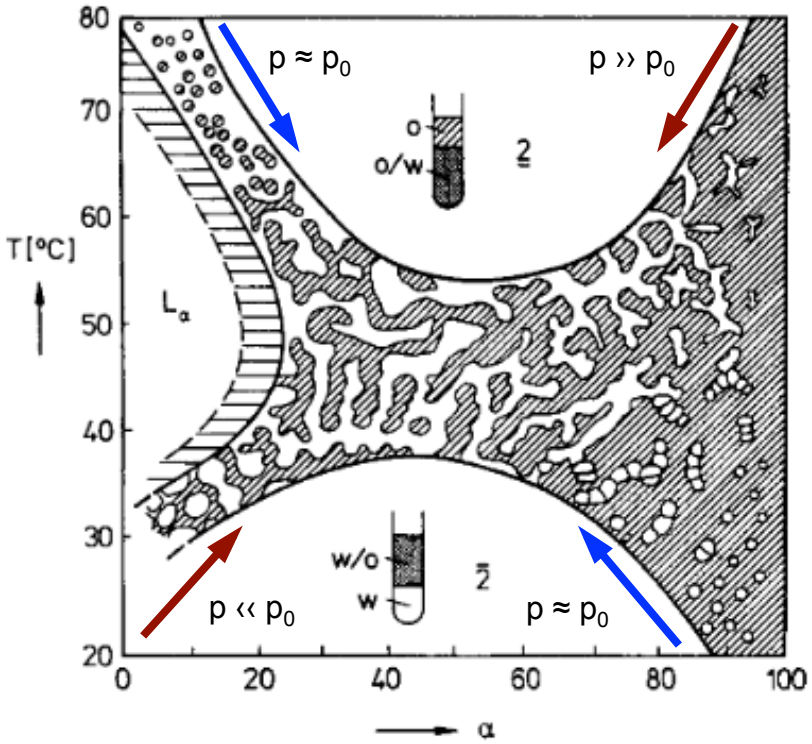

Figure II-19 – χ-plot of n-decane, AOT, $\varepsilon_{brine} = 0.6$ as a function of Z (here temperature) and $\alpha_{\mathrm{n-dodecane}}$. This figure is a schematic representation to highlight the frustrated (red arrows) and non-frustrated regions (blue arrows).

The opposite behaviour is observed when increasing the temperature. $For\ T > 60\ °C$, the monophasic region separates into two branches. According to the increased HLB with rising temperature, AOT now prefers to curve towards n-dodecane. As a result, the non-frustrated branch is at low the values of $\alpha_{\mathrm{n-dodecane}}$, while the frustrated branch is on the solvent-rich side.

Judging the effective surface of the ionic head-group when comparing the molecular structures of NaDEHP with AOT, it would be appropriate to state that AOT has the bigger head-group, given the additionally integrated succinate. Nevertheless, in literature, it was reported that AOT has a smaller head-group than NaDEHP ($a_0(AOT) = 60\ \text{Å}^2$ vs. $a_0(NaDEHP) = 64\ \text{Å}^2$) and judging this result by comparing the molecular structures is counter-intuitive.[59] The large effective head-group of NaDEHP can be explained when comparing the pK_a-values of the respective of phosphoric and sulfuric acid. The pK_a for sulfuric acid is at $pK_{a,1} = -3$, while the pK_a for phosphoric acid is $pK_{a,1} = 2.16$.[168] Thus, the

driving force for deprotonating the sulfuric acid is 5 orders of magnitudes higher than the phosphoric acid. The resulting corresponding base of the sulfuric acid, $NaHSO_4$ has thus a significantly smaller urge to dissociate compared to the corresponding phosphoric acid base. As a result, the charge density of the phosphate anion is significantly increased and thus the effective surface a_0 is bigger than the polar surface of AOT. This also explains the preferential solubilization of NaDEHP in water. Therefore, NaDEHP behaves at room temperatures as AOT at $T = 80\,°C$. This could be a crucial reason, why the physico-chemical properties are opposite when comparing AOT with NaDEHP solutions.[54,55,169]

3.4.3.2) Possible structuring on a nanoscopic scale in the frustrated branch

In the frustrated branches, interface is forced to bend against its natural curvature.[92] Looking at the monophasic region on the solvent-rich side for the ternary phase diagram of toluene/NaDEHP/water, the surfactant wants to bend towards oil, however oil is the dominant phase with a high volume fraction. As a consequence, the system has to compensate for this unpleasant situation by locally adapting the curvature, e.g. by merging two spherical aggregates to one barbell-shaped (figure 20).[170] Since such a conformation is only convenient for the surfactant molecules sitting at the convex area. Therefore, such conformations are highly dynamic, which is not in conflict with the interfacial rigidity, since the phase separates due to an attractive interaction between the mesoscopic aggregates.

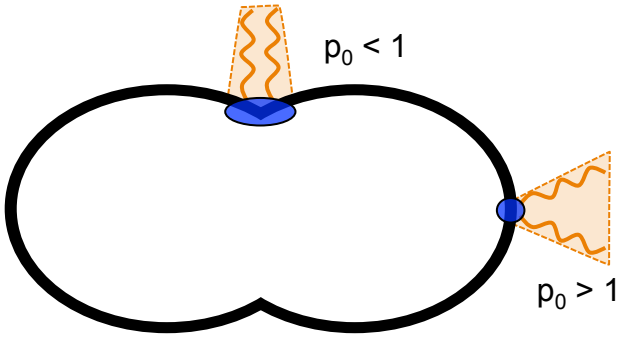

Figure II-20 – Barbell-shaped dimer of a frustrated microemulsion. Adapted figure from [170]

To go even further, the urge to curve towards oil can be so high, that the formation of such a barbell can enthuse an attractive interaction between aggregates and may be the origin of the phase separation.[171]

3.4.3.3) Comparing the frustration on the water-rich vs. oil-rich side

In section 3.3, we elaborated that the dominating motor for phase separation is either an emulsification failure, for counter-ion ratios below the solubility maximum, or a liquid-gas transition, for Z-values above the maximum (see and modified in figure 21). Combining the χ-

plot and the fish-plot representation, we can correlate the type of phase separation with the frustration of the extracting microemulsion. If the system separates according to a liquid-gas phase separation, the system can be declared as frustrated. It is yet flexible microemulsion, in the sense that water can still be added, thus leading to further swelling of the aggregates in the microemulsion. If the system separates due to an emulsification failure, the system can be regarded as a non-frustrated, but rigid microemulsion, as the aggregates cannot be inflated any further.

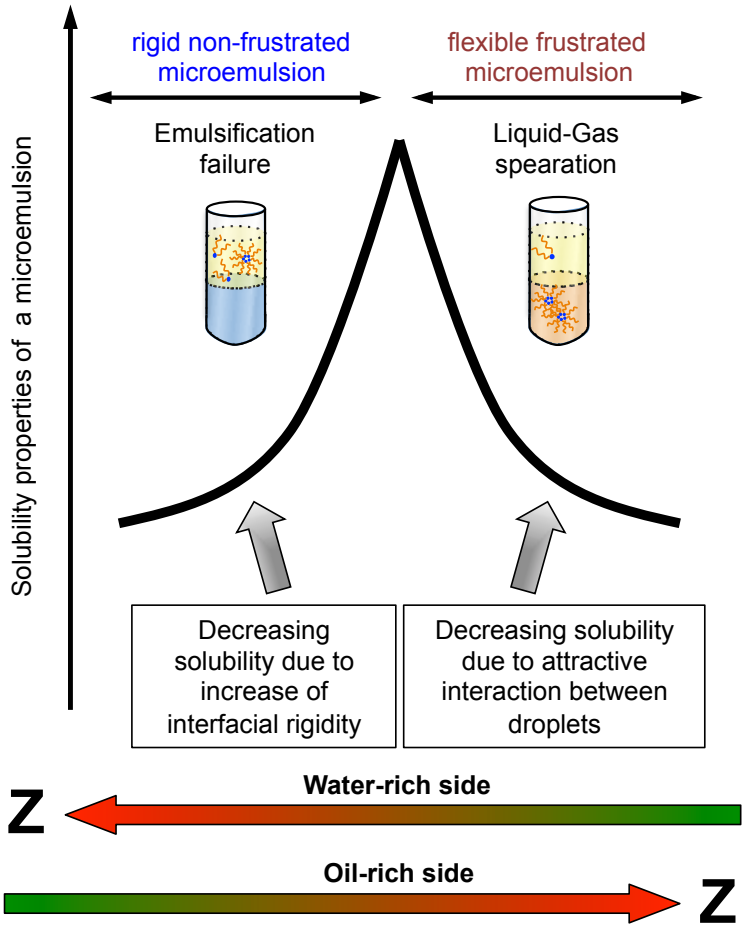

Figure II-21 – Modified scheme of Shah. On the water-rich side, decreasing Z leads to an increase in rigidity and decrease of frustration. The opposite is observed on the oil-rich side of the phase diagram.

The transition between the two types of microemulsions can be controlled by the counter-ion ratio Z. Extracted from the location of the bluish phases, observed in the opposite side of the solubility maximum in the fish-plots, a major factor is the water-to-solvent-ratio. On the solvent-rich side, the frustration increases with increasing Z. On the water-rich side, the opposite is observed, as the frustration increases with a decreasing counter-ion ratio.

To conclude this convergent study of prism, χ- and fish-cut representations (that had never been done to our best knowledge for an extractant used in hydrometallurgy) helped

fundamentally understanding that the reverse micellar behaviour of the extractant as a function of its counter-ion ratio Z. In analogy to the temperature T, Z can be viewed as a thermodynamic variable, since it is the vertical axis for our system, as the temperature is for non-ionics.[90] This provides a "chemical control" over curvature: What is true for the replacement of H^+ by Na^+ should be valid also for other cations. Therefore Z is correlated to p_0. Determining the variation of p_0 with Z is the major task for extractants, as it was for non-ionic surfactants.

3.4) Off-plane tie lines in a quaternary system

The choice of using a pseudo-ternary approach for a quaternary system has a crucial inconvenience. Upon entering a multiphasic region, a distribution of the components between the apparent phases, in particular NaDEHP and HDEHP, is quite certain. The first objective of this experiment is therefore to determine if the tie lines are directed towards pure water, or if the extractant is soluble in the aqueous phase to a certain degree. Secondly, in case that the extractant is actually soluble in the aqueous phase, a different distribution of HDEHP and NaDEHP between both phases is awaited. As a consequence, the tie lines cannot be drawn perpendicularly to the prism, but "off-plane".

3.4.1) Distribution of the extractant between the aqueous and the organic phase

The separation of all four components has been evaluated for three compositions in the pseudo-ternary phase diagram at $Z = 0.5$, as depicted in figure 22(i). All three compositions are on a dilution line towards pure water. The initially chosen compositions are listed in table 3, alongside the experimentally determined compositions of the aqueous and organic phases.

In 22(i), a frontal view on the phase triangle shows that the tie lines are not directly pointing towards pure water. A considerable amount of extractant resides in the aqueous phase ($\gamma_{extractant} \sim 3.5 wt\%$). As a result, the biphasic regime cannot be declared as a classical Winsor II regime. Further, as the sample is diluted with water, the total extractant concentration decreases in the organic phase, while it increases in the aqueous phase, as indicated by the arrows.

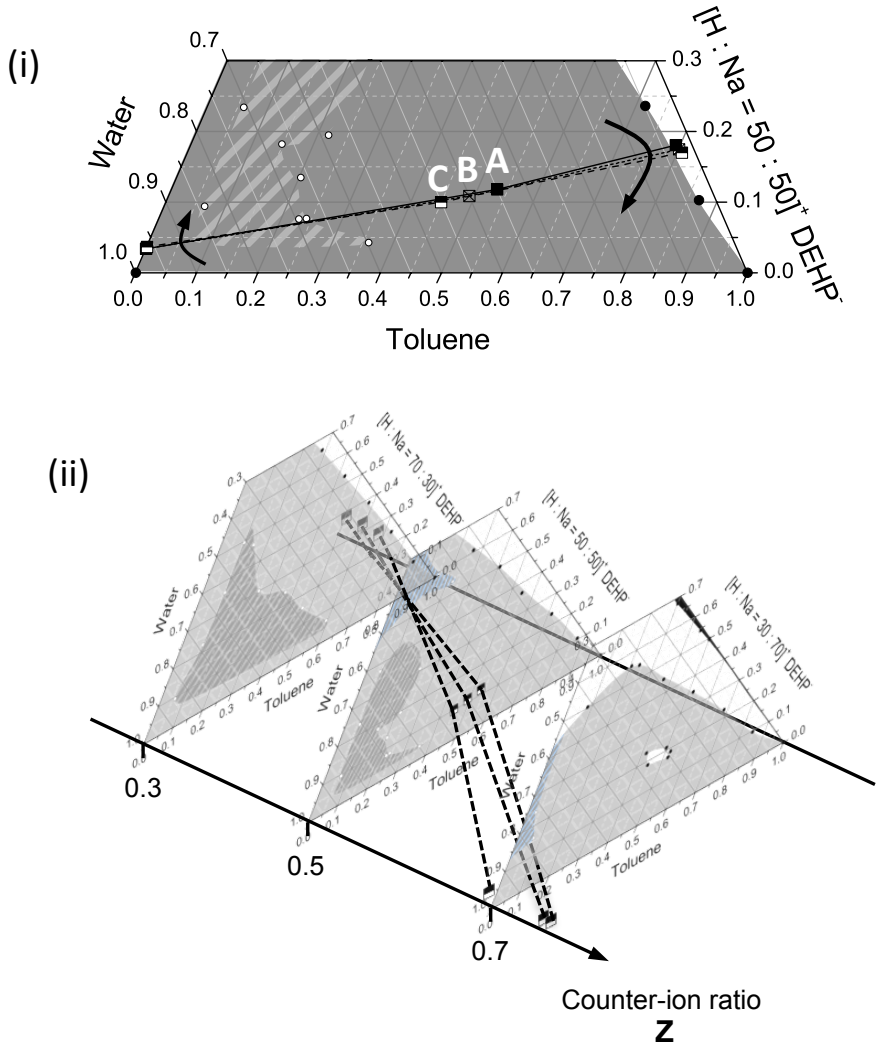

Figure II-22 – (i) Tie lines in the biphasic region of the phase diagram of the phase diagram with $Z = 0.5$. (ii) Tie lines taking into account the ratio of HDEHP to NaDEHP in each of the phases.

In figure 22(ii), the tie lines are shown in a three dimensional representation. Since the tie line is not in the same plane as the initial compositions in the pseudo-phase diagram, the extractant is distributing between the two phases. The counter-ion ratio in the aqueous phase is higher than in the initial phase diagram, while it is lower in the organic phase. Thus, this confirms that NaDEHP has a preferred solubility of in aqueous phase. Nevertheless, around 1 molecule HDEHP per 3 molecules NaDEHP is co-extracted in the aqueous phase. The opposite is observed in the organic phase, where one NaDEHP molecule is found per three molecules of HDEHP.

As the system is diluted, the counter-ion ratio decreases in the aqueous phase, while it increases in the organic phase. Thus, with increasing water-content, the solubility of HDEHP in the aqueous phase increases.

Table II-3 – Composition of the initial samples prepared in the binary region of the phase diagram as well as the compositions of the resulting organic and aqueous phase.

Initial composition in the biphasic region

	w(Toluene)	*w*(DEHP)	*w*(Water)	Z	*w*(NaDEHP)	*w*(HDEHP)
A	53.2%	11.8%	3.5%	0.50	5.9%	5.9%
B	49.1%	10.9%	4.0%	0.50	5.5%	5.5%
C	45.0%	10.0%	4.5%	0.50	5.0%	5.0%

Organic Phase

	w(Toluene)	*w*(DEHP)	*w*(Water)	Z	*w*(NaDEHP)	*w*(HDEHP)
A	79.3%	18.0%	2.7%	0.27	4.9%	13.1%
B	80.1%	17.5%	2.4%	0.26	4.5%	13.0%
C	80.8%	17.0%	2.2%	0.23	3.9%	13.1%

Aqueous Phase

	w(Toluene)	*w*(DEHP)	*w*(Water)	Z	*w*(NaDEHP)	*w*(HDEHP)
A	0.11%	3.37%	96.52%	0.76	2.57%	0.80%
B	0.09%	3.42%	96.49%	0.75	2.58%	0.84%
C	0.08%	3.65%	96.27%	0.70	2.54%	1.11%

3.4.2)Correlation of the distribution ratio with structuring and dissociation

We infer from table 3 that there is a negligible amount of toluene in the aqueous phase. Therefore, we find direct micellar structures in the aqueous phase, while the organic phase contains reverse spherical aggregates with a W_0-value of 3, as deduced from the structural study of the 2 coexisting phases (figure 23, SAXS-Spectra of organic (i) and aqueous phase (ii)).

The spectrum of the organic phase was fitted at first approximation with a simple spherical form factor and a hard sphere interaction term only. Note that there is a significant amount of HDEHP in the organic phase that is not contributing to the micelle formation and thus part of the organic pseudo-phase. Therefore, the contribution of HDEHP in the solvent had to be subtracted. As a result, we find spherical reverse aggregates in the organic phase with a radius of $R_{sphere} = 1.13\ nm$.

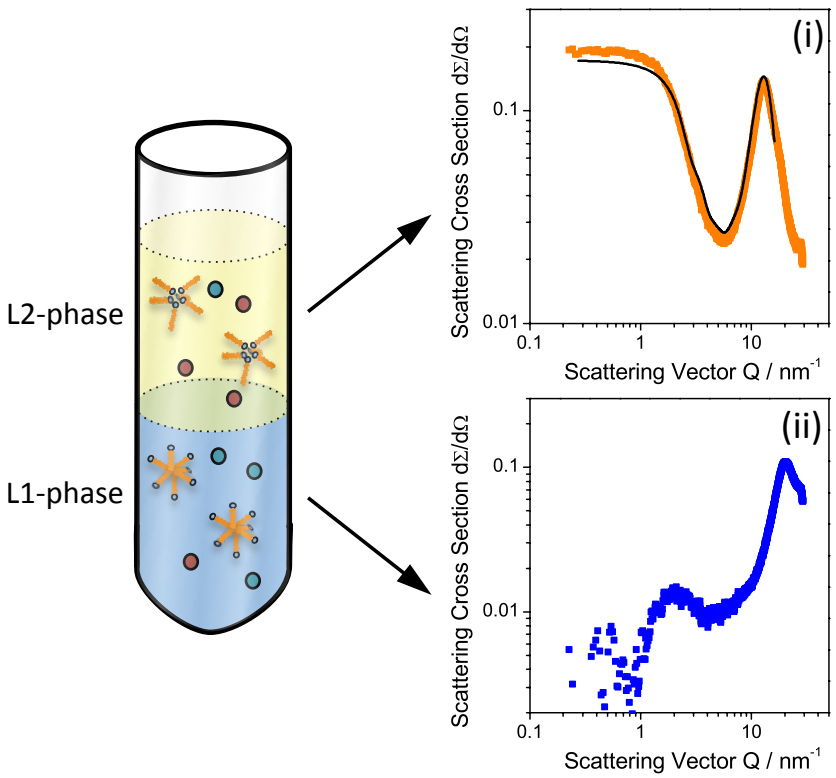

Figure II-23 – Schematic partition of liquid-liquid regime into a heavy L1 phase and a light L2 phase. SAXS-spectra show the presence of structures in the mesoscopic domain.

Since no toluene co-extracted into the aqueous phase (see table 2), the aggregates in the organic phase are only be composed of HDEHP and NaDEHP. The resulting contrast of the surfactants is nearly equal to water, resulting in a phenomenon called “zero average contrast”.[172] Since the forward scattering $I(0)$ is directly proportional of the square of the contrast $\Delta\rho^2$, the spectrum exhibits no scattering intensity, hence a spherical aggregation is the simplest approximation.

As deduced from table 3, the counter-ion ratio in the organic phase is in the range of $Z = 0.75$. Though the counter-ion ratio is based on the weight-fraction the calculation into the molecular counter-ion ratio Z* is neglected, since the molecular mass of the two derivatives is nearly identical ($M_{HDEHP} = 322.43$ and $M_{NaDEHP} = 344.23$). Therefore, the correction factor to obtain Z^* is omitted, since this calculation is done as a demonstration. Three “red” HDEHP-molecules, alongside one “blue” NaDEHP-molecule are drawn in the organic phase. The aqueous phase contains respectively three “blue” and one “red” molecule, in accordance with table 3. Based on a thermodynamic calculation using the distribution coefficients, one can deduce a free energy of transfer for the individual cations between the phases.

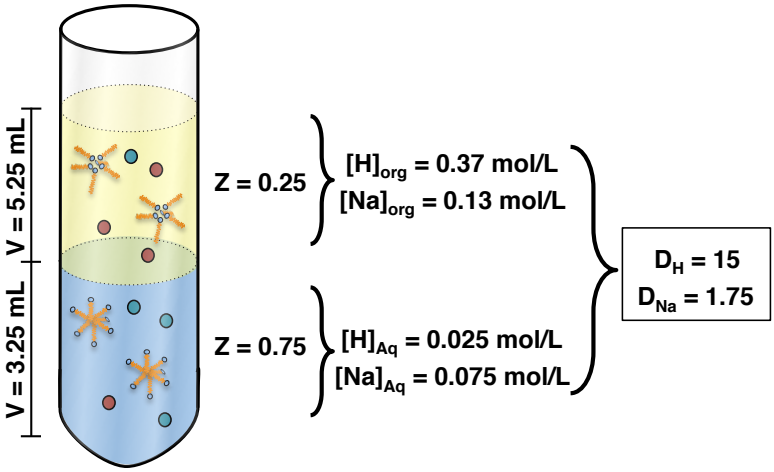

Figure II-24 – Schematic representation of the mesoscopic aggregation in both phases and the distribution of the cations between the two phases.

After phase separation and settling, the system is at a thermodynamic equilibrium, therefore the difference in chemical potential is zero between oil and water for all species present. Determining then the distribution ratio gives an idea about the difference in reference chemical potential of the two cations, that are more or less "happy" in different locations of the phase diagram. It must be stressed that the chosen "reference state" for each anion is a state with $c_0 = 1\, mol/L$, since we use the concentration scale. This is the most realistic choice in the case of liquid-liquid extraction, since species are typically 1 nm apart. This choice is adapted to quantify ion transfer problems. In the case of hydration, the scale of mole fraction implying a dilution in solvent and not an ion transfer is much else adapted since the reference state has an infinite negative chemical potential.[173] Since the system is in a thermodynamic equilibrium, hence the free energy of the system is at a global minimum:

$$\Delta G = 0 \qquad (iv)$$

As a consequence, the chemical potential of the proton is equal in both phases. The same is true for the sodium cation.

$$\mu_{Na}{}^{oil} = \mu_{Na}{}^{\circ,oil} + RT\, lnc_{Na}^{oil} = \mu_{Na}{}^{\circ,water} + RT\, lnc_{Na}^{water} = \mu_{Na}{}^{water} \qquad (v)$$

$$\mu_{H}{}^{oil} = \mu_{H}{}^{\circ,oil} + RT\, lnc_{H}^{oil} = \mu_{H}{}^{\circ,water} + RT\, lnc_{H}^{water} = \mu_{H}{}^{water} \qquad (v')$$

where $\mu_i{}^{\circ,\alpha}$ is the standard chemical potential based on the concentration scale, $\mu_i{}^{\alpha}$ is the chemical potential of cation i in phase α.[173] In a first approximation the standard chemical reference potential can be assumed to be identical in both phases and therefore be neglected. As a result, the chemical potential for transfer of an ion from one phase to the other can be written as function of the distribution ratio D_i

$$\Delta_{trans}G_i^{water \to oil} = RT \ln D_i \qquad (vi)$$

As a result of this elementary evaluation, the free energy of transfer for a proton is at $\Delta_{trans}G_H^{water \to oil} = 6.7\ kJ/mol$, while the energy to transfer a sodium cation is at $\Delta_{trans}G_{Na}^{water \to oil} = 1.5\ kJ/mol$. As introduced in the fundamental section (I-1.1), the ratio of the two distribution ratios give the separation factor $S_H = 8.57$. Thus the difference in free energies gives:

$$\Delta\Delta_{Trans}G_H{}^{water \to oil} = RT \ln S_H = 5.2\ kJ/mol \qquad (vii)$$

Therefore, when present, nearly all protons stay in the solvent-rich phase while the sodium ions distribute. This confirms that extractants are badly soluble in the aqueous phase and highly prefer to solubilise in an organic solvent.

The notion of intrinsic pK_a is very clear in diluted solution, but irrelevant as soon as charge regulation occurs, i.e. in concentrated solutions.[174] Using a pK_a-value for HDEHP, one can formally write a dissociation-reaction of HDEHP as:[175]

$$HDEHP + H_2O \rightarrow DEHP^- + H_3O^+ \quad ; \quad pK_a = 1.3 \qquad (viii)$$

And the free energy for dissociation can be calculated according to:

$$\Delta G_{Diss,H} = RT \ln K_a = -7.42\ \mathrm{kJ/mol} \qquad (ix)$$

In total, we identified that there are three competing equilibria: the dissociation of the counter-ions from the of phosphate head-groups, competition of H^+/Na^+ in the water-continuous to the oil-continuous phases and oil-water equilibrium of the extracting anion. Aside from non-ideal behaviour, all these terms are influenced largely by structuration: we know from structural study that adjacent phosphate groups are 1 nm apart. Thus, the charge regulation effect is strong. Multiple equilibrium alone without the structural knowledge can only be fitted to the values observed at different points of the phase diagram requires at least three different "constants": The modelling of the free energy of transfer requires explicit calculation of the different terms involved; The structural study will be useful for the evaluation of the different terms of the free energy of transfer. To our knowledge, this has been done in the whole literature only once.[39] Our evaluation shows, how intricate these mechanisms interact when the species considered are at a reference concentration of $c_0 = 1\ mol/L$:

- The free energy of association, which can be deduced from:

$$\Delta_{micellization}G = RT \cdot ln\ \frac{cmc}{c_0} \qquad (x)$$

- The separation factor to transfer a proton from the aqueous to the organic phase $\Delta\Delta_{Trans}G = 5.2\ kJ/mol$.
- Dissociation of phosphate $\Delta G_{Dissociation} = -6.5\ kJ/mol$ plus quenching by nearest neighbour by charge regulation.

For NaDEHP the free energy for dissociation can approximated by:

$$pK_a + pK_b = 14 \quad \Leftrightarrow \quad pK_b = 12.7 \quad \Rightarrow \quad \Delta G_{Diss,Na} = -72.49\ kJ/mol \qquad (xi)$$

As already mentioned earlier, the phase behaviour of NaDEHP is like that of AOT at $T = 80\ °C$. From this calculation, it can be deduced that NaDEHP strongly prefers to be in a dissociated state. Hence, this explains the strong affinity towards water. Association of a sodium-cation and transfer into the organic phase is strongly unfavourable from a molecular point of view. Exploring all the aspects is beyond the scope of this work and cannot be done without investigations about the different regimes of charge transport in the different single-phase regions, i.e. the conductivity.

4. Variation of Solvents

The choice of a *good solvent* for liquid-liquid extraction is not evident. From a formulator's point of view, a diluent has to fulfil several criteria in order to serve as a good solvent, i.e. it needs appropriate physico-chemical properties (low vapour pressure, low viscosity, low density). However, the significance of a diluent on a mesoscopic scale is often neglected. Only few publications actively focus on the impact of solvent on an extraction process. Berthon *et al.* determined that solvent penetration is crucial to evade the formation of third phases.[132] Short-chained branched alkanes migrate into the apolar shell of a complex, interacting with the chains of an extractant. This creates a "solvation shell" around reverse micelles and increases the hard-sphere radius. In return, this inhibits the splitting of the organic phase, as the short-range attractive interactions are not strong enough to remove this solvation shell. For the synergistic extraction system HDEHP-TOPO, it has been identified that solvent penetration strongly influences the extraction efficacy.[38] Using a poorly penetrating solvent (n-hexadecane versus n-heptane) increases the distribution ratio of Uranium by a factor 4. If the solvent has a good penetration property, this is correlated with

an increase of the spontaneous packing parameter p_0, since the volume of the apolar region v increases, thus modifying the stability of the complex. These two examples show the significance of the choice of diluent in a metal-extracting microemulsion. Even in surfactant science, the choice of solvent is often neglected. For Aerosol OT, a large spectrum of alkanes of different chain length and branching is used. Yet, to the best of our knowledge only few publication are available, which specifically correlates the choice of solvent with different physico-chemical properties (e.g. size and shape of aggregates, influence of solvent on the interactions between reverse micelles).[96,176,177]

The aim of this study is to compare the phase behaviour of three fundamentally different diluents with the phase behaviour of "reference" solvent toluene. A particular focus is on the phase behaviour in the frustrated regime, where phase separation is dominated by attractive interactions. The major interest is how the choice of solvent influences the interactions on a macroscopic scale.

4.1) The "theta solvent" – Iso-octane

In polymer solutions, solubility of a polymer in a solvent depends on the intermolecular interactions between polymer chain segments with coordinated solvent molecules.[40] If the interaction energy between a polymer with the solvent is equal to the interaction energy with other polymer chain segments, the solvent is called a *theta solvent*. The free energy of mixing is independent of the enthalpy and is driven by entropy. We make this reference towards iso-octane as solvent, as the solvent perfectly interacts with the apolar 2-ethylhexyl-chains of the extractant. Therefore, we consider iso-octane as a well-penetrating solvent

4.1.1)The two faces of the prism – Z = 0 and Z = 1

Iso-octane is miscible in any proportion with HDEHP, however shows complete immiscibility towards water. Extending this miscibility into the ternary regime results in a large miscibility gap, as depicted in figure 25(i). Only trace amounts of water (the phase boundary runs along a constant value of $W_0 = 0.14$) are soluble in a binary mixture HDEHP and iso-octane and any further added water separates to give a second phase in excess. Given this behaviour, tie lines have been drawn towards pure water in analogy to the "reference" solvent toluene. Hence, the biphasic region is a Winsor II-phase and the origin of phase separation is an emulsification failure.

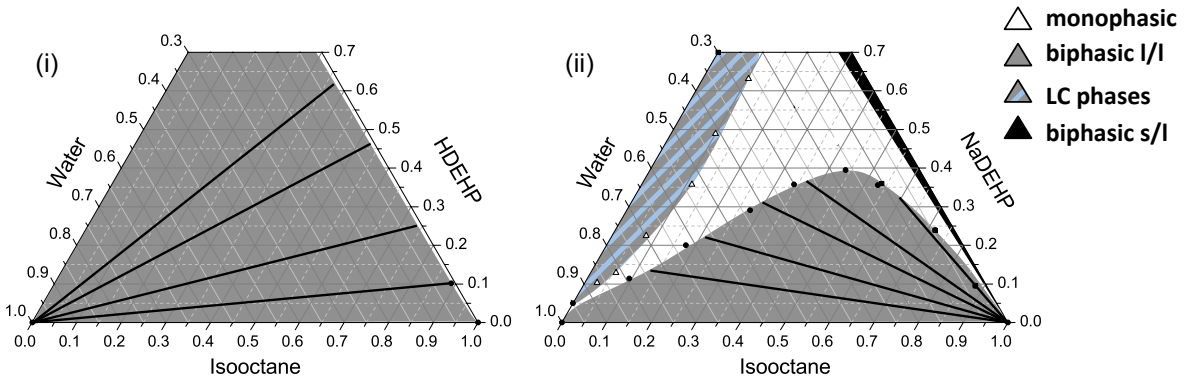

Figure II-25 – Phase diagram of iso-octane/HDEHP/water in wt% (i). Phase diagram of iso-octane/NaDEHP/water in wt% (ii). Tie lines are schematically presented.

In contrast, NaDEHP is insoluble in iso-octane, giving rise to a solid-liquid domain on the solvent-extractant binary edge of triangle. Addition of water results in a transition into a monophasic, clear and transparent solution. On the water-rich side, addition of iso-octane extends LC-regime into the ternary regime. This region is clearly discontinuous with the miscibility gap, separated by a small monophasic channel. The miscibility gap is of type I, which inclines that NaDEHP is capable of closing the gap and a maximum at $\gamma_{extractant} = 39\ wt\%$. The phase boundary on the oil-rich side runs along a constant value of $W_0 = 4$. The tie lines point towards pure oil, hence the biphasic region is a Winsor I-phase. In analogy to toluene, the phase separation is thus due to a splitting of the organic phase.

Overall, the phase behaviour of the ternary systems iso-octane/HDEHP/water and iso-octane/NaDEHP/water vary only little when comparing to isooctane.

4.1.2)Impact of the counter-ion ratio on the development of the phase diagrams

Using iso-octane as solvent, the macroscopic phase behaviour along the prism is presented. First, the results are presented, starting by a brief description on the solid-liquid regime on the solvent-rich side. Then the liquid-liquid regime is evaluated as function of the counter-ion ratio. The tie lines have been omitted due to the pseudo-nature of the phase diagrams.

NaDEHP is not miscible in apolar solvents. This is true for toluene as well as for iso-octane. Successive replacement of the sodium by a proton increases the solubility of NaDEHP in an apolar diluent. Therefore, the solid-liquid regime disappears with decreasing Z. For $Z \leq 0.5$, NaDEHP can be completely solubilized without further addition of water.

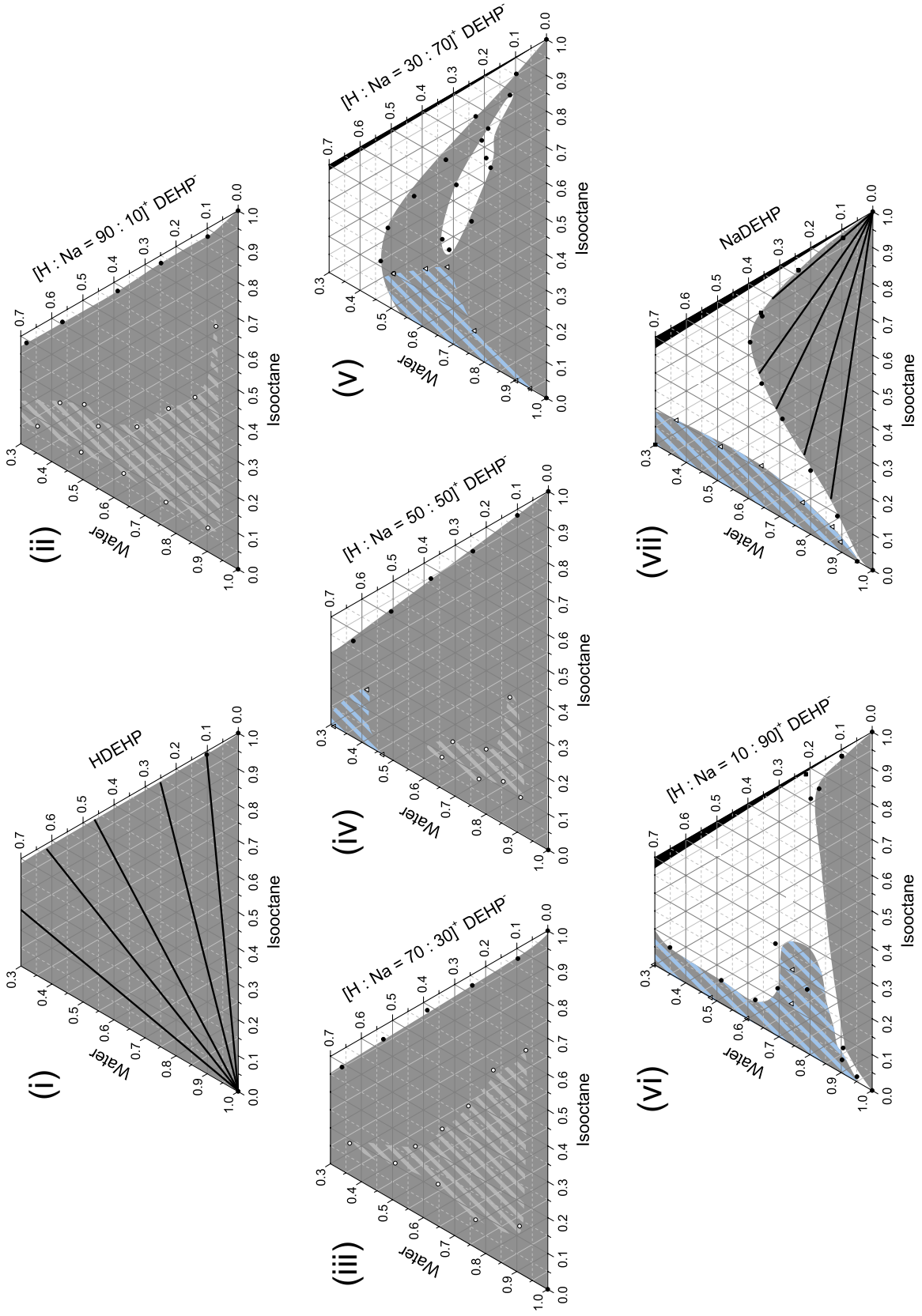

Figure II-26 – Pseudo-ternary phase diagrams of iso-octane/H-Na-DEHP/water in wt% for different ratios of H to Na. (i) $Z = 0$; (ii) $Z = 0.1$; (iii) $Z = 0.3$; (iv) $Z = 0.5$; (v) $Z = 0.7$; (vi) $Z = 0.9$; (vii) $Z = 1$.

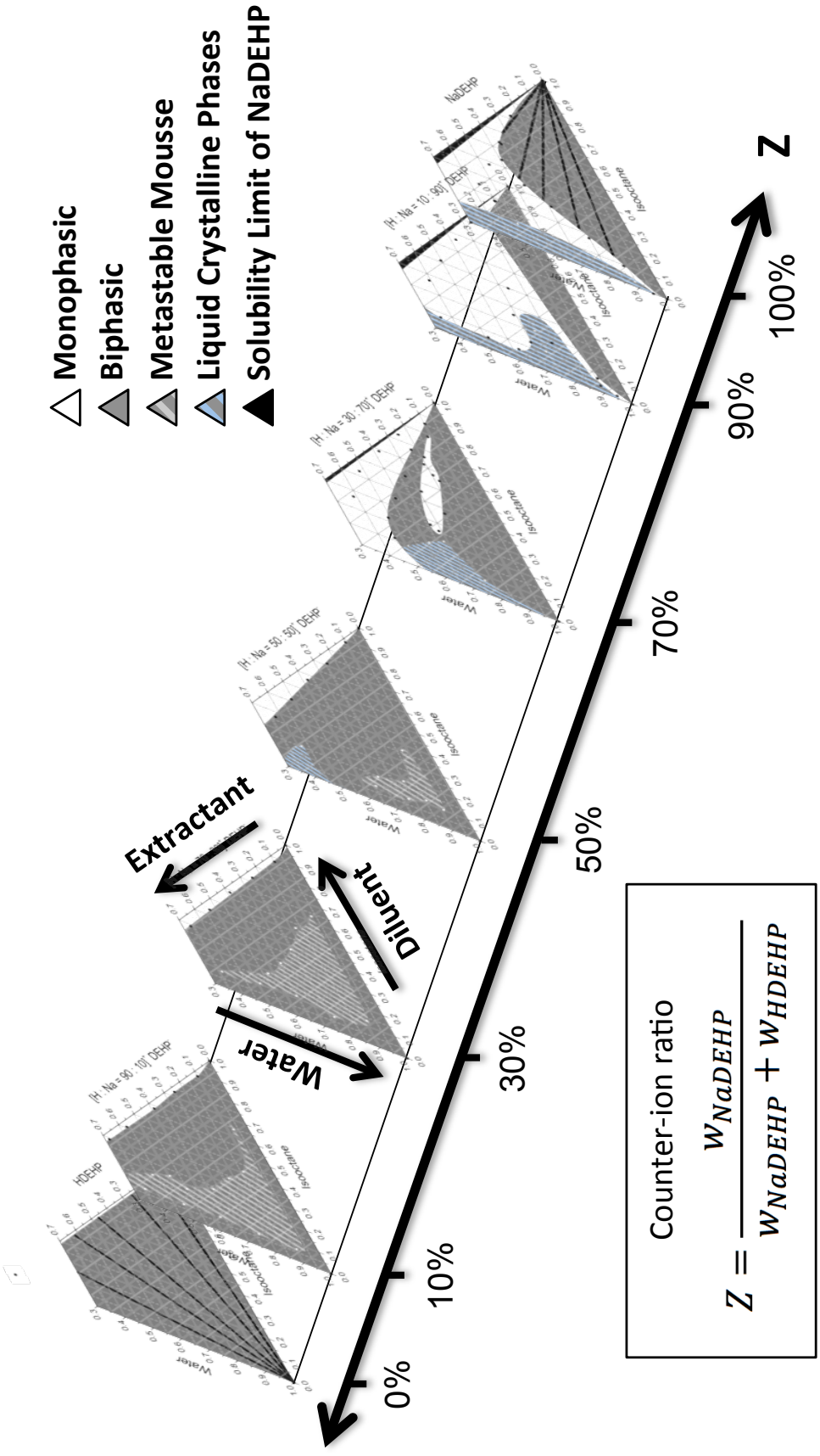

Figure II-27 – Quaternary phase prism of iso-octane/NaDEHP/HDEHP/water. The Z-axis gives the ratio of NaDEHP with respect to the total amount of extractant. 7 phase diagrams for different Z are plotted, including the two "faces" for $Z = 0$ and $Z = 1$.

The miscibility of water on the oil-rich side gradually increases when increasing the counter-ion ratio Z. For $Z = 0.7$, a maximum of the miscibility gap is pronouncing, indicating a transition from a type II to a type I miscibility gap. A drastic increase of the monophasic region is observed for the phase diagram in figure 27(vi) ($Z = 0.9$). This increased miscibility is only partially pronounced in the pseudo-ternary phase diagram where $Z = 0.7$, where a large monophasic lens is located in the centre of the miscibility gap. The formation of a liquid-foam-like third phase, as the case with toluene as solvent, has been detected when adding slight amounts of NaDEHP to the bottom face of the prism (figure 24(ii), $Z = 0.1$) up the half of the prism ($Z = 0.5$), with a decreasing area the higher the sodium content. The evolution of this phase can be best traced in the prism, represented in figure 27.

4.2) Phase behaviour with a poorly penetrating solvent – n-Dodecane

In contrast to iso-octane and toluene, n-dodecane is a long-chained alkane, which poorly penetrates the micellar shell. However, it finds a significant application on an industrial scale, since the vapour pressure is significantly lower compared to short-chained alkanes.

4.2.1)The two faces of the prism – Z = 0 and Z = 1

The ternary phase diagram with dodecane as solvent and HDEHP, depicted in figure 28(i) shows the same phase morphology as observed for the other solvents. Due to the bad solubility of dodecane with water, but a complete miscibility with HDEHP, a large biphasic domain is present in the ternary region. Residual water is expelled from the system and forms an excess aqueous phase, therefore the tie lines are pointing towards water. Thus the biphasic region is a Winsor II-phase. The phase separation is due to an emulsification failure.

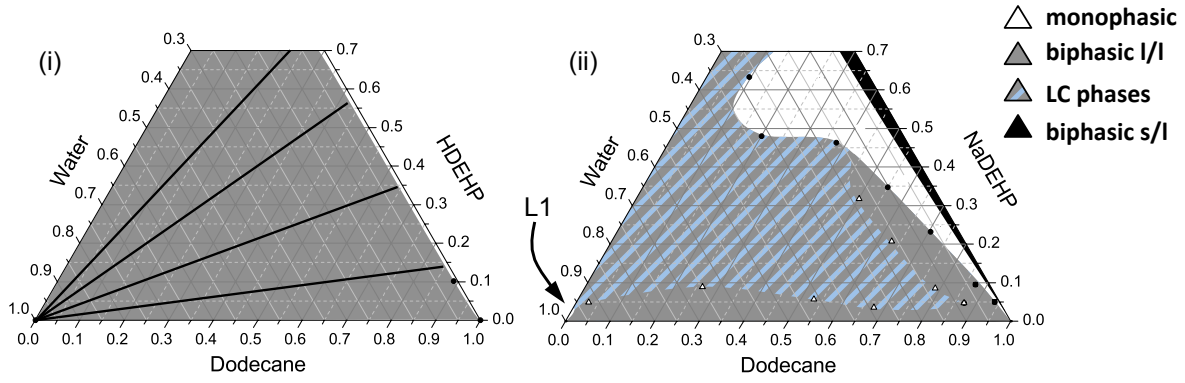

Figure II-28 – Phase diagram of n-dodecane/HDEHP/water in wt% (i). Phase diagram of dodecane/NaDEHP/water in wt% (ii). Tie lines are schematically presented.

The binary phase behaviour of dodecane with NaDEHP further confirms the bad solubility of the NaDEHP in organic diluents. Addition of water however can solubilize the surfactant in dodecane, resulting in a monophasic regime on the oil-rich side of the phase diagram. The phase boundary runs along a constant value of $W_0 = 3.9$. Above $\gamma_{extractant} > 48wt\%$, the miscibility gap is partially closed. However, the regime where lyotropic mesophases have been observed extends in a wedge-like form from the water-rich side towards the oil-rich side (blue-grey shaded area). As a result, the narrow channel connecting the small monophasic region L1 on the water-rich with the microemulsion on the oil-rich side is absent. Due to this odd phase behaviour, the tie lines have been omitted.

4.2.2)Impact of the counter-ion ratio on the development of the phase diagrams

Addition of HDEHP to the top face of the prism gradually decreases the s/l-regime on the n-dodecane-rich side of the phase diagram. For $Z \leq 0.5$, the extractant is completely miscible in n-dodecane for any given ratio. Starting on the bottom face, for $Z = 0$, the monophasic region gradually increases on the solvent-rich side with increasing Z. For $Z \leq 0.7$, a maximum of the miscibility is observed, indicating a transition from a type II miscibility gap towards a type I miscibility gap. However, for higher Z, no transition towards a type I miscibility gap is observer. For $Z = 0.9$, the region where lyotropic phases are observed extends from the water-rich side to the oil rich side. A slight decrease of the monophasic region is detected, however no channel towards the water-rich corner.

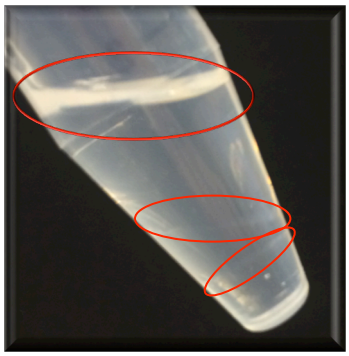

Figure II-29 – Formation of a third phase, where an aqueous and organic phase coexist in the presence of a liquid-crystalline phase. Red circles highlight the three meniscuses.

A surprising feature is the formation of a third phase, as illustrated in figure 29. Instead of a monophasic lens, as observed for Z=0.7 in the prisms with toluene and iso-octane, the solution separates into three phases. This is observed in the phase diagrams in figures 30(v,vi). The bottom phase exerts a high viscosity, indicating that it is a lyotropic phase in equilibrium with an aqueous and organic phase in excess.

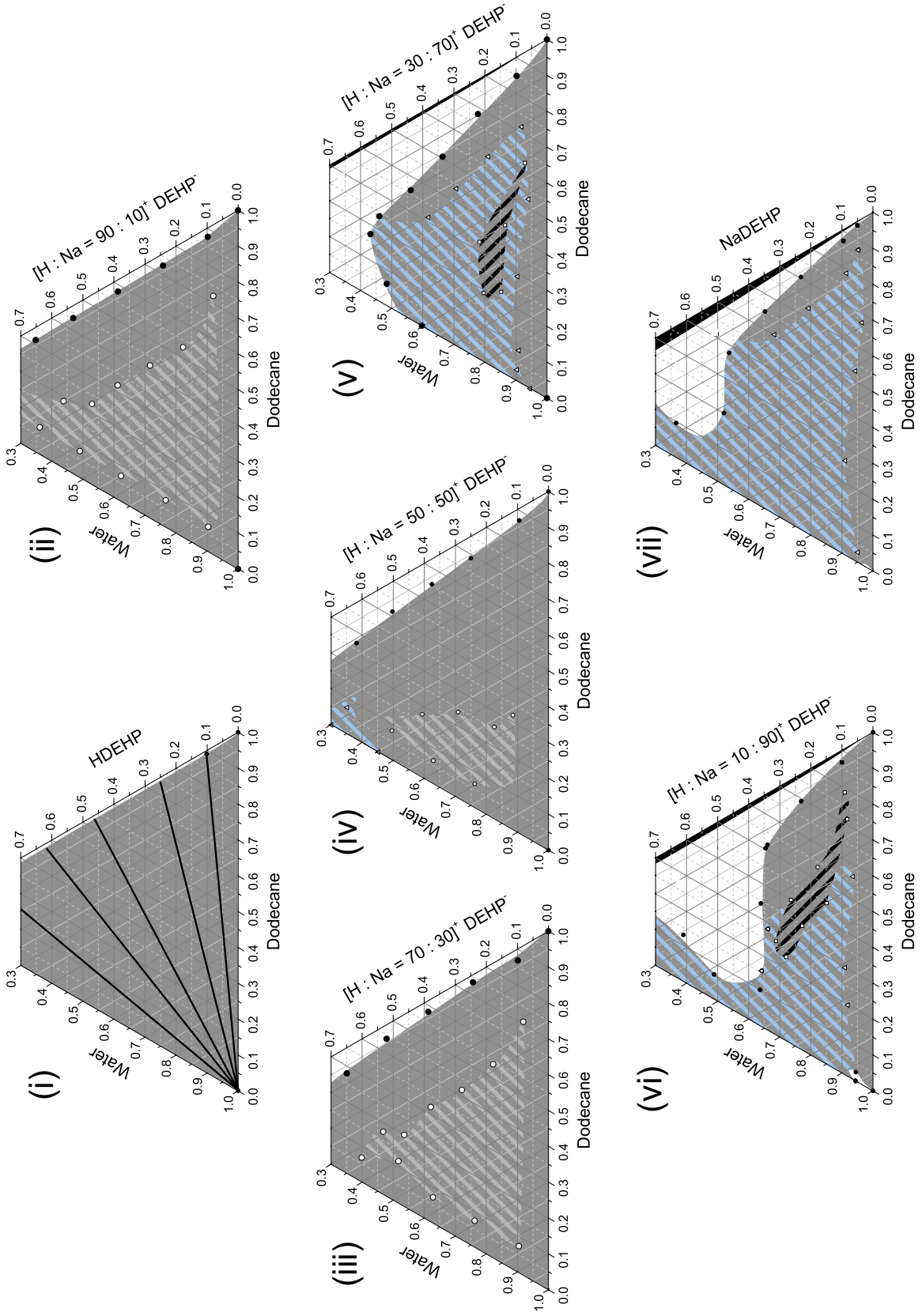

Figure II-30 – Pseudo-ternary phase diagrams of n-dodecane/H-Na-DEHP/water in wt% for different ratios of H to Na. (i) $Z = 0$; (ii) $Z = 0.1$; (iii) $Z = 0.3$; (iv) $Z = 0.5$; (v) $Z = 0.7$; (vi) $Z = 0.9$; (vii) $Z = 1$.

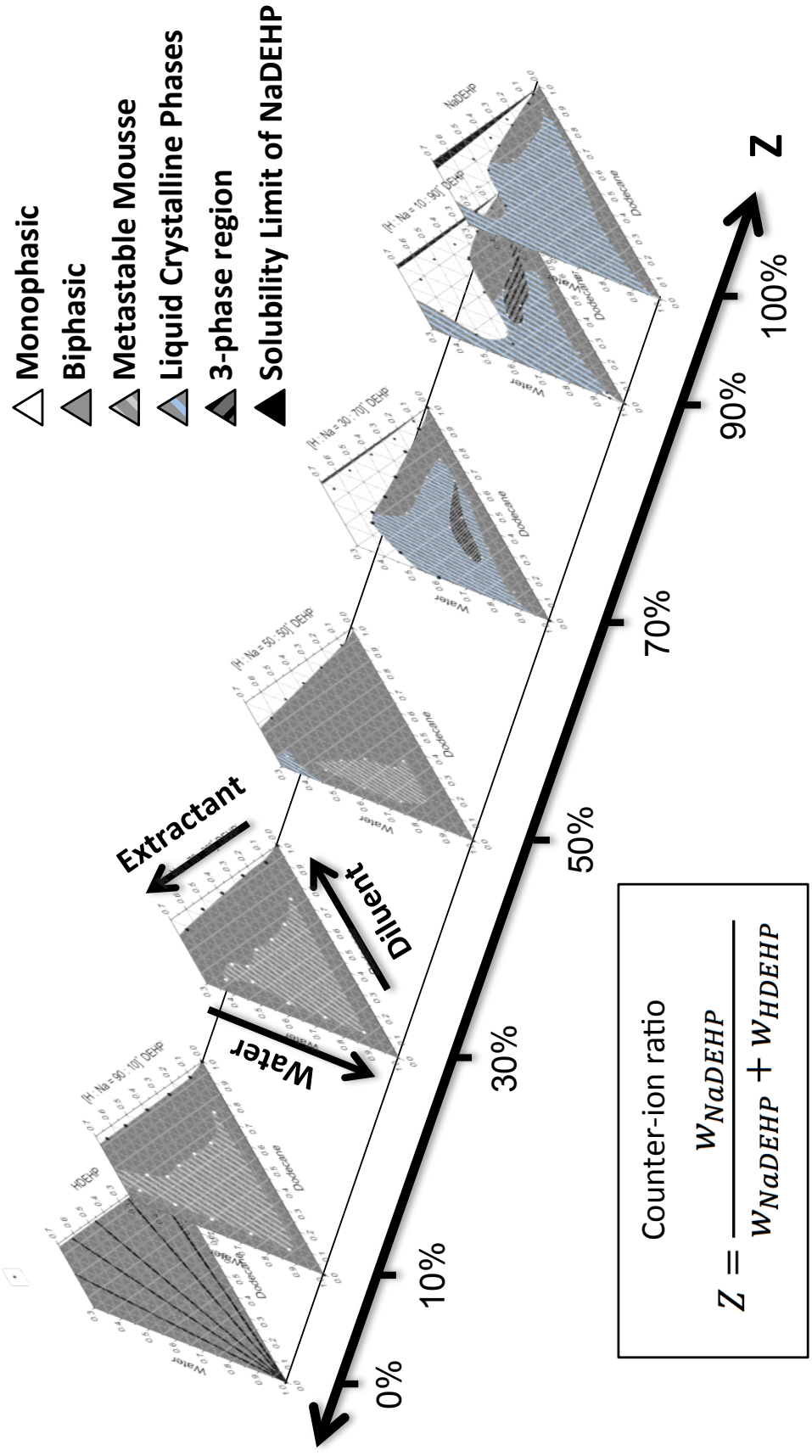

Figure II-31 – Quaternary phase prism of n-dodecane/NaDEHP/HDEHP/water. The Z-axis gives the ratio of NaDEHP with respect to the total amount of extractant. 7 phase diagrams for different Z are plotted, including the two "faces" for $Z = 0$ and $Z = 1$.

4.3) Effect of high polarity – Nitrobenzene

Nitrobenzene is a derivative of toluene, where the methyl group is exchanged by a nitro-moiety. This has a significant effect on the polarity of the molecule, as the dipole moment is at $\mu = 4.03\,D$, whereas toluene has a permanent dipole moment of $\mu = 0.31\,D$.[6] Even though nitrobenzene has a higher dipolar moment than water, the two solvents are basically immiscible ($w_{Nbz\ in\ water} = 0.19wt\%$ and $w_{water\ in\ Nbz} = 0.24wt\%$). Attractive interactions that lead to a splitting of the organic phase are often ascribed to attractive dipole-dipole interactions between micellar cores. Thus, a major interest is whether nitrobenzene is capable of increasing the monophasic region in the frustrated region by screening the electrostatic potential between reverse micelles.

4.3.1)The two faces of the prism – Z = 0 and Z = 1

HDEHP is completely soluble with nitrobenzene, while the solvent is completely immiscible with water. Therefore, and in common with all previous observations for other solvents, water is only soluble in trace amounts in the organic phase. Additional water is excluded from the organic phase to give an additional aqueous phase in excess. This is indicated by the tie lines pointing towards water, as depicted in figure 32(i). Therefore, the biphasic region is a Winsor II-phase and the phase separation due to a maximum swelling of the reverse micelles (phase separation type I, emulsification failure).

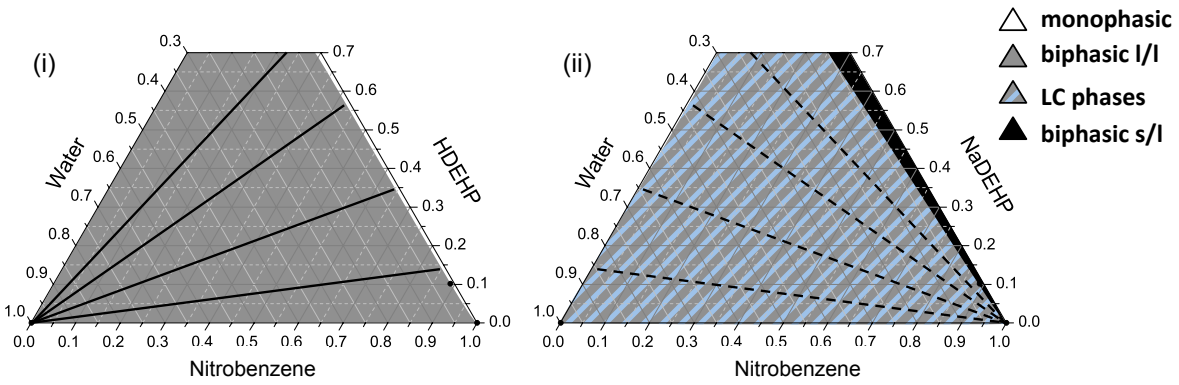

Figure II-32 – Phase diagram of nitrobenzene/HDEHP/water in wt% (i). Schematic representation of the phase diagram nitrobenzene/NaDEHP/water in wt% (ii). Tie lines are schematically presented.

In contrast, NaDEHP is poorly soluble in either nitrobenzene or water. When all three components are present, NaDEHP will form a lyotropic phase with water, with an excess organic phase. The miscibility gap cannot be closed. The only possible explanation for this phenomenon is the high permittivity of nitrobenzene. The high polarity enhances dissociation

of the counter-ion, thus drastically decreasing the solubility of a charged species in an apolar environment.

4.3.2)Impact of the counter-ion ratio on the development of the phase diagrams

In figure 33, three pseudo-ternary phase diagrams are depicted alongside the bottom face of the prism. The macroscopic phase behaviour beyond a counter-ion ratio of Z ≥ 0.7 has been omitted, since no monophasic regimes have been detected and phase diagrams look essentially like the “top face”. The main objective was to elucidate the evolution of the monophasic region, therefore samples on the water-rich side have been omitted and the thorough analysis of the biphasic region, depicted in grey has been neglected. In the prism in figure 34, the “top face” is added for the sake of completeness.

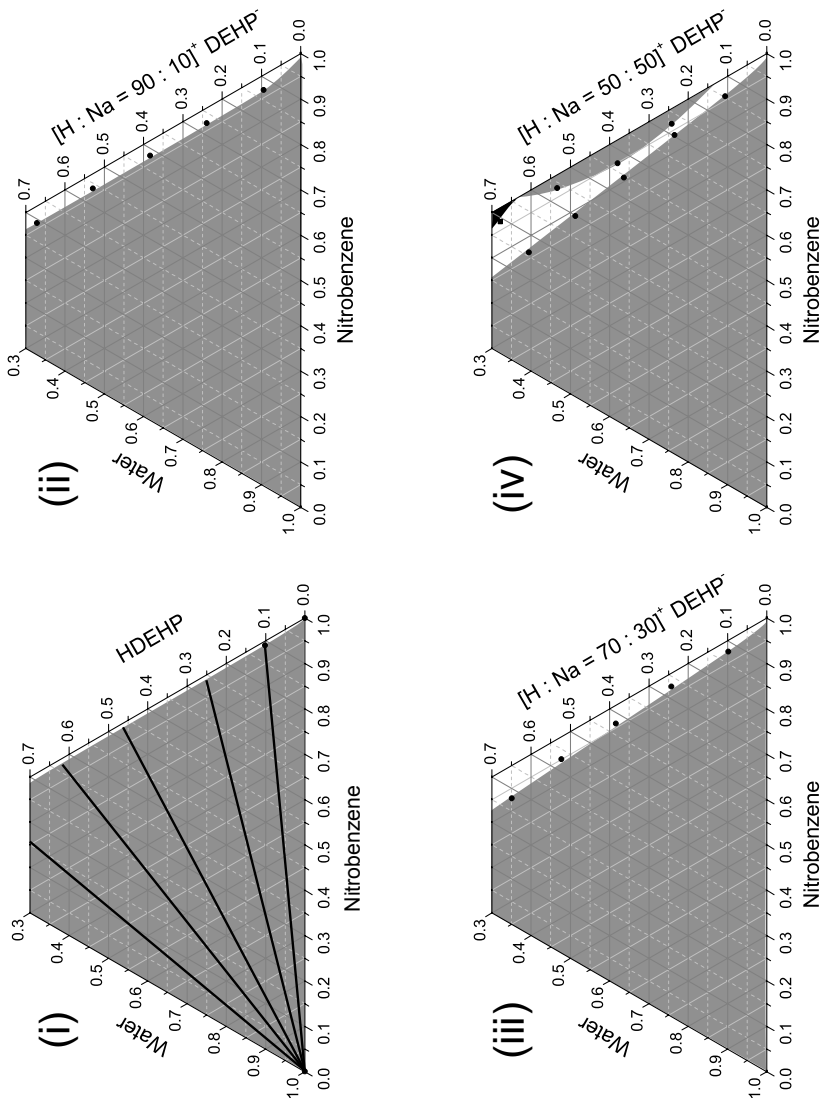

Figure II-33 – Pseudo-ternary phase diagrams of iso-octane/H-Na-DEHP/water in wt% for different ratios of H to Na. (i) $Z = 0$; (ii) $Z = 0.1$; (iii) $Z = 0.3$; (iv) $Z = 0.5$.

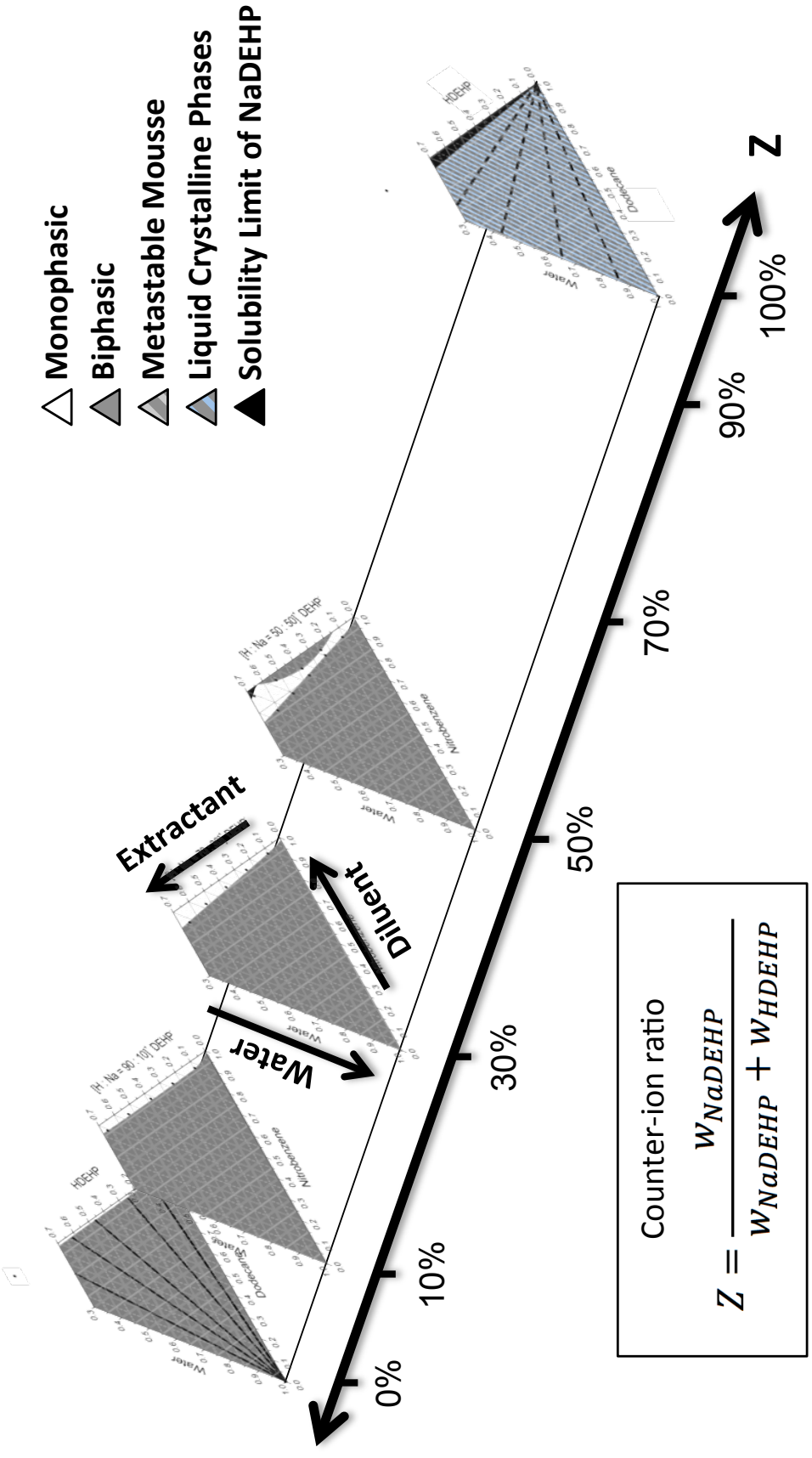

Figure II-34 – Quaternary phase prism of nitrobenzene/NaDEHP/HDEHP/water. The Z-axis gives the ratio of NaDEHP with respect to the total amount of extractant. 5 phase diagrams for different Z are plotted, including the two face for $Z = 0$ and $Z = 1$.

The solubility of water on in the microemulsion increases with increasing Z. The phase boundary runs along a constant W_0-value. For $Z = 0.5$, pseudo-binary solvent-extractant line exhibits a second miscibility gap and upon addition of water, this miscibility gap is closed. Further, at for $\gamma_{extractant} > 55wt\%$, the extractant is not fully soluble in the organic solvent. This confirms the bad solubility of NaDEHP in very polar solvents.

4.4) Comparing the macroscopic phase behaviour as a function of the solvent

For all four solvents, the phase behaviour in the non-frustrated regime, at low counter-ion ratios is identical: the solubility of water in an organic solvent containing pure HDEHP is very low. Increasing the counter-ion ratio Z gradually increases the solubility of water in the microemulsion and the phase boundary runs along a constant W_0-value. This confirms that the origin for phase separation is due to a maximum swelling of reverse aggregates. Further addition of water leads to the formation of an excess aqueous phase.
A significant difference is observed for $Z > 0.5$, where the microemulsion is classified as *frustrated.* The biggest monophasic region is observed for toluene. For the *theta solvent* iso-octane a smaller monophasic regime is detected, nevertheless a continuous path from the water-rich side to the solvent-rich side can be drawn for $Z \geq 0.9$. In contrast, using the poorly penetrating solvent dodecane, the miscibility gap cannot be closed, but large domains of lyotropic phases are observed, as well as a regime where even three phases are present. Using a highly polar solvent (nitrobenzene), the surfactant NaDEHP is unable to form a "frustrated microemulsion" and only lyotropic phases are observed in equilibrium with an excess organic phase.

The phase separation in the frustrated branch is mainly due to attractive interaction and given the strong deviation of the macroscopic phase behaviour for different solvents it can be concluded that the solvent has a significant impact on the stability of a microemulsion in this region. The nature of these interactions can be of different origin and to the best of our knowledge no discrete identification of different types of interactions is present in literature.

In the frame of solvent extraction, the attractive potential that drives metallo-amphiphilic solutions towards the formation of a third phase is assigned to a dipole-dipole attraction between polar cores.[36,116,178] Thus, when using a slightly polar diluent (e.g. toluene with a permittivity of $\varepsilon = 2.2$ compared to alkanes with a permittivity of $\varepsilon = 1.8$), these electrostatic

interactions can be screened to a certain degree and thus increase the solubility in the frustrated regime. This explains why the miscibility gap for $Z \geq 0.9$ is significantly smaller for toluene than iso-octane. For Aerosol OT, Huang *et al.* proposed a model showing that if the hydrophobic shell is badly penetrated, interactions of overlapping shells is highly favourable.[179] Therefore, a "stickiness" between reverse micellar aggregates may not only arise from interactions between the core. Besides screening of the electrostatic, the attractive interactions can be prevented increasing the hard-sphere radius of a reverse aggregate. An important factor is the penetration properties of a solvent. Partial occupation of the apolar volume of a reverse micelle by the solvent increases the hard-sphere radius and thus the sterical repulsion between aggregates. However, the residence of a solvent molecule in the hydrophobic shell is favourable from an enthalpic point of view, if the molecule is able to interact well with the apolar chains. However, from an entropic point of view, the solvent molecule has less degree of freedom, as this volume is confined.

In case of long-chained alkanes, penetration of the shell can be highly unfavourable from an entropic point of view, leading to an additional "attractive force" which we will compare to depletion forces known form colloidal systems.
In a first approximation, dodecane can be considered as a stiff cylinder. Using the tanford-approach to calculate the length l of the cylinder yields:[60]

$$l_{dodecane} = 2 \cdot 0.15\ nm + 10 \cdot 0.127\ nm = 1.57\ nm \qquad (xii)$$

Further, the volume V can be deduced using the molecular volume of moieties, presented by Fedor:[180]

$$V_{dodecane} = 2 \cdot 0.056\ nm^3 + 10 \cdot 0.027\ nm^3 = 0.38\ nm^3 \qquad (xiii)$$

With the volume and the length, the radius R of the cylinder can be determined

$$V_{cylinder} = 2\pi R^2 l \Leftrightarrow R_{cylinder} = \sqrt{\frac{V}{2\pi l}} = 0.2\ nm \qquad (xiv)$$

Therefore, the radius of gyration for a cylinder gives and the respective diameter d can be calculated as

$$R_G = \sqrt{\frac{R^2}{2} + \frac{l^2}{12}} = 0.47\ nm \Rightarrow d_{dodecane} = 2 * R_G = 0.94\ nm \qquad (xv)$$

The shell of a reverse aggregate with NaDEHP as a surfactant will have the aliphatic chains oriented towards the outside, therefore, irrespective of the actual shape of the aggregate, the thickness of the shell l_{shell} can be approximated by the length of the apolar moiety,

$$l_{shell} = 0.15\ nm + 5 \cdot 0.127\ nm = 0.785\ nm \qquad (xvi)$$

Since the diameter of the solvent is superior to the thickness of the film, the origin of the attractive force can be explained by the appearance of depletion forces, visualized in figure 35.

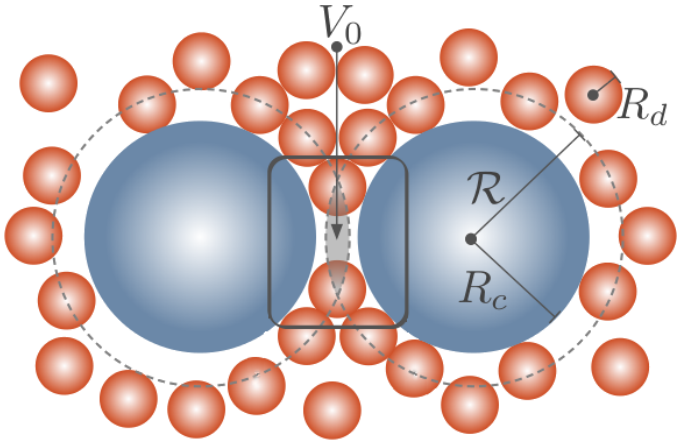

Figure II-35 – Schematic representation of attractive depletion forces of two colloids in the presence of smaller aggregates.[181]

Considering dodecane as a small entity, which is incapable of penetrating the shell of a reverse aggregate, the reduced osmotic pressure in the excluded volume when the shell of two aggregates overlap, induces a net attractive force on the two colloids.

When using a too polar solvent, dissociation of the counter-ion inhibits a solubility of the extractant in the apolar phase.

5. Conclusion

In order to analyse the macroscopic phase behaviour of a metal-extracting microemulsion, the essential ingredients have been identified and a model system has been determined: water and solvent for the respective aqueous and organic phase, and an extractant in a non-extracted form (HDEHP) and engaged in the extraction of a cation (NaDEHP). We defined the ratio of the two forms as the counter-ion ratio Z.

In the first part of this chapter, using toluene as a “reference solvent”, the macroscopic phase behaviour was evaluated as a function of the counter-ion ratio. Starting with the two “faces” of the prism & $Z = 1$), two main mechanisms for phase separation have been identified: the emulsification failure and the liquid-gas separation. Further, the liquid-liquid regime in the bottom face ($Z = 0$) is a Winsor II-phase, while it is a Winsor I-phase in the top face ($Z = 1$). The transition between the converse nature of the two faces has been analysed using the prism analysis introduced by Kahlweit for non-ionic surfactants.[90] Along the prism, HDEHP has been identified as a co-surfactant, which increases the solubility-properties of the surfactant (NaDEHP). The χ-cut analysis allowed correlating the regions where phase separation is dominated by interactions between aggregates on a mesoscopic scale with the concept of *frustration.* The packing parameter of the aggregates is dissimilar to the spontaneous packing. Therefore, the microemulsion is *frustrated* and attractive interactions can be attributed to the urge to have locally lamellar curvatures. Further, the tie lines in quaternary regime are not in the same plane as the initial pseudo-compositions, but different solubility of NaDEHP and respectively HDEHP in the two solvents leads to an uneven distribution between the two phases. Thus, the tie lines have to be 3-dimensional.

In the second part, the macroscopic phase behaviour of the prism is analysed as a function of alternative solvents. In the non-frustrated regime, where aggregates poorly interact with each other, the choice of solvent has nearly no effect on the macroscopic phase behaviour. In the frustrated regime, where the phase separation is driven by interaction between aggregates, the choice of solvent has a significant effect. Different types of attractive interactions have been identified in literature in order to explain the (in-)stability domains, however the results only allow a qualitative statement.

In conclusion, this model system will help understanding the phase behaviour of metal-extracting microemulsions, in particular adaptive for rare-earth elements. In chapter III, we will exploit these maps, in order to understand the conducting along well-chosen dilution lines along the prism. In chapter IV, a link between the model and an actual extracting microemulsion is discussed.

Chapter III

Exploring the conducting properties of a metal-extracting microemulsion

1. CONDUCTIVITY IN IN SOLVENT EXTRACTION SYSTEMS 105

1.1) THE ROLE OF CHARGED AGGREGATES IN SOLVENT-EXTRACTION 105

1.2) EXPERIMENTAL CONSIDERATIONS 107

1.2.1) A concise introduction in physically relevant dilution lines 107

1.2.2) Conductivity in the model system with the "reference" solvent toluene 110

2. DILUTION TOWARDS WATER 111

2.1) THE NON-FRUSTRATED REGION – Z = 0.5 111

2.1.1) Conductivity in the non-frustrated regime 111

2.1.2) Origin of the conductivity signal in the non-frustrated regime 112

2.2) THE FRUSTRATED REGION – Z = 1 113

2.2.1) Conductivity in the frustrated regime 113

2.2.2) Is the sharp increase in conductivity a percolation phenomenon? 114

2.2.3) Plotting the conductivity in reduced units 116

2.2.4) Origin of the sharp increase in conductivity 118

3. DILUTION TOWARDS OIL 120

3.1) THE NON-FRUSTRATED REGION – Z = 0.5 120

3.1.1) Conductivity in the non-frustrated regime 120

3.1.2) Qualitative interpretation of the scattering signal 123

3.1.3) Origin of the conducting signal 123

3.2) CONDUCTIVITY IN FRUSTRATED REGION – Z = 1 125

4. CONDUCTIVITY FOR INTERMEDIATE Z 129

5. CONDUCTIVITY AS A FUNCTION OF THE COUNTER-ION VARIATION Z 131

6. CONCLUSION 134

1. Conductivity in solvent extraction systems

1.1) The role of charged aggregates in solvent-extraction

One of the main objectives of the ERC-project REEcycle is to gain a comprehensive understanding of the fundamental driving forces in solvent extraction formulations. The colloidal approach describes the free energy of transfer $\Delta_{trans}G$ as a sum of multiple equilibria:[10]

$$\Delta_{trans}G = \Delta_{comp}G + \Delta_{LRI}G + \Delta_{bend}G + \Delta_{sol}G + T\Delta S \qquad (i)$$

The term $\Delta_{comp}G$ takes into account the free energy for formation of a complex, i.e. self-assembly of extractant molecules around a desired metal-cation. The bending energy, which defines the properties of the interfacial film, between the "pseudo-aqueous" phase inside the micelle and the organic phase, is comprised in the term $\Delta_{bend}G$, as introduced in Chapter I. The term $\Delta_{sol}G$ describes the cohesion energy that has to be overcome in order to form a cavity in the diluent. The entropic term $T\Delta S$ takes into account the degrees of freedom from different configurations of complexation. If a metallo-amphiphilic complex has a higher aggregation number (i.e. number of extractants participating in formation of an aggregate) than complexation number (i.e. number of extractants directly coordinating the metal-cation), the encapsulated cation can swap its coordination-partners.

The term of interest in this equation is the one assembling the possible interactions between aggregates: $\Delta_{LRI}G$ comprises all types of long-ranged interactions between reverse complexes and are the origin of non-ideal behaviour, e.g. due to electrostatics, dispersion and hydration forces. Water-poor reverse aggregates in an organic solvent have always been assumed to be electrically neutral. Therefore, the electrostatic term only takes into account multi-pole interactions. Yet, since the work of Weitz *et al.* there is a great consensus that reverse micellar solutions may produce charged aggregates arising from a dismutation mechanism.[182] Examination of a binary AOT-dodecane solution revealed a linear increase of the specific conductivity. It has been evaluated by the formula:

$$\sigma = \frac{e^2 n_{ion}}{6\pi\eta a_h} \qquad (ii)$$

With the elementary charge e, the viscosity η and the hydrodynamic radius a_h. In this equation, the conductivity is thus proportional to the number of charged micelles n_{ion}. Further, he deduced that the fraction of charged micelles is constant and in the range of $\alpha = n_{ion}/n_{tot} = 1.2 \cdot 10^{-5}$.

In solvent extraction, the conductivity of an organic solvent has rarely been in the focus of interest, which is a result of the assumption that reverse micelles are electrically neutral. However, Erlinger *et al.* reported a significant increase in conductivity in the organic phase of a solvent extraction system.[34] For the system DMDBTDMA in n-dodecane, used in the DIAMEX process of the French CEA, increase of acid concentration in the aqueous phase leads to a splitting of the organic phase. The extractant co-extracts nitric acid into the organic phase and above a critical value of $c(HNO_3)_{org} = 0.5\, mol/L$, the formation of a third phase is observed. As shown in figure 1, the conductivity increases by 3 orders of magnitude in the order of $\sigma = 10^{-5}\, S/m$, just before splitting of the organic phase. Yet, aside from correlation of an increase in conductivity when approaching the third phase, the origin for this conductivity could not be explained.

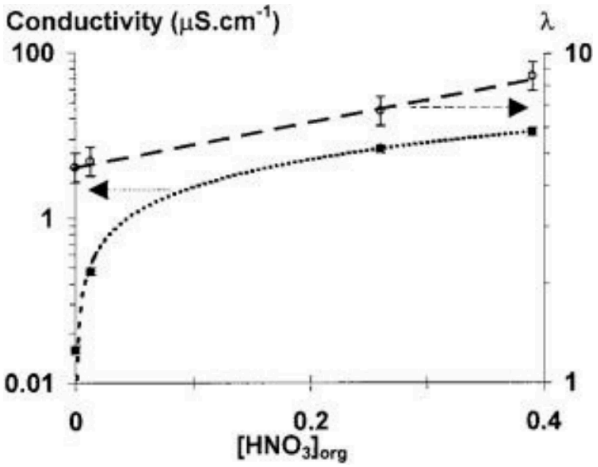

Figure III-1 – Conductivity of the organic phase (squares, dotted line) for the solvent extraction system DMDBTDMA as a function of the co-extracted nitric acid concentration in the organic phase. Figure taken from [178].

As a result of the poorly documented conducting profile of apolar solutions, the primary objective of this work is to map the conducting behaviour of a metal-extracting microemulsion in the water-poor regime. With help of the phase prism and the χ-cut analysis, the aim is to rationalize the conductivity as observed in the monophasic regions in terms of frustration, shape and size of aggregation.[154] To the best of our knowledge, a clearly represented

mapping of different conducting regimes is not available and will be of great help identifying the origin of phase behaviour, e.g. the third-phase formation, as well as fundamentally supporting the general equation for the free energy of transfer.

1.2) Experimental considerations

1.2.1)A concise introduction in physically relevant dilution lines

From an experimental point of view, measuring the conductivity in the monophasic regions of the prism is the most straightforward approach.[167] Dilution along a monophasic pathway can be entirely controlled and offers an easy experimental preparation. Every point of the prism can be defined as a set of the three variables α, γ and Z.[90] However, three different types of dilution lines are of considerable interest, as they modify specific internal parameters of the microstructure.

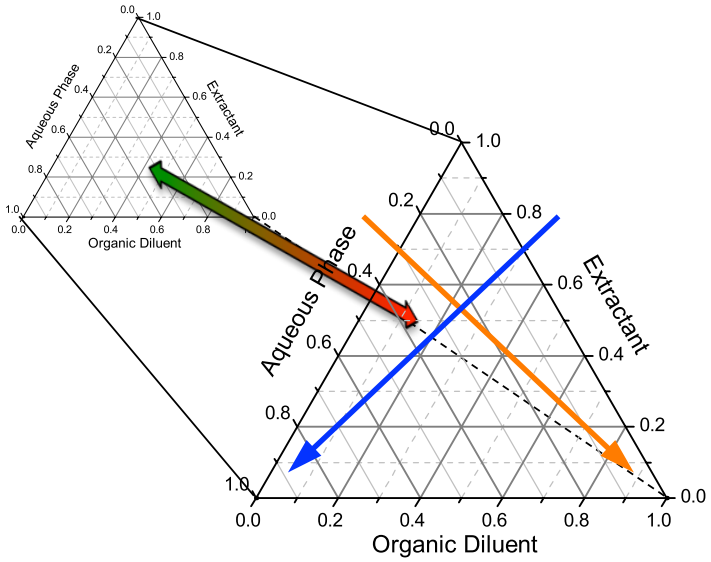

Figure III-2 – Representation of the three dilutions paths that will be compared: dilution with water (blue arrow), dilution with solvent (orange arrow) and variation of the counter-ion mole ratio, everything else being constant.

a) Dilution line towards water – blue arrow in figure 2

In reverse micellar solutions, the main factor determining the size of an aggregate is the volume-fraction of the dispersed phase.[165] Diluting a binary extractant-solvent solution with water is always decreasing the packing parameter p. Aggregates with a reverse spherical geometry $(p = 2 - 3)$ swell to large aggregates, which implies that the curvature of the interface is decreasing. At high contents of water, the spherical aggregates coalesce and form a bicontinuous regime, which can be described by the model of disconnected open

cylinders or lamellae. Here, the packing parameter is at $p = 1$.[79] As a result of bicontinuity, charged entities may move freely in a continuous water-environment, giving rise to a drastic increase in conductivity, related to percolation.[104,183,184] The progress along this dilution line is expressed as the ratio of the number of water molecules to the number of surfactant molecules W_0:

$$W_0 = \frac{n_{water}}{n_{amphiphile}} \qquad (iii)$$

With n_i as the number of molecules of component i. In microemulsion systems where a co-surfactant is necessary to enhance emulsification properties of the surfactant, different adaptations of this equation are possible, depending on whether the co-surfactant is included in the denominator. For this work, we will include the "co-extractant" HDEHP into this equation:

$$W_0 = \frac{n_{water}}{n_{HDEHP} + n_{NaDEHP}} \qquad (iv)$$

This approach facilitates the comparison of the conductivity profiles at different counter-ion ratios. In return, the ratio of extractant to solvent is constant and will be expressed as S_0^*:

$$S_0^* = \frac{w_{extractant}}{w_{extractant} + w_{diluent}} \qquad (v)$$

Where w_i is the mass fraction of component i.

b) Dilution line towards oil – orange arrow in figure 2

On a dilution line towards oil, the ratio of water-to-surfactant W_0 is constant. Neglecting interactions between clusters (also referred to as inter-cluster interactions (ICI)[37]), the mean aggregation number N_{Agg} is constant and only the number density varies (as in direct micellar systems, introduced in Chapter I). This means that the packing parameter p, as well as the curvature H of an aggregate is constant. A general effect of the dilution towards the solvent and seeing "bound" species within an aggregate decrease is to evaluate the enthalpy of binding in micelles.[185] In our case, not only the presence of aggregates will be accessed, but also their ability to transport the charges present. The motivation to rationalize the conductivity along this dilution line is therefore ion one hand to verify if a critical micellar concentration can be detected and on the other hand if the conductivity can be correlated with interactions between aggregates.

c) Variation of Z – green/red arrow in figure 2

As introduced in Chapter II, the counter-ion ratio Z defines the progress of an extraction. The more the extractant is engaged in complex formation, the higher Z. Further, it was concluded from the cut-analysis, that Z can be viewed as an analogon to the temperature in surfactant systems, since the spontaneous packing parameter p_0 decreases with increases Z, as well as the solubility of NaDEHP decreases in the organic phase.

In surfactant systems, percolation occurs not only above a critical concentration of water, but also by modification of the temperature (non-ionic surfactants) or salinity (ionic surfactants) leads to a percolation of the microstructure.[186,187]

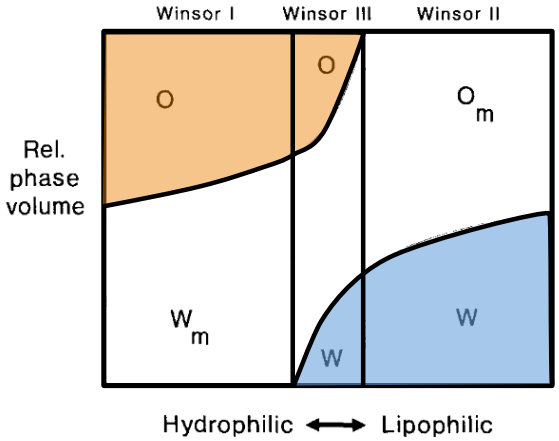

Figure III-3 – Changing the solubility of a surfactant by modifying the temperature or salinity can transform a Winsor II microemulsion into a Winsor I microemulsion by passing through a Winsor III-regime. Taken from [19].

As demonstrated in figure 3, a lipophilic surfactant prefers to form a Winsor II-phase, i.e. discrete reverse aggregates in equilibrium with an excess aqueous phase. Changing the temperature or adding salt modifies the solubility of the surfactant. The microemulsion is transformed into a Winsor I-phase. In-between these two phases, as defined in Chapter I, the system crosses a Winsor III-phase, where the morphology on a mesoscopic scale is bicontinuous. Therefore, the transition from Winsor II to Winsor III and Winsor III to Winsor I can also be described by percolation.[188] As a consequence, it is of great interest to see whether the conductivity shows the same behaviour when plotted against the counter-ion ratio Z.

1.2.2)Conductivity in the model system with the “reference” solvent toluene

Using the pseudo-ternary phase triangles, which have been evaluated in Chapter II, we can now chose specific paths along the prism in order to study the conductivity behaviour as a function of three identified dilution lines. As rationalized in the χ-cut, the monophasic region on the oil-side can be divided into two branches of the prism: for $Z < 0.85$, the microemulsion is non-frustrated, for $Z > 0.9$ it is frustrated, illustrated in figure 4.

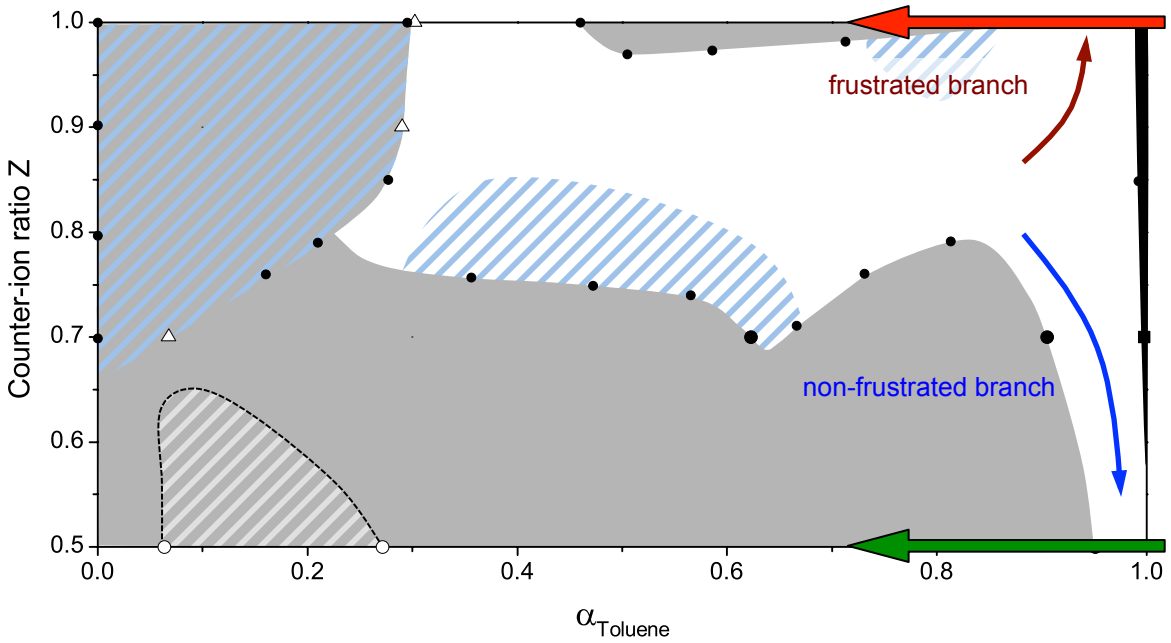

Figure III-4 – Partial χ-cut for the quaternary system toluene/HDEHP/NaDEHP/water in the range of $0.5 \leq Z \leq 1$. The same colours as in the previous chapter for frustration (wine red) and non-frustrated (blue) has been maintained and depicted by the arrows. The green and red arrows indicate the conductivity paths analysed in this section.

In a comparative study, the first sub-section addresses the conductivity in the frustrated (pseudo-ternary phase diagram: $Z = 1$) versus non-frustrated (pseudo-ternary phase diagram: $Z = 0.5$) region when diluting a binary solvent-extractant mixture with water (blue dilution line in figure 2). In the second sub-section, the conductivity profiles towards the oil-rich corner are investigated for the same phase diagrams (orange dilution line in figure 2). The conductivity in the pseudo-ternary phase diagram where the maximum solubility of water and oil was observed is in the focus of interest in the third sub-section ($Z = 0.9$). Last, the evolution of the conductivity is determined as a function of the counter-ion ratio.

The scope of this chapter is to probe the conducting behaviour for an extracting microemulsion using the model system. As a function of the three demonstrated dilution lines, the monophasic region is extensively screened for the “reference” solvent toluene.

2. Dilution towards water

2.1) The non-frustrated region – Z = 0.5

2.1.1)Conductivity in the non-frustrated regime

In the non-frustrated branch, the packing parameter p of the extractant is close to the spontaneous packing p_0. In figure 3, the phase diagram of toluene/NaDEHP/HDEHP/water with a counter-ion ratio of $Z = 0.5$ is depicted. The conductivity was measured along a dilution line towards water in the monophasic region is illustrated by the blue triangles for an initial extractant-to-solvent ratio of $S_0^* = 0.5$.

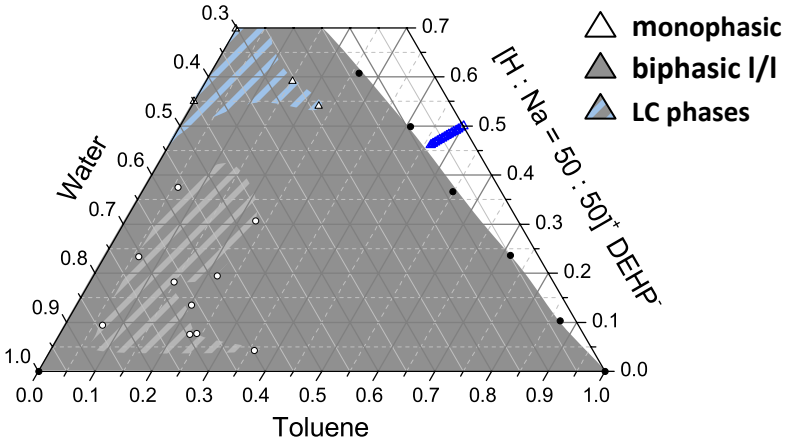

Figure III-5 – Pseudo-ternary phase diagram of toluene/NaDEHP/HDEHP/water with indication of conductivity path in the monophasic region (blue triangles). One dilution line for S_0^* = 0.5.

The phase separation upon crossing the phase boundary towards the multiphasic regime (beyond the white monophasic domain) is an emulsification failure. Hence the internal phase (water) is expelled to form an excess aqueous phase.

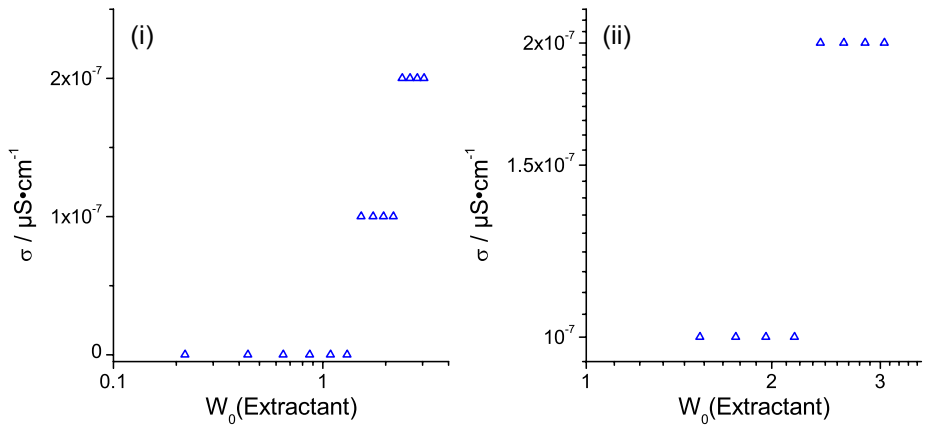

Figure III-6 – Specific conductivity in a non-frustrated extracting microemulsion as a function of the water-to-extractant ratio W_0. (i) lin-log representation; (ii) log-log representation.

The conductivity along the dilution line in the phase diagram (blue triangles) is depicted in figure 6. Upon dilution with water, the conductance of the solution increases slightly, but the conductivity-signal is just above the limit of detection ($\sigma_{LOD} = 1 \cdot 10^{-7}\, S/cm$). Hence, the numerical value indicated should be handled with care. Nevertheless the slight increase of conductivity observed upon approaching the phase boundary is real.

2.1.2)Origin of the conductivity signal in the non-frustrated regime

The conductivity in apolar solvents has been reported to be in the order of $\sigma_{organic\ solvent} = 10^{-16} - 10^{-12}\, S/cm^2$.[189] From a physical point of view, the conductivity in apolar media is zero, since no charge carriers are present. Nevertheless, the fact that conductivities in the pS/cm-regime are measured is mostly a result of impurities solubilized in an apolar media.[93]

The conductivity in the non-frustrated regime in figure 6 is far below the conductivity measured in aqueous systems,[190] or in bicontinuous percolated microemulsion microemulsions,[191] where ions can move freely in a continuous medium with high permittivity.[187] Nevertheless, the conductivity is several orders of magnitude above the conductivity of pure apolar liquids, which is a sign that low concentration of charge carriers is present. The specific conductance of reverse micellar media, before the onset of percolation, has been reported to be in the order of $\sigma = 10^{-8}\, S/cm$ for the system dodecane/AOT/water,[192] and $\sigma = 10^{-7}\, S/cm$ for chlorobenzene/alkylbenzydimethyl-ammonium chloride/water.[193] The question therefore is: what is the origin of the conductivity discrepancy between a pure apolar solvent and the reverse micellar solutions investigated along the blue dilution path towards water?

The only possibility is the formation of charged micelles through a dismutation process, as depicted in figure 7, that was reported by Weitz *et al.*[182]

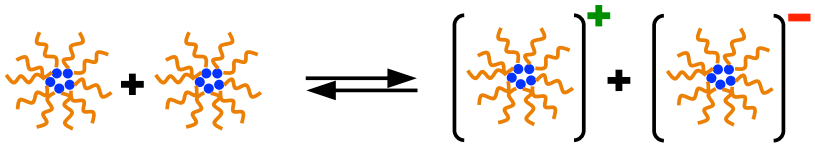

Figure III-7 – Dismutation mechanism of reverse micelles.

Upon collision of two reverse micelles, exchange of material can lead to formation of charged aggregates.[182] The resulting conductivity has been reported to be in the $pS/cm - nS/cm$ regime for very dilute binary surfactant/solvent systems.[194] As the concentration of extractant is high in this experiment ($S_0^* = 0.5, c(extractant) = 1.25\, mol/L$) this may explain why the

specific conductance is one 1-2 orders of magnitude higher. The formation of charged micelles has been further confirmed analysing transient currents of binary solvent-surfactant solutions.[195]

2.2) The frustrated region – Z = 1

2.2.1) Conductivity in the frustrated regime

In the frustrated region, the effective packing parameter p, imposed by the microstructure without tearing of the film of the extractant, is far to the spontaneous packing p_0. Despite the molecular geometry of NaDEHP, which favours a curvature towards water, the surfactant has a higher activity in the organic phase, hence preferring to solubilize in the aqueous phase, if water and oil are both present. As a consequence, monophasic oil-rich compositions of toluene/NaDEHP/water are *frustrated*. The phase separation approaching the phase boundary is to attractive interactions, thus leading to a liquid-gas phase separation.

In order to cover not only the conductivity in the channel on the oil-rich side (for $\gamma_{extractant} < 33wt\%$), but also the microemulsion regime at intermediate $\alpha_{toluene}$, three dilution lines by water at $S_0^* = 50wt\%, 25wt\%$ & $10wt\%$ have been analysed, as depicted in figure 8.

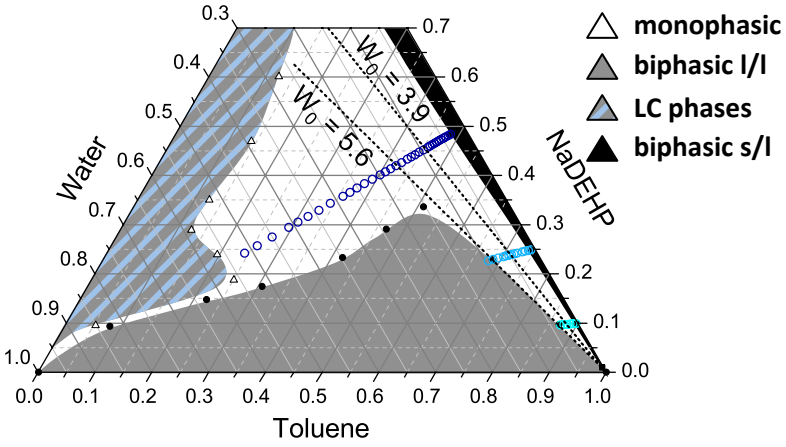

Figure III-8 – Ternary phase diagrams of toluene/NaDEHP/HDEHP/water with indication of conductivity pathways in the monophasic region. Three dilution lines for $S_0^* = 0.5$ (navy blue), 0.25 (blue) & 0.1 (light blue). The two changes of the slope of the conductivity measurement at water-to-solvent ratios are added in this plot for a more visual representation.

The phase boundary from monophasic to biphasic upon dilution with water has been recorded at $W_0 = 5.6$ for $S_0^* = 0.1$ and $W_0 = 7.8$ for $S_0^* = 0.25$. For $W_0 < 1.1$, no conductivity is recorded, since the system is in the insolubility-regime of NaDEHP in toluene (zone depicted in black).

In figure 9, the specific conductivity of these dilution lines is depicted in lin-log and log-log representation as a function of the water-to-extractant ratio W_0.

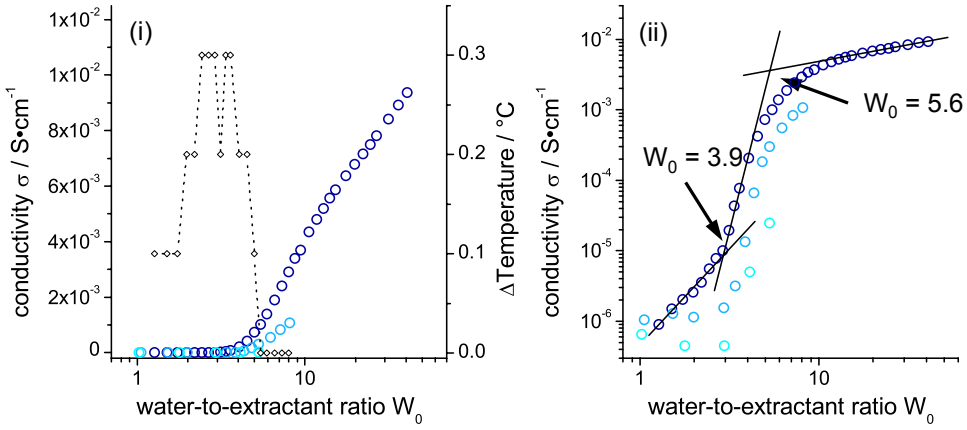

Figure III-9 – The specific conductivity plotted as a function of W_0. (i) lin-log-scale: illustration of increase in temperature, upon addition of water: the clear inflection at $W_0 = 3.9$ is the origin of the first hydration layer concept in micellar systems. (ii) log-log scale: this scale allows identifying the three different conduction regimes involved (see text). All measurements were carried out at $T = 25\,°C$.

In the lin-log representation in figure 9(i), the specific conductivity for $W_0 < 3.9$ is very low and in the order of $\sigma = 10^{-6}\,S/cm$. The conductivity drastically increases by 2-3 orders of magnitude above $W_0 > 3.9$ for all three dilution lines. The slopes differ, depending on the initial S_0^*-value and is steeper, the higher the initial extractant concentration. The log-log plot in figure 7(ii) reveals that the slopes are actually similar in the regime of $3.9 \leq W_0 \leq 5.6$. A second inflection of the curve is observed at higher water-to-extractant ratios. Fitting the linear parts reveal that the two straights converge at a value of $W_0 = 5.6$.

For $W_0 < 3.9$, an increase in temperature is detected after each consecutive addition of water. The maximum difference of $\Delta T = 0.3\,°C$ is measured in the regime of $2.4 \leq W_0 \leq 4$. For $W_0 > 5$, the temperature of the solution remained constant. The two transitions are also shown in the phase diagram in figure 8. In particular a correlation of the conductivity with the macroscopic phase behaviour is observed at $W_0 = 5.6$. The inflection of the conductivity curve is observed at the same ratio of water-to-surfactant as the phase boundary transition for lower extractant weight-fractions. This may indicates a transition of the structure on a mesoscopic level.

2.2.2)Is the sharp increase in conductivity a percolation phenomenon?

The significant increase in conductivity observed in figure 9 is typical for percolation phenomena observed in microemulsion systems.[196] A convenient way to determine if a percolation phenomenon is responsible for the significant increase in conductivity is a so-

called “percolation-plot”, as depicted in figure 10.[197] This plot allows deducing the critical exponents μ and $|s|$, which give an indication on the type of percolation.

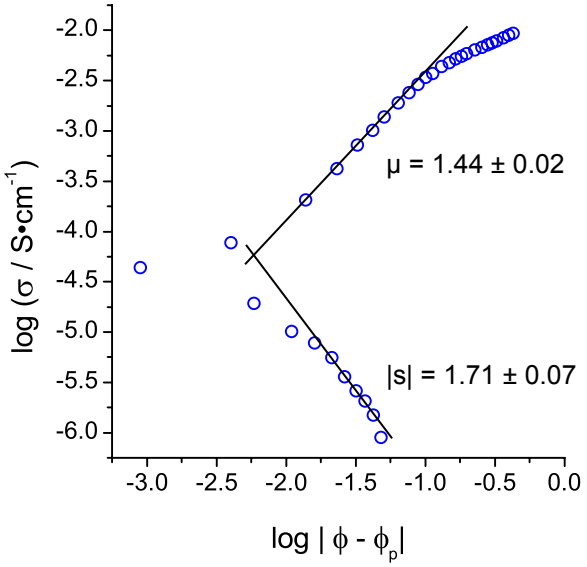

Figure III-10 – Determination of the percolation scaling exponents μ and $|s|$ of the conductivity line at $S_0^* = 0.5$.

Linear regimes, sufficiently far away from the transition region have been chosen to evaluate these exponents. As average values, $\mu = 1.44$ and $|s| = 1.71$ were found, with standard deviations of $\Delta\mu = 0.02$ and $\Delta s = 0.07$.

The critical exponents deduced from figure 10 are listed in table 1, alongside values taken from literature. The experimentally deduced critical exponents are in disagreement with values reported in literature, which means that asymptotic conductivity above and below the steep increase is atypical for percolation, irrespective whether the origin is static or dynamic percolation. In particular, the onset of percolation, determined by the critical exponent $|s|$, is higher than values reported in literature. This means that the increase in conductivity is too abrupt for a dynamic or static percolation only responsible for the slope observed: there is also a morphology variation, as was already observed for the cationic surfactant/water/oil systems.[79]

Table III-1 – Comparison of experimentally determined critical exponents with literature.

	System	μ	$\|s\|$	percolation
Experimental	toluene/NaDEHP/water	1.44	1.71	-
Blattner *et al.*[197]	$scCO_2$/ClPFPE-NH_4/water	1.75	1.28	dynamic
Bhattacharya *et al.*[107]	n-decane/AOT/water	1.68	1.17	dynamic
Kim and Huang[198]	n-decane/AOT/water	1.6	1.2	static

Further, the volume fraction of water at the percolation threshold is far below the typical values observed if aggregates are spherical. For the system water/potassium oleate/butan-1-ol/toluene, the percolation threshold has been reported to be at $\phi_{water} = 33 vol\%$.[199] For the system water/SDS/pentan-1-ol/dodecane the threshold has been reported at $\phi_{water} = 20 vol\%$.[200] The volume fractions of water at the experimentally observed thresholds for the three different dilution lines are listed in table 2.

Table III-2 – Volume fraction of water dispersed in the microemulsion at the onset of the conductivity increase.

S_0*	Conductivity threshold at ϕ_{water} / vol%
0.5	0.078
0.25	0.051
0.1	0.016

2.2.3)Plotting the conductivity in reduced units

In order to determine the origin of the sharp increase, specific conductivity is normalized to a *reduced equivalent conductivity*. The scheme in figure 11 schematically represents a bicontinuous microemulsion between two electrodes. Dissociated counter-ions may migrate in the continuous water-channels and contribute to the overall conduction.[106]

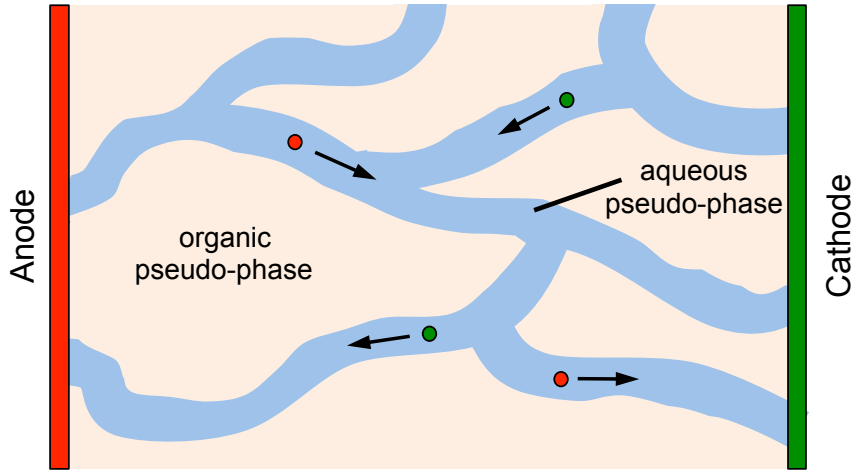

Figure III-11 – Conductance in a bicontinuous microemulsion system. Dissociated counter-ions primarily migrate in the continuous water-channels.

Therefore, the conductivity in microemulsion systems depend on two critical factors:

- The concentration of charge carriers present in a solution
- The volume in which these charge carriers can move

Thus we normalize the experimentally determined specific conductivity σ and translate it the reduced equivalent conductivity Λ^*, according to:

$$\Lambda^* = \frac{\sigma}{c(NaDEHP) \cdot \phi^*_{water}} = \left[\frac{S \cdot cm^2}{mol}\right] \qquad (vi)$$

Where ϕ^*_{Water} takes into account the volume fraction of water with respect to the total volume of solvent and water in the sample,

$$\phi^*_{Water} = \frac{\phi_{water}}{\phi_{water} + \phi_{solvent}} \qquad (vii)$$

Thus, irrespective of the amount of extractant in the solution.

We call Λ^* the "reduced conductivity" or "reduced equivalent conductivity" of the system, in order to avoid confusion with notations of the equivalent conductivity Λ. This normalization is based on the conductivity introduced in charge-fluctuation model presented by Eicke et al., where the specific conductivity normalized by the volume fraction of water.[104] Further, the background to normalize the conductivity by the concentration of NaDEHP stems from the classical aqueous model, which has also been adapted in one of Eicke's earlier works.[103] This reduced conductivity is thus the contribution of a single charge carrier the total conductivity.

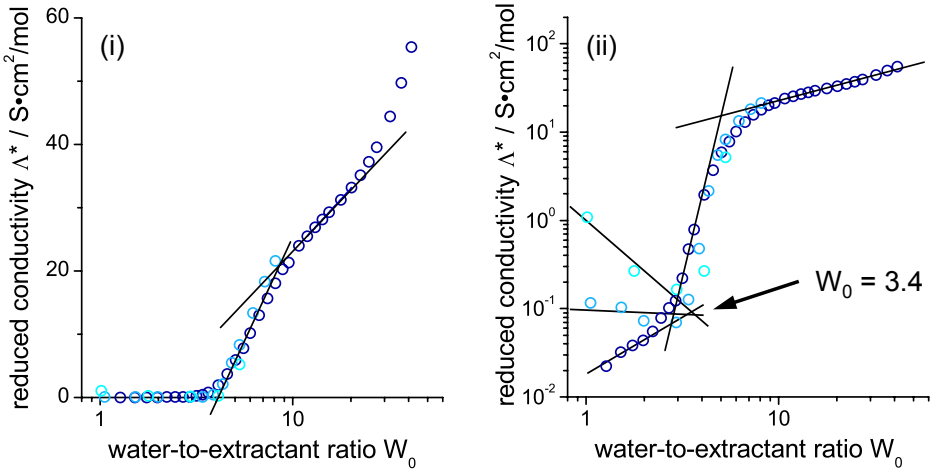

Figure III-12 – Conductivity of figure 9 depicted in "reduced conductivity" versus the water-to-extractant ratio W_0. (i) lin-log representation, (ii) log-log representation.

In figure 12, the reduced equivalent conductivities along three dilution lines in figure 8 are plotted as the function of the water-to-surfactant ratio W_0. In the lin-log representation in figure 12(i), all three curves are superposed. Above $W_0 \geq 3.9$ the reduced conductivity increases sharply by 3 orders of magnitude. A second inflection at $W_0 \geq 5.6$ is observed.

In the log-log representation in figure 12(ii), merging of the three curves is observed for $W_0 \geq 3.9$. However, the reduced conductivity below this critical region exerts an odd behaviour. For a low initial extractant concentration (light blue curve, $S_0^* = 0.1$), the conductivity Λ^* is the highest and decreases upon dilution with water. For $S_0^* = 0.5$ (navy blue curve), the equivalent conductance is two orders of magnitude lower and increases upon dilution. Linear regression of the available data-points reveals that the three data-points converge for $W_0 = 3.4$.

2.2.4)Origin of the sharp increase in conductivity

Searching for an alternative explanation for the increase in conductivity, Faure *et al.* has been conducting spin-echo NMR-measurements.[126] For the system benzene/NaDEHP/water in was determined that above a critical water-to-surfactant ratio of $W_0 = 3.6$, the relaxation time of water-protons increase significantly, meaning that they are more mobile with a correlation time of the magnetic field fluctuation "killing" some of the dipolar relaxation mechanisms. Above this critical value, the rotational diffusion coefficient of water is enhanced, giving rise to the formation of a water-core, where water exerts properties similar to bulk water.[59] Below this critical value, water is adsorbed at the head-groups of the surfactant and their rotational mobility is therefore handicapped. Further, the relaxation time of sodium also increases for $W_0 \geq 4$, indicating an increased mobility of sodium ions upon formation of a water core.

In contrast to Faure, who assumed at that time (1986) that the shape of the reverse aggregates is restricted to perfect spheres, Yu and Neuman showed that giant rod-like micelles of NaDEHP are present in the case of the penetrating solvent n-heptane.[125] The chosen concentration of NaDEHP in n-heptane was chosen in the order of $c(NaDEHP) = 30 - 80\ mmol/L$, which corresponds roughly to $\gamma_{NaDEHP} = 1 - 2wt\%$.

Therefore, the origin of the sharp increase of the conductivity can be explained as follows: Below the critical value $W_0 < 3.9$, water is completely immobilized and forms a hydration shell around the polar head-groups of NaDEHP. This explains the increase in temperature observed in the regime for $W_0 < 3.9$, highlighted in figure 9. Upon addition of water, the head-groups of NaDEHP are hydrated, resulting in a release of heat from the hydration enthalpy. Above this critical value, the reverse micelles transition into *swollen reverse micelles*, as they now possess a water-core where water has "bulk-water"-like properties, i.e. it may form a dynamic hydrogen-bond network. Therefore, dissociation of a cation is possible, thus giving

rise to a drastic increase in conductivity. This is illustrated by the positive charge in figure 13 which can freely migrate in the core of a reverse swollen micelle.

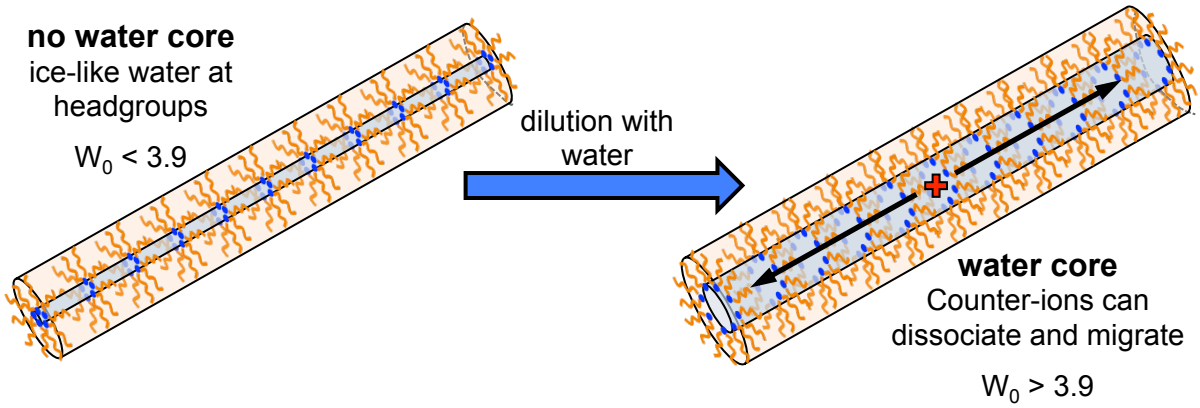

Figure III-13 – Rod-like sections of a percolating DOC-system: below the critical hydration where water is adsorbed at the surfactant head-groups. Above the critical hydration, the formation of a water core enables the dissociation of counter-ions. These counter-ions can migrate along these cylinders giving rise to a drastic increase in conductivity.

As NaDEHP forms rod-like micelles at low concentrations it is safe to assume that at higher concentrations (as chosen in this experiment, since γ_{NaDEHP} was chosen 10-50 times higher) the system is already percolated, thus giving rise to a conductivity signal in the order of magnitude of $\sigma_{W_0>4} = 10^{-3}\ S/cm$, as observed in figure 8.

A logical consequence is that the domain of increase in conductivity is independent of the volume fraction of water, but is primarily determined by the ratio of water to extractant. We can therefore define a limit on the water-poor side of the phase diagram, separating the ternary regime into a reverse micellar region and a microemulsion region. For the counter-ion ratio of $Z = 1$, a *first hydration layer* at a critical value of $W_0 = 3.9$.

This conclusion is illustrated in figure 14, where a hydration limit is defined at a constant W0-value, i.e. a dilution line towards pure toluene. Below this value, water is ice-like and adsorbed at the head-groups. The origin for conductivity in this region, as observed in the reduced conductivity is in the focus of interest in the next section. Yet, a decrease of the reduced equivalent conductivity with increasing extractant concentration indicates that the origin of conductivity is due to a dismutation mechanism.

Above this value a polar water-core is present, thus there is an actual interface between water and oil separated by a film of surfactants.

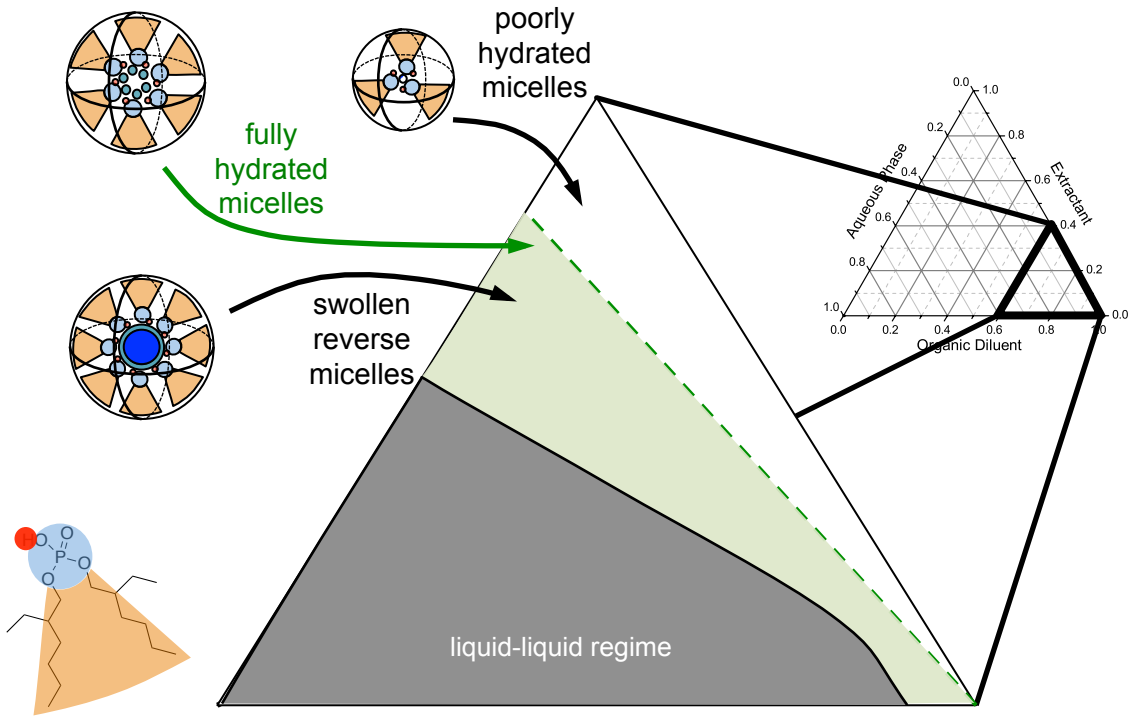

Figure III-14 – Limit of hydration and distinction between reverse micellar systems as w/o weak aggregates and swollen reverse w/o microemulsions. The water inside the swollen micelles behaves like bulk water and thus we can define this region as a real L2 microemulsion, where oil and water are separated by a hydrated surfactant film and a real interface.

3. Dilution towards oil

3.1) The non-frustrated region – Z = 0.5

3.1.1)Conductivity in the non-frustrated regime

In figure 15, the pseudo-ternary phase diagram of toluene/NaDEHP/HDEHP/water with a counter-ion ratio of $Z = 0.5$ is shown. Pseudo-binary extractant-toluene solutions (at different S_0^*-values) have been prepared and diluted with water until phase separation. The compositions of the samples are indicated by the blue triangles (detailed composition in table 3). The phase separation in the two-phase regime is due to an *emulsification failure*, therefore the extracting microemulsion is in equilibrium with an excess water phase (Winsor II-equilibrium). Since the compositions are located just beyond the phase transition the volume of the excess aqueous phase can be neglected.

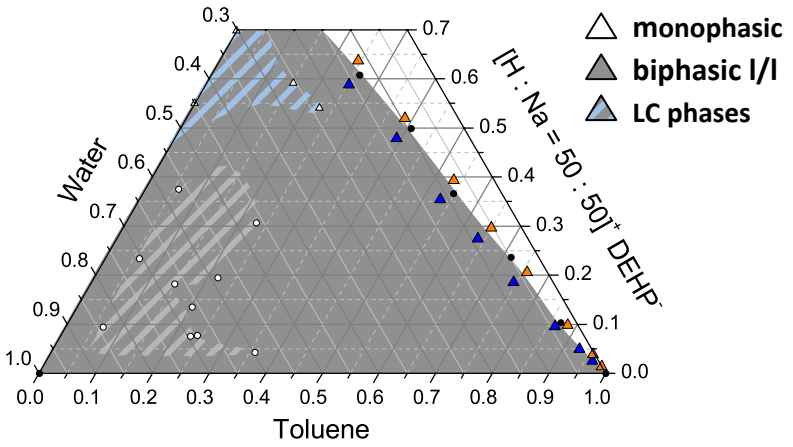

Figure III-15 – Pseudo-ternary phase diagram of toluene/NaDEHP/HDEHP/water at a counter-ion ratio of $Z = 0.5$. The blue triangles indicate the initially prepared compositions in the biphasic region. The orange triangles denote the compositions of the organic phase after phase separation.

The respective contents of DEHP and toluene in the organic phases have been determined via quantitative NMR and the water-content has been deduced using Karl-Fischer titration. The resultant compositions of the organic phases are illustrated as orange triangles in figure 15 and appropriately listed in table 3. Naturally, the composition of the organic phase superposes with the experimentally deduced phase boundary in Chapter II, thus confirming that the organic phase can be considered as a Winsor II microemulsion. Since the volume of the excess aqueous phase is negligible, the initially chosen ratio of NaDEHP to HDHEP of $Z = 0.5$ is considered as unchanged, irrespective of the tie lines being strictly out of the plane at constant Z (see section I-3.4).

Table III-3 – Composition of samples in the organic phase deduced by quantitative NMR and Karl-Fischer titration.

Weighed-in compositions			**quant. NMR**			**KF**	
$w_{toluene}$	$w_{extractant}$	w_{water}	$w_{toluene}$	$w_{extractant}$	w_{water}	W_0	$\Phi_{water + extr}$
0.965	0.025	0.011	0.988	0.021	0.0002	0.34	0.053
0.930	0.049	0.021	0.955	0.038	0.003	1.47	0.066
0.863	0.095	0.041	0.897	0.099	0.018	3.38	0.123
0.745	0.185	0.070	0.776	0.202	0.037	3.37	0.229
0.638	0.273	0.089	0.645	0.298	0.056	3.49	0.329
0.531	0.354	0.115	0.529	0.393	0.075	3.54	0.431
0.392	0.479	0.130	0.398	0.515	0.097	3.48	0.569
0.253	0.588	0.159	0.246	0.639	0.119	3.45	0.715

In table 3, the ratio of water-to-solvent W_0 has been calculated based on the compositions of the organic phase. Above $\gamma_{extractant} > 9.9wt\%$, a constant value of $W_0 = 3.45 \pm 0.06$ is detected, which is in good agreement with the results obtained in the previous chapter ($W_0 = 3.3$). However at lower concentrations of extractant, the water-uptake is below this

value (see two rows marked in light red). The conductivity of the organic phase has been measured using impedance-spectroscopy. Using the Cole-Cole-plot, the conductivity of the organic phases has been deduced and plotted in figure 16, as function of the volume fraction of extractant plus water in a lin-lin and a lin-log representation.

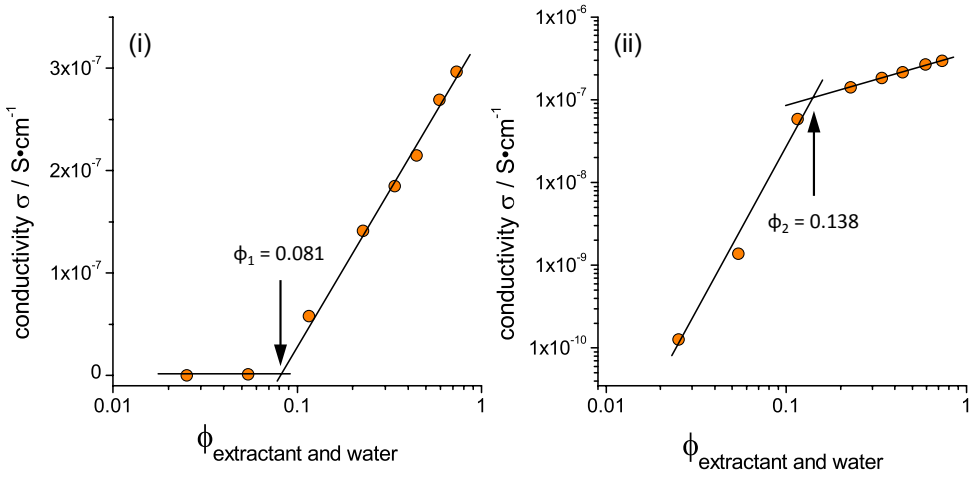

Figure III-16 – Conductivity deduced from impedance spectroscopy versus the volume fraction of dispersed phase. (i) lin-log representation; (ii) log-log-representation.

In figure 16(i), a sharp increase in conductivity is observed at $\phi_{extractant+water} = 8.1 vol\%$, above which the conductivity increases linearly. In the log-log plot (figure 16(ii)), two linear domains have been detected. Below the critical value $\phi_{extractant+water} = 13.8 vol\%$, the conductivity significantly increases by 4 orders of magnitude, while above this value, the conductance stays in the order of $\sigma = 10^{-7}\ S/cm$.

Applying the reduced equivalent conductivity in figure 17, introduced in the previous sub-section. The conductivity is plotted as a function of the square root of the concentration of the surfactant, in accordance with Kohlrausch's law. A sharp maximum is observed at $\sqrt{c(NaDEHP)} = 1.24\ (mol/L)^{1/2}$. Below this critical concentration, the conductivity decreases sharply, whereas above this value, the conductivity is decreasing asymptotically.

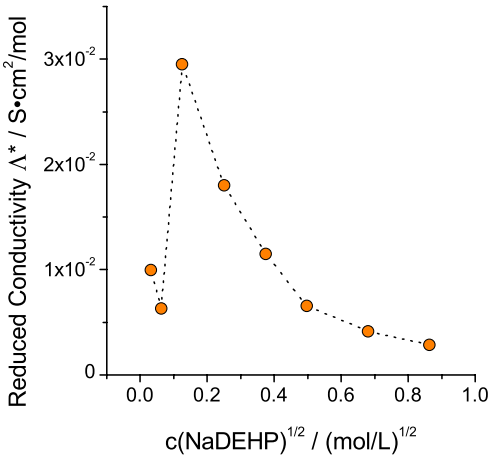

Figure III-17 – Reduced equivalent conductivity versus the square root of extractant concentration.

3.1.2)Qualitative interpretation of the scattering signal

Small angle X-ray scattering is among the few appropriate techniques to probe the morphology of a microemulsion on a nanoscopic scale. Along the dilution line towards the toluene-rich corner, three different types of morphologies have been observed, as depicted in figure 17(i). For low weight-fractions of extractant, no signal was detected in the low-angle regime (red curve). For intermediate weight-fractions of extractant, a typical spherical form-factor is observed (green spectrum).[70] Further increase of the extractant-concentration leads to a decrease of the intensity in the low-angle regime and the pronunciation of a structure-peak in the intermediate regime (blue curve). This is due to a decrease in compressibility of the solution.[201]

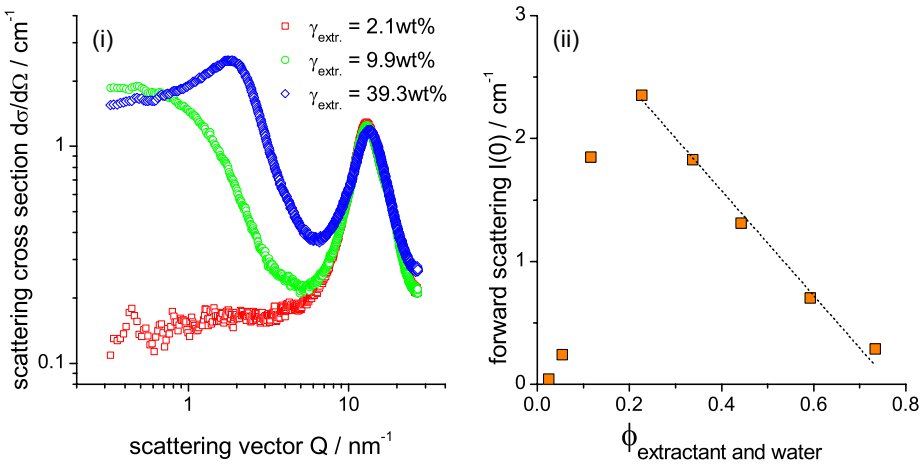

Figure III-17 – (i) Three observed morphologies of SAXS-spectra along the dilution line towards oil. (ii) Forward scattering $I(0)$ of the spectra.

The forward scattering $I(0)$ of the spectra has been deduced in figure 17(ii).[201] Above the maximum at $\phi_{extractant+water} = 22.5vol\%$ ($\gamma_{extractant} = 18.5wt\%$), the signal decreases linearly with increasing volume fraction of the dispersed aggregates.

3.1.3)Origin of the conducting signal

The phase diagram and the scattering signal give valuable information from a macroscopic and microscopic point of view. As a result of the bad solubility of water for $\gamma_{extractant} = 4.9wt\%$, as listed in table 3 (the two red lines), the macroscopic phase behaviour suggests that no reverse micelles are formed below this critical value. This is confirmed by small angle X-ray scattering, where no signal in the small-angle regime is detected for the first two points (see figure 17(ii)). For $\gamma_{extractant} > 4.9wt\%$, the solubility of water, as well as the scattering signal at small Q increase. Therefore, the cmc is in the regime between $0.095 > \gamma_{extractant} > 4.9wt\%$.

The same behaviour is observed for the conductivity plotted in figure 16. Below the apparent cmc, the conducting behaviour is in the order of $\sigma_{<cmc} = 10^{-10} - 10^{-9}\, S/cm$ and increases significantly when increasing the extractant concentration, as well as the amount of co-extracted water. A critical micellar concentration, extracted from the lin-log plot is extracted at a volume fraction of $\phi_{extractant+water} = 8.1 vol\%$.

Plotting the conductivity in reduced conductivities reveals a sharp peak at $\sqrt{c(NaDEHP)} = 1.24\ (mol/L)^{1/2}$. The increasing conductivity below this maximum may be due to charges that are a hydrated sodium or Hydronium ion dissociated from monomeric DEHP-anions. Thus, this occurs in the most diluted stage. It is important to note that this regime merges in the dismutation regime: when all aggregates are not neutral, but some aggregates have a positive while some have an excess anion. The probability of dissociation is low, but typically only a fraction of $\alpha = 10^{-5} - 10^{-4}$, where α is the degree of dissociation:[100,202]

$$\alpha = \frac{n_{charged\ micelle}}{n_{micelle}} \qquad (viii)$$

Thus, the distance between neighbouring dismutated aggregates. This regime has the peculiarity that neighbouring dismutation interact, hence reduced conductivity decreases with concentration, as observed for $\sqrt{c(NaDEHP)} > 1.24\ (mol/L)^{1/2}$.[98,203] Since only two data points are available in dilute regime, deduction of the mathematical dependence of the conductivity from the concentration in this region is ambiguous. However, as soon as the amphiphiles start to auto-assemble into reverse spherical aggregates (at $\gamma_{extractant} = 9.9 wt\%$, $\phi_{extractant+water} = 12.3 vol\%$, $\sqrt{c(NaDEHP)} = 1.24\ (mol/L)^{1/2}$), the conductivity increases linearly. This can be explained by a mechanism of micelle dismutation, presented Weitz *et al.*, where the same linear dependence of the specific conductivity was observed for the binary system AOT/dodecane.[182]

Further, from the phase boundary, which runs along a constant value of $W_0 = 3.45 \pm 0.06$, it can be inferred that no change of the structures on a mesoscopic scale occurs when increasing the extractant-concentration. Additionally, the linear decrease of the scattering signal confirms that the reverse micelles essentially behave like hard-spheres and do not exert an attraction on each other. This confirms that the microemulsion essentially behaves like a non-frustrated microemulsions, where the phase separation is driven by a maximum swelling of the aggregates.[83]

Thus, it can be concluded that the conducting behaviour in the non-frustrated branch on the water-poor side arises only from the formation of charged reverse micelles due to a dismutation-mechanism.

3.2) Conductivity in frustrated region – Z = 1

Sample preparation in the biphasic region as in the non-frustrated region is not possible, since the biphasic region is a liquid-gas type phase separation. After determination of the hydration limit in the previous section, the main question is how the conductivity is affected below and above this critical hydration limit.

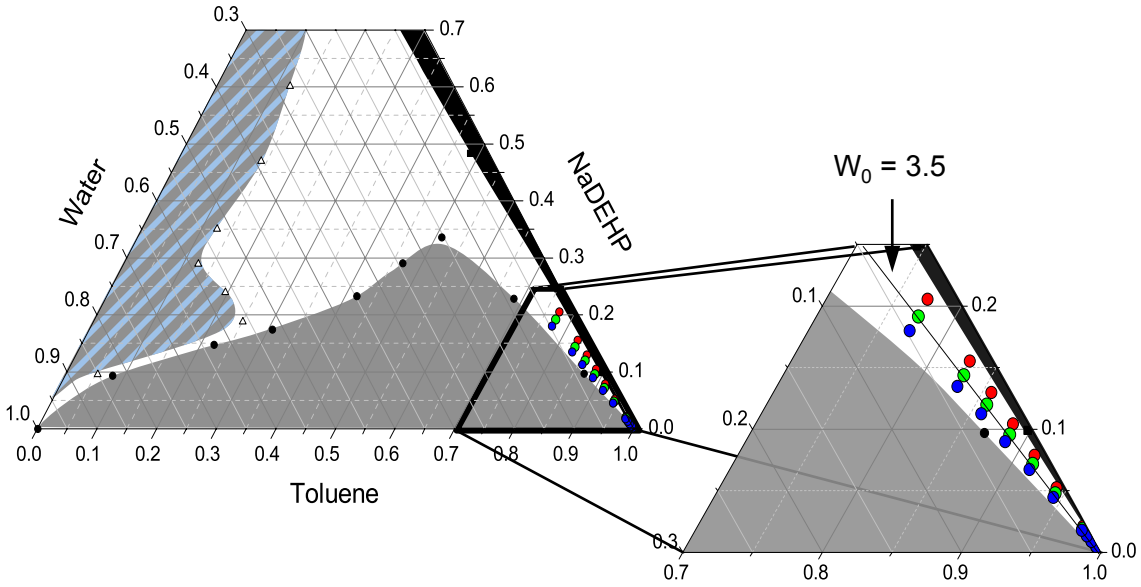

Figure III-19 – Ternary phase diagram of toluene/NaDEHP/water, with three dilution lines towards water at $W_0 = 2; 3.5; 5$. The zoom into the oil-rich corner highlights the dilution lines towards toluene in the monophasic channel.

In figure 19, the phase diagram of toluene/NaDEHP/water is illustrated with a zoom into the monophasic channel on the oil-rich side. Three dilution lines towards toluene have been prepared, one below the critical hydration limit ($W_0 = 2$, orange dilution line), one at the hydration limit ($W_0 = 3.5$, green dilution line) and in the swollen reverse micellar regime ($W_0 = 5$, blue dilution line).

The conductivity, which was deduced via impedance-spectroscopy, is depicted in figure 19 as a function of the volume fraction of dispersed extractant and water.

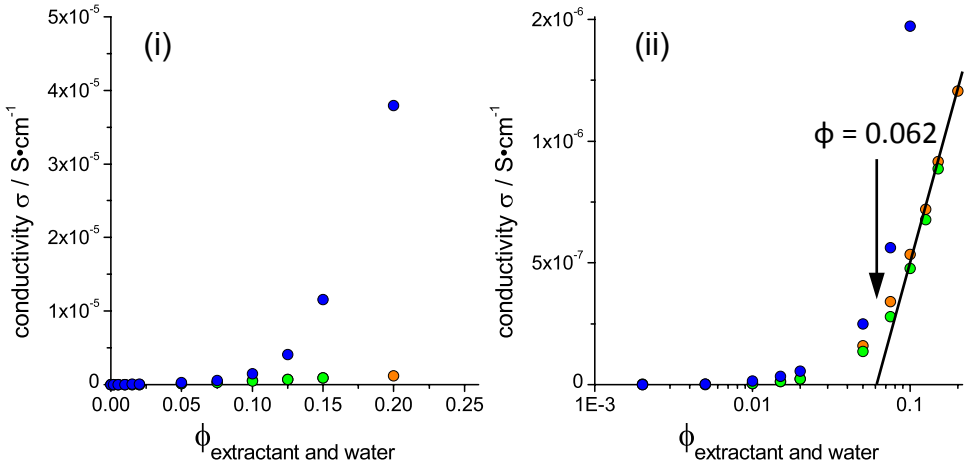

Figure III-20 – Conductivity profile towards pure toluene as a function of $\phi_{extractant+water}$ for $W_0 = 2$ (orange), $W_0 = 3.5$ (green) and $W_0 = 5$ (blue). (i) lin-lin representation, (ii) lin-log representation.

If a water core is present (blue dilution line), the conductivity increases significantly, up to $\sigma_{swollen\ micelles} = 5 \cdot 10^{-5}\ S/cm$. In the absence of the water core the signal is 1-2 orders of magnitudes lower. Below the hydration-limit ($W_0 \leq 3.5$), the conductivity is increasing as well, however the steepness is much less pronounced if no water-core is present. Nevertheless, an onset of conductivity is detected at $\phi_{extractant+water} = 6.2 vol\%$ and the specific conductivity increases linearly $\phi_{extractant+water}$.

Below this critical concentration, the specific conductivity is in the order of pS/cm – nS/cm, as observed in the non-frustrated branch, therefore the arising conductivity can be attributed to the dissociation of monomers. Above this critical concentration, the specific conductivity increases linearly as a function of ϕ, and is in the μS/cm regime. As in the non-frustrated microemulsion, this conductivity can be assigned to the formation of some charged micelles by dismutation. The conducting behaviour is greatly influenced if a water-core containing mobile water molecules that are not bound in the first hydration shell of head-groups is present.

Plotting the reduced conductivity as a function of the square root of the concentration reveals the same behaviour as observed in the non-frustrated regime: for low concentration of extractant, the reduced equivalent conductivity increase, however above a critical micellar concentration, the conductivity decreases linearly. An intriguing feature is the second onset in conductivity for $\sqrt{c(NaDEHP)} = 0.5\ (mol/L)^{1/2}$, which indicates the onset of a percolation phenomenon, as the contribution of an ion to the overall conductivity is significantly enhanced if it can travel in a continuous water-path.

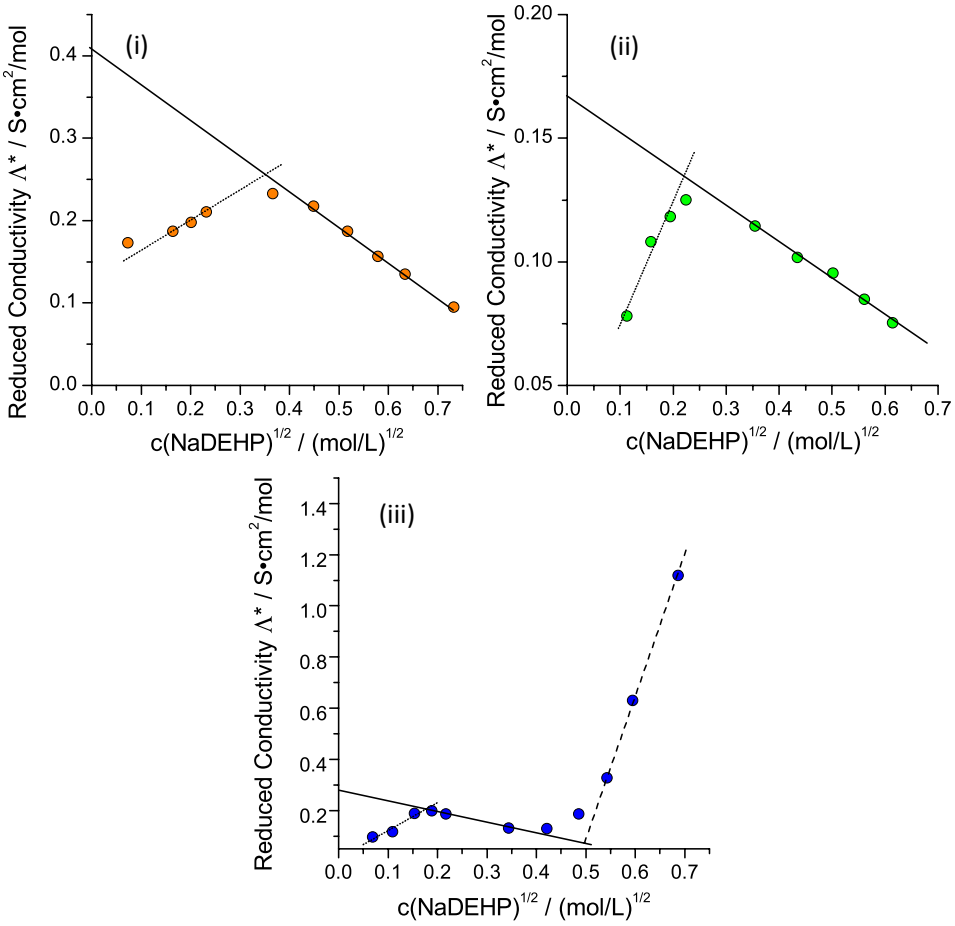

Figure III-21 – Reduced equivalent conductivities as a function of the square root of the extractant concentration. (i) $W_0 = 2$ (orange). (ii) $W_0 = 3.5$ (green). (iii) $W_0 = 5$ (blue).

An illustrative way to evidence these different regimes is by looking at the reduced equivalent conductivity plot in figure 21(iii) (blue curve). Here, the same profile is found in the low $\sqrt{c}$-regime, where a maximum and then decreasing equivalent conductivity indicates the formation of microstructures. However at sufficiently high concentrations, the conductivity increases significantly.

Therefore, we can state that the percolation is not only dependent on the volume fraction of dispersed water and thus the ratio of water-to-surfactant W_0, but also on the number-density of available micelles. Thus is schematically represented in figure 22, where the monophasic region can be divided into five different regions:

In the most diluted state, conductance arises from dissociation of monomers and is in the order of $\sigma_{monomers} = 10^{-10}\ S/cm$. This can is in good accordance with the conductivity of very dilute salt solutions, which can dissociate due to charge-fluctuations.[95,204] Above the cmc (above the red curve in figure 22), the monomers self-assemble into higher-ordered

structures, giving rise to a linear increase in specific conductivity. This is the regime where electrical conductance is correlated with the formation of charged micelles due to a dissociation (or dismutation) process, as proposed by Weitz *et al.,*[182] and confirmed by the work of Beunis and co-workers using transient current measurements.[97,205] Translated into the reduced equivalent conductivity, the contribution of a charged micelle to the overall conductivity decreases, as the number of adjacent aggregates increases. Thus, the association of charged micelles is enhanced.[203] Above a critical extractant concentration a second increase in conductivity is due to a percolation phenomenon is observed in the swollen micellar regime, as indicated by the blue regime.

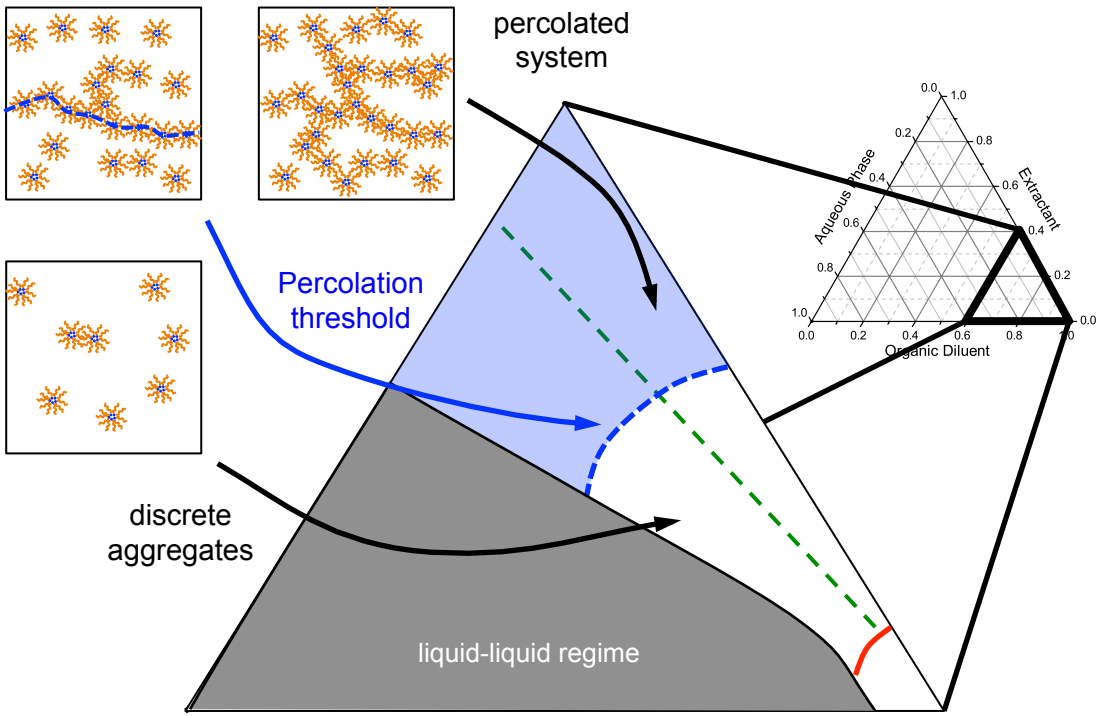

Figure III-22 – At very dilute concentrations of the extractant, the system is in a monomeric state. Above a cmc (red line), the aggregates self-assemble into discrete reverse micellar aggregates. Above a second critical concentration (percolation threshold, blue dotted line), the aggregates coalesce to form a continuous cluster. The reverse micellar regime beyond the cmc is further divided by the hydration limit as shown in figure 14.

However, above the percolation threshold it has to be clearly differentiated between two cases, depending on whether the system is below or beyond the hydration limit (green-dotted line in figure 22):

If no water-core is present, the system may be percolated, however since the ions cannot migrate in a polar environment, no sharp increase of the electrical conductance is observed. This is the origin of the low conductance below $W_0 < 3.9$, when diluting with water. The system is percolated, yet the charge carriers are inhibited to migrate and thus contribute in

the overall conductance. If a water-core is present, conductivity can serve as a valuable experimental method to detect the onset of percolation, as the ions can move freely in the core of swollen reverse micelles

4. Conductivity for intermediate Z

In order to evaluate the conducting behaviour in a regime located in-between the two frustrated branches, the electrical conductance is explored in the pseudo-ternary phase diagram, where the maximum solubility of water and toluene has been detected in Chapter II of this work: $Z = 0.9$, as represented by the orange arrow in the χ-cut in figure 23.

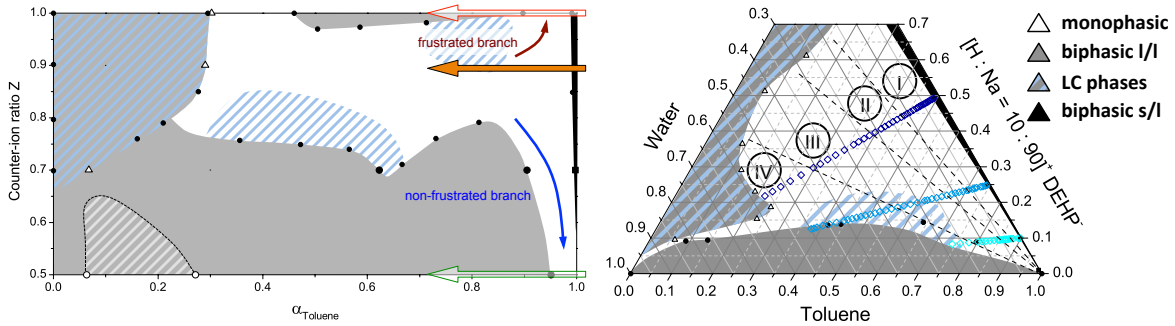

Figure III-23 – (i) Partial χ-cut for the quaternary system toluene/HDEHP/NaDEHP/water in the range of $0.5 \leq Z \leq 1$. The same colours as in the previous chapter for frustration (wine red) and non-frustrated (blue) has been maintained and depicted by the arrows. The orange arrow indicates the conductivity-pathway as a function of the water-content for a counter-ion ratio of $Z = 0.9$. (ii) pseudo-ternary phase diagram of toluene/NaDEHP/HDEHP/water at a counter-ion ratio of $Z = 0.9$. The three dilution lines towards water for which the conductivity has been measured have been inserted.

The conductivity has been explored by diluting pseudo-binary extractant-toluene solutions with water, as depicted in the ternary diagram in figure 23(ii).

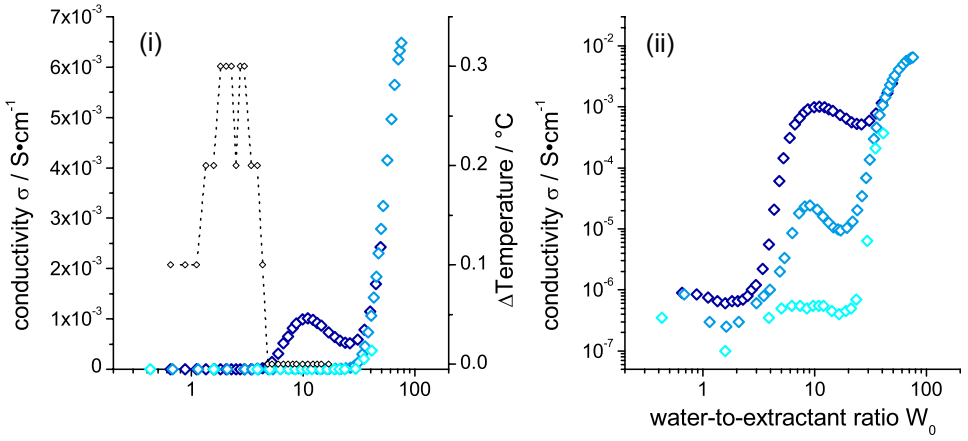

Figure III-24 – Conductivity in the monophasic region of the pseudo-ternary phase diagram toluene/NaDEHP/HDEHP/water at a counter-ion ratio of $Z = 0.9$. $S_0^* = 0.5$ (navy blue), $S_0^* = 0.25$ (blue) and $S_0^* = 0.1$ (light blue). (i) lin-log representation; (ii) log-log representation.

The conductivity profile along this dilution line is shown in figure 24. In the lin-lin representation, the conductivity is very low ($\sigma = 10^{-6}\, S/cm$) and a sharp increase in conductivity is observed for $W_0 > 12$. Additionally, an odd peak is observed for the dilution line at $S_0^* = 0.5$ at intermediate regimes. In the log-log representation, this peak is also visible for the lower initial extractant concentration, however much less pronounced. Thus, this peak is clearly dependent on the concentration of extractant in the solution. Below the first onset of conductivity ($W_0 < 3.5$), the temperature of the solutions increased with each successive addition of water, indicating a hydration of the head-groups.

The results can be explained when transferring the specific conductivity into the reduced equivalent conductivity, as depicted in figure 25. The conductivity profile can be divided onto 4 different regimes as a function of the water-to-surfactant ratio:
At very low contents of water, in region I, the conductivity is due to a dissociation of micelles, as elucidated in the previous subsections. The absence of a water-core is confirmed by the small increase in temperature as the system is diluted with water, which is due to an enthalpic hydration of the head-groups. As soon as a water-core is present, the equivalent conductivity significantly increases by 3 orders of magnitude, which is correlated to the presence of an aqueous core, which is due to a dynamic percolation. The aggregates are too diluted to make a continuous path. Therefore, the charge carriers are part of the time moving "inside" a cylinder aggregate (black paths) and sometimes "hopping" from one micelle to another, which is indicated by the green paths.[107,206] The regime III is the most intriguing one, as there is a regime in between the dynamic and static percolation regime, where the conductivity in reduced units decreases upon the increase of polar volume fraction. This behaviour is not compatible with the model of flexible microemulsions in any means, but can be reconciled within the importance of curvature.[80] Upon increasing the polar volume fraction by diluting with water, the local morphology changes form long connected cylinders to much less coalesced swollen droplet. This cylinder-to-sphere morphology transition explains the very strange behaviour observed: upon adding water, the morphology tends towards slightly coalesced globular water-in-oil aggregates. Therefore, the continuous path inside a micelle is shorter and an ion is forced to "hop" more frequently between aggregates. As can be seen on figure 25, the amount of "green" paths of charge carrier in the solvent increases while the continuous path "inside" polar cores decreases. Hence, the transition regime between dynamic percolation (regime II) and static percolation (regime IV) implies this sigmoidal shape of the transition in the regime III, when static and dynamic percolation coexist.[207]

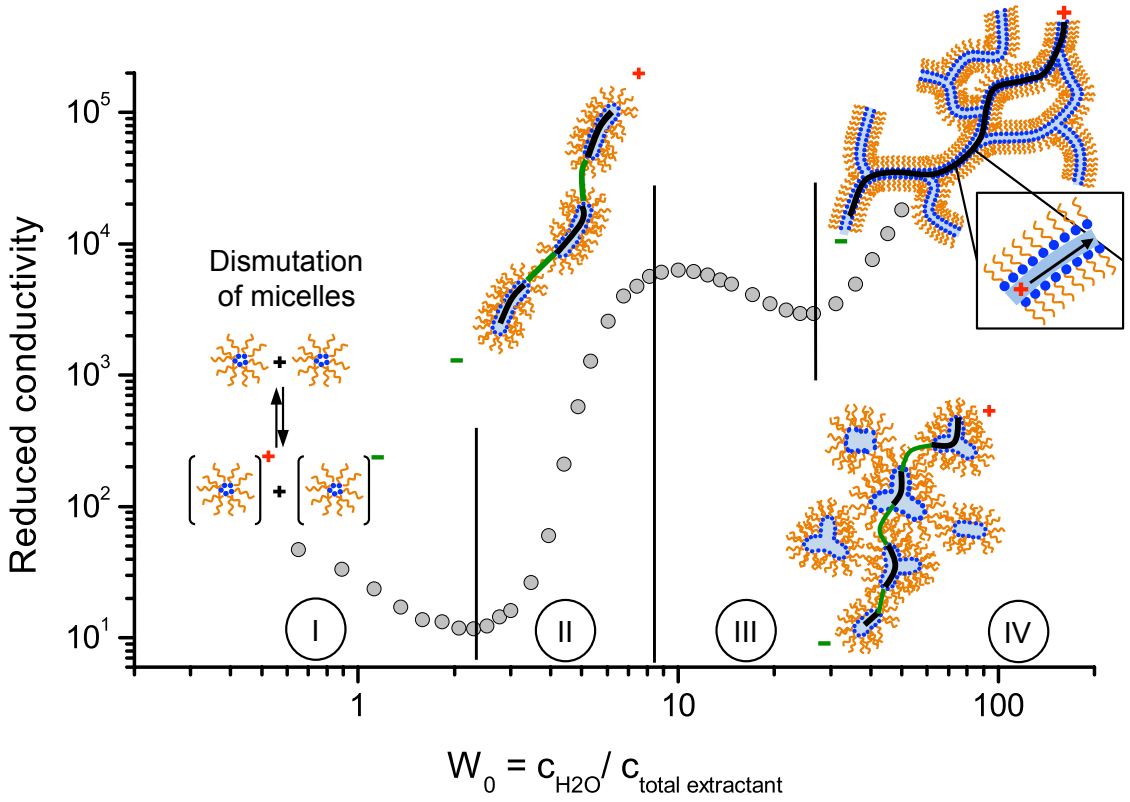

Figure III-25 – Dilution line towards water in the pseudo-ternary phase diagram toluene/NaDEHP/HDEHP/water at a counter-ion ratio of $Z = 0.9$. The initial extractant-to-toluene ratio is $S_0^* = 0.5$. Plot of the reduced conductivity of the dilution line and schematic evolution of the microstructure as a function the water-content (expressed as W_0).

At high concentration, the classical static percolation regime is observed (regime IV): paths of charge carries are in a bicontinuous network, that is either as connected cylinders in most of the cases described, or close to bi-liquid foam, locally lamellar in the narrow channel linking the water and the solvent corner.[79,148,208] The whole path of charge carriers is inside the polar volumes of the microemulsions, therefore charge carriers migrate “inside” the tubes.

5. Conductivity as a function of the counter-ion variation Z

The last variable defined in section 1.2.1 is the variation of the conductivity when changing the counter-ion ratio Z. Along this dilution line, the composition in terms of the extractant concentration $\gamma_{extractant}$ and the ratio of toluene-to-water $\alpha_{toluene}$ is held constant and only the degree of neutralization is the crucial factor. Illustrated in a map, this is shown in the χ-

plot in figure 26: When increasing the counter-ion ratio Z, the solution gradually evolves from a non-frustrated microemulsion into a frustrated microemulsion.

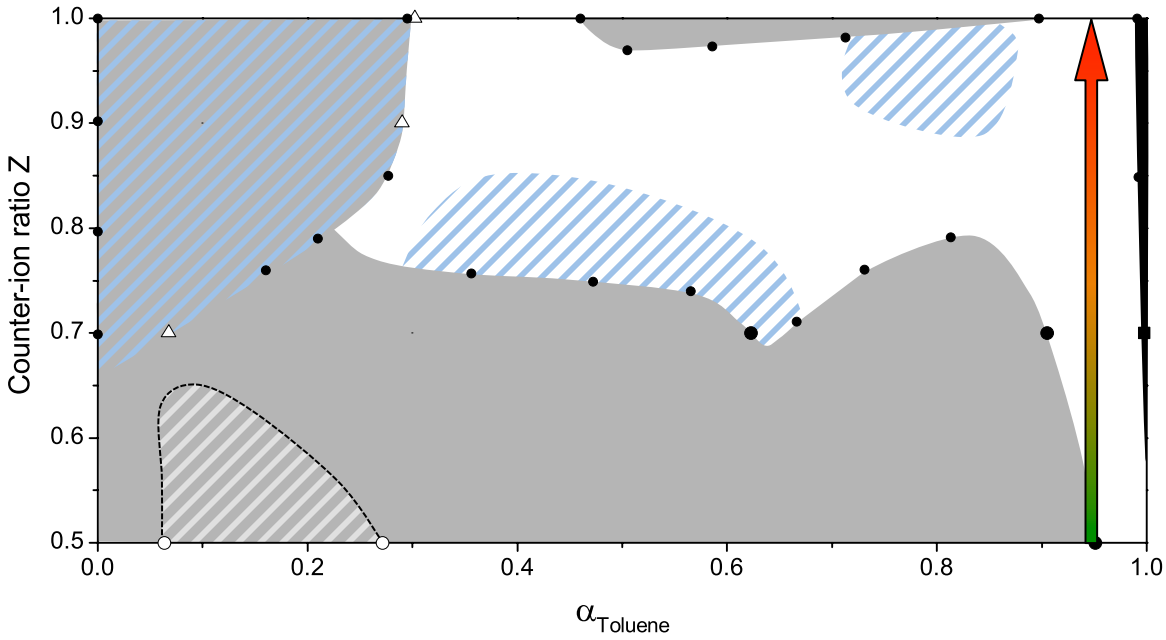

Figure III-26 – Partial χ-cut for the quaternary system toluene/HDEHP/NaDEHP/water in the range of $0.5 \leq Z \leq 1$. The arrow indicates a transition from the non-frustrated branch (green) towards the frustrated branch.

The specific conductivity in the water-poor region is plotted in figure 27. The conductivity is plotted with a composition of $\gamma_{extractant} = 50wt\%$ and at a constant water-to-surfactant ratio of $W_0 = 5$. In the linear representation in 26(i), the conductivity increases significantly by 4 orders of magnitude ($\sigma_{Z=0.5} = 2 \cdot 10^{-7}\ S/cm$ to $\sigma_{Z=1} = 1 \cdot 10^{-3}\ S/cm$).

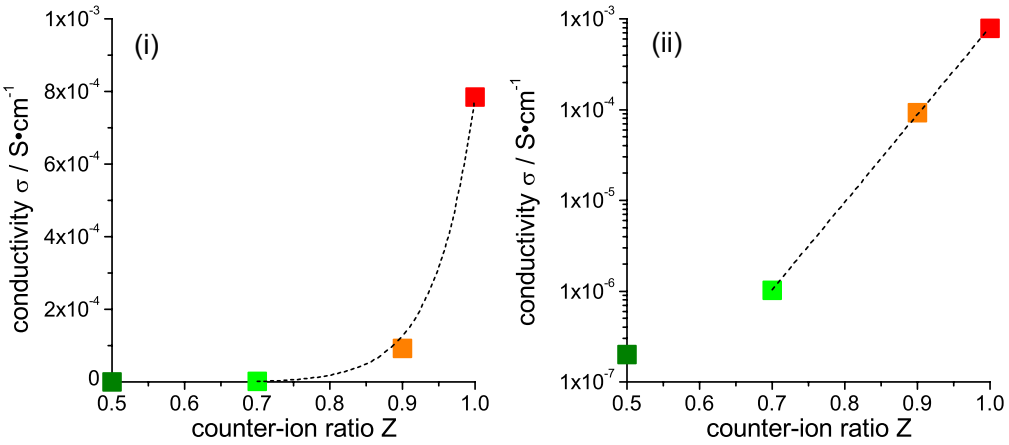

Figure III-27 – Conductivity as a function of the counter-ion ratio Z. The surfactant concentration was held at a constant weight-fraction of $\gamma_{extractant} = 50wt\%$ and a constant value of $W_0 = 5$. (i) lin-lin representation; (ii) log-lin representation.

If the graph is represented in a log-representation (figure 26(ii)), a linear dependence of the conductivity as a function of the counter-ion ratio is observed for $Z \geq 0.7$, which confirms an exponential increase of the conductivity. Nevertheless, due to the lack of experimental points, deduction of the critical exponents is not possible.

In analogy to the increase in temperature in surfactant systems, this behaviour can indeed be correlated to a percolation phenomenon.[209,210] This result shows the complexity in analysing the percolation phenomenon: The percolation threshold is not only dependent on the volume fraction of the dispersed phase, but also on the concentration of surfactant present in the solution, as well as the *degree of frustration*.

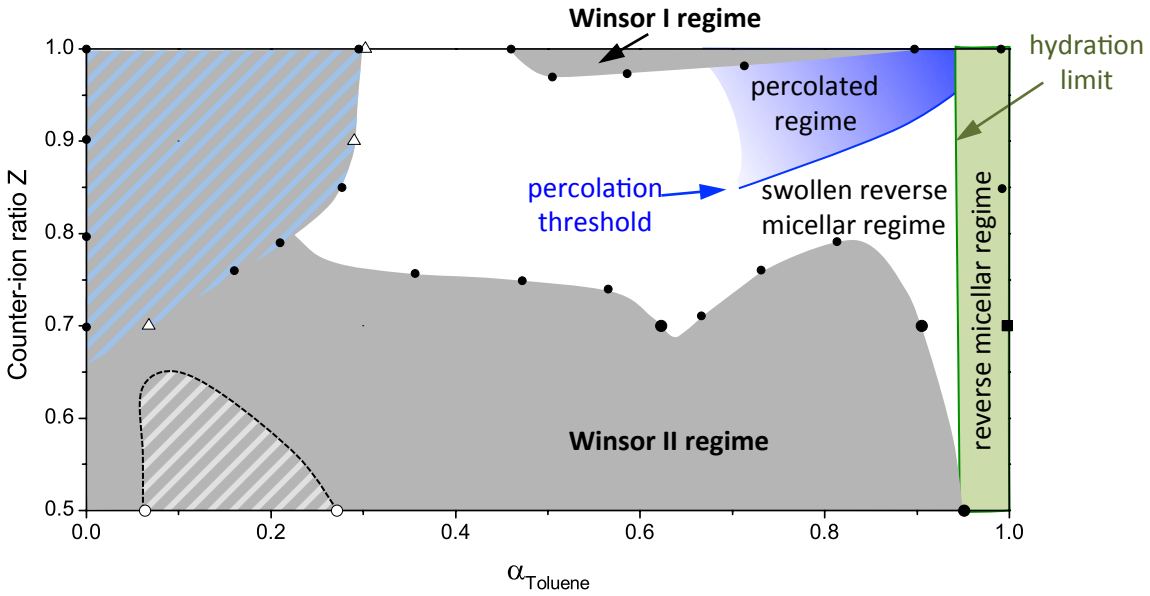

Figure III-28 – Mapping the of the morphology on a microscopic state in terms of percolation, discrete swollen micelles and the *true* reverse micellar regime, where free water is present in the micellar core.

Therefore, a proper percolation threshold needs to be mapped as a 3-dimensional surface in the phase prism. The schematic representation in figure 28 gives an overlook on the evolution of the percolation threshold in a 2-dimensional χ-phase diagram. The higher the counter-ion ratio Z, the lower the necessary volume fraction of water in order to achieve bicontinuity. Determining the onset of percolation using electrical conductivity as experimental method requires being above the hydration limit. In the green region, counter-ions are tightly bound by the head-groups if the extractants and are thus unable to conduct an electrical current.

6. Conclusion

This chapter shows the significance of the experimental composition of a microemulsion and the correlation of the electrical conductance.

In the non-frustrated regime, where the packing parameter p is close to the spontaneous packing p_0 of an extractant, the electrical conductance ($\sigma_{non-frustrated} = 10^{-9} - 10^{-7}\ S/cm$) is significantly higher compared to the conductivity of an apolar solvent ($\sigma_{organic\ solvent} = 10^{-16} - 10^{-12}\ S/cm$). This is attributed to the formation of charged micelles as a result of a dismutation process. However, even at very high concentrations of extractant where X-ray spectra show a strong correlation peak ($\gamma_{extractant} > 30wt\%$), the conductivity is still very low compared to percolated or dynamic structures.

In contrast, the conductivity in the frustrated branch may be significantly higher, but depends if the (pseudo-)ternary solution is below or above the hydration limit. If below the hydration limit, the conductivity may only be due to a dismutation of micelles. However, a “jump” of a charge carrier, as in dynamic percolation is not possible. If however enough water is solubilized in the micellar core to form a “water-pool”, the conductance increases significantly even at low extractant concentrations ($\gamma_{extractant} \sim 2 - 3wt\%$). The percolation threshold is dependent on three different factors: the *degree of frustration* (thus the water-poor region at high Z), the water-content (expressed as W_0) and the concentration of extractant in the solution ($\gamma_{extractant}$).

Chapter IV

Relation of the reference model with a solvent extraction system

A comprehensive conclusion and outlook

1. LESSONS FROM PHASE DIAGRAMS 141

2. LESSONS FROM CONDUCTIVITY 142

3. CONSEQUENCES ON PHASE INSTABILITY 144

3.1) NOVEL INTERPRETATION OF THIRD PHASE FORMATION IN SOLVENT EXTRACTION SYSTEMS 144

3.2) INTRODUCING: THE FORMULATOR'S CUT 146

3.3) FROM SOLVENTS TO CO-SOLVENTS – GREEN ALTERNATIVES FOR SOLVENT EXTRACTION USING ULTRAFLEXIBLE MICROEMULSION 148

3.3.1) Introducing: Ultraflexible microemulsions 148

3.3.2) Towards an alternative solvent extraction procedure 150

4. CONCLUSION 152

Osseo-Asare once stated that "o*nce the amphiphilic nature metal-extractant complexes is accepted, we can take advantage of the theoretical and experimental tools available for the study of reversed micelles and microemulsions. Such a marriage between surfactant science and solvent extraction stands to benefit both fields*".[31]

In this spirit, we chose to analyse a model system, which can be interpreted as an intermediate between microemulsions known from surfactant science and a metal-extracting microemulsion used in hydrometallurgy.

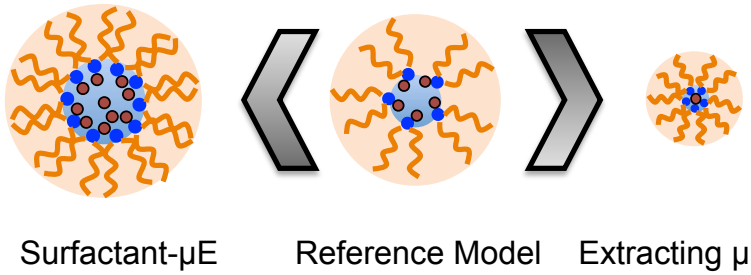

Figure IV-1 – Classification of the model used in this work compared to surfactant microemulsions and an extracting microemulsion.

This model is based on one of the most used extractants, bis(2-ethylhexyl) phosphoric acid and using its surfactant form NaDEHP as a counter-part. Completed by water and a diluent, this quaternary system adequately represents a solvent extraction system, where the sodium cation adopts the function of an extracted ion.

1. Lessons from phase diagrams

The aim of this work was to apply known concepts from surfactant science on a solvent extraction system. By introducing a new coordinate, the counter-ion ratio Z between the protonated and sodium form of the extractant HDEHP, we are able to analyse the variation of the phase behaviour upon successively changing the counter-ion ratio. Assembling the phase diagrams together to a phase prism as a function of Z, we are able to identify the transitions of the phase behaviour using the prism analysis introduced by Kahlweit *et al.*[90]

The prism allowed identifying Z as an analogue to the temperature: A sodium cation has a high enthalpy of hydration and dissociates easily from the phosphate group. As in ionic surfactant solutions, when increasing the temperature, the effective water-oil contact area per molecular headgroup a_0 increases. Everything else being equal (average length and effective

volume of the apolar moieties) the spontaneous packing p_0 decreases. Therefore, NaDEHP is a strong water-soluble surfactant while HDEHP is a weak oil-soluble extractant.
Performing a so-called χ-cut analysis of the prism allows us to rationalize that NaDEHP goes naturally in Winsor I equilibrium, while HDEHP forms to Winsor II-phases. Mismatch between p and p_0 induces a frustration in oil-rich media at high values for Z (high NaDEHP content). In reverse, the opposite effect is observed on the water-rich side, as elucidated from the fish-cuts. Therefore, we were able to locate frustrated and non-frustrated regions in the phase prism for any Z, γ, α. We noticed that bluish regions are close to the phase boundaries with two phase regions and close to frustrated regions: These are failed phase transitions and the structures fluctuate between two frustrated morphologies. This is additionally confirmed by the fish-plot, where the vertical axis is Z. The dominant mechanism for instability of the monophasic regime below the critical "Z-value" is an emulsification failure. Above this critical value, the dominating mechanism for instability is due to attractive interactions between aggregates, thus leading to coalescence. Difference affinities of the two forms of the extractant between oil and water are at the origin of cation-segregation in coexisting phases: In the prism, the end of the tie lines are not in the same pseudo-ternary phase diagram, but are 3-dimensional. With values of $\Delta\mu^{w\to o} = 6.7\ kJ/mol$ for HDEHP and $\Delta\mu^{w\to o} = 1.5\ kJ/mol$ for NaDEHP. This complicates analysis and predictive modelling of phase diagrams in the biphasic region, but once understood it is a crucial property in the design of efficient separation plants.

2. Lessons from conductivity

In a multi-component system, sample-preparation and choice of an experimental path is not evident. Every component in a microemulsion, as well as in a solvent extraction system has a strong influence on the physico-chemical properties of the system, e.g. on a macroscopic scale (e.g. the phase behaviour, viscosity, density) and on a microscopic scale (e.g. morphology on a mesoscopic scale or extraction efficacy).

Therefore, based on the phase diagrams acquired in Chapter II, the conductivity of the monophasic region is first explored as a function of two dilution lines: Dilution towards water affects the packing parameter p of the solution. In return, this modifies the aggregation number, as well as the local curvature. In a reverse (swollen) micellar regime, dilution towards the organic solvent does not modify the aggregation number or the size of

aggregates, but the number of aggregates per unit volume. The conducting behaviour along these two dilution lines has been analysed, comparing the frustrated branch (for $Z = 1$) with in the non-frustrated branch of the prism ($Z = 0.5$).

In the frustrated branch, a hydration limit has been determined at $W_o = 3.9$. Below this critical value, water is tightly bound by the head-groups of the extractants. In this confined environment, the counter-ions (H^+ and Na^+) are unable to dissociate and migrate freely in an aqueous pseudo-phase. Therefore, the water-poor regime has to be classified into: a $true\ reverse\ micellar\ solution$, where no free water is present, and a *swollen reverse micellar regime*, i.e. an L2 microemulsion, where a water-core is present. As shown, conductivity measurements offer an easy measurement to determine the boundary between these two regimes. The conductivity signal below the hydration limit is yet several orders of magnitudes higher than compared to pure apolar solvents ($\sigma_{below\ hydration\ limit} \sim 10^{-7}\ S/cm$ compared to $\sigma_{apolar\ diluent} \sim 10^{-12}\ S/cm.$) Thus, the conducting signal is attributed due to the formation of charged micelles as a result of a dissociation (also dismutation) mechanism. Above the hydration limit, a water-pool is present in the micellar core. Thus, the conductivity beyond the percolation threshold increases exponentially and is in the order of $\sigma_{above\ hydration\ limit,percolated} \sim 10^{-4} - 10^{-3}\ S/cm.$

In the non-frustrated branch, the conductivity signal is in the order of $\sigma_{non-frustrated} \sim 10^{-7}\ S/cm$. Supported by small angle X-ray scattering, micelles in this regime essentially behave like hard spheres and poorly interact with each other, apart from a sterical repulsion. The conductivity signal arises thus only due to the formation of charged aggregates due to a dismutation mechanism.

The percolation threshold has been identified to be dependent of three crucial parameters: The extractant concentration $\gamma_{extractant}$, the volume fraction of dispersed water (expressed as the water-to-surfactant ratio W_0) and the *degree of frustration* (when approaching the frustrated branch at high Z).

3. Consequences on phase instability

3.1) Novel interpretation of third phase formation in solvent extraction systems

As a consequence for solvent extraction, we are able to propose a new explanation for the occurrence of third phases, as it is often observed in metal-extracting microemulsions.[36,132]

Extracting microemulsions have a Winsor II type phase behaviour, i.e. an excess aqueous phase is in equilibrium with an extracting organic phase.[10] The formation of third phases is explained as a "splitting" of the organic phase due to attractive interactions between complexes. The attraction leads to the forming of a heavy organic phase, where reverse micellar complexes form a "condensed" phase in equilibrium with a light organic phase, mainly composed of the diluent. As a result of the high spontaneous packing parameter p_0 (usually in the order of $p_0 = 2 - 3$),[39] metalloamphiphilic complexes are unable to solubilize high amounts of water, leading to an aqueous phase in excess. Therefore, three phases are in equilibrium (heavy organic phase, diluent and aqueous phase in excess).

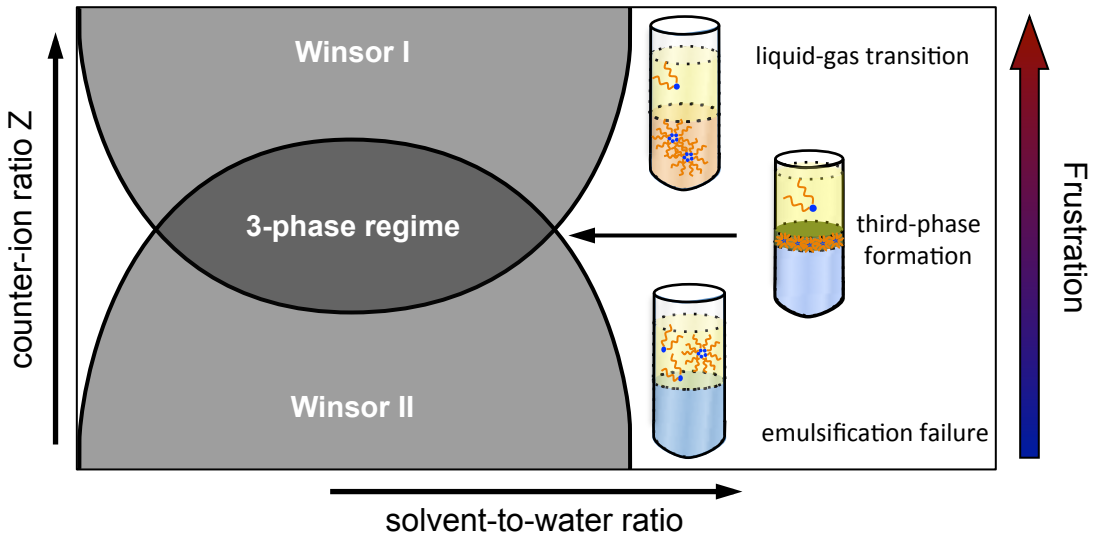

Figure IV-2 – Schematic representation of a χ-cut, where the Winsor I and Winsor II regimes overlap. In the cross-section, the system exhibits both types of phase separation: an emulsification failure and a liquid-gas-type separation.

As demonstrated in figure 2 and elucidated in Chapter II, the degree of frustration increases on the oil-rich side, the more the extractant participates in a complexation. Specifically observing the solvent-rich side, the phase separation in the Winsor II regime is driven by an emulsification failure (phase separation of type 1). In contrast, the main motor for phase

separation in the Winsor I regime is the attractive interaction between aggregates, hence the formation of a condensed phase (separation of type 2). The origin of the third phase can be explained as an overlap of a Winsor I and a Winsor II regime, thus leading to a cross-section where both types of phase separation are present. This has been mentioned by Shah *et al.* as a "phase separation of type 3", however notes that the occurrence of a third phase is only "*suggested*".[83] To revert to Osseo-Asare's statement, extracting microemulsions can thus be considered as a "special type" of microemulsions, for which this third type of phase separation is a common observation at appropriate conditions.

As a consequence, the microemulsion inside the third phase is at the same time rigid (as the aggregates are not able to solubilize more water) and frustrated.[92] This interpretation is further supported, as the structure on a mesoscopic scale is no longer that of spherical aggregates, but forms cylindrical chain-like structures called "coordination polymers".[211]

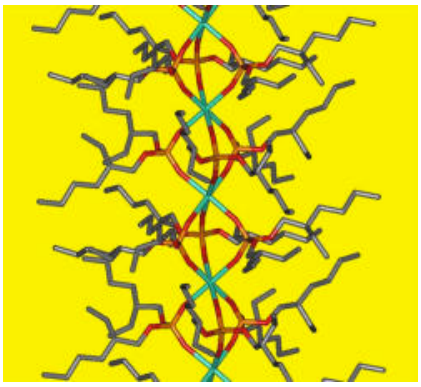

Figure IV-3 – Bottlebrush structure of complexes formed by Lanthanum and HDEHP.[212]

In frustrated phases, where the packing parameter p of the solution is dissimilar to the spontaneous packing, the amphiphiles try to compensate the unfavourable geometries by forming locally lamellar structures. Thus, cylindrical aggregation, as observed in bottlebrush structures, can be considered as a 1-dimensional lamellar extension.

As introduced in Chapter III, Erlinger *et al*. observed an increase in conductivity of the organic phase, approaching a third-phase regime, however was not able to further explain this observation.[178] With the presented approach that the third phase can be interpreted as a frustrated microemulsion, this phenomenon can be rationalized: As shown in Chapter III.5, the specific conductivity of the microemulsion increases significantly as the microemulsion approaches the frustrated regime.

3.2) Introducing: the Formulator's Cut

In order comprehensively understand the phase behaviour along the quaternary phase prism a cut-analysis has been performed, according to classical concepts known from surfactant science, namely the Chi-cut and Fish-cut. From a formulator's point of view, elaboration of a phase prism as a function of e.g. the pH, salinity in the aqueous phase, or temperature as the "edge" coordinate is accompanied by a tremendous experimental effort. Thus, a novel cut is presented, reducing the 3-dimensional representation of the phase behaviour into a 2-dimensional representation, which has been adapted for the sake of solvent extraction: the formulator's cut.

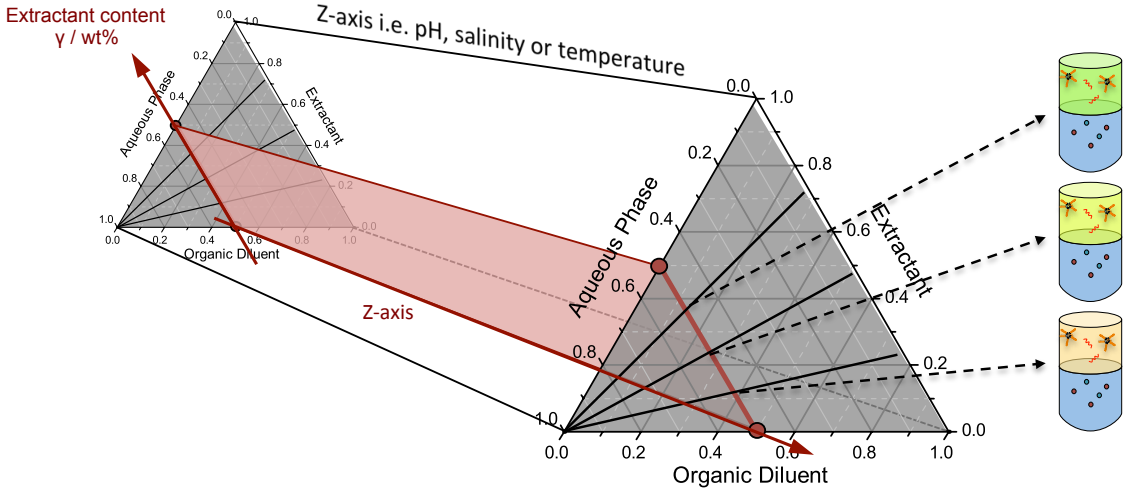

Figure IV-4 – Schematic representation of the formulator's cut: The tie lines (black lines) are cut at half their length (represented by the red line). The compositions at the intersection of the tie lines with the red line posses an equal volume of the aqueous and the organic phase.

In a solvent extraction systems, the volume of the aqueous and the organic phases are (usually) equal. In the language of phase diagrams, this means that the tie lines of a phase diagram (in vol%) are cut at half of their length, in accordance with the lever rule and as depicted in figure 4. At the intersection of the red line and the tie lines, the volume of the aqueous and the organic phase are identical, as represented by the tubes. Recording the phase behaviour as a function of e.g. the pH, salinity, the ratio of two extractants or temperature allows stretching the pseudo-ternary phase representation in a 3-dimensional prism. The relevant information on the macroscopic phase behaviour from the point of view of solvent extraction can be extracted from formulator's cut. Thus, this cut plots the phase behaviour with increasing concentration of extractant in the organic phase as a function of the "edge" coordinate of choice.

In figure 5, the formulator's cut for the prism with toluene as a solvent is shown. Since the orientation of the tie lines is not in the same plan as the pseudo-ternary phase diagrams, a simplified cut was chosen for a demonstration purpose. The prism was cut at a constant

weight fraction of $w_{water} = 50wt\%$, thus giving the cut as illustrated by the red surface in figure 4.

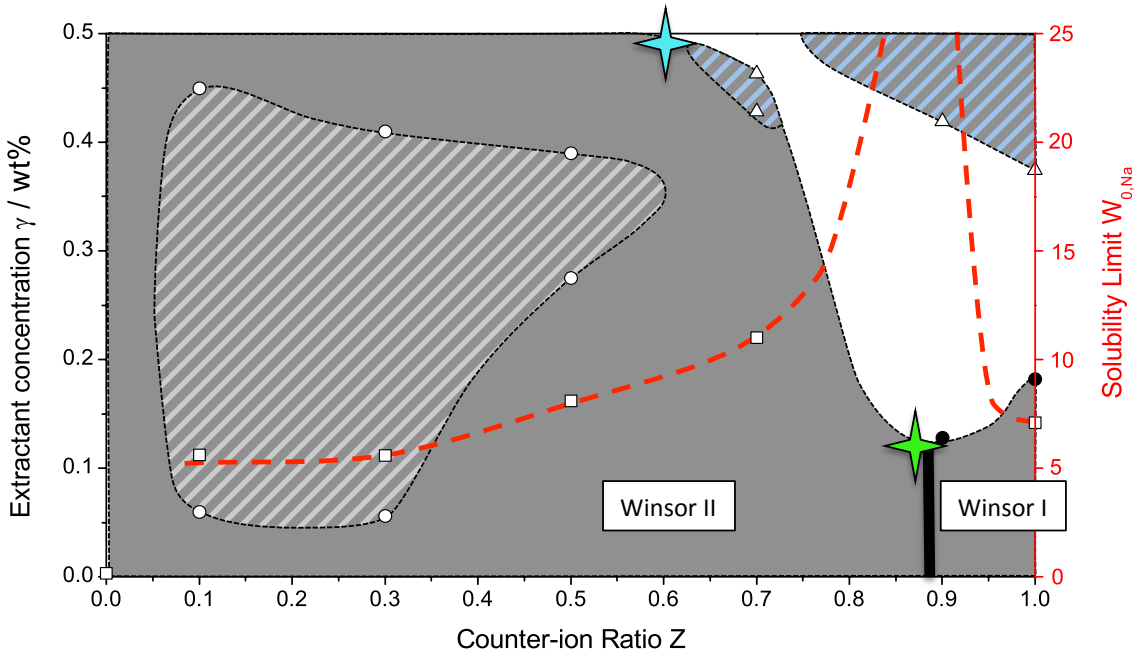

Figure IV-5 – Formulator's cut for the quaternary system toluene/NaDEHP/HEHP/water at a constant weight fraction of $w_{water} = 50wt\%$. The phase behaviour with increasing extractant concentration is plotted as a function of the counter-ion ratio Z. Additionally, the solubility of water in the organic phase is plotted as a function of the counter-ion ratio, using the right Y-axis. The solubility is illustrated by the red dashed curve. The black line at $Z = 0.9$ indicates the maximum solubility of the quaternary system.

The advantage of this plot is the easy deduction of the phase behaviour. In this representative case the assumption is made that the volumes of the aqueous and organic phase in the liquid-liquid regime are equal and that the extractant (HDEHP as well as NaDEHP) are entirely solubilized in the organic phase. The sodium-ion imitates the function of an extracted ion, thus the objective is to find a formulation with a high distribution ratio (high counter-ion ratio in the organic phase), as well as a high concentration of extractant in the organic phase. Above the solubility maximum at $Z = 0.9$, the microemulsion will transition into a Winsor I-phase (liquid-gas phase transition). As a result, there are 2 different "optimum formulations" available:

1) A high distribution ratio before the system enters a monophasic region (green cross) or enters a Winsor I-phase
2) A lower distribution ratio, where increase of the counter-ion ratio would lead to a transition into a liquid-crystalline phase (blue cross)

Though this is only a demonstration, this plot can serve as a versatile tool for chemical engineers in order to find an optimum formulation and yet decreasing the experimental effort.

3.3) From solvents to co-solvents – Green alternatives for solvent extraction using ultraflexible microemulsion

In the process of re-inventing industrial procedures, there is always a need for to replace chemical compounds, which do not comply with the European REACH regulation.[213] In solvent extraction of precious metals, this regulation afflicts e.g. the use of non-phosphorous extractants, or the replacement of organic diluents stemming from petroleum production. Towards greener solvents, one route is the replacements of organic diluents by ionic liquids.[214] A second alternative and innovative route anticipates a departure from classical liquid-liquid extraction when replacing the organic diluent for a hydrotrope, using so-called *ultraflexible microemulsions*.

3.3.1)Introducing: Ultraflexible microemulsions

The formation of micelle-like structures in ternary solutions of three solvents of differential polarities has been postulated in the 70s by Barden and co-workers.[215] However it has only been recently that their significance has been realized. The first hint on the existence of mesoscopic heterogeneities in the vicinity of the phase boundary in the ternary system octan-1-ol/ethanol/water has been reported using DLS-measurements.[216] In a series of experimental,[217] and theoretic approaches,[218,219] existence of direct micelle-like aggregates have been proven. The self-assembly of octanol-molecules to a loose aggregate is supported by the adsorption of ethanol at the interface (as highlighted in figure 6).

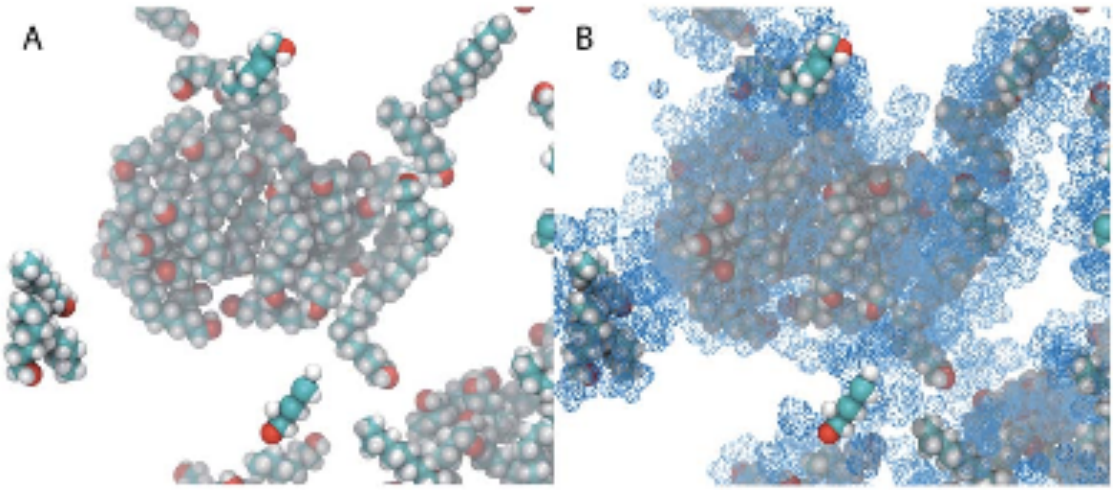

Figure IV-6 – A) Octan-1-ol cluster in a water-continuous environment. B) Same cluster as a with ethanol molecules adsorbed at the interface.[218]

Further, it could be revealed, that the structuring is not limited to the water-rich side of the phase diagram, but depending on the ratio of water to solvent, the system can transition from direct aggregates towards reverse micellar aggregates, passing by a bicontinuous regime.[ii]

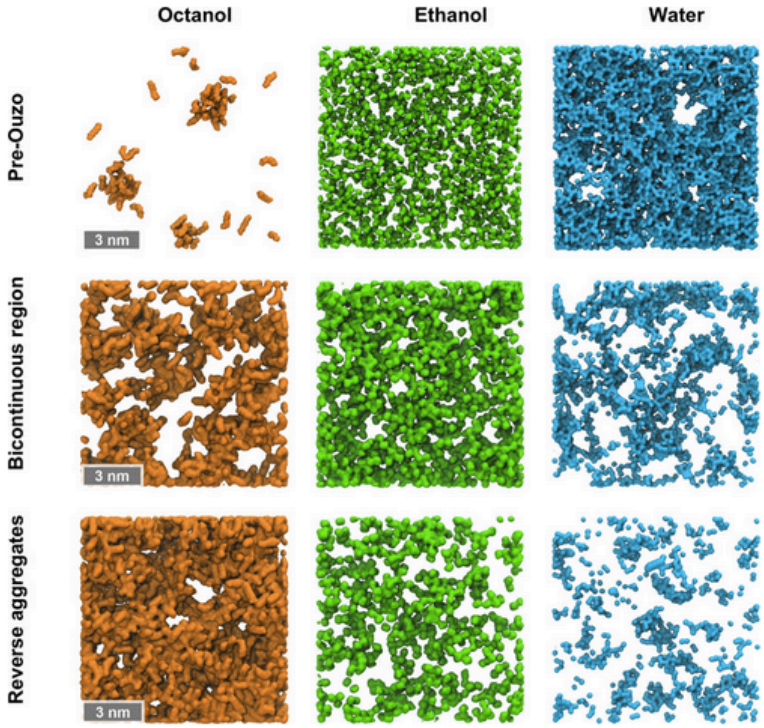

Figure IV-7 – Simulated structure of ultraflexible microemulsion, depending on the composition

As depicted in figure 7, on the water-rich "pre-Ouzo" side, discrete octan-1-ol aggregates are observed in a water-continuous environment. In the bicontinuous regime, water as well as octan-1-ol forms a bicontinuous network. On the octan-1-ol rich side, polydisperse, but discrete water-pools are found in an oil-continuous environment.

The interaction between ethanol and octanol are primarily dispersion forces,[219] however the repulsive force between two aggregates is of entropic origin, resulting from the hydration forces.[iii] Since the interactions are in the order of 1 kT, the UFME have a highly dynamic and flexible nature, thus the terminus *ultraflexible microemulsions* has been established.

[ii] T. Lopian, S. Schöttl, S. Prévost, S. Pellet-Rostaing, D. Horinek, W. Kunz, T. Zemb, Morphologies observed in ultraflexible microemulsions with and without the oresence of a strong acid, *ACS Central Science* **2016**, *2(7)*, 467-475.
[iii] T. Zemb, M. Klossek, T. Lopian, J. Marcus, S. Schoettl, D. Horinek, S. Prévost, D. Touraud, O. Diat, S. Marcelja, W. Kunz, How to explain microemulsions formed by solvent mixtures without conventional surfactants, PNAS 2016,

3.3.2)Towards an alternative solvent extraction procedure

There are many requirements towards the formulation of a solvent extraction system for application on an industrial scale. One of the major drawbacks is often a slow kinetic of complex-formation at the interface.[114] The high interfacial tension between the aqueous and organic phase, even in the presence of amphiphilic extractants is certainly contribution to this dilemma.[220] Therefore, surfactants are added as additives in order to decrease the interfacial tension and increase the reaction kinetics of complex formation.[6] Ultraflexible microemulsions offer not only the a very low interfacial tension, but using a hydrotropic co-solvent enables not only to dispense the organic solvent, but also the addition of toxic surfactants.[221]

Most extractants, such as HDEHP, DMDOHEMA, DEHCNPB, TODGA, octan-1-ol, TBP, etc. are (at ambient temperatures) in a liquid matter of state, with a poor solubility in water. Therefore, the main idea is to overcome this immiscibility towards an aqueous phase by adding a hydrotropic co-solvent, where the interface between the extractants and the aqueous phase can be maximized. By positioning in a direct-micelle like condition, several extractant molecules form a cluster, ready to complex a metal-cation from the pseudo-aqueous phase.

In a pilot study, the system was based on the most studied UFME system octan-1-ol/ethanol/water, where octan-1-ol has been reported to be an excellent extractant for Tantalum and Niobium. [iv] At high temperatures (60 °C), the miscibility gap is smaller than at ambient conditions, therefore a formulation in-between the binodals was chosen and phase separation is induced upon cooling of the solution. However, due to the small net increase of the monophasic region upon variation of the temperature, a more thermo-sensible hydrotrope was chosen: 1-propoxy-2-propanol (PnP). At room temperature, PnP is completely soluble with water for any given ratio, however increase of the temperature leads to a lower critical separation temperature and thus a de-mixing.[222] With this approach, the operation procedure of the pilot study is reversed. The extraction in a monophasic UFME is conducted at room temperature, whereas the separation of the organic phase is induced upon increasing the temperature, transforming the miscibility gap of type 1 (RT) towards a type 2 phase behaviour (at increased temperatures).[223,224]

[iv] T. Lopian, Selective liquid-liquid extraction using the pre-Ouzo effect, Master Thesis **2014**

In a contribution towards a greener approach in solvent extraction, the macroscopic phase behaviour of HDEHP and water was analysed, replacing organic diluent by the hydrotrope PnP.

Figure IV-8 – Quaternary phase prism of 1-propoxy-2-propanol/HDEHP/NaDEHP/water, for ratios of $Z = 0;\ 0.3;\ 0.7$. Biphasic regimes are depicted in grey, monophasic regimes in white.

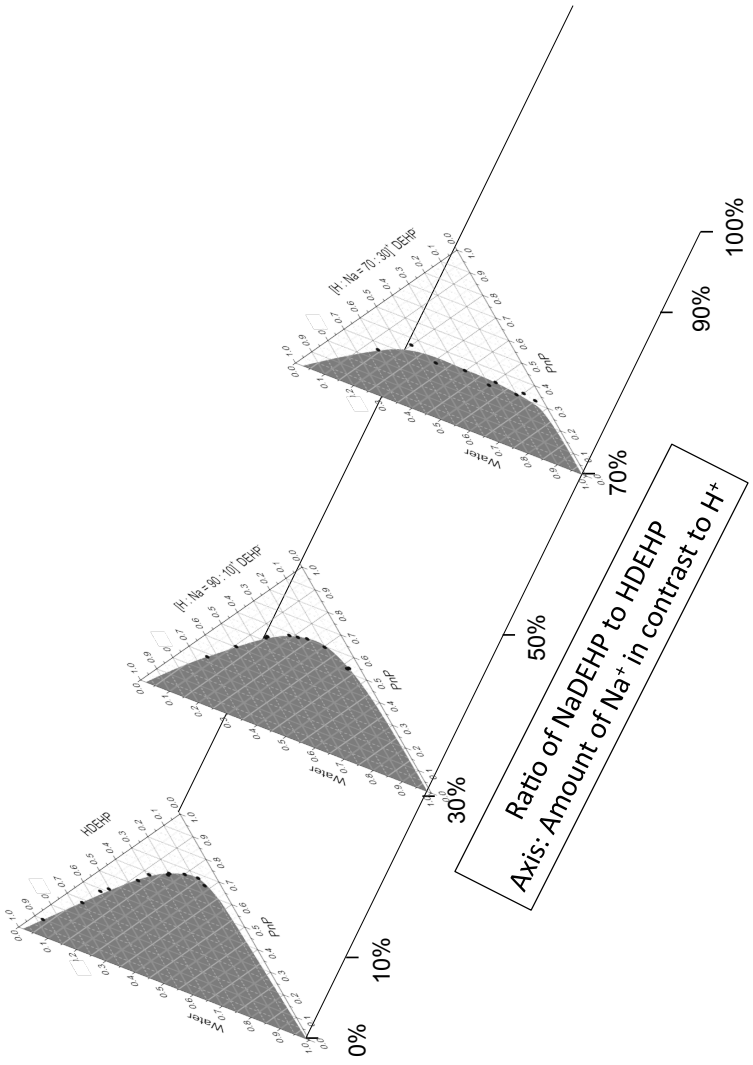

Figure IV-8 – Quaternary phase prism of 1-propoxy-2-propanol/HDEHP/NaDEHP/water, for ratios of $Z = 0;\ 0.3;\ 0.7$. Biphasic regimes are depicted in grey, monophasic regimes in white.

In figure 8, three pseudo-ternary phase diagrams are depicted as a function of the counter-ion ratio Z. In the phase diagram for $Z = 0$, PnP is able to successfully close the miscibility gap of HDEHP and water. Partial replacement of the proton by a sodium-cation leads to a decrease of the miscibility gap as the counter-ion variation increases. This is a natural consequence of NaDEHP being a surfactant. However, this little demonstration serves as a motivation using HDEHP as an extractant for an alternative extraction using UFME. In

contrast to previously studied extractants, HDEHP offers an easy control of distribution ratio and separation coefficient by modifying the acidity. Further, it was be shown that ultraflexible microemulsions are nearly unaffected of the acidic concentration in the aqueous phase.[225]

Therefore, peri-critical extraction, i.e. using ultraflexible microemulsions as extraction media offers a versatile, novel and green approach towards the extraction of rare earth elements.

4. Conclusion

This chapter gives an overview on the results obtained in Chapter II and III of this work, namely the evolution of the macroscopic phase behaviour and the conductivity profiles. Transferring the acquired knowledge for the model system with HDEHP and NaDEHP on a solvent extraction system offers a new perspective on the interpretation of fundamental hurdles encountered in solvent extraction. On one hand, the origin of third-phase formation can be explained with the concept of frustration. On the other hand, a novel and versatile cut is presented, reducing the experimental effort to obtain a comprehensive map for solvent extraction: the formulator's cut. Finally, a new route towards a greener solvent extraction procedure is presented, where a hydrotropic co-solvent replaces the organic diluent: towards solvent extraction using ultraflexible microemulsions.

General conclusion

Rare earth elements have a significant importance for the transition towards a green and sustainable economy due to their unique physical and chemical properties. However, only 1% of the worldwide annual production of rare earths stems from a recycling process. Therefore, sustainable energy and environmentally benign technology still run on resources of non-sustainable origin. The objective of the ERC-project REEcycle is to address this problematic. On one hand, the scope is to fundamentally understand the physico-chemical properties in of solvent extraction systems, which are the core separation process in hydrometallurgy. On the other hand, the aim is to develop a new, cost efficient and environmentally friendly recycling process, adapted for rare earths.

In the frame of the ERC-project REEcycle, this work addresses two fundamental questions, which are yet poorly understood for solvent extraction systems: the macroscopic phase behaviour and the conductivity profiles in an extracting microemulsion. In order to challenge these questions, a model system is introduced, based on the well-known extractant HDEHP. Its sodium form (NaDEHP) plays the role of an extractant engaged in complex formation. Thus, the sodium-ion adopts the function of an extracted ion. Completed with water and an organic diluent, this system has all necessary components to appropriately imitate a solvent extraction system.

A quaternary phase prism was established, in analogy to a Gibbs prism for surfactant systems. In surfactant systems, the “edge” coordinate in such a prism is the temperature. The temperature modifies not only the solubility of a surfactant in water or oil, but also the spontaneous packing parameter p_0 of the amphiphile. In our case, we replaced the intensive variable (temperature) by the counter-ion ratio between the sodium and protonated form of the extractant, which we call Z. This approach is justified, as variation of the counter-ion of an extractant affects the same properties: it modifies the solubility, as well as the effective surface of the head group and thus the spontaneous packing parameter.

The macroscopic phase behaviour is comprehensively investigated using toluene as a reference solvent. Analysis of the two “faces” of the prism, where the ternary phase diagrams are *truly* ternary, two main mechanisms for phase separation have been detected: For the fully protonated form of the extractant, the organic phase separates as water is no more soluble in the organic phase. Thus, it is excluded to form an aqueous phase in excess. This separation is called an *emulsification failure*, where the dispersed solvent can no longer be

solubilized and is ejected from the microemulsion. This phase separation is driven by rigidity constraints, as the reverse aggregates cannot be inflated any further. As the microemulsion is in equilibrium with an excess aqueous phase, this regime is also called a Winsor II regime. In contrast, if the extractant is solubilized in toluene as a sodium salt, a splitting of the organic phase is detected. At the phase boundary, the organic phase separates into a "condensed" microemulsion phase and an organic phase in excess. The surrounding solvent in the microemulsion is still toluene, thus not the interior, but the exterior solvent is ejected. The main driving force for phase separation upon addition of water has been recognized to be due to attractive interactions between reverse micelles. Thus, we call this a *liquid-gas type separation*. When adding water, it can still be solubilized in the microemulsion, thus the interface is still flexible. The microemulsion is in equilibrium with an excess organic phase, thus referring to this region as a Winsor I-phase.

If NaDEHP and HDEHP are mixed, a maximum solubility of water and toluene is detected for a ratio of $HDEHP : NaDEHP = 1:9$. Thus, HDEHP can be considered as a co-surfactant. Due to the two different types of phase separations, HDEHP on one hand increases the flexibility of the interfacial film, on the other hand it decreases the attractive interactions between NaDEHP micelles.

Performing a fish-cut and χ-cut analysis, where sections of the prism are cut at either a constant water-to-toluene ratio or constant extractant content allows correlating the previous results with the concept of *frustration:* If the packing parameter p for a given composition is close to the spontaneous packing parameter p_0 of the extractant, the system is non-frustrated. In case that the packing parameter strongly deviates, the microemulsion is *frustrated*. From the χ-cut representation it was derived, that systems in the frustrated branches of the plot succumb to a liquid-gas type separation. In the non-frustrated branches, the phase separation is due to an emulsification failure.

The tie lines in the quaternary regime have been investigated. Due to the preferential solubility of NaDEHP in water and HDEHP in toluene, the tie lines are not in the same plane as the initial composition, but are arranged diagonal in the prism.

The Gibbs prism has been prepared for three alternative solvents, in order to investigate the influence of diluents on the macroscopic phase behaviour: iso-octane, dodecane and nitrobenzene. For all three cases, the non-frustrated part is nearly unaffected when replacing toluene for an alternative. In the frustrated regime, where interactions between reverse micelles dominate the phase separation, the choice of solvent has a significant consequence. Different types of interactions between reverse micelles in the frustrated regime have been identified, which play a role in the liquid-gas phase transition: Entropic

depletion forces, dipole-dipole interactions between polar cores and Van der Waals interactions between overlapping shells.

Using the Gibbs prism as a map, the conductivity in the oil-rich region of the diagram has been explored as a function of three variables: the water content (described as the water to extractant ratio W_0), the extractant concentration $\gamma_{extractant}$ and the counter-ion ratio Z.

Comparison of the conductivity profile in the non-frustrated and frustrated regions have been in the focus of interest. In the non-frustrated regime, the electrical conductance ($\sigma_{non-frustrated} = 10^{-9} - 10^{-7}\ S/cm$) is significantly higher compared to the conductivity of an apolar solvent ($\sigma_{organic\ solvent} = 10^{-16} - 10^{-12}\ S/cm$) and is assigned to the formation of charged micelles, due to a dismutation phenomenon. Even at very high concentrations of extractant where X-ray spectra show a strong correlation peak ($\gamma_{extractant} > 30wt\%$), the conductivity is still very low compared to percolated or dynamic structures.

In contrast, the conductivity in the frustrated branch may be significantly higher, but depends if the (pseudo-)ternary solution is below or above the hydration limit. If below the hydration limit, the conductivity may only be due to a dismutation of micelles. However, a “jump” of a charge carrier, as in dynamic percolation is not possible. If however enough water is solubilized in the micellar core to form a “water-pool”, the conductance increases significantly even at low extractant concentrations ($\gamma_{extractant} \sim 2 - 3wt\%$).

The percolation threshold is dependent on three different factors: the *degree of frustration* (thus the water-poor region at high Z), the water-content (expressed as W_0) and the concentration of extractant in the solution ($\gamma_{extractant}$).

Fundamental analysis of the phase behaviour and the conductivity profile in these maps allows drawing important conclusions for solvent extraction of rare earths:

As a result of this phase behaviour, a novel interpretation of third-phase formation in extracting microemulsion is formulated: Overlap of Winsor I and Winsor II regime lead to a regime where both types of phase separation are observed at the same time: an emulsification failure and a liquid-gas transition. Thus, splitting of the organic phase is driven by frustration. In order to avoid an extensive experimental effort to deduce the phase behaviour of extracting microemulsions in form of a Gibbs prism, a new cut is introduced that

we call the *formulator's cut*. Since the volume of the aqueous and the organic phase in a solvent extraction procedure are equal, a 2-dimensional phase diagram is proposed. For a green approach in solvent extraction, a new extraction principle is introduced, based on ultraflexible microemulsions.

References

(1) Svedberg, T. The Ultracentrifuge. *Nobel Lect.* **1926**.

(2) Gomes, P. B.; Mata, V. G.; Rodrigues, A. E. Production of Rose Geranium Oil Using Supercritical Fluid Extraction. *J. Supercrit. Fluids* **2007**, *41* (1), 50–60.

(3) Myasoedov, P. B. F. The Science and Technology of Tributyl Phosphate. *Solvent Extr. Ion Exch.* **1986**, *4* (5), 1077–1078.

(4) Serrano-Purroy, D.; Christiansen, B.; Glatz, J.-P.; Malmbeck, R.; Modolo, G. Towards a DIAMEX Process Using High Active Concentrate. Production of Genuine Solutions. *Radiochim. Acta* **2007**, *93* (6), 357–361.

(5) Hoogerstraete, T. V.; Wellens, S.; Verachtert, K.; Binnemans, K. Removal of Transition Metals from Rare Earths by Solvent Extraction with an Undiluted Phosphonium Ionic Liquid: Separations Relevant to Rare-Earth Magnet Recycling. *Green Chem.* **2013**, *15* (4), 919–927.

(6) Rydberg, J. *Solvent Extraction Principles*; CRC Press, 2004.

(7) Schwedt, G.; Schmidt, T. C.; Schmitz, O. J. *Analytische Chemie: Grundlagen, Methoden und Praxis*, 3rd ed.; Wiley-VCH Verlag GmbH & Co. KGaA: Weinheim, 2016.

(8) Motschmann, H. *Physikalische Chemie: Für die Bachelorprüfung*; De Gruyter: Berlin ; Boston, 2014.

(9) Nernst, W. Verteilung Eines Stoffes Zwischen Zwei Lösungsmitteln Und Zwischen Lösungsmittel Und Dampfraum. *Z. Für Phys. Chem.* **1891**, No. 8, 110.

(10) Zemb, T.; Bauer, C.; Bauduin, P.; Belloni, L.; Déjugnat, C.; Diat, O.; Dubois, V.; Dufrêche, J.-F.; Dourdain, S.; Duvail, M.; et al. Recycling Metals by Controlled Transfer of Ionic Species between Complex Fluids: En Route to “Ienaics.” *Colloid Polym. Sci.* **2014**, *293* (1), 1–22.

(11) Hiskey, B. Metallurgy, Survey. In *Kirk-Othmer Encyclopedia of Chemical Technology*; John Wiley & Sons, Inc., 2000.

(12) Wenzel, M.; Schnaars, K.; Kelly, N.; Götzke, L.; Robles, S. M.; Kretschmer, K.; Le, P. N.; Tung, D. T.; Luong, N. H.; Duc, N. A.; et al. Hydrometallurgical Recovery of Rare Earth Metals from Spent FCC Catalysts. In *Rare Metal Technology 2016*;

Springer, Cham, 2016; pp 37–45.

(13) Coulson, J. M.; Richardson, J. F. *Coulson and Richardson's Chemical Engineering: Chemical Engineering Vol 2*, New ed of 2 Revised ed edition.; Sinnott, R. K., Ed.; Butterworth-Heinemann Ltd: Oxford ; Boston, 1996.

(14) Rice, N. M.; Irving, H. M. N. H.; Leonard, M. A. Nomenclature for Liquid-Liquid Distribution (Solvent Extraction) (IUPAC Recommendations 1993). *Pure Appl. Chem.* **2009**, *65* (11), 2373–2396.

(15) Peligot, M. E. Recherches Sur l'uranium. *Ann Chim Phys* **1842**, *5*, 5–47.

(16) Mayorov, V. G.; Nikolaev, A. I. Tantalum (V) and Niobium (V) Extraction by Octanol. *Hydrometallurgy* **2002**, *66* (1), 77–83.

(17) Agulyansky, A.; Agulyansky, L.; Travkin, V. F. Liquid–liquid Extraction of Tantalum with 2-Octanol. *Chem. Eng. Process. Process Intensif.* **2004**, *43* (10), 1231–1237.

(18) Bauer, C. Metal Ion Extractant in Microemulsions: Where Solvent Extraction and Surfactant Science Meet, 2011.

(19) Paatero, E.; Sjöblom, J. Phase Behaviour in Metal Extraction Systems. *Hydrometallurgy* **1990**, *25* (2), 231–256.

(20) Pierce, T. B.; Peck, P. F. The Extraction of the Lanthanide Elements from Perchloric Acid by Di-(2-Ethylhexyl) Hydrogen Phosphate. *Analyst* **1963**, *88* (1044), 217–221.

(21) Tait, B. K. Cobalt-Nickel Separation: The Extraction of Cobalt(II) and Nickel(II) by Cyanex 301, Cyanex 302 and Cyanex 272. *Hydrometallurgy* **1993**, *32* (3), 365–372.

(22) Tsakiridis, P. E.; Agatzini, S. L. Process for the Recovery of Cobalt and Nickel in the Presence of Magnesium and Calcium from Sulphate Solutions by Versatic 10 and Cyanex 272. *Miner. Eng.* **2004**, *17* (4), 535–543.

(23) Dembiński, W.; Mioduski, T. Europium Isotope Separation in the HCl/HDEHP Extraction System. *J. Radioanal. Nucl. Chem.* **1995**, *199* (2), 159–171.

(24) Coca, J.; Díez, F. V.; Morís, M. A. Solvent Extraction of Molybdenum and Tungsten by Alamine 336 and DEHPA. *Hydrometallurgy* **1990**, *25* (2), 125–135.

(25) Sato, T.; Watanabe, H.; Suzuki, H. Liquid-Liquid Extraction of Molybdenum(VI) from Aqueous Acid Solutions by TBP and TOPO. *Hydrometallurgy* **1990**, *23* (2), 297–308.

(26) Carrott, M.; Geist, A.; Hères, X.; Lange, S.; Malmbeck, R.; Miguirditchian, M.; Modolo, G.; Wilden, A.; Taylor, R. Distribution of Plutonium, Americium and Interfering Fission Products between Nitric Acid and a Mixed Organic Phase of TODGA and DMDOHEMA in Kerosene, and Implications for the Design of the "EURO-GANEX" Process. *Hydrometallurgy* **2015**, *152*, 139–148.

(27) Bollesteros, M.-J.; Calor, J.-N.; Costenoble, S.; Montuir, M.; Pacary, V.; Sorel, C.; Burdet, F.; Espinoux, D.; Hérès, X.; Eysseric, C. Implementation of Americium Separation from a PUREX Raffinate. *Procedia Chem.* **2012**, *7* (Supplement C), 178–183.

(28) McDowell, W. J.; Coleman, C. F. Interface Mechanism for Uranium Extraction by Amine Sulphate. *J. Inorg. Nucl. Chem.* **1967**, *29* (5), 1325–1343.

(29) Cupples, H. L. Interfacial Tension by the Ring Method: The Benzene-Water Interface. *J. Phys. Colloid Chem.* **1947**, *51* (6), 1341–1345.

(30) Lo, T. C.; Baird, M. H. I.; Hanson, C. *Handbook of Solvent Extraction*; Wiley: New York, 1983.

(31) Osseo-Asare, K. Aggregation, Reversed Micelles, and Microemulsions in Liquid-Liquid Extraction: The Tri-n-Butyl Phosphatediluent-Water-Electrolyte System. *Adv. Colloid Interface Sci.* **1991**, *37* (1–2), 123–173.

(32) Gaonkar, A. G.; Garver, T. M.; Neuman, R. D. 1H-NMR Spectroscopic Investigation of Reversed Micellization in Metal/Organophosphorous Surfactant System. *Colloids Surf.* **1988**, *30* (3), 265–273.

(33) Gaonkar, A. G.; Neuman, R. D. Interfacial Activity, Extractant Selectivity, and Reversed Micellization in Hydrometallurgical Liquid/Liquid Extraction Systems. *J. Colloid Interface Sci.* **1987**, *119* (1), 251–261.

(34) Erlinger, C.; Gazeau, D.; Zemb, T.; Madic, C.; Lefrançois, L.; Hebrant, M.; Tondre, C. Effects of Nitric Acid Extraction on Phase Behaviour, Microstructure and Interactions between Primary Aggregates in the System Dimethyldibutyltetradecylmalinamide (DMDBTDMA/ Dodecane / Water: A Phase Analysis and Small-Angle X-Ray Scattering (SAXS) Characterization Study. *Solvent Extr. Ion Exch.* **1998**, *16* (3), 707–738.

(35) Marinet, L. Effet Des Ions Multivalents Sur l'instabilité Des Solutions Concentrées d'extractants, 2005.

(36) Nave, S.; Mandin, C.; Martinet, L.; Berthon, L.; Testard, F.; Madic, C.; Zemb,

T. Supramolecular Organisation of Tri-n-Butyl Phosphate in Organic Diluent on Approaching Third Phase Transition. *Phys. Chem. Chem. Phys.* **2004**, *6* (4), 799–808.

(37) Qiao, B.; Ferru, G.; Olvera de la Cruz, M.; Ellis, R. J. Molecular Origins of Mesoscale Ordering in a Metalloamphiphile Phase. *ACS Cent. Sci.* **2015**, *1* (9), 493–503.

(38) Julien Rey, S. D. Synergy in Extraction System Chemistry: Combining Configurational Entropy, Film Bending, and Perturbation of Complexation. *Langmuir ACS J. Surf. Colloids* **2015**, *31* (25).

(39) Bley, M.; Siboulet, B.; Karmakar, A.; Zemb, T.; Dufrêche, J.-F. A Predictive Model of Reverse Micelles Solubilizing Water for Solvent Extraction. *J. Colloid Interface Sci.* **2016**, *479*, 106–114.

(40) Evens, D. F.; Wennerström, H. *The Colloidal Domain: Where Physics, Chemisry, Biology and Technology Meet*, Second Edition.; Wiley-VCH, 1999.

(41) Rosen, M. J.; Kunjappu, J. T. *Surfactants and Interfacial Phenomena*, 4 edition.; Wiley: Hoboken, N.J, 2012.

(42) Holmberg, K.; Shah, D. O.; Schwuger, M. J. *Handbook of Applied Surface and Colloid Chemistry*; Wiley, 2002.

(43) Holmberg, K.; Jönsson, B.; Kronberg, B.; Lindman, B. Surfactant Micellization. In *Surfactants and Polymers in Aqueous Solution*; John Wiley & Sons, Ltd, 2002; pp 39–66.

(44) Klaus, A. Solubility of Triglycerides in Water Using Extended Surfactants, Regensburg, 2011.

(45) Turro, N. J.; Yekta, A. Luminescent Probes for Detergent Solutions. A Simple Procedure for Determination of the Mean Aggregation Number of Micelles. *J. Am. Chem. Soc.* **1978**, *100* (18), 5951–5952.

(46) Mukerjee, P.; Mysels, K. J. Critical Micelle Concentrations of Aqueous Surfactant Systems. *J. Pharm. Sci.* **1972**, *61* (2), 319–319.

(47) Chevalier, Y.; Zemb, T. The Structure of Micelles and Microemulsions. *Rep. Prog. Phys.* **1990**, *53* (3), 279.

(48) Dill, K.; Bromberg, S. *Molecular Driving Forces: Statistical Thermodynamics in Biology, Chemistry, Physics, and Nanoscience*, 2 Revised edition.; Taylor & Francis Inc: London ; New York, 2010.

(49) Chandler, D. Hydrophobicity: Two Faces of Water. *Nature* **2002**, *417* (6888), 491.

(50) Kronberg, B.; Costas, M.; Silveston, R. Thermodynamics of the Hydrophobic Effect in Surfactant Solutions: Micellization and Adsorption. *Pure Appl. Chem.* **2009**, *67* (6), 897–902.

(51) Maibaum, L.; Dinner, A. R.; Chandler, D. Micelle Formation and the Hydrophobic Effect. *J. Phys. Chem. B* **2004**, *108* (21), 6778–6781.

(52) Fowkes, F. M. The Interactions of Polar Molecules, Micelles and Polymers in Nonaqueous Media. In *Solvent properties ov surfactant solutions*; Dekker, 1967; pp 65–115.

(53) Eicke, H.-F.; Christen, H. Is Water Critical to the Formation of Micelles in Apolar Media?? *Helv. Chim. Acta* **1978**, *61* (6), 2258–2263.

(54) Eicke, H. F.; Christen, H. Nucleation Process of Micelle Formation in Apolar Solvents. *J. Colloid Interface Sci.* **1974**, *48* (2), 281–290.

(55) Yu, Z. J.; Zhou, N. F.; Neuman, R. D. On the Role of Water in the Formation of Reversed Micelles: An Antimicellization Agent. *Langmuir* **1992**, *8* (8), 1885–1888.

(56) Ravey, J. C.; Buzier, M.; Picot, C. Micellar Structures of Nonionic Surfactants in Apolar Media. *J. Colloid Interface Sci.* **1984**, *97* (1), 9–25.

(57) Zulauf, M.; Eicke, H. F. Inverted Micelles and Microemulsions in the Ternary System Water/Aerosol-OT/Isooctane as Studied by Photon Correlation Spectroscopy. *J. Phys. Chem.* **1979**, *83* (4), 480–486.

(58) Kotlarchyk, M.; Huang, J. S.; Chen, S. H. Structure of AOT Reversed Micelles Determined by Small-Angle Neutron Scattering. *J. Phys. Chem.* **1985**, *89* (20), 4382–4386.

(59) Faure, A.; Tistchenko, A. M.; Zemb, T.; Chachaty, C. Aggregation and Dynamical Behavior in Sodium Diethylhexyl Phosphate/Water/Benzene Inverted Micelles. *J. Phys. Chem.* **1985**, *89* (15), 3373–3378.

(60) Tanford, C. *The Hydrophobic Effect: Formation of Micelles and Biological Membranes*, 2nd Revised edition edition.; John Wiley & Sons Inc: New York, 1980.

(61) Déjugnat, C.; Dufrêche, J.-F.; Zemb, T. Ion-Specific Weak Adsorption of Salts and Water/Octanol Transfer Free Energy of a Model Amphiphilic Hexapeptide. *Phys. Chem. Chem. Phys.* **2011**, *13* (15), 6914–6924.

(62) Ekwall, P.; Mandell, L.; Fontell, K. Solutions of Alkali Soaps and Water in Fatty

Acid V. Measurements of Water Vapour Pressure and Electrical Conductivity. *Colloid Polym. Sci.* **1986**, *264* (6), 542–551.

(63) Danielsson, I.; Lindman, B. The Definition of Microemulsion. *Colloids Surf.* **1981**, *3* (4), 391–392.

(64) Abbe, E. Beiträge zur Theorie des Mikroskops und der mikroskopischen Wahrnehmung. *Arch. Für Mikrosk. Anat.* **1873**, *9* (1), 413–418.

(65) Ruckenstein, E.; Chi, J. C. Stability of Microemulsions. *J. Chem. Soc. Faraday Trans. 2 Mol. Chem. Phys.* **1975**, *71* (0), 1690–1707.

(66) Sagisaka, M.; Narumi, T.; Niwase, M.; Narita, S.; Ohata, A.; James, C.; Yoshizawa, A.; Taffin de Givenchy, E.; Guittard, F.; Alexander, S.; et al. Hyperbranched Hydrocarbon Surfactants Give Fluorocarbon-like Low Surface Energies. *Langmuir* **2014**, *30* (21), 6057–6063.

(67) Griffin, W. C. Classification of Surface-Active Agents by "HLB." *J. Cosmet. Sci.* **1949**, *1* (5), 311–326.

(68) Winsor, P. A. *Solvent Properties of Amphiphilic Compounds.*; Butterworths: London, 1954.

(69) Shinoda, K.; Arai, H. The Correlation between Phase Inversion Temperature In Emulsion and Cloud Point in Solution of Nonionic Emulsifier. *J. Phys. Chem.* **1964**, *68* (12), 3485–3490.

(70) Prévost, S.; Gradzielski, M.; Zemb, T. Self-Assembly, Phase Behaviour and Structural Behaviour as Observed by Scattering for Classical and Non-Classical Microemulsions. *Adv. Colloid Interface Sci.* **2017**.

(71) Hoar, T. P.; Schulman, J. H. Transparent Water-in-Oil Dispersions: The Oleopathic Hydro-Micelle. *Nature* **1943**, *152*, 102–103.

(72) Kumar, P.; Mittal, K. L. *Handbook of Microemulsion Science and Technology*; Marcel Dekker Inc: New York, 1999.

(73) Eicke, H.-F. On the Cosurfactant Concept. *J. Colloid Interface Sci.* **1979**, *68* (3), 440–450.

(74) Graciaa, A.; Lachaise, J.; Cucuphat, C.; Bourrel, M.; Salager, J. L. Improving Solubilization in Microemulsions with Additives. 2. Long Chain Alcohols as Lipophilic Linkers. *Langmuir* **1993**, *9* (12), 3371–3374.

(75) N. Israelachvili, J.; John Mitchell, D.; W. Ninham, B. Theory of Self-Assembly of Hydrocarbon Amphiphiles into Micelles and Bilayers. *J. Chem. Soc. Faraday*

Trans. 2 Mol. Chem. Phys. **1976**, *72* (0), 1525–1568.

(76) Salim, M.; Minamikawa, H.; Sugimura, A.; Hashim, R. Amphiphilic Designer Nano-Carriers for Controlled Release: From Drug Delivery to Diagnostics. *MedChemComm* **2014**, *5* (11), 1602–1618.

(77) Helfrich, W. Elastic Properties of Lipid Bilayers: Theory and Possible Experiments. *Z. Für Naturforschung C* **2014**, *28* (11–12), 693–703.

(78) Georgiev, A. Membrane Stress and the Role of GYF Domain Proteins. **2008**.

(79) Zemb, T. N. The DOC Model of Microemulsions: Microstructure, Scattering, Conductivity and Phase Limits Imposed by Sterical Constraints. *Colloids Surf. Physicochem. Eng. Asp.* **1997**, *129*, 435–454.

(80) Hyde, S. T.; Ninham, B. W.; Andersson, S.; Larsson, K.; Landh, T.; Blum, Z.; Lidin, S. *The Language of Shape*; Elsevier: Amsterdam, 1997.

(81) Winsor, P. A. Hydrotropy, Solubilisation and Related Emulsification Processes. *Trans. Faraday Soc.* **1948**, *44* (0), 376–398.

(82) Schwarze, M.; Pogrzeba, T.; Volovych, I.; Schomäcker, R. Microemulsion Systems for Catalytic Reactions and Processes. *Catal. Sci. Technol.* **2015**, *5* (1), 24–33.

(83) Leung, R.; Shah, D. O. Solubilization and Phase Equilibria of Water-in-Oil Microemulsions. *J. Colloid Interface Sci.* **1987**, *120* (2), 320–329.

(84) Safran, S. A.; Turkevich, L. A. Phase Diagrams for Microemulsions. *Phys. Rev. Lett.* **1983**, *50* (24), 1930–1933.

(85) Miller, C. A.; Hwan, R.-N.; Benton, W. J.; Fort, T. Ultralow Interfacial Tensions and Their Relation to Phase Separation in Micellar Solutions. *J. Colloid Interface Sci.* **1977**, *61* (3), 554–568.

(86) Foucault, A. P. *Centrifugal Partition Chromatography*, 1 edition.; CRC Press: New York, 1994.

(87) Strey, R. On the Stability Range of Microemulsions: From the Tricritical Point to the Lamellar Phase in Water/Formamide-Octane-CiEj Systems. *Berichte Bunsenges. Für Phys. Chem.* **1993**, *97* (5), 742–750.

(88) Roux, D.; Bellocq, A. M.; Leblanc, M. S. An Interpretation of the Phase Diagrams of Microemulsions. *Chem. Phys. Lett.* **1983**, *94* (2), 156–161.

(89) Kahlweit, M.; Strey, R.; Firman, P.; Haase, D.; Jen, J.; Schomaecker, R. General Patterns of the Phase Behavior of Mixtures of Water, Nonpolar Solvents,

Amphiphiles, and Electrolytes. 1. *Langmuir* **1988**, *4* (3), 499–511.

(90) Kahlweit, M.; Strey, R.; Haase, D.; Kunieda, H.; Schmeling, T.; Faulhaber, B.; Borkovec, M.; Eicke, H.-F.; Busse, G.; Eggers, F.; et al. How to Study Microemulsions. *J. Colloid Interface Sci.* **1987**, *118* (2), 436–453.

(91) Ahmad, S. I.; Shinoda, K.; Friberg, S. Microemulsions and Phase Equilibria. Mechanism of the Formation of so-Called Microemulsions Studied in Connection with Phase Diagram. *J. Colloid Interface Sci.* **1974**, *47* (1), 32–37.

(92) Duvail, M.; Dufrêche, J.-F.; Arleth, L.; Zemb, T. Mesoscopic Modelling of Frustration in Microemulsions. *Phys. Chem. Chem. Phys.* **2013**, *15* (19), 7133–7141.

(93) Morrison, I. D. Electrical Charges in Nonaqueous Media. *Colloids Surf. Physicochem. Eng. Asp.* **1993**, *71* (1), 1–37.

(94) Fuoss, R. M. Conductance of Dilute Solutions of 1-1 Electrolytes1. *J. Am. Chem. Soc.* **1959**, *81* (11), 2659–2662.

(95) Dukhin, A.; Parlia, S. Ions, Ion Pairs and Inverse Micelles in Non-Polar Media. *Curr. Opin. Colloid Interface Sci.* **2013**, *18* (2), 93–115.

(96) Hou, M. J.; Kim, M.; Shah, D. O. A Light Scattering Study on the Droplet Size and Interdroplet Interaction in Microemulsions of AOT—oil—water System. *J. Colloid Interface Sci.* **1988**, *123* (2), 398–412.

(97) Karvar, M.; Strubbe, F.; Beunis, F.; Kemp, R.; Smith, N.; Goulding, M.; Neyts, K. Charging Dynamics of Aerosol OT Inverse Micelles. *Langmuir* **2015**, 150916160758009.

(98) Schmidt, J.; Prignitz, R.; Peschka, D.; Münch, A.; Wagner, B.; Bänsch, E.; Peukert, W. Conductivity in Nonpolar Media: Experimental and Numerical Studies on Sodium AOT-Hexadecane, Lecithin-Hexadecane and Aluminum(III)-3,5-Diisopropyl Salicylate-Hexadecane Systems. *J. Colloid Interface Sci.* **2012**, *386* (1), 240–251.

(99) Beunis, F.; Strubbe, F.; Marescaux, M.; Beeckman, J.; Neyts, K.; Verschueren, A. R. M. Dynamics of Charge Transport in Planar Devices. *Phys. Rev. E* **2008**, *78* (1), 011502.

(100) Beunis, F.; Strubbe, F.; Karvar, M.; Drobchak, O.; Brans, T.; Neyts, K. Inverse Micelles as Charge Carriers in Nonpolar Liquids: Characterization with Current Measurements. *Curr. Opin. Colloid Interface Sci.* **2013**, *18* (2), 129–136.

(101) Karvar, M.; Strubbe, F.; Beunis, F.; Kemp, R.; Smith, N.; Goulding, M.; Neyts, K. Investigation of Various Types of Inverse Micelles in Nonpolar Liquids Using

Transient Current Measurements. *Langmuir* **2014**, *30* (41), 12138–12143.

(102) Eicke, H.; Shepherd, J. C. W.; Steinemann, A. Exchange of Solubilized Water and Aqueous Electrolyte Solutions between Micelles in Apolar Media. *J. Colloid Interface Sci.* **1976**, *56* (1), 168–176.

(103) Eicke, H. F.; Hammerich, H.; Vasta, G. A Thermodynamic Analysis of the Molar Conductivity of the Ternary System: Water-Aerosol OT-Isooctane. *J. Colloid Interface Sci.* **1983**, *93* (2), 593–595.

(104) Eicke, H. F.; Borkovec, M.; Das-Gupta, B. Conductivity of Water-in-Oil Microemulsions: A Quantitative Charge Fluctuation Model. *J. Phys. Chem.* **1989**, *93* (1), 314–317.

(105) *Percolation | Geoffrey R. Grimmett | Springer*.

(106) De Gennes, P. G.; Taupin, C. Microemulsions and the Flexibility of Oil/Water Interfaces. *J. Phys. Chem.* **1982**, *86* (13), 2294–2304.

(107) Bhattacharya, S.; Stokes, J. P.; Kim, M. W.; Huang, J. S. Percolation in an Oil-Continuous Microemulsion. *Phys. Rev. Lett.* **1985**, *55* (18), 1884–1887.

(108) Gutfleisch, O.; Willard, M. A.; Brück, E.; Chen, C. H.; Sankar, S. G.; Liu, J. P. Magnetic Materials and Devices for the 21st Century: Stronger, Lighter, and More Energy Efficient. *Adv. Mater.* **2011**, *23* (7), 821–842.

(109) Constantinides, S. Rare Earth Science Community Help Needed for Clean Energy Initiatives.; Santa Fe, New Mexico, USA, 2011.

(110) Yu, Z.; Chen, M. Rare Earth Elements and Their Applications. *Metall. Ind. Press Beijing* **1995**, 286–294.

(111) Bredol, M.; Kynast, U.; Ronda, C. Leuchtstoffe Für Kathodenstrahlröhren. *Chem. Unserer Zeit* **1994**, *28* (1), 36–43.

(112) Binnemans, K.; Jones, P. T.; Blanpain, B.; Van Gerven, T.; Yang, Y.; Walton, A.; Buchert, M. Recycling of Rare Earths: A Critical Review. *J. Clean. Prod.* **2013**, *51*, 1–22.

(113) Anitha, M.; Kotekar, M. K.; Singh, D. K.; Sharma, J. N.; Singh, H. Solvent Extraction Studies of Rare Earths from Thiocyanate Medium with N,N,N´,N´-Tetra(2-Ethylhexyl) Diglycolamide. *Sep. Sci. Technol.* **2015**, *50* (3), 430–436.

(114) Danesi, P. R.; Chiarizia, R.; Coleman, C. F. The Kinetics of Metal Solvent Extraction. *C R C Crit. Rev. Anal. Chem.* **1980**, *10* (1), 1–126.

(115) Pathak, P. N.; Kanekar, A. S.; Prabhu, D. R.; Manchanda, V. K. Comparison of

Hydrometallurgical Parameters of N,N-Dialkylamides and of Tri-n-Butylphosphate. *Solvent Extr. Ion Exch.* **2009**, *27* (5–6), 683–694.

(116) Rao, P. R. V.; Kolarik, Z. A Review of Third Phase Formation in Extraction of Actinides by Neutral Organophosphorus Extractants. *Solvent Extr. Ion Exch.* **1996**, *14* (6), 955–993.

(117) Chiarizia, R.; Jensen, M. P.; Borkowski, M.; Nash, K. L. A New Interpretation of Third-Phase Formation in the Solvent Extraction of Actinides by TBP. In *Separations for the Nuclear Fuel Cycle in the 21st Century*; ACS Symposium Series; American Chemical Society, 2006; Vol. 933, pp 135–150.

(118) Paatero, E.; Ernola, P.; Sjöblom, J.; Hummelstedt, L. Formation of Microemulsion in Solvent Extraction Systems Containing Cyanex 272; Institut de Génie Chimique, Toulouse, 1987; Vol. E-1, pp 124–127.

(119) Paatero, E.; Lantto, T.; Ernola, P. The Effect of Trioctylphosphine Oxide on Phase and Extraction Equilibria in Systems Containing Bis(2,4,4-Trimethylpentyl) Phosphinic Acid. *Solvent Extr. Ion Exch.* **1990**, *8* (3), 371–388.

(120) Bauer, C.; Bauduin, P.; Dufrêche, J. F.; Zemb, T.; Diat, O. Liquid/Liquid Metal Extraction: Phase Diagram Topology Resulting from Molecular Interactions between Extractant, Ion, Oil and Water. *Eur. Phys. J. Spec. Top.* **2012**, *213* (1), 225–241.

(121) Dourdain, S.; Hofmeister, I.; Pecheur, O.; Dufrêche, J.-F.; Turgis, R.; Leydier, A.; Jestin, J.; Testard, F.; Pellet-Rostaing, S.; Zemb, T. Synergism by Coassembly at the Origin of Ion Selectivity in Liquid–Liquid Extraction. *Langmuir* **2012**, *28* (31), 11319–11328.

(122) Yu, Z.-J.; Neuman, R. D. Reversed Micellar Solution-to-Bicontinuous Microemulsion Transition in Sodium Bis(2-Ethylhexyl) Phosphate/n-Heptane/Water System. *Langmuir* **1995**, *11* (4), 1081–1086.

(123) Shioi, A.; Harada, M.; Matsumoto, K. Phase Equilibrium of Sodium Bis(2-Ethylhexyl)Phosphate/Water/n-Heptane/Sodium Chloride Microemulsion. *J. Phys. Chem.* **1991**, *95* (19), 7495–7502.

(124) Shioi, A.; Harada, M.; Tanabe, M. Static Light Scattering from Oil-Rich Microemulsions Containing Polydispersed Cylindrical Aggregates in Sodium Bis(2-Ethylhexyl) Phosphate System. *J. Phys. Chem.* **1995**, *99* (13), 4750–4756.

(125) Yu, Z.-J.; Neuman, R. D. Giant Rodlike Reversed Micelles Formed by Sodium Bis(2-Ethylhexyl) Phosphate in n-Heptane. *Langmuir* **1994**, *10* (8), 2553–2558.

(126) Faure, A.; Ahlnas, T.; Tistchenko, A. M.; Chachaty, C. Surfactant Conformation and Solvent Penetration in Sodium Di-2-Ethylhexyl Phosphate Reversed Micelles. A Multinuclear Relaxation Study. *J. Phys. Chem.* **1987**, *91* (7), 1827–1834.

(127) Li, Q.; Li, T.; Wu, J. Water Solubilization Capacity and Conductance Behaviors of AOT and NaDEHP Systems in the Presence of Additives. *Colloids Surf. Physicochem. Eng. Asp.* **2002**, *197* (1–3), 101–109.

(128) Quintana, S. S.; Falcone, R. D.; Silber, J. J.; Correa, N. M. Comparison between Two Anionic Reverse Micelle Interfaces: The Role of Water–Surfactant Interactions in Interfacial Properties. *ChemPhysChem* **2012**, *13* (1), 115–123.

(129) Alexander, S.; Eastoe, J.; Lord, A. M.; Guittard, F.; Barron, A. R. Branched Hydrocarbon Low Surface Energy Materials for Superhydrophobic Nanoparticle Derived Surfaces. *ACS Appl. Mater. Interfaces* **2016**, *8* (1), 660–666.

(130) Nave, S.; Eastoe, J.; Penfold, J. What Is So Special about Aerosol-OT? 1. Aqueous Systems. *Langmuir* **2000**, *16* (23), 8733–8740.

(131) Nave, S.; Eastoe, J.; Heenan, R. K.; Steytler, D.; Grillo, I. What Is So Special about Aerosol-OT? 2. Microemulsion Systems. *Langmuir* **2000**, *16* (23), 8741–8748.

(132) Berthon, L.; Martinet, L.; Testard, F.; Madic, C.; Zemb, T. Solvent Penetration and Sterical Stabilization of Reverse Aggregates Based on the DIAMEX Process Extracting Molecules: Consequences for the Third Phase Formation. *Solvent Extr. Ion Exch.* **2007**, *25* (5), 545–576.

(133) Kahlweit, M.; Strey, R. Phase Behavior of Ternary Systems of the Type H2O-Oil-Nonionic Amphiphile (Microemulsions). *Angew. Chem. Int. Ed. Engl.* **1985**, *24* (8), 654–668.

(134) *Solubilities of Toluene and Water*; NIST Database, 1986.

(135) Mukherjee, S.; Miller, C. A.; Fort, T. Theory of Drop Size and Phase Continuity in Microemulsions I. Bending Effects with Uncharged Surfactants. *J. Colloid Interface Sci.* **1983**, *91* (1), 223–243.

(136) Eicke, H.-F. Surfactants in Nonpolar Solvents. In *Micelles*; Topics in Current Chemistry; Springer Berlin Heidelberg, 1980; pp 85–145.

(137) Prince, L. *Microemulsions Theory and Practice*; Elsevier, 2012.

(138) Ekwall, P.; Mandell, L.; Fontell, K. Some Observations on Binary and Ternary Aerosol OT Systems. *J. Colloid Interface Sci.* **1970**, *33* (2), 215–235.

(139) Ekwall, P.; Mandell, L. Solutions of Alkali Soaps and Water in Fatty Acids I. Region of Existence of the Solutions. *Kolloid-Z. Z. Für Polym.* **1969**, *233* (1–2), 938–944.

(140) Ekwall, P.; Solyom, P. Solutions of Alkali Soaps and Water in Fatty Acids II. Density and Viscosity Measurements. *Kolloid-Z. Z. Für Polym.* **1969**, *233* (1–2), 945–955.

(141) Friberg, S.; Mandell, L.; Ekwall, P. Solutions of Alkali Soaps and Water in Fatty Acids III. IR and NMR Investigations. *Kolloid-Z. Z. Für Polym.* **1969**, *233* (1–2), 955–962.

(142) Ekwall, P.; Mandell, L.; Fontell, K. Solutions of Alkali Soaps and Water in Fatty Acids VI. Studies of the Refractive Index and Light Scattering. In *Surface Forces and Surfactant Systems*; Progress in Colloid & Polymer Science; Steinkopff, 1987; pp 3–16.

(143) Ekwall, P.; Fontell, K. Solutions of Alkali Soaps and Water in Fatty Axids VII. X-Ray Scattering of the Isotropic Liquid L2-Phase. *Colloid Polym. Sci.* **1988**, *266* (2), 184–191.

(144) Ekwall, P. Solutions of Alkali Soaps and Water in Fatty Acids VIII. Correlations of X-Ray Data with Other Experimental Observations. *Colloid Polym. Sci.* **1988**, *266* (3), 261–278.

(145) Ekwall, P. Solutions of Alkali Soaps and Water in Fatty Acids IX. The Location of TheL2-Phase in Three-Component Systems of Sodium Soap — Fatty Acid — Water, in View of the Occurrence of Acid Soaps. *Colloid Polym. Sci.* **1988**, *266* (3), 279–282.

(146) Ekwall, P. Solutions of Alkali Soaps and Water in Fatty Acids X. The Basic Structure of the Molecules and the Size of the Particles of Acid Octanoates in the L2-Phase at Water Contents below 40%. *Colloid Polym. Sci.* **1988**, *266* (8), 721–728.

(147) Ekwall, P. Solutions of Alkali Soaps and Water in Fatty Acids XI. Correlation between the Acid Sodium Octanoate in the Most Water-Rich Part of the L2-Phase and the Acid Soaps in Two Adjacent Phases. *Colloid Polym. Sci.* **1988**, *266* (8), 729–733.

(148) Barnes, I. S.; Derian, P.-J.; Hyde, S. T.; Ninham, B. W.; Zemb, T. N. A Disordered Lamellar Structure in the Isotropic Phase of a Ternary Double-Chain Surfactant System. *J. Phys.* **1990**, *51* (22), 2605–2628.

(149) Wolf, L.; Hoffmann, H.; Teshigawara, T.; Okamoto, T.; Talmon, Y. Microemulsions with a HIPME (High Internal Phase Microemulsion) Structure. *J. Phys. Chem. B* **2012**, *116* (7), 2131–2137.

(150) Williams, C.; Pierański, P.; Cladis, P. E. Nonsingular $S=+1$ Screw Disclination Lines in Nematics. *Phys. Rev. Lett.* **1972**, *29* (2), 90–92.

(151) Shioi, A.; Harada, M.; Tanabe, M. X-Ray and Light Scattering from Oil-Rich Microemulsions Containing Sodium Bis(2-Ethylhexyl) Phosphate. *Langmuir* **1996**, *12* (13), 3201–3205.

(152) Miller, C. A.; Neogi, P. Thermodynamics of Microemulsions: Combined Effects of Dispersion Entropy of Drops and Bending Energy of Surfactant Films. *AIChE J.* **1980**, *26* (2), 212–220.

(153) Kahlweit, M.; Strey, R.; Schomaecker, R.; Haase, D. General Patterns of the Phase Behavior of Mixtures of Water, Nonpolar Solvents, Amphiphiles, and Electrolytes. 2. *Langmuir* **1989**, *5* (2), 305–315.

(154) Hyde, S. T.; Ninham, B. W.; Zemb, T. Phase Boundaries for Ternary Microemulsions: Predictions of a Geometric Model. *J. Phys. Chem.* **1989**, *93* (4), 1464–1471.

(155) Bagchi, D.; Kumar, A.; Menon, R. Ion-Induced Multiply Reentrant Liquid-Liquid Transitions and the Nature of Criticality in Ethanol-Water Mixture. *J. Chem. Phys.* **2006**, *125* (3), 34511.

(156) Gazeau, D.; Bellocq, A. M.; Roux, D.; Zemb, T. Experimental Evidence for Bicontinuous Structures in L3 Phases. In *Trends in Colloid and Interface Science III*; Progress in Colloid & Polymer Science; Steinkopff, 1989; pp 226–232.

(157) Leung, R.; Shah, D. O. Solubilization and Phase Equilibria of Water-in-Oil Microemulsions. *J. Colloid Interface Sci.* **1987**, *120* (2), 330–344.

(158) Hornfeck, U.; Gradzielski, M.; Mortensen, K.; Thunig, C.; Platz, G. Highly Swollen Lamellar Phases in the System Calcium Dodecyl Sulfate, Pentanol or Hexanol, and Water. *Langmuir* **1998**, *14* (11), 2958–2964.

(159) Meziani, A.; Touraud, D.; Zradba, A.; Clausse, M.; Kunz, W. Co-Surfactant Properties of Ketones. *J. Mol. Liq.* **2000**, *84* (3), 301–311.

(160) Kim, M. W.; Huang, J. S. Dynamic Scaling in a Critical Microemulsion System. *Phys. Rev. B* **1982**, *26* (5), 2703–2706.

(161) Lemaire, B.; Bothorel, P.; Roux, D. Micellar Interactions in Water-in-Oil

Microemulsions. 1. Calculated Interaction Potential. *J. Phys. Chem.* **1983**, *87* (6), 1023–1028.

(162) Baxter, R. J. Percus–Yevick Equation for Hard Spheres with Surface Adhesion. *J. Chem. Phys.* **1968**, *49* (6), 2770–2774.

(163) Czajka, A.; Hazell, G.; Eastoe, J. Surfactants at the Design Limit. *Langmuir* **2015**, *31* (30), 8205–8217.

(164) Pileni, M. P. *Structure and Reactivity in Reverse Micelles*; Elsevier: Amsterdam, 1989.

(165) Day, R. A.; Robinson, B. H.; Clarke, J. H. R.; Doherty, J. V. Characterisation of Water-Containing Reversed Micelles by Viscosity and Dynamic Light Scattering Methods. *J. Chem. Soc. Faraday Trans. 1 Phys. Chem. Condens. Phases* **1979**, *75* (0), 132–139.

(166) Cabos, C.; Delord, P.; Marignan, J. Local Lamellar Structure in Dense Microemulsions. *Phys. Rev. B* **1988**, *37* (16), 9796–9799.

(167) Chen, S. -H.; Chang, S. -L.; Strey, R. Structural Evolution within the One-phase Region of a Three-component Microemulsion System: Water–n-decane–sodium-bis-ethylhexylsulfosuccinate (AOT). *J. Chem. Phys.* **1990**, *93* (3), 1907–1918.

(168) Holleman, A. F.; Wiberg, E. *Lehrbuch der Anorganischen Chemie*; Gruyter: Berlin, 1995.

(169) Li, Q.; Li, T.; Wu, J. Comparative Study on the Structure of Reverse Micelles. 2. FT-IR, 1H NMR, and Electrical Conductance of H2O/AOT/NaDEHP/n-Heptane Systems. *J. Phys. Chem. B* **2000**, *104* (38), 9011–9016.

(170) Safran, S. A. Fluctuations of Spherical Microemulsions. *J. Chem. Phys.* **1983**, *78* (4), 2073–2076.

(171) Auvray, L. Deviations from the Spontaneous Curvature in Surfactant Films : Effects on the Second Virial Coefficient and Interfacial Properties of the Microemulsions. *J. Phys. Lett.* **1985**, *46* (4), 163–172.

(172) Benmouna, M.; Hammouda, B. The Zero Average Contrast Condition: Theoretical Predictions and Experimental Examples. *Progress. Polym. Sci.* **1997**, *22*, 49–92.

(173) Moeser, B.; Horinek, D. The Role of the Concentration Scale in the Definition of Transfer Free Energies. *Biophys. Chem.* **2015**, *196*, 68–76.

(174) Parsegian, V. A.; Ninham, B. W. Van Der Waals Forces in Many-Layered Structures: Generalizations of the Lifshitz Result for Two Semi-Infinite Media. *J. Theor. Biol.* **1973**, *38* (1), 101–109.

(175) Dzido, T. Modification of Retention of Some Alkaloids in the System Silanized Silica/Methanol + Water + Di(2-Ethylhexyl)Orthophosphoric Acid. *J. Chromatogr. A* **1988**, *439* (2), 257–266.

(176) Hou, M. J.; Shah, D. O. Effects of the Molecular Structure of the Interface and Continuous Phase on Solubilization of Water in Water/Oil Microemulsions. *Langmuir* **1987**, *3* (6), 1086–1096.

(177) Chen, S. J.; Evans, D. F.; Ninham, B. W.; Mitchell, D. J.; Blum, F. D.; Pickup, S. Curvature as a Determinant of Microstructure and Microemulsions. *J. Phys. Chem.* **1986**, *90* (5), 842–847.

(178) Erlinger, C.; Belloni, L.; Zemb, T.; Madic, C. Attractive Interactions between Reverse Aggregates and Phase Separation in Concentrated Malonamide Extractant Solutions. *Langmuir* **1999**, *15* (7), 2290–2300.

(179) Huang, J. S. Surfactant Interactions in Oil Continuous Microemulsions. *J. Chem. Phys.* **1985**, *82* (1), 480–484.

(180) Fedors, R. F. A Method for Estimating Both, the Solubility Parameters and Molar Volumes of Liquids. *Polym. Eng. Sci.* **1974**, *14* (2), 147–157.

(181) Jun, S. Chromosome, Cell Cycle, and Entropy. *Biophys. J.* **2015**, *108* (4), 785–786.

(182) Hsu, M. F.; Dufresne, E. R.; Weitz, D. A. Charge Stabilization in Nonpolar Solvents. *Langmuir* **2005**, *21* (11), 4881–4887.

(183) Clausse, M.; Peyrelasse, J.; Heil, J.; Boned, C.; Lagourette, B. Bicontinuous Structure Zones in Microemulsions. *Nature* **1981**, *293* (5834), 636–638.

(184) Jada, A.; Lang, J.; Zana, R.; Makhloufi, R.; Hirsch, E.; Candau, S. J. Ternary Water in Oil Microemulsions Made of Cationic Surfactants, Water, and Aromatic Solvents. 2. Droplet Sizes and Interactions and Exchange of Material between Droplets. *J. Phys. Chem.* **1990**, *94* (1), 387–395.

(185) Tanford, C. Simple Model for the Chemical Potential Change of a Transported Ion in Active Transport. *Proc. Natl. Acad. Sci.* **1982**, *79* (9), 2882–2884.

(186) Dutkiewicz, E.; Robinson, B. H. The Electrical Conductivity of a Water-in-Oil Microemulsion System Containing an Ionic Surfactant. *J. Electroanal. Chem.*

Interfacial Electrochem. **1988**, *251* (1), 11–20.

(187) Eicke, H.-F.; Hilfiker, R.; Holz, M. Percolative Phenomena in Microemulsions of the 'One-Component Macrofluid' Type. *Helv. Chim. Acta* **1984**, *67* (2), 361–372.

(188) Borkovec, M.; Eicke, H. F.; Hammerich, H.; Das Gupta, B. Two Percolation Processes in Microemulsions. *J. Phys. Chem.* **1988**, *92* (1), 206–211.

(189) Dukhin, A. Critical Concentration of Ion-Pairs Formation in Nonpolar Media: General. *ELECTROPHORESIS* **2014**, *35* (12–13), 1773–1781.

(190) Stockhausen, M. J. M. G. Barthel, H. Krienke, and W. Kunz: Physical Chemistry of Electrolyte Solutions: Modern Aspects (Topics in Physical Chemistry, Vol. 5, Ed. by Deutsche Bunsengesellschaft), Steinkopff, Darmstadt/Springer, New York, 1998, ISBN 3-7985-1076-8, XVII+401 S., DM 84,-. *Berichte Bunsenges. Für Phys. Chem.* **1998**, *102* (10), 1521–1521.

(191) Cazabat, A.-M.; Chatenay, D.; Langevin, D.; Meunier, J. Percolation and Critical Points in Microemulsions. *Faraday Discuss. Chem. Soc.* **1983**, *76* (0), 291–303.

(192) Jada, A.; Lang, J.; Zana, R. Relation between Electrical Percolation and Rate Constant for Exchange of Material between Droplets in Water in Oil Microemulsions. *J. Phys. Chem.* **1989**, *93* (1), 10–12.

(193) Zana, R.; Lang, J.; Canet, D. Ternary Water-in-Oil Microemulsions Made of Cationic Surfactants, Water, and Aromatic Solvents. 3. Self-Diffusion Studies in Relation to Exchange of Material between Droplets and Percolation. *J. Phys. Chem.* **1991**, *95* (8), 3364–3367.

(194) Schmidt, J.; Prignitz, R.; Peschka, D.; Münch, A.; Wagner, B.; Bänsch, E.; Peukert, W. Conductivity in Nonpolar Media: Experimental and Numerical Studies on Sodium AOT–hexadecane, Lecithin–hexadecane and Aluminum(III)-3,5-Diisopropyl Salicylate–hexadecane Systems. *J. Colloid Interface Sci.* **2012**, *386* (1), 240–251.

(195) Neyts, K.; Beunis, F.; Strubbe, F.; Marescaux, M.; Verboven, B.; Karvar, M.; Alwin Verschueren. Charge Transport and Current in Non-Polar Liquids. *J. Phys. Condens. Matter* **2010**, *22* (49), 494108.

(196) van Dijk, M. A.; Casteleijn, G.; Joosten, J. G. H.; Levine, Y. K. Percolation in Oil-continuous Microemulsions. A Dielectric Study of Aerosol OT/Water/Isooctane. *J. Chem. Phys.* **1986**, *85* (1), 626–631.

(197) Blattner, C.; Bittner, J.; Schmeer, G.; Kunz, W. Electrical Conductivity of

Reverse Micelles in Supercritical Carbon Dioxide. *Phys. Chem. Chem. Phys.* **2002**, *4* (10), 1921–1927.

(198) Kim, M. W.; Huang, J. S. Percolationlike Phenomena in Oil-Continuous Microemulsions. *Phys. Rev. A* **1986**, *34* (1), 719–722.

(199) Lagourette, B.; Peyrelasse, J.; Boned, C.; Clausse, M. Percolative Conduction in Microemulsion Type Systems. *Nature* **1979**, *281* (5726), 60–62.

(200) Dekker, M. L.; Clausse, M.; Rosano, H. L.; Zradba, A. *Microemulsion Systems*; Microemulsion Series; 1987.

(201) Sivia, D. S. *Elementary Scattering Theory: For X-Ray and Neutron Users*; Oxford University Press: Oxford, New York, 2011.

(202) Beunis, F.; Strubbe, F.; Karvar, M.; Drobchak, O.; Brans, T.; Neyts, K.; Verschueren, A. R. M. Electric Charging of Inverse Micelles in a Nonpolar Liquid with Surfactant. *Colloids Surf. Physicochem. Eng. Asp.* **2014**, *440*, 10–19.

(203) Gourdin-Bertin, S.; Chassagne, C. Application of Classical Thermodynamics to the Conductivity in Non-Polar Media. *J. Chem. Phys.* **2016**, *144* (24), 244501.

(204) Dukhin, A. Critical Concentration of Ion-Pairs Formation in Nonpolar Media. *ELECTROPHORESIS* **2014**, *35* (12–13), 1773–1781.

(205) Beunis, F.; Strubbe, F.; Marescaux, M.; Neyts, K.; Verschueren, A. R. M. Micellization and Adsorption of Surfactant in a Nonpolar Liquid in Micrometer Scale Geometries. *Appl. Phys. Lett.* **2010**, *97* (18), 181912.

(206) Grest, G. S.; Webman, I.; Safran, S. A.; Bug, A. L. R. Dynamic Percolation in Microemulsions. *Phys. Rev. A* **1986**, *33* (4), 2842–2845.

(207) Testard, F. De La Molécule Aux Propriétés Macroscopiques d'une Solution Complexe : Relation Structure-Réactivité de Solutions Complexes et Nucléation Croissance de Nanoparticules, 2009.

(208) Ninham, B. W.; Barnes, I. S.; Hyde, S. T.; Derian, P.-J.; Zemb, T. N. Random Connected Cylinders: A New Structure in Three-Component Microemulsions. *EPL Europhys. Lett.* **1987**, *4* (5), 561.

(209) Schrödle, S.; Buchner, R.; Kunz, W. Percolating Microemulsions of Nonionic Surfactants Probed by Dielectric Spectroscopy. *Chemphyschem Eur. J. Chem. Phys. Phys. Chem.* **2005**, *6* (6), 1051–1055.

(210) Pileni, M.-P.; Zemb, T.; Petit, C. Solubilization by Reverse Micelles: Solute Localization and Structure Perturbation. *Chem. Phys. Lett.* **1985**, *118* (4), 414–420.

(211) Grimes, T. S.; Jensen, M. P.; Debeer-Schmidt, L.; Littrell, K.; Nash, K. L. Small-Angle Neutron Scattering Study of Organic-Phase Aggregation in the TALSPEAK Process. *J. Phys. Chem. B* **2012**, *116* (46), 13722–13730.

(212) Ellis, R. J.; Demars, T.; Liu, G.; Niklas, J.; Poluektov, O. G.; Shkrob, I. A. In the Bottlebrush Garden: The Structural Aspects of Coordination Polymer Phases Formed in Lanthanide Extraction with Alkyl Phosphoric Acids. *J. Phys. Chem. B* **2015**, *119* (35), 11910–11927.

(213) REACH - Chemicals - Environment - European Commission http://ec.europa.eu/environment/chemicals/reach/reach_en.htm (accessed Oct 3, 2017).

(214) Sukhbaatar, T.; Dourdain, S.; Turgis, R.; Rey, J.; Arrachart, G.; Pellet-Rostaing, S. Ionic Liquids as Diluents in Solvent Extraction: First Evidence of Supramolecular Aggregation of a Couple of Extractant Molecules. *Chem. Commun.* **2015**, *51* (88), 15960–15963.

(215) Smith, G. D.; Donelan, C. E.; Barden, R. E. Oil-Continuous Microemulsions Composed of Hexane, Water, and 2-Propanol. *J. Colloid Interface Sci.* **1977**, *60* (3), 488–496.

(216) Klossek, M. L.; Touraud, D.; Zemb, T.; Kunz, W. Structure and Solubility in Surfactant-Free Microemulsions. *ChemPhysChem* **2012**, *13* (18), 4116–4119.

(217) Diat, O.; Klossek, M. L.; Touraud, D.; Deme, B.; Grillo, I.; Kunz, W.; Zemb, T. Octanol-Rich and Water-Rich Domains in Dynamic Equilibrium in the Pre-Ouzo Region of Ternary Systems Containing a Hydrotrope. *J. Appl. Crystallogr.* **2013**, *46* (6), 1665–1669.

(218) Schöttl, S. Emergence of Micelles in Ternary Solutions Without Surfactants. 2013.

(219) Schöttl, S.; Touraud, D.; Kunz, W.; Zemb, T.; Horinek, D. Consistent Definitions of “the Interface” in Surfactant-Free Micellar Aggregates. *Colloids Surf. Physicochem. Eng. Asp.* **2015**, *480*, 222–227.

(220) Scoppola, E. Extraction Par Solvant: Étude d’une Interface Liquide/Liquide Contenant Des Ligands En Associant Des Mesures de Réflectivité de Rayons X et de Neutrons, 2015.

(221) Kunz, W.; Holmberg, K.; Zemb, T. Hydrotropes. *Curr. Opin. Colloid Interface Sci.*

(222) Bauduin, P.; Touraud, D.; Kunz, W. Design of Low-Toxic and Temperature-Sensitive Anionic Microemulsions Using Short Propyleneglycol Alkyl Ethers as Cosurfactants. *Langmuir* **2005**, *21* (18), 8138–8145.

(223) Pleines, M. Extractant-Free Extraction Using the Pre-Ouzo to Ouzo Effect. 2015.

(224) Kühnhammer, M. Extraction of Lanthanides Using the Pre-Ouzo and Ouzo Effect.

(225) Lopian, T.; Schöttl, S.; Prévost, S.; Pellet-Rostaing, S.; Horinek, D.; Kunz, W.; Zemb, T. Morphologies Observed in Ultraflexible Microemulsions with and without the Presence of a Strong Acid. *ACS Cent. Sci.* **2016**.

Annex

1. TABLE OF CONTENTS 180

1.1) LIST OF FIGURES 180

Chapter I 180

Chapter II 181

Chapter III 184

Chapter IV 186

1.2) LIST OF TABLES 186

2. EXPERIMENTAL SECTION 187

2.1) CHEMICAL PRODUCTS 187

2.1.1) Provided products 187

2.1.2) A novel method for preparation of NaDEHP 187

2.2. PREPARATION OF PHASE DIAGRAMS 189

2.2.1) Experimental evaluation 189

2.2.2) Plotting 190

2.3. TIE LINE ANALYSIS 190

2.3.1) Karl-Fischer analysis 190

2.3.2) Quantitative NMR 190

2.3.3) ICP-OES 191

2.4. CONDUCTIVITY MEASUREMENTS 191

2.4.1) Impedance spectroscopy 191

2.4.2) Conductivity-meter 192

2.5. SMALL ANGLE X-RAY SCATTERING 192

3. LIST OF PUBLICATIONS 192

4. REFERENCES 193

1. Table of contents

1.1) List of figures

Chapter I

Figure I-1 – Schematic representation of a solvent extraction experiment. Two liquids, e.g. water and oil are not miscibile. Two compounds are solubilized in the aqueous phase. After contacting the aqueous phase with an organic phase, the solutes distribute between the two phases according to their solubility in each of the respective phases.

Figure I-2 – Schematic representation of an extraction process, based on the distribution of ions between an aqeous and an organic phase.

Figure I-3 – Simplistic scheme of a hydrometallurgic process with solvent extraction as the core separation step. The first step is the leaching of metals from ores or waste material with an acidic solution. The second step is the enrichment of desired metal species from the feed solution with a formulated organic solution. In the third step, the precious metals are recuperated from the organic phase by a stripping step.

Figure I-4 – Artist view of a water-solvent interface (minisc underligned in green) in a liquid-liquid exraction system on a nanometer scale. Amphiphilic extractant molecules pick up an electrolyte at this interface and encapulated them into a organo-soluble complex. The red circle illustrates the polar cavity where the electrolyte is embedded after extraction.

Figure I-5 – Molecular structure of commonly used amphiphilic extractants. The blue areas denote the hydrophilic head-groups, responsible for complexation of cations. The orange areas shows the lipophilic tails, solubilizing the complex in an apolar environment.

Figure I-6 – Schematic representation of the molecular structure of an amphiphile and the organisation at the interface of a two-phase system containing water and oil.

Figure I-7 – Classification of surfactants according to their head-groups and apolar chains.

Figure I-8 – Change of some physico-chemical properties of a micellar solution before and after the cmc.

Figure I-9 – The two possible orientations of a surfactant in an organic solvent at the interface towards air. Since both are unfavourable for the free energy of the interface, they are crossed out by the red crosses.

Figure I-10 – Definition of the packing parameter and illsutration of the preferred spontaneous geometry.

Figure I-11 – Orientation of the spontaneous curvature of an interfactial surfactant film.

Figure I-12 – The four different types of phase behaviour in microemulsion systems named after Winsor.

Figure I-13 – Schematic representation of the two types of phase separation. Type I is an *emulsufication failure*, where mesoscopic aggregates are unable to solubilize higher quantities of the dispersed solvent. Type II is a *liquid-gas separation* and is a splitting of the organic phase into a “condensed“ lower phase, and a gas-like organic phase, only containing negligible amounts of the amphiphile.

Figure I-14 – How to read a phase diagram. (i) Extracting the composition of a sample with respect to the fraction of each component. (ii) Line towards component 2: the ratio between C1 and C3 is constant; Line parallel to the base: along this line, C3 is constant and the ratio between C1 and C2 varies.

Figure I-15 – Differentiation between phase diagrams with miscibility gaps of type 1 and type 2.

Figure I-16 – Tie line analysis in binary systems. A sample in the biphasic region will separate according to the orientation of the tie line. The compositions of the respective organic and aqueous phase can be deduced from the intersection of the tie line with the binodal. The ratio of the volumes is deduced from the lever rule.

Figure I-17 – Ternary phase diagram of water, octane and a non-ionic surfactant at a fixed temperature of $T = 44.6\,°C$.

Figure I-18 – Pseudo-ternary phase representations of a 5-component system. The surfactant SDS and butan1-ol as co-surfactant are unified on the top corner, water and NaCl as electrolyte are unified as a common aqueous medium. The influene of the salt concentration on the macroscopic phase behaviour is shown in three different ternary diagrams.

Figure I-19 – Gibbs prism of a quaternary system water + salt, oil and surfactant. Each triangle represents the phase behaviour at a specific temperature. Stacking of the triangles give a prism, for which the temperature-dependent phase behaviour can be analysed. Two sections are shown, to represent the 3-dimensional in a more visual 2-dimensional phase diagram. The section in blue is a cut at a constant surfactant-concentration, in green at a fixed ratio of aqueous to organic solvent.

Figure I-20 – Cut-analysis of a Gibbs prism: schematic representation of a (i) χ-diagram and (ii) Fish-diagram for an ionic surfactant. The white areas are monophasic. The grey areas show two liquid phases in equilibrium. The green area indicates where three phases are in equilibirum and the blue phase shows the presence of liquid crystalline phases.

Figure I-21 – Schematic representation of a percolation phenomenon upon dilution. Increase of the volume fraction of the dispersed phase, in this case water for an inverse system, leads to a swelling of aggregates. Beyond a critical volume fraction of the dispersed phase, the system is percolating. Here, it can be differed between two distinct cases: (i) dynamic percolation, where the aggregates are still discrete, however due to reversible coalescence, charge carriers can hop from micelle to micelle. (ii) static percolation, where the aggregates coalesce irreversibly to form continuous water-channels in which charge carriers can freely move.

Chapter II

Figure II-1 – Life cycle of a permanent magnet used in a wind turbine, highlighting the role of solvent extraction as separation procedure.

Figure II-2 – Schematic phase behaviour of a solvent extraction system expressed in a ternary diagram (in vol%). The grey and white areas denote the biphasic and monophasic areas. The striped area in (ii) shows a region where a splitting of the organic phase is observed. The red line indicates the compositions for which the volumes of the aqueous and organic phases are equal. The black lines show the tie lines. The test tubes with two phases represent the compositions in the diagrams, where the tie lines cross the red line.

Figure II-3 – Pseudo-ternary phase diagrams of hexane/Cyanex/water + NaOH for different contents of NaOH in the aqueous solution. Monophasic regions are presented in white, biphasic domains in grey and regions where the system separates into three co-existing phases.

Figure II-4 – Molecular structures of NaDEHP and Aerosol OT in a Van der Waals representation.

Figure II-5 – Scheme of a quaternary phase prism and introduction of the thermodynamic variable Z. The two faces represent the two limits for which the phase diagrams are true ternary systems. Every point of the prism can therefore be given as a function of the water-to-oil ratio, the extractant/surfactant concentration and the counter-ion ratio.

Figure II-6 – Ternary phase diagrams of toluene/HDEHP/water in wt%. The biphasic liquid-liquid domain is represented in grey, the monophasic region in white. The tie lines point towards pure water.

Figure II-7 – Ternary phase diagrams of toluene/NaDEHP/water in wt%. The biphasic liquid-liquid domain is represented in grey, the monophasic region in white, lyotropic mesophases in grey-blue and the biphasic solid-liquid regime in black. The tie lines point towards pure toluene.

Figure II-8 – Ternary phase diagrams of n-heptane/NaDEHP/water in wt% presented by Yu and Neuman ($T = 20\,°C$) (i) and by Shioi *et. al* ($T = 25\,°C$) (ii).

Figure II-9 – Miscibility gap of the ternary system toluene/NaDEHP/water in wt% at 25°C. The tie lines point towards pure oil, resulting in a critical point on the oil-rich side of the phase diagram (red circle). Two compositions (red and green cross) are represented on a dilution line towards water (blue line). The tubes illustrate the different types of phase separations, depending on whether the system is on the water-rich or solvent-rich side. The s/l-regime and most of the lyotropic phases have been omitted for clarity.

Figure II-10 – Pseudo-ternary phase diagrams of toluene/H-Na-DEHP/water in wt% for different ratios of H to Na. (i) Z = 0; (ii) Z = 0.1; (iii) Z = 0.3; (iv) Z = 0.5; (v) Z = 0.7; (vi) Z = 0.9; (vii) Z = 1.

Figure II-11 – Quaternary phase prism of toluene/NaDEHP/HDEHP/water. The Z-axis gives the ratio of NaDEHP with respect to the total amount of extractant. 7 phase diagrams for different Z are plotted, including the two “faces” for Z = 0 and Z = 1.

Figure II-12 – Amount of water molecules per molecule NaDEHP necessary in order to observe a phase transition, plotted as a function of Z.

Figure II-13 – Image of the apparently monophasic transparent low-viscous microemulsion for the system toluene/HDEHP/NaDEHP/water, exhibiting a bluish appearance designed as Tyndall effect corresponding to efficient diffusion of blue light (blue sky) without the strong diffusion due to local index variation that would produce a “milky” appearance.

Figure II-14 – Images of a stable “*liquid-foam-like*”-phase.

Figure II-15 – Solubility-limit of water in binary mixtures of extractant and toluene plotted versus different counter-ion ratios of Z.

Figure II-16 – Schematic presentation of the transition for a phase separation of class 2 (attractive interactions) to class 1 (emulsification failure).

Figure II-17 – χ-cut the prism toluene/HDEHP/NaDEHP/water for γ = 20wt%. The typical X-shaped form of the monophasic region has been highlighted by two lines. The dashed line represents the so-called “non-frustrated” regime. The dotted line traces the so-called “frustrated regimes”. The black arrow indicates a re-entrant pathway, where a monophasic-biphasic-monophasic transition is observed for decreasing α. Lyotropic phases; the s/l-phase and the LFL-phase are added for the sake of completeness.

Figure II-18 – Vertical prism sections at constant water-to-toluene ratio. (i) $\alpha_{toluene}$ = 0.25, (ii) $\alpha_{toluene}$ = 0.75. A maximum solubility for in the water- as well as on the oil-rich side is detected for $Z = 0.9$. Lyotropic phases; the s/l-phase and the LFL-phase are added for the sake of completeness.

Figure II-19 – χ-plot of n-decane, AOT, $\varepsilon_{brine} = 0.6$ as a function of Z (here temperature) and α_{decane}. This figure is a schematic representation to highlight the frustrated (red arrows) and non-frustrated regions (blue arrows).

Figure II-20 – Barbell-shaped dimer of a frustrated microemulsion.

Figure II-21 – Modified scheme of Shah. On the water-rich side, decreasing Z leads to an increase in rigidity and decrease of frustration. The opposite is observed on the oil-rich side of the phase diagram.
Figure II-22 – (i) Tie lines in the biphasic region of the phase diagram of the phase diagram with Z = 0.5. (ii) Tie lines taking into account the ratio of HDEHP to NaDEHP in each of the phases.

Figure II-23 – Schematic partition of liquid-liquid regime into a heavy L1 phase and a light L2 phase. SAXS-spectra show the presence of structures in the mesoscopic domain.

Figure II-24 – Schematic representation of the mesoscopic aggregation in both phases and the distribution of the cations between the two phases.

Figure II-25 – Phase diagram of iso-octane/HDEHP/water in wt% (i). Phase diagram of iso-octane/NaDEHP/water in wt% (ii). Tie lines are schematically presented.

Figure II-26 – Pseudo-ternary phase diagrams of iso-octane/H-Na-DEHP/water in wt% for different ratios of H to Na. (i) Z = 0; (ii) Z = 0.1; (iii) Z = 0.3; (iv) Z = 0.5; (v) Z = 0.7; (vi) Z = 0.9; (vii) Z = 1.

Figure II-27 – Quaternary phase prism of iso-octane/NaDEHP/HDEHP/water. The Z-axis gives the ratio of NaDEHP with respect to the total amount of extractant. 7 phase diagrams for different Z are plotted, including the two "faces" for $Z = 0$ and $Z = 1$.

Figure II-28 – Phase diagram of dodecane/HDEHP/water in wt% (i). Phase diagram of dodecane/NaDEHP/water in wt% (ii). Tie lines are schematically presented.

Figure II-29 – Schematic representation of attractive depletion forces of two colloids in the presence of smaller aggregates.

Figure II-30 – Pseudo-ternary phase diagrams of iso-octane/H-Na-DEHP/water in wt% for different ratios of H to Na. (i) $Z = 0$; (ii) $Z = 0.1$; (iii) $Z = 0.3$; (iv) $Z = 0.5$; (v) $Z = 0.7$; (vi) $Z = 0.9$; (vii) $Z = 1$.

Figure II-31 – Quaternary phase prism of iso-octane/NaDEHP/HDEHP/water. The Z-axis gives the ratio of NaDEHP with respect to the total amount of extractant. 7 phase diagrams for different Z are plotted, including the two "faces" for $Z = 0$ and $Z = 1$.

Figure II-32 – Formation of a third phase, where an aqueous and organic phase coexist in the presence of a liquid-crystalline phase. The three meniscus are highlighted by red circles.

Figure II-33 – Ternary phase diagram of nitrobenzene/HDEHP/water in wt% at $T = 25\ °C$. The tie lines have been added schematically to highlight the expulsion of water from the organic phase.

Figure II-34 – Pseudo-ternary phase diagrams of iso-octane/H-Na-DEHP/water in wt% for different ratios of H to Na. (i) $Z = 0$; (ii) $Z = 0.1$; (iii) $Z = 0.3$; (iv) $Z = 0.5$.

F**igure II-35** – Quaternary phase prism of nitrobenzene/NaDEHP/HDEHP/water. The Z-axis gives the ratio of NaDEHP with respect to the total amount of extractant. 4 phase diagrams for different Z are plotted, including the two "bottom" for $Z = 0$.

Chapter III

Figure III-1 – Conductivity of the organic phase (squares, dotted line) for the solvent extraction system DMDBTDMA as a function of the co-extracted nitric acid concentration in the organic phase.

Figure III-2 – Representation of the three dilutions paths that will be compared: dilution with water (blue arrow), dilution with solvent (orange arrow) and variation of the counter-ion mole ratio, everything else being constant.

Figure III-3 – Changing the solubility of a surfactant by modifying the temperature or salinity can transform a Winsor II microemulsion into a Winsor I microemulsion by passing through a Winsor III-regime.

Figure III-4 – partial χ-cut for the quaternary system toluene/HDEHP/NaDEHP/water in the range of $0.5 \leq Z \leq 1$. The same colours as in the previous chapter for frustration (wine red) and non-frustrated (blue) has been maintained and depicted by the arrows. The green and red arrows indicate the conductivity paths analysed in this section.

Figure III-5 – Pseudo-ternary phase diagram of toluene/NaDEHP/HDEHP/water with indication of conductivity path in the monophasic region. One dilution line for $S_0^* = 0.5$.

Figure III-6 – Specific conductivity in a non-frustrated extracting microemulsion as a function of the water-to-extractant ratio W_0. (i) lin-log representation; (ii) log-log representation.

Figure III-7 – Dismutation mechanism of reverse micelles.

Figure III-8 – Ternary phase diagrams of toluene/NaDEHP/HDEHP/water with indication of conductivity pathways in the monophasic region. Three dilution lines for $S_0^* = 0.5$ (navy blue), 0.25 (blue) & 0.1 (light blue). The two changes of the slope of the conductivity measurement at water-to-solvent ratios are added in this plot for a more visual representation.

Figure III-9 – The specific conductivity plotted as a function of W_0. (i) lin-log-scale: illustration of increase in temperature, upon addition of water: the clear inflection at $W_0 = 3.9$ is the origin of the first hydration layer concept in micellar systems. (ii) log-log scale: this scale allows to identify the three different conduction regimes involved (see text). All measurements were carried out at $T = 25\ °C$.

Figure III-10 – Determination of the percolation scaling exponents μ and s of the conductivity line at $S_0^* = 0.5$.

Figure III-11 – Conductance in a bicontinuous microemulsion system. Dissociated counter-ions primarily migrate in the continuous water-channels.

Figure III-12 – Conductivity of figure 9 depicted in “reduced conductivity” versus the water-to-extractant ratio W_0. (i) lin-log representation, (ii) log-log representation.

Figure III-13 – Rod-like sections of a percolating DOC-system: below the critical hydration where water is adsorbed at the surfactant head-groups. Above the critical hydration, the formation of a water core enables the dissociation of counter-ions. These counter-ions can migrate along these cylinders giving rise to a drastic increase in conductivity.

Figure III-14 – Limit of hydration and distinction between reverse micellar systems as w/o weak aggregates and swollen reverse w/o microemulsions. The water inside the swollen micelles behaves like bulk water and thus we can define this region as a real L2 microemulsion, where oil and water are separated by a hydrated surfactant film and a real interface.

Figure III-15 – Pseudo-ternary phase diagram of toluene/NaDEHP/HDEHP/water at a counter-ion ratio of $Z = 0.5$. The blue triangles indicate the initially prepared compositions in the biphasic region. The orange triangles denote the compositions of the organic phase after phase separation.

Figure III-16 – Conductivity deduced from impedance spectroscopy versus the volume fraction of dispersed phase. (i) lin-log representation; (ii) log-log-representation.

Figure III-17– Reduced equivalent conductivity versus the square root of extractant concentration.

Figure III-18 – (i) Three observed morphologies of SAXS-spectra along the dilution line towards oil. (ii) Forward scattering $I(0)$ of the spectra.

Figure III-19 – Ternary phase diagram of toluene/NaDEHP/water, with three dilution lines towards water at $W_0 = 2; 3.5; 5$. The zoom into the oil-rich corner highlights the dilution lines towards toluene in the monophasic channel.

Figure III-20 – Conductivity profile towards pure toluene as a function of $\phi_{extractant+water}$ for $W_0 = 2$ (orange), $W_0 = 3.5$ (green) and $W_0 = 5$ (blue). (i) lin-lin representation, (ii) lin-log representation.

Figure III-21 – Reduced equivalent conductivities as a function of the square root of the extractant concentration. (i) $W_0 = 2$ (orange). (ii) $W_0 = 3.5$ (green). (iii) $W_0 = 5$ (blue).

Figure III-22 – At very dilute concentrations of the extractant, the system is in a monomeric state. Above a cmc (red line), the aggregates self-assemble into discrete reverse micellar aggregates. Above a second critical concentration (percolation threshold, blue dotted line), the aggregates coalesce to form a continuous cluster. The reverse micellar regime beyond the cmc is further divided by the hydration limit as shown in figure 13.

Figure III-23 – (i) Partial χ-cut for the quaternary system toluene/HDEHP/NaDEHP/water in the range of $0.5 \leq Z \leq 1$. The same colours as in the previous chapter for frustration (wine red) and non-frustrated (blue) has been maintained and depicted by the arrows. The orange arrow indicates the conductivity-pathway as a function of the water-content for a counter-ion ratio of $Z = 0.9$. (ii) pseudo-ternary phase diagram of toluene/NaDEHP/HDEHP/water at a counter-ion ratio of $Z = 0.9$. The three dilution lines towards water for which the conductivity has been measured have been inserted.

Figure III-24 – Conductivity in the monophasic region of the pseudo-ternary phase diagram toluene/NaDEHP/HDEHP/water at a counter-ion ratio of $Z = 0.9$. $S_0^* = 0.5$ (navy blue) , $S_0^* = 0.25$ (blue) and $S_0^* = 0.1$ (light blue). (i) lin-log representation; (ii) log-log representation.

Figure III-25 – Dilution line towards water in the pseudo-ternary phase diagram toluene/NaDEHP/HDEHP/water at a counter-ion ratio of $Z = 0.9$. The initial extractant-to-toluene ratio is $S_0^* = 0.5$. Plot of the reduced conductivity of the dilution line and schematic evolution of the microstructure as a function the water-content (expressed as W_0).

Figure III-26 – Partial χ-cut for the quaternary system toluene/HDEHP/NaDEHP/water in the range of $0.5 \leq Z \leq 1$. The arrow indicates a transition from the non-frustrated branch (green) towards the frustrated branch.

Figure III-27 – Conductivity as a function of the counter-ion ratio Z. The surfactant concentration was held at a constant weight-fraction of $\gamma_{extractant} = 50wt\%$ and a constant value of $W_0 = 5$. (i) lin-lin representation; (ii) log-lin representation.

Figure III-28 – Mapping the of the morphology on a microscopic state in terms of percolation, discrete swollen micelles and the *true* reverse micellar regime, where free water is present in the micellar core.

Chapter V

Figure IV-1 – Classification of the model used in this work compared to surfactant microemulsions and an extracting microemulsion.

Figure IV-2 – Schematic representation of a χ-cut, where the Winsor I and Winsor II regimes overlap. In the cross-section, the system exhibits both types of phase separation: an emulsification failure and a liquid-gas-type separation.

Figure IV-3 – Bottlebrush structure of complexes formed by Lanthanum and HDEHP.

Figure IV-4 – Schematic representation of the formulator's cut: The tie lines (black lines) are cut at half their length (represented by the red line). The compositions at the intersection of the tie lines with the red line posses an equal volume of the aqueous and the organic phase.

Figure IV-5 – Formulator's cut for the quaternary system toluene/NaDEHP/HEHP/water at a constant weight fraction of $w_{water} = 50wt\%$. The phase behaviour with increasing extractant concentration is plotted as a function of the counter-ion ratio Z. Additionally, the solubility of water in the organic phase is plotted as a function of the counter-ion ratio, using the right Y-axis. The solubility is illustrated by the red dashed curve.

Figure IV-6 – A) Octan-1-ol cluster in a water-continuous environment. B) Same cluster as a with ethanol molecules adsorbed at the interface.[17]

Figure IV-7 – Simulated structure of ultraflexible microemulsion, depending on the composition

Figure IV-8 – Quaternary phase prism of 1-propoxy-2-propanol/HDEHP/NaDEHP/water, for ratios of $Z = 0;\ 0.3;\ 0.7$.

1.2) List of tables

Table I-1 – Permittivity and corresponding Bjerrum-length in different solvents, considering the valency of the ions: $m = n = 1$.

Table II-1 – Selected properties of water soluble and insoluble solvents. V is the molecular volume, μ the electric dipole moment, ε the dielectric permittivity and δ the Hildebrandt coefficient. Solvent of significance for this work are highlighted in orange.[7]

Table II-2 – Consolidation and comparison of phase behaviour for the two ternary systems.

Table II-3 – Composition of the initial samples prepared in the binary region of the phase diagram as well as the compositions of the resulting organic and aqueous phase.

Table III-1 – Comparison of experimentally determined critical exponents with literature.

Table III-2 – Volume fraction of water dispersed in the microemulsion at the onset of the conductivity.

Table III-3 – Composition of samples in the organic phase deduced by quantitative NMR and Karl-Fischer titration.

2. Experimental section

2.1) Chemical products

2.1.1)Provided products

Toluene (purity > 99%) and iso-octane (purity > 99.5%) were provided by Carlo Erba. n-Dodecane (purity > 99%), nitrobenzene (purity > 98.5%) and bis(2-ethylhexyl) phosphoric acid (purity > 97%) were purchased from Sigma Aldrich. NaOH (purity >99.9%) was bought from Merck. Water was obtained from a Millipore source with a resistivity $R > 12.8\ \Omega$.

All chemical products were used without further purification.

2.1.2)A novel method for preparation of NaDEHP

NaDEHP is a component that is not found in a regular portfolio of big companies providing chemical products for laboratory use, such as Sigma Aldrich, Merck or Carlo Erba. Its acidic counterpart however, bis(2-ethylhexyl) phosphoric acid, or HDEHP, is easily accessible at a low price as it is one of the most used extractants on a laboratory as well as on an industrial scale.

For synthesis of the sodium salt, several procedures have been identified in literature, such as the reaction of HDEHP with metallic sodium[4] or neutralization with sodium hydroxide until a certain pH.[5,6] While the first description was discarded beforehand due to safety reasons, the reports on neutralization with a base are ambiguously described. In one case, the equivalent point was set at pH = 6,[5] in the second case at pH = 9.[6] One of the reasons for deviation of the neutralization point could be the different choice of solvent (e.g. methanol and n-heptane) in which HDEHP was solubilized before addition of aqueous NaOH. From a practical point of view, first essays have been tested with either of proposed pathways, however the presence of water at higher quantities has posed severe problems during evaporation of the solvent. Due to the surfactant properties of NaDEHP as the solution exhibits a gel-like texture with strong foam formation as the solution is more and more reduced.

As a consequence of the elusive procedures in literature, a novel concept has been developed in order to synthesize NaDEHP at high quantities on a laboratory scale (~30 g per batch), with high yields and purity, in addition to a concise pathway.

2.1.2.1) The chemical reaction and challenges towards an easy purification

As this is a simple acid-base reaction, water is produced as a side product. Further, being a phosphoric acid, HDEHP is considered as strong acid (pK_a = 1.8)[7] the balance of the reaction is quantitatively towards the formation of NaDEHP.

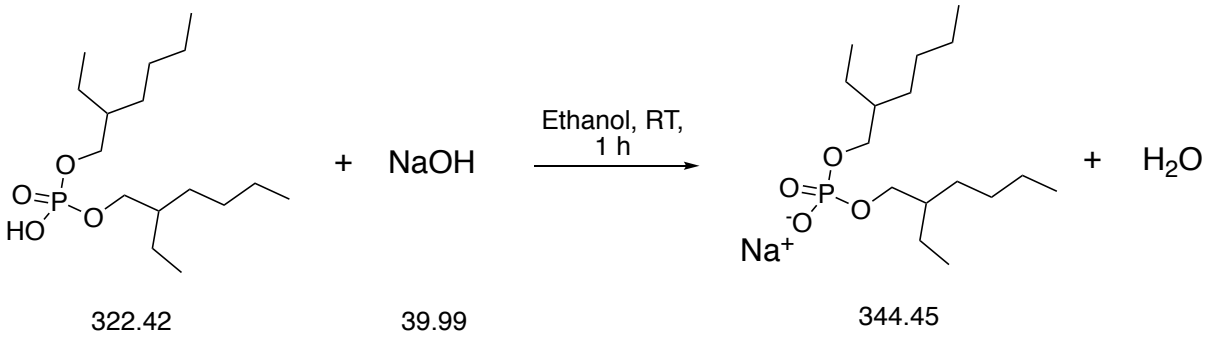

Figure A-1 – Neutralization of bis(2-ethylhexyl) phosphoric acid by sodium hydroxide to obtain sodium bis(2-ethylhexyl) phosphate.

The crucial points of this reaction have been identified to be the addition of water and volatility of the solvent. Therefore, a solvent has been chosen to commonly solubilize the reagents NaOH and HDEHP, which has been found in the short-chained alcohols, like methanol and ethanol. As additional advantage, both alcohols form an azeotrope with water, thus facilitating the removal of water as side-product of the reaction.[8]

The second point is to ensure a complete reaction towards the salt, hence either the acid or the base need to be added with a slight excess. It was chosen to add NaOH in slight excess, since after evaporation of the solvent after reaction, NaOH and NaDEHP remain as precipitates on the bottom of the flaks and washing with water easily dissolves the base, while the salt remains solid. Finally, the overall reaction is depicted in scheme 1.

2.1.2.2) Working procedure

The first step is the solubilization of crushed sodium hydroxide pellets (1.05 eq, 91.45 mmol, 3.657 g) in ethanol (50 mL) in a flask (250 mL). To accelerate this process, the flask is put in an ultrasonic bath (20 min, RT). After obtaining a clear transparent solution, the flask is placed on a microbalance and HDEHP is added with a pasteur pipette (1 eq, 87.1 mmol, 28.081 g). The solution is then stirred for 1 h at ambient conditions before evaporating the solvent under reduced pressure (180 mbar, 40 °C, 15 min) until a white, waxy solid remains. Residual NaOH is removed by washing the product with water (3 x 20 mL). Water was removed by freeze-drying (12 h) to remove the major part, then under vacuum (24 h, 80 °C) to eliminate any residues. In the end, 29.6 g of pure NaDEHP was obtained (98.6% yield).

2.2. Preparation of phase diagrams

2.2.1)Experimental evaluation

The phase diagrams have been evaluated preparing 10 samples per triangle as schematically presented in figure 2. Per water or respectively oil-rich side, five samples have been prepared and diluted with the last component.

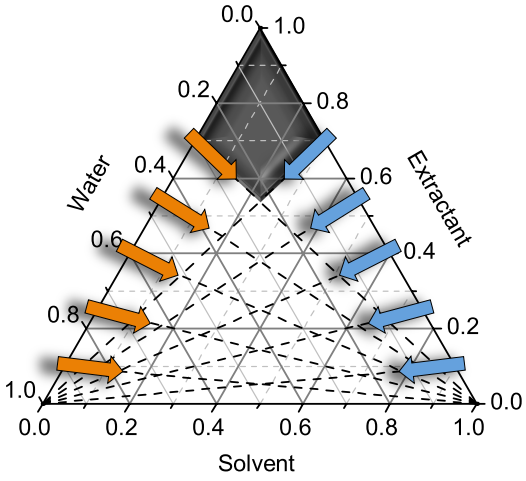

Figure A-2 – Ternary phase plot with location of water, extractant and the solvent. The orange arrows indicate the dilution lines performed by adding the diluent as the last component. The blue arrows indicate the dilution lines performed by adding water as the last component.

The initial (pseudo-)binary compositions were chosen for:

$$S_0^* = \frac{w_{extractant}}{w_{extractant} + w_{solvent}} \; ; \; W_0^* = \frac{w_{extractant}}{w_{extractant} + w_{water}} \qquad (i)$$

With $S_0^*/W_0^* = 0.1, 0.25, 0.4, 0.55, 0.7$.

The initial composition of a sample before adding the last component was $m = 2g$. All phase diagrams have been determined at ambient temperatures ($T = 25\,°C$). The samples were prepared in screw tubes of borosilicate glass provided from Pyrex.

Monophasic regions have been evaluated by diluting with the last component until a phase separation was observed by the naked eye (cloud-point method).[9] Multiphasic regions have been evaluated by gradual screening. The last component was added in steps of 3-5 wt%, the solution was thoroughly shaken and left 24 h for settling. If no phase separation occurred within 48 h, the tubes were centrifuged 30 mins at 4500 rpm.

2.2.2)Plotting

The phase transitions have been plotted using the program Origin 8.5 from OriginLab. Interpolation of the phase transitions to give a phase boundary has been done using PowerPoint form Microsoft. The legend for the defined phases, which have been observed during this investigation are tabled in figure 3.

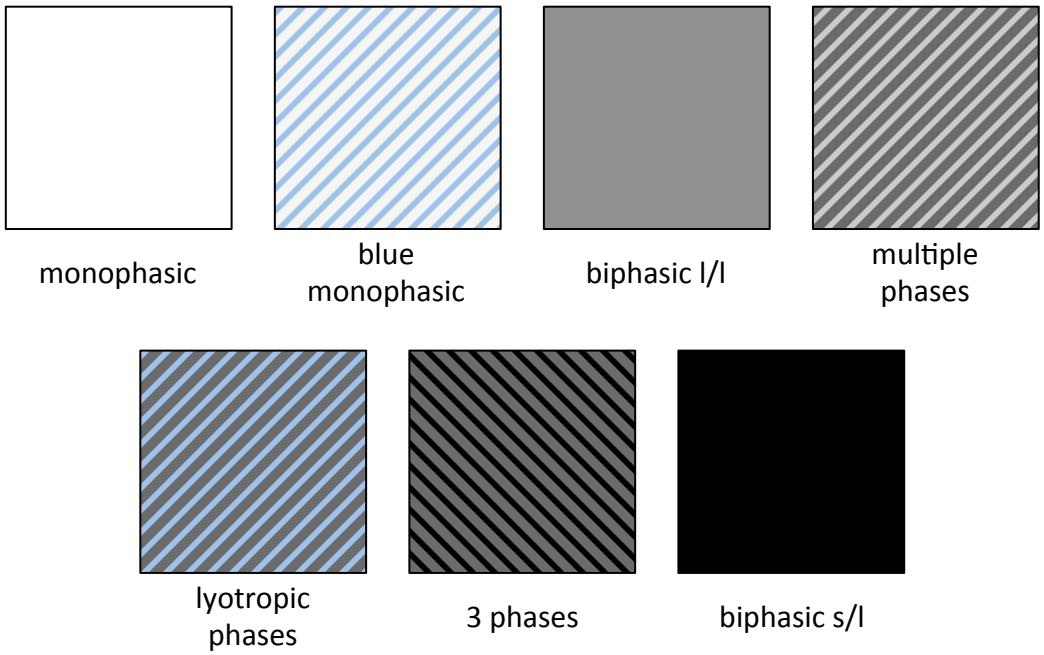

Figure A-3 – Legend of observed phases in ternary phase diagrams in this work.

2.3. Tie line analysis

The compositions of the quaternary solutions have been analysed using different techniques in order to quantify a component in an organic or aqueous phase.

2.3.1)Karl-Fischer analysis

The water-content in water-poor organic solutions has been determined by volumetric Karl-Fischer titration. An automated KF Titrando (Metrohm) device has been used, with a Composite 2 solution provided by Sigma Aldrich (2 mL of solutions are equivalent to 1 mg water).

2.3.2)Quantitative NMR

The content of toluene and the DEHP-anion has been determined using quantitative NMR with dimethylformamide as internal standard, as it is soluble in water as well as apolar

solvents. Further, the chemical shift of the 1H spectrum can be clearly distinct from the signal of DEHP and toluene. NMR-measurements have been carried out with a Bruker 400 device.

2.3.3)ICP-OES

The concentration of sodium in the aqueous and organic phase were analysed by ICP-OES. The samples were analyzed by an ICP-OES spectrometer from Archos equipped with an autosampler. In order to avoid and notice cross contamination, the system was rinsed with 2% (v/v) nitric acid and blancs were placed in regular intervals.

2.4. Conductivity measurements

2.4.1)Impedance spectroscopy

Conductivity by diluting with the solvent has been obtained using impedance spectroscopy. The spectra have been recorded with a Solartron ModuLab XM MTS frequency response analyser from Modulab Analytics. The measurement cell has been provided from Keysight Technologies (16452A Liquid Test Fixture) with a minimum volume of 4.5 mL per sample. The impedance spectra have been recorded in the frequency range from $\omega = 5 \cdot 10^{-2}$ - $1 \cdot 10^{6}$ Hz. The amplitude was chosen to be in the range of |V| = ±100 mV. The minimum of the half-circle obtained from a Cole-Cole-plot was obtained by fitting the spectrum with a circular fit, implemented in the evaluation software.

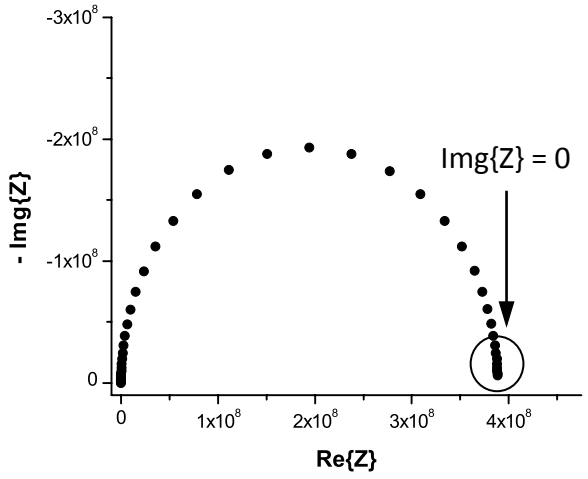

Figure A-3 – Cole-Cole-plot of an impedance spectrum. The conductivity was determined using the purely resistive signal where the half-circle is at a minimum.

2.4.2)Conductivity-meter

Conductivity measurements were carried out in a thermostatic measurement cell (25.0 °C) under permanent stirring using a low-frequency WTW inoLab Cond 730 conductivity meter connected with a WTW TetraCon 325 electrode (Weilheim, Germany). 20 g of a sample were filled in the measurement cell and successively diluted with pure water. The electrode has been calibrated with potassium chloride and a cell constant of $R = 0.472\ cm^{-1}$ has been determined.

2.5. Small angle X-ray scattering

Small-and-wide-angle X-ray scattering (SWAXS) measurements were performed on a bench built by XENOCS using Mo radiation (l= 0.071 nm). The scattered beam was recorded using a large online scanner detector (diameter: 345 mm, from MAR Research). A large q-range (0.2 to 40 nm^{-1}) was covered with an off-center detection. Collimation was applied using a 12:∞ multilayer Xenocs mirror (for Mo radiation) coupled to two sets of scatterless FORVIS slits providing a 0.8 0.8 mm X-ray beam at the sample position. Preanalysis of data was performed using FIT2D software. The scattered intensities are recorded versus the magnitude of the scattering vector q = [(4p)/λ]sin(y/2), where λ is the wavelength of incident radiation and y the scattering angle. 2 mm quartz capillaries were used as sample containers for the solutions. The usual corrections for background (empty cell and detector noise) subtractions and intensity normalization using a high density polyethylene film as a standard were applied. Experimental resolution was Δq/q= 0.05. Silver behenate in a sealed capillary was used as the scattering vector calibration standard. Measurements were performed at room temperature.

3. List of Publications

Zemb, T.; Klossek, M. L.; **Lopian, T**.; Marcus, J.; Schöttl, S.; Horinek, D.; Prévost, S. F.; Touraud, D.; Diat, O.; Marčelja, S.; Kunz, W., How to explain microemulsions formed by solvent mixtures without conventional surfactants. *Proceedings of the National Academy of Sciences* 2016, *113*, 4260-4265.

Lopian, T.; Schöttl, S.; Prévost, S; Pellet-Rostaing, S.; Horinek, Kunz. W; Zemb, T, Morphologies observed in ultra-flexible microemulsions with and without the presence of a strong acid. *ACS Central Science* 2016, *2*, 467–475.

Prévost, S.; **Lopian, T**.; Pleines, M.; Diat, O.; Zemb, T., Small-angle scattering and morphologies ultra-flexible microemulsions. *Journal of Applied Cristallography* 2016, *49*, 2063-2072.

Brock, D.; **Lopian, T**.; Khoshsima, A.; Bauduin, P.; Diat, O.; Touraud, D.; Kunz, W., Nanostructuring in ethanol/"ethanolotrope"/rapeseed oil automotive biofuels; *Colloid and Interface Science Communications* 2016, *16*, 1-3.

4. References

(1) Kahlweit, M.; Strey, R.; Firman, P.; Haase, D.; Jen, J.; Schomaecker, R. General Patterns of the Phase Behavior of Mixtures of Water, Nonpolar Solvents, Amphiphiles, and Electrolytes. 1. *Langmuir* **1988**, *4* (3), 499–511.

(2) Yu, Z.-J.; Neuman, R. D. Reversed Micellar Solution-to-Bicontinuous Microemulsion Transition in Sodium Bis(2-Ethylhexyl) Phosphate/n-Heptane/Water System. *Langmuir* **1995**, *11* (4), 1081–1086.

(3) Evens, D. F.; Wennerström, H. *The Colloidal Domain: Where Physics, Chemisry, Biology and Technology Meet*, Second Edition.; Wiley-VCH, 1999.

(4) Yu, Z. J.; Zhou, N. F.; Neuman, R. D. On the Role of Water in the Formation of Reversed Micelles: An Antimicellization Agent. *Langmuir* **1992**, *8* (8), 1885–1888.

(5) Faure, A.; Tistchenko, A. M.; Zemb, T.; Chachaty, C. Aggregation and Dynamical Behavior in Sodium Diethylhexyl Phosphate/Water/Benzene Inverted Micelles. *J. Phys. Chem.* **1985**, *89* (15), 3373–3378.

(6) Shioi, A.; Harada, M.; Matsumoto, K. Phase Equilibrium of Sodium Bis(2-Ethylhexyl)Phosphate/Water/n-Heptane/Sodium Chloride Microemulsion. *J. Phys. Chem.* **1991**, *95* (19), 7495–7502.

(7) Ellis, R. J.; Demars, T.; Liu, G.; Niklas, J.; Poluektov, O. G.; Shkrob, I. A. In the Bottlebrush Garden: The Structural Aspects of Coordination Polymer Phases Formed in Lanthanide Extraction with Alkyl Phosphoric Acids. *J. Phys. Chem. B* **2015**, *119* (35), 11910–11927.

(8) Gould, R. F. Azeotropic Data—III, Copyright, Advances in Chemistry Series, FOREWORD. In *Azeotropic Data—III*; Gould Robert F., Ed.; Advances in Chemistry; AMERICAN CHEMICAL SOCIETY, 1973; Vol. 116, pp i–vi.

(9) Klossek, M. L.; Touraud, D.; Zemb, T.; Kunz, W. Structure and Solubility in Surfactant-Free Microemulsions. *ChemPhysChem* **2012**, *13* (18), 4116–4119.